INVESTIGATING THE STERIC AND ELECTRONIC EFFECTS OF LOW-VALENT URANIUM COMPLEXES ON THE ACTIVATION OF SMALL MOLECULES

by

Rachel Jennifer Kahan

Submitted for the degree of Doctor of Philosophy

University of Sussex

February 2015

The work detailed in this thesis was carried out at the University of Sussex from September 2011 to February 2015, under the supervision of Professor F. G. N. Cloke. All the work is my own, unless stated to the contrary and has not been previously submitted for any degree at this or any other university.

Rachel J. Kahan

February 2015

RACHEL JENNIFER KAHAN, DOCTOR OF PHILOSOPHY IN CHEMISTRY

INVESTIGATING THE STERIC AND ELECTRONIC EFFECTS OF LOW-VALENT URANIUM COMPLEXES ON THE ACTIVATION OF SMALL MOLECULES

SUMMARY

In the last decade substantial progress has been made in our understanding of uranium organometallic chemistry, specifically regarding the activation of small molecules by uranium(III) complexes. Research by Cloke and colleagues has employed dianionic eight- and monoanionic five-membered aromatic ligands around a uranium(III) centre to make mixed-sandwich systems, which have demonstrated novel reactivity with carbon monoxide and carbon dioxide. This thesis continues this work and furthers our understanding of the properties and reactivity of these complexes.

The first part of this thesis describes the preparation of novel mixed-sandwich complexes incorporating the $COT^{(SiiPr3)2}$ ligand and either a substituted cyclopentadienyl ring or a heterocyclic analogue. The steric parameters of these complexes have been quantitatively evaluated and provide insight into the molecular structures and reactivity observed. The electronic properties of the complexes have been investigated using cyclic voltammetry and complement results obtained by other researchers from the group.

The second part of this thesis describes the reactivity of the novel mixed-sandwich complexes with small molecules. Whilst it was found the cyclopentadienyl complexes exhibit similar reactivity with carbon monoxide and carbon dioxide to previously reported complexes, the heterocyclic analogues provided a wealth of new reactivity, including facile cleavage of carbon monoxide at ambient temperatures, synthesis of an unusual phosphacarbonate fragment, and unprecedented synthesis of a 2,2'-bis(arsenine) species.

The third part of this thesis explores the reactivity of potential precursors to uranium(II) metallocene complexes. Uranium complexes in this oxidation state have only recently been synthesised and the formation of a uranium(II) sandwich complex is desirable for its anticipated reactivity with small molecules. Reactivity studies include the attempted reduction of uranium(III) iodide precursors with potassium-based reducing agents and the synthesis of a novel uranium(II) tetraphenylborate complex.

Acknowledgements

I would like to start by thanking Geoff for all his support and for allowing me to carry out some truly bizarre chemistry. Thanks are given to John Turner for keeping me motivated during some dark hours and to Ian Crossley for all the good careers advice. Thanks to Drs Frey and Frey and Nikos Tsoureas for the odd helping hand. Thanks also to Nikos, Mark and the NCS for attempting to run and solve many 'crystals' that were powdery in nature. To Zoë Button for teaching me the magic of the Toepler line. Special thanks goes to Sandy for the perseverance to read this whole thesis when it was double the length and less than half as good. Also for his patience when I bombarded him with questions about crystals/cyclic voltammetry/chemistry/life in general.

Thanks to Iain Day for not complaining about the many random 'cheeky' 2+ hour silicon NMR experiments that took place in a 20 minute slot. To Mark Roe who was always apologetic when informing me the structure 'was not what I wanted'. To Ali Abdul-Sada for the express MS-EI service, and optimism that we might find the molecular ion of an unstable species if we try enough times! To Chris Dadswell for running some 'emergency' GC-MS when Ali wasn't around. To Mick and Fran for lending me glassware, and for the donation of two shiny new lab coats.

Thanks are given to Professor Meyer for the donation of COS *via* Sandy, which prompted another 20 pages of work. Thanks also to Professor Nief for his donation of potassium arsolyl, which saved me months of work and Geoff hundreds of £££s!!! To Professor Maron and Christos Kefalidis for the calculations on the tetraphenylborate complex. To Dr Wildgoose for the two instructive visits on cyclic voltammetry. I would also like to thank the mystery benefactor of the 'box' which provided me with an extra six inches of height when it mattered.

To Vicki for showing me I had nothing to complain about when she found yet another unit cell for $[Rh(COD)Cl]_2$. To Matt for the random comments that have made me laugh and to Chris for his lack of tact. To Hope for being a delightful student. To mum and dad for their unwavering support and the many frogs that have accumulated over the years.

And most of all to Gary, for everything else.

List of New Compounds

$[U(COT^{(SiiPr3)2})(Cp^{tBu})]$	2.1
$[U(COT^{(SiiPr3)2})(Cp^{tBu2})]$	**2.2**
$[U(COT^{(SiiPr3)2})(Cp^{tBu3})]$	**2.3**
$[U(COT^{(SiiPr3)2})(Cp^{(SiiPr3)2})]$	**2.4**
$[U(COT^{(SiiPr3)2})(Cp^{NMe4})]$	**2.5**
$[U(COT^{(SiiPr3)2})(Cp^{PMe4})]$	**2.6**
$[U(COT^{(SiiPr3)2})(Cp^{AsMe4})]$	**2.7**
$[U(COT^{1,4\text{-}SiiPr3})(COT^{1,3\text{-}SiiPr3})]$	**2.8**
$[U(COT^{(SiiPr3)2})(Cp^{AsMe4})I]$	**2.9**
$[U(COT^{(SiiPr3)2})(Cp^{PMe4})(O^{n}Bu)]$	**2.10**
$[U(COT^{(SiiPr3)2})(Cp^{AsMe4})(O^{n}Bu)]$	**2.11**
$[U(COT^{(SiiPr3)2})(Cp^{NMe4})(O^{n}Bu)]$	**2.12**
$[(COT^{(SiiPr3)2})U(\mu\text{-}\eta^{5}\text{:}\eta^{1}\text{-}NC_4Me_3CH)U(COT^{(SiiPr3)2})(NC_4Me_4)]$	**2.13**
$[\{U(COT^{(SiiPr3)2})(Cp^{tBu})\}_2(\mu\text{-}O)]$	**3.1**
$[\{U(COT^{(SiiPr3)2})(Cp^{tBu3})\}_2(\mu\text{-}O)]$	**3.2**
$[\{U(COT^{(SiiPr3)2})(Cp^{(SiiPr3)2})\}_2(\mu\text{-}O)]$	**3.3**
$[\{U(COT^{(SiiPr3)2})(Cp^{tBu})\}_2(\mu\text{:}\eta^{1}\text{:}\eta^{2}\text{-}CO_3)]$	**3.4**
$[U(COT^{(SiiPr3)2})(Cp^{tBu})Cl]$	**3.5**
$[U(COT^{(SiiPr3)2})(Cp^{PMe4})(2\text{-}O\text{-}PC_5Me_4)]$	**4.1**
[1,2-bis(1,2,3,4-tetramethylphospholyl)acetylene]	**4.2**
$[\{U(COT^{(SiiPr3)2})\}_2(\mu\text{-}O)(\mu\text{-}\eta^{1}\text{:}\eta^{1}\text{-}O_2SOCF_3)_2]$	**4.3**

$[U(COT^{(SiiPr3)2})(Cp^{AsMe4})(2\text{-}O\text{-}AsC_5Me_4)]$ **4.4**

[2,2'-bis(3,4,5,6-tetramethylarsenine)] **4.5**

$[U(COT^{(SiiPr3)2})(Cp^{PMe4})(CN^tBu)]$ **4.6**

$[\{U(COT^{(SiiPr3)2})\}_2(\mu\text{-}O)\{\mu\text{-}\eta^1\text{:}\eta^1\text{-}O_2C(NC_4Me_4)\}_2]$ **4.8**

$[(COT^{(SiiPr3)2})(Cp^{NMe4})U(\mu\text{-}O)(\mu\text{-}\eta^1\text{:}\eta^5\text{-}Cp^{NMe4})U(COT^{(SiiPr3)2})]$ **4.9**

$[\{U(COT^{(SiiPr3)2})\}_2(\mu\text{-}O)\{\mu\text{-}\eta^1\text{:}\eta^1\text{-}O_2C(PC_4Me_4)\}_2]$ **4.11**

$[\{(COT^{(SiiPr3)2})U\}_2(\mu\text{-}O)_2]$ **4.12**

[1,1'-bis(2,3,4,5-tetramethylphosphole)] **4.13**

$[C_4Me_4PCO_2SiMe_3]$ **4.14**

$[C_4Me_4PSiMe_3]$ **4.15**

$[\{U(COT^{(SiiPr3)2})(OSiMe_3)\}_2(\mu\text{-}Cl)_2]$ **4.16**

$[\{U(COT^{(SiiPr3)2})(OSiMe_3)\}_2(\mu\text{-}I)_2]$ **4.17**

$[\{U(COT^{(SiiPr3)2})(Cp^{PMe4})\}_2(\mu\text{-}S)]$ **4.18**

$[\{U(COT^{(SiiPr3)2})(Cp^{PMe4})\}_2(\mu\text{-}CO_2S)]$ **4.19**

$[\{U(COT^{(SiiPr3)2})(Cp^{PMe4})\}(\mu\text{-}CO_2S)\{U(COT^{(SiiPr3)2})(\eta^1\text{:}\eta^1\text{-}O_2CPC_4Me_4)\}]$ **4.20**

$[\{U(Cp^{tBu2})_2\}_2(\mu\text{-}I)_2]$ **6.1**

$[\{U(Cp^{(SiiPr3)2})_2\}_2(\mu\text{-}I)_2]$ **6.2**

$[U(Cp^{tBu2})_3]$ **6.3**

$[\{U(Cp^{tBu2})_2\}_2(BH_x)]$ **6.4**

$[\{U(Cp^{(SiiPr3)2})_2\}_2(BH_x)]$ **6.5**

$[(Cp^{(SiiPr3)2})U(\mu\text{-}Ph)_2BPh_2]$ **6.6**

List of Abbreviations Used in the Text

Å	Angstrom
Ad	adamantyl
An	actinide
Ar	generic aryl
Bz	benzyl
ca.	*circa*, approximately
cm^{-1}	wavenumbers
crown	generic crown ether
crypt	generic cryptand
CSD	Cambridge Structural Database
°	degree
°C	degree Celsius
ΔG	Gibbs free energy change
DCM	dichloromethane
DFT	density functional theory
DME	1,2-dimethoxyethane
dmpz	dimethylpyrazolyl
E	unspecified element
EA	elemental analysis
EI	electron impact
Et	ethyl
F	Faraday constant, 9.6485×10^4 C·mol^{-1}
FTIR	Fourier transform infrared
GC-MS	Gas chromatography – mass spectrometry
HOMO	highest occupied molecular orbital
^{i}Pr	*iso*-propyl
Ind	indenyl
IR	infrared spectroscopy
kcal	kilocalorie
kJ	kilojoules
L	unspecified ligand
Ln	lanthanide

LUMO	lowest unoccupied molecular orbital
M	unspecified metal
m/z	mass-to-charge ratio
Me	methyl
Mes	mesityl
MO	molecular orbital
mol	mole(s)
MS	mass spectrometry
^{n}Bu	*n*-butyl
ODtbp	2,6-di-*tert*-butylphenoxy
OTtbp	2,4,6-tri-*tert*-butylphenoxy
OTf	triflate
Ph	phenyl
pmdta	N.N.N',N',N''-pentamethyldiethylenetriamine
R	generic alkyl
RT	room temperature
^{t}Bu	*tert*-butyl
tacn	unspecified triazacyclononane ligand
($^{R,R'}$ArO)tacn	R,R'-derivatized aryloxide-functionalised triazacyclononane ligand
THF	tetrahydrofuran
TMS	trimethylsilyl
Tp^{Me2}	3,5-dimethyltrispyrazolylborate
tpy	2,2':6',2''-terpyridine
X	generic anionic ligand
XRD	X-ray diffraction
$[U]^{R}$	generic uranium(III) or uranium(IV) metal centre with the ancillary ligands $COT^{(Si\mathit{i}Pr3)2}$ and Cp^{R}

Aromatic Ligands

COT	cyclooctatetraenyl
$COT^{(Si\mathit{i}Pr3)2}$	1,4-bis(tri-*iso*-propylsilyl)cyclooctatetraenyl
$COT^{(SiMe3)2}$	1,4-bis(trimethylsilyl)cyclooctatetraenyl

COT^{BIG}	1,4-bis(triphenylsilyl)cyclooctatetraenyl
Cp	cyclopentadienyl
Cp^{-PPh2}	diphenyphosphinocyclopentadienyl
$Cp^{(Si\mathit{i}Pr3)2}$	1,3-bis(tri-*iso*-propylsilyl)cyclopentadienyl
Cp^{AsMe4}	2,3,4,5-tetramethylarsolyl
Cp^{EMe4}	2,3,4,5-tetramethyl-substituted heterocyclic aromatic ring, where E = N, P or As
Cp^{NMe4}	2,3,4,5-tetramethylpyrrolyl
Cp^{PMe4}	2,3,4,5-tetramethylphospholyl
Cp^{R}	R-substituted cyclopentadienyl
$Cp^{\mathit{t}Bu}$	*tert*-butylcyclopentadienyl
$Cp^{\mathit{t}Bu2}$	1,3-di-*tert*-butylcyclopentadienyl
$Cp^{\mathit{t}Bu3}$	1,2,4-tri-*tert*-butylcyclopentadienyl
Cp^{Me}	methylcyclopentadienyl
Cp^{Me4}	tetramethylcyclopentadienyl
Cp^{Me4Et}	tetramethylethylcyclopentadienyl
$Cp^{Me4\mathit{i}Pr}$	tetramethyl-*iso*-propylcyclopentadienyl
$Cp^{Me4SiMe3}$	tetramethyl-trimethylsilylcyclopentadienyl
$Cp^{Me4\mathit{t}Bu}$	tetramethyl-*tert*-butylcyclopentadienyl
Cp^{Me5} or Cp*	pentamethylcyclopentadienyl
Cp^{SiMe3}	trimethylsilylcyclopentadienyl
Ct	centroid
Pn	pentalene

Electrochemistry Abbreviations

$[FeCp_2]^{+/0}$	ferrocenium/ferrocene reference potential
ΔE	difference in half-wave potentials
CV	cyclic voltammetry
E^0	standard electrode potential
$E_{½}$	half-wave potential
Ep_a	oxidation peak potential
Ep_c	reduction peak potential

V	Volt

Nuclear Magnetic Resonance Abbreviations

$\{^1H\}$	proton decoupled
δ	chemical shift
^xJ	coupling constant over x bonds
br	broad
d	doublet
dd	doublet of doublets
DOSY	diffusion ordered spectroscopy
HMBC	heteronuclear multiple bond correlation spectroscopy
HSQC	heteronuclear single-quantum correlation spectroscopy
Hz	hertz
K	Kelvin
t	triplet
m	multiplet
MHz	megahertz
NMR	nuclear magnetic resonance spectroscopy
ppm	parts per million
s	singlet
VT	variable temperature
$w_{½}$	half-height linewidth

Solid-G Abbreviations

G	shielding parameter, expressed as a percentage
Gγ	overlap parameter, expressed as a percentage

Abstract

Investigating the Steric and Electronic Effects of Low-Valent Uranium Complexes on the Activation of Small Molecules

Rachel Jennifer Kahan

An introduction to the use of aromatic ligands in organouranium chemistry is reviewed in Chapter 1, with reference to electrochemical studies on the thermodynamic stability of the published complexes where appropriate. The synthesis of seven new uranium(III) mixed-sandwich complexes $[U(COT^{(Si\textit{i}Pr3)2})(Cp^{R})]$ is described in Chapter 2 and these complexes have been studied by cyclic voltammetry. Three of these complexes incorporate the heterocyclic five-membered rings Cp^{EMe4} (E = N, P or As), which are structurally similar to their carbocyclic analogues. Thermolysis of the heterocyclic mixed-sandwich complexes results in the formation of *n*-butoxide complexes $[U(COT^{(Si\textit{i}Pr3)2})(Cp^{EMe4})(O^{\textit{n}}Bu)]$ by ring-opening of THF, and an additional tuck-in tuck-over complex, $[(COT^{(Si\textit{i}Pr3)2})U(\mu\text{-}\eta^5\text{:}\eta^1\text{-}NC_4Me_3CH)U(COT^{(Si\textit{i}Pr3)2})(NC_4Me_4)]$ is observed from $[U(COT^{(Si\textit{i}Pr3)2})(Cp^{NMe4})]$.

Chapter 3 is introduced with a summary of the activation of small molecules by organouranium complexes, which is followed by reactivity studies of the synthesised carbocyclic mixed-sandwich complexes, $[U(COT^{(Si\textit{i}Pr3)2})(Cp^{R})]$ (R = ^{t}Bu, $^{t}Bu_3$ or $(Si^{i}Pr_3)_2$), with CO, CO_2 and N_2O. These studies are limited with the larger complexes, however $[U(COT^{(Si\textit{i}Pr3)2})(Cp^{\textit{t}Bu})]$ is observed to form an oxo complex $[\{U(COT^{(Si\textit{i}Pr3)2})(Cp^{\textit{t}Bu})\}_2(\mu\text{-}O)]$ and a carbonate complex $[\{U(COT^{(Si\textit{i}Pr3)2})(Cp^{\textit{t}Bu})\}_2(\mu\text{-}CO_3)]$ from N_2O and CO_2 respectively. The mixed-sandwich chloride complex $[U(COT^{(Si\textit{i}Pr3)2})(Cp^{\textit{t}Bu})Cl]$ was also synthesised and its redox behaviour compared with its uranium(III) analogue.

Chapter 4 explores the reactivity of the heterocyclic mixed-sandwich complexes with small molecules. Reaction of $[U(COT^{(Si\textit{i}Pr3)2})(Cp^{PMe4})]$ and $[U(COT^{(Si\textit{i}Pr3)2})(Cp^{AsMe4})]$

with carbon monoxide results in initial insertion of CO into the heterocyclic ring to yield oxy-phosphinine and oxy-arsenine fragments. This is followed by cleavage of the C≡O bond, resulting the formation of [1,2-bis(2,3,4,5-tetramethylphospholyl)acetylene] and [2,2'-bis(3,4,5,6-tetramethylarsenine)].

Carbon dioxide demonstrated both reduction and insertion reactivity with $[U(COT^{(Si\textit{i}Pr3)2})(Cp^{EMe4})]$ (E = N or P) with the formation of $[\{U(COT^{(Si\textit{i}Pr3)2})\}_2(\mu\text{-}O)\{\mu\text{-}\eta^1\text{:}\eta^1\text{-}O_2C(NC_4Me_4)\}_2]$ and $[\{U(COT^{(Si\textit{i}Pr3)2})\}_2(\mu\text{-}O)\{\mu\text{-}\eta^1\text{:}\eta^1\text{-}O_2C(PC_4Me_4)\}_2]$ respectively. The carbamate complex is formed *via* the mixed-sandwich oxo complex $[(COT^{(Si\textit{i}Pr3)2})(Cp^{NMe4})U(\mu\text{-}O)(\mu\text{-}\eta^1\text{:}\eta^5\text{-}Cp^{NMe4})U(COT^{(Si\textit{i}Pr3)2})]$, however the phosphacarbonate complex is formed *via* $[\{(COT^{(Si\textit{i}Pr3)2})U\}_2(\mu\text{-}O)_2]$ and [1,1'-bis(2,3,4,5-tetramethylphosphole)]. Attempts to probe the mechanism of the latter reaction using COS resulted in the formation of a bridging sulfide complex $[\{U(COT^{(Si\textit{i}Pr3)2})(Cp^{PMe4})\}_2(\mu\text{-}S)]$, which was found to react with carbon dioxide to yield two thiocarbonate complexes, $[\{U(COT^{(Si\textit{i}Pr3)2})(Cp^{PMe4})\}_2(\mu\text{-}CO_2S)]$ and $[\{U(COT^{(Si\textit{i}Pr3)2})(Cp^{PMe4})\}(\mu\text{-}CO_2S)\{U(COT^{(Si\textit{i}Pr3)2})(\eta^1\text{:}\eta^1\text{-}O_2CPC_4Me_4)\}]$.

Chapter 5 details the work undertaken to evaluate the steric parameters of uranium(III) mixed-sandwich complexes A brief literature review introduces the methods available and their applications, and a comprehensive study of the mixed-sandwich complexes is then described. The steric parameters obtained for individual ligands and entire complexes are compared and trends pertaining to the solid-state molecular structures and the reactivity of these complexes are discussed.

Chapter 6 presents the syntheses of $[\{U(Cp^R)_2\}_2(\mu\text{-}I)_2]$ (R = ^{t}Bu$_2$, (Si^{i}Pr$_3$)$_2$), which have been studied by cyclic voltammetry and their steric properties evaluated. Attempts to reduce $[\{U(Cp^{tBu2})_2\}_2(\mu\text{-}I)_2]$ with potassium-based reagents yielded the tris(cyclopentadienyl)uranium complex, $[U(Cp^{tBu2})_3]$, by possible disproportionation of a uranium(II) intermediate. Attempts to trap this species with BH_3·THF gave rise to a bridging borane/borohydride complex, $[\{U(Cp^{tBu2})_2\}_2(\mu\text{-}BH_x)_2]$. Attempts to synthesise

a bis(cyclopentadienyl)uranium(III) cation resulted in the formation of a mono(cyclopentadienyl)uranium tetraphenylborate complex, [($Cp^{(Si\mathit{i}Pr3)2}$)U(μ-Ph)$_2$BPh$_2$]. Summaries of the results and experimental details are included at the end of each chapter and additional data are presented in the appendices.

TABLE OF CONTENTS

Acknowledgements ..... **iv**

List of New Compounds ..... **v**

List of Abbreviations Used in the Text ..... **vii**

Abstract ..... **xi**

CHAPTER 1: INTRODUCTION TO ORGANOURANIUM CHEMISTRY **1**

1.1 Introduction **1**

1.2 Properties of the f-Block elements **1**

1.3 Aromatic ligands in organouranium Chemistry **4**

1.3.1 Five-membered carbocycles *4*

1.3.1.1 Properties of cyclopentadienyl ligands 4

1.3.1.2 Tetrakis(cyclopentadienyl)uranium complexes 4

1.3.1.3 Tris(cyclopentadienyl)uranium complexes 5

1.3.1.4 Bis(cyclopentadienyl)uranium complexes 9

1.3.1.5 Electrochemical studies of bis(cyclopentadienyl)uranium complexes 12

1.3.1.6 Mono(cyclopentadienyl)uranium complexes 14

1.3.2 Five-membered heterocycles *15*

1.3.2.1 Properties of heterocyclic ligands 15

1.3.2.2 Uranium heterocyclic complexes 16

1.3.3 Six-membered carbocycles *20*

1.3.3.1 Properties of arene ligands 20

1.3.3.2 Terminal arene uranium complexes 21

1.3.3.3 Bridging arene complexes 23

1.3.4 Seven-membered carbocycles *26*

1.3.4.1 Properties of cycloheptatrienyl ligands 26

1.3.4.2 Uranium cycloheptatriene complexes 26

1.3.5 Eight-membered carbocycles *27*

1.3.5.1 Properties of cyclooctatetraene ligands 27

1.3.5.2 Uranocene 27

1.3.5.3 Monocyclooctatetraene uranium complexes 30

1.3.5.4 Inverse cyclooctatetraene uranium complexes 32

1.3.5.5 Properties of pentalene 33

1.3.5.6 Uranium pentalene complexes 34

1.4 Summary **35**

1.5 References **35**

CHAPTER 2: URANIUM(III) MIXED-SANDWICH COMPLEXES 47

2.1 Introduction **47**

2.2 Synthesis and characterisation of cyclopentadienyl-based uranium(III) mixed-sandwich complexes **49**

2.2.1 Synthetic route to mixed-sandwich complexes *49*

*2.2.2 NMR studies of mixed-sandwich complexes **2.1** - **2.4*** *50*

*2.2.3 Molecular structure of [U(COT$^{(SiiPr3)2}$)(Cp^{tBu})(THF)] (**2.1THF**)* *53*

*2.2.4 Molecular structures of the desolvated mixed-sandwich complexes (**2.1** – **2.4**)* *54*

2.2.5 Cyclic voltammetry of cyclopentadienyl mixed-sandwich complexes *56*

2.3 Synthesis and characterisation of heterocyclic uranium(III) mixed-sandwich complexes **61**

2.2.1 Synthetic route to heterocyclic mixed-sandwich complexes *61*

2.3.2 Characterisation of heterocyclic mixed-sandwich complexes *63*

*2.3.3 Molecular structures of **2.5THF** – **2.7THF*** *66*

*2.3.4 Molecular structure of [U(COT$^{(SiiPr3)2}$)(Cp^{NMe4})] (**2.5**)* *69*

2.3.5 Cyclic voltammetry of heterocyclic mixed-sandwich complexes *71*

2.3.6 Identification and characterisation of side products *73*

2.3.6.1 Characterisation of [U(COT$^{1,4\text{-Si}i\text{Pr}3}$)(COT$^{1,3\text{-Si}i\text{Pr}3}$)] (**2.8**) 73

2.3.6.2 Characterisation of [U(COT$^{(\text{Si}i\text{Pr}3)2}$)(Cp$^{\text{AsMe}4}$)I] (**2.9**) 74

2.3.7 Thermolysis of mixed-sandwich complexes *75*

2.4 Summary **80**

2.5 Experimental details for chapter 2 ..... **80**

2.6 References **91**

CHAPTER 3: ACTIVATION OF CARBON OXIDES BY URANIUM(III) MIXED-SANDWICH COMPLEXES WITH SUBSTITUTED CYCLOPENTADIENYL LIGANDS 95

3.1 Binding and activation of small molecules by uranium complexes **95**

3.1.1 Dinitrogen *95*

3.1.1.1 Features and applications of dinitrogen activation by uranium(III) complexes 95

3.1.1.2 Coordination of dinitrogen 97

3.1.1.3 Reductive activation of dinitrogen 98

3.1.2 Carbon monoxide *100*

3.1.2.1 Properties and applications of carbon monoxide 100

3.1.2.2 Carbonyl complexes 101

3.1.2.3 Insertion chemistry 103

3.1.2.4 Activation of CO 107
3.1.3 Carbon dioxide *110*
3.1.3.1 Properties and coordination of carbon dioxide 110
3.1.3.2 Insertion chemistry 111
3.1.3.3 Reduction of carbon dioxide by uranium complexes 115
3.1.3.4 Reductive disproportionation 116
3.1.3.5 Reductive coupling reactions 118
3.1.4 Scope for Chapter 3 ..... *119*

3.2 Activation of carbon monoxide **120**
*3.2.1 Reactivity of [U(COT$^{(SiiPr3)2}$)(Cp^{tBu})] (**2.1**) with carbon monoxide* *120*
*3.2.2 Alternative synthesis of [{U(COT$^{(SiiPr3)2}$)(Cp^{tBu})}$_2$(μ-O)] (**3.1**)* *121*

3.3 Activation of carbon dioxide **124**
*3.3.1 Synthesis and characterisation of uranium(IV) oxo complexes (**3.2** and **3.3**)* *124*
*3.3.2 Synthesis and characterisation of [{U(COT$^{(SiiPr3)2}$)(Cp^{tBu})}$_2$(μ-η^1:η^2-CO$_3$)] (**3.4**)* *125*
*3.3.3 Cyclic voltammetry of [{U(COT$^{(SiiPr3)2}$)(Cp^{tBu})}$_2$(μ-η^1:η^2-CO$_3$)] (**3.4**)* *129*
3.3.4 Extraction of the carbonate fragment *130*
*3.3.5 Alternative synthesis of [U(COT$^{(SiiPr3)2}$)(Cp^{tBu})Cl] (**3.5**)* *132*
*3.3.6 Cyclic voltammetry of [U(COT$^{(SiiPr3)2}$)(Cp^{tBu})Cl] (**3.5**)* *134*
*3.3.7 Regeneration of **2.1** by reduction of [U(COT$^{(SiiPr3)2}$)(Cp^{tBu})Cl]* *135*

3.4 Summary **135**

3.5 Experimental details for Chapter 3 ..... **136**

3.6 References **139**

CHAPTER 4: ACTIVATION OF SMALL MOLECULES BY HETEROCYCLIC MIXED-SANDWICH COMPLEXES **146**

4.1 Introduction **146**

4.2 Activation of carbon monoxide **147**
4.2.1 Reactivity of [U(COT$^{(SiiPr3)2}$)(Cp^{PMe4})] with carbon monoxide *147*
4.2.1.1 Characterisation of [U(COT$^{(SiiPr3)2}$)(Cp^{PMe4})(2-O-PC$_5$Me$_4$)] (**4.1**) 149
4.2.1.2. Infrared studies of the reaction of [U(COT$^{(SiiPr3)2}$)(Cp^{PMe4})] with CO 151
4.2.1.3 Characterisation of [bis(2,3,4,5-tetramethylphospholyl)acetylene] (**4.2**) 153
4.2.1.4 Synthesis of [{U(COT$^{(SiiPr3)2}$)}$_2$(μ-O)(μ-η^1:η^1-O$_2$SOCF$_3$)$_2$] (**4.3**) 156
4.2.1.5 Molecular structure of [{U(COT$^{(SiiPr3)2}$)}$_2$(μ-O)(μ:η^1:η^1-O$_2$SOCF$_3$)$_2$] (**4.3**) 157
4.2.2. Reactivity of [U(COT$^{(SiiPr3)2}$)(Cp^{AsMe4})] with carbon monoxide *158*
4.2.2.1 Characterisation of [2,2'-bis(3,4,5,6-tetramethylarsenine)] (**4.5**) 160
4.2.3. Reactivity of [U(COT$^{(SiiPr3)2}$)(Cp^{PMe4})(THF)] with isonitriles *161*
4.2.3.1 Molecular structure of [U(COT$^{(SiiPr3)2}$)(Cp^{PMe4})(CN^{t}Bu)] (**4.6**) 162

4.3 Activation of carbon dioxide 163

4.3.1 Reactivity of [U(COT$^{(SiiPr3)2}$)(Cp^{NMe4})] with carbon dioxide 164

4.3.1.1 Characterisation of **4.8** 165

4.3.2 Reactivity of [U(COT$^{(SiiPr3)2}$)(Cp^{NMe4})] with nitrous oxide 169

4.3.2.1 Reactivity of **4.9** with carbon dioxide 171

4.3.3 Reactivity of [U(COT$^{(SiiPr3)2}$)(Cp^{PMe4})] with carbon dioxide 172

4.3.3.1 Characterisation of **4.11** 174

4.3.4 Reactivity of [U(COT$^{(SiiPr3)2}$)(Cp^{PMe4})] with nitrous oxide 176

4.3.2.1 Characterisation of [{(COT$^{(SiiPr3)2}$)U}$_2$(μ-O)$_2$] (**4.12**) 177

4.3.2.1 Characterisation of [1,1'-bis(2,3,4,5-tetramethylphosphole)] (**4.13**) 180

*4.3.4 Reactivity of **4.12** and **4.13** with carbon dioxide 180*

4.3.5 Reactivity of [U(COT$^{(SiiPr3)2}$)(Cp^{AsMe4})] with carbon dioxide 181

4.3.6 Removal of the phosphacarbonate moiety 182

4.3.6.1 Characterisation of **4.16** and **4.17** 184

4.4 Alternative heteroallenes 187

4.4.1 Introduction 187

4.4.2 Reactivity of [U(COT$^{(SiiPr3)2}$)(Cp^{PMe4})(THF)] with carbonyl sulfide 189

4.4.2.1 Characterisation of [{U(COT$^{(SiiPr3)2}$)(Cp^{PMe4})}$_2$(μ-S)] 191

4.4.3 Reactivity of [{U(COT$^{(SiiPr3)2}$)(Cp^{PMe4})}$_2$(μ-S)] with carbon dioxide 193

4.4.3.1 Characterisation of **4.19** 195

4.4.3.2 Characterisation of **4.20** 196

4.4.4 Carbon disulfide reactivity 199

4.4.4.1 Reactivity of [U(COT$^{(SiiPr3)2}$)(Cp^{PMe4})] with CS_2 199

4.4.4.2 Reactivity of **4.12** and **4.13** with CS_2 199

4.5 Summary 200

4.6 Experimental details for Chapter 4 200

4.7 References 216

CHAPTER 5: STERIC EFFECTS OF THE FIVE-MEMBERED RING 221

5.1 Introduction 221

5.2 Calculating the steric parameters 230

5.3 Steric effects on molecular structures 231

5.4 Steric effects on reactivity 235

5.5 Summary 241

5.6 Computational details for Chapter 5 242

5.7 References **242**

CHAPTER 6: STUDIES TOWARDS A URANIUM(II) METALLOCENE **246**

6.1 Introduction **246**

6.2 Synthesis of bis(cyclopentadienyl)uranium(III) iodides **247**

*6.2.1 Synthesis and characterisation of [{U(Cp^{tBu2})$_2$}$_2$(μ-I)$_2$] (**6.1**)* *247*

*6.2.2 Synthesis and characterisation of [{U(Cp$^{(SiiPr3)2}$)$_2$}$_2$(μ-I)$_2$] (**6.2**)* *249*

6.2.2.1 Molecular structure of [{U(Cp$^{(SiiPr3)2}$)$_2$}$_2$(μ-I)$_2$] (**6.2**). 250

6.2.2.2 Molecular structures of [UI(Cp$^{(SiiPr3)2}$)$_2$(THF)] and [U(Cp$^{(SiiPr3)2}$)$_2$I$_2$K(DME)$_2$] 252

*6.2.3 Cyclic voltammetry of [{U(Cp^{tBu2})$_2$}$_2$(μ-I)$_2$] (**6.1**) and [UI(Cp$^{(SiiPr3)2}$)$_2$(THF)]$_2$ (**6.2THF**)* *253*

6.2.4 Calculating the G-parameter for bis(cyclopentadienyl)uranium(III) iodides *255*

6.3 Reactivity of [{U(Cp^{R})$_2$}$_2$(μ-I)$_2$] with reducing agents **257**

*6.3.1 Attempted reduction of [{U(Cp$^{(SiiPr3)2}$)$_2$}$_2$(μ-I)$_2$] (**6.2**)* *257*

*6.3.2 Reactivity of [{U(Cp^{tBu2})$_2$}$_2$(μ-I)$_2$] (**6.1**) with potassium graphite* *257*

6.3.1.1 Characterisation of [U(Cp^{tBu2})$_3$] (**6.3**) 258

6.3.3 Reactivity of [{U(Cp^{R})$_2$}$_2$(μ-I)$_2$] with potassium graphite in the presence of a Lewis acid *260*

6.3.3.1 Characterisation of [{U(Cp^{tBu2})$_2$}$_2$(μ-BH$_x$)$_2$] (**6.4**) 261

6.4 Synthesis of a uranium tetraphenylborate complex **263**

6.4.1 Reactivity of [{U(Cp^{R})$_2$}$_2$(μ-I)$_2$] with potassium benzyl and [NEt$_3$H][BPh$_4$] *263*

6.4.1.1 Characterisation of [(Cp$^{(SiiPr3)2}$)U(μ-Ph)$_2$BPh$_2$] 265

6.5 Summary **268**

6.6 Experimental details for Chapter 6 ..... **268**

6.7 References **273**

APPENDIX I: GENERAL EXPERIMENTAL DETAILS **276**

APPENDIX II: DATA AND ERROR ANALYSIS OF THE G-PARAMETERS GENERATED BY SOLID-G **283**

APPENDIX III: DATA AND ERROR ANALYSIS FOR THE CALCULATION OF THE EQUILIBRIUM CONSTANT FOR [U(COT$^{(SIIPR3)2}$)(CP^{NME4})] **298**

APPENDIX IV ..... **CD ATTACHED**

Anything that can go wrong, will.

Finagle's Law of Dynamic Negatives

CHAPTER 1: INTRODUCTION TO ORGANOURANIUM CHEMISTRY

1.1 Introduction

The defining feature of organometallic chemistry is the bonding between carbon-based ligands and metals. One of the dominant classes of ligand in the literature is the aromatic carbocycle, which significantly features the five-membered cyclopentadienyl ligand. The review below briefly introduces the properties of uranium and outlines some of the most significant, and the most unusual, uranium complexes synthesised that incorporate one or more aromatic ligands.

1.2 Properties of the f-Block elements

Despite the early progress of organometallic chemistry of the transition metals in the 1800s, analogous f-block chemistry did not begin until over a century later.[1] Earliest reports of lanthanide, thorium and uranium organometallic complexes appeared in the literature in the mid 1900s, but keen interest in this area did not develop until the discovery of uranocene.[2] The late development of organolanthanide and actinide chemistry can be attributed to the sensitivity of most of these species towards air and moisture, and for some elements, the levels of radioactivity.

Lanthanide and actinide elements have a fourth angular momentum quantum number, and therefore have s, p, d and f-orbitals, which can accommodate 32 electrons.[3] The lanthanides have contracted, core-like 4f-orbitals, which are lower in energy than the 5d-orbitals. As a consequence electrons fill the f-orbitals prior to the d-orbitals giving rise to a series of elements which are chemically very similar. Exceptions are however found for lanthanum and cerium, whose 5d subshell is lower in energy than the 4f; and

gadolinium and lutetium, where addition of an electron to the 5d orbitals maintains the favoured half-filled and filled 4f-subshell.

The electronic configuration of the lanthanides can be observed by the ionisation energies, which illustrate the +3 oxidation state is most favoured.[4] Despite this, many divalent lanthanide complexes have been reported, as modification of the ligand environment has given rise to stable complexes in this oxidation state.[5,6] Ln^{3+} ions are Lewis-acidic, and form complexes that are predominantly ionic in character.

The 5f-orbitals have a radial node, and therefore exhibit greater extension than the 4f-orbitals. In addition, relativistic effects for the actinides give rise to contraction of the s and p orbitals, but expansion and destabilisation of the d and f orbitals. Consequently, the early actinide 5f-orbitals have greater availability for covalent bonding and access to multiple oxidation states. For the later actinides however, ineffective shielding gives rise to contraction of the f-orbitals and lanthanide-like properties. Behaviour comparable to transition metals is therefore only seen in the early actinides up to neptunium, however the higher levels of radioactivity for most actinide elements render thorium and uranium the only actinides that have been extensively studied in organometallic chemistry. Thorium is most commonly found in the +4 oxidation state, which has a [Rn] electronic configuration. Reduction to thorium(III) is non-trivial and only a few examples have been synthesised to date.[7–11] As such the organometallic chemistry of thorium has attracted less interest and organoactinide chemistry is dominated by uranium.

Uranium exhibits properties that are individual to the early actinide elements, which gives rise to a combination of transition metal- and lanthanide-like behaviour. As the heaviest naturally occurring element, uranium has a large coordination sphere which allows the coordination of more and/or larger ligands than transition metals.[4] However, the participation of the f-orbitals gives rise to additional bonding interactions and therefore the coordination geometries of the ligands are not constrained by overlap with

the d-orbitals. In comparison to the lanthanides, uranium-ligand bonding has more covalent character and the positioning of the ligands around the metal centre is therefore not solely dependent on electrostatic interactions and packing.

Another feature of uranium is its oxophilicity, which renders organometallic complexes highly reactive towards oxygen and water. As a result, the chemistry of the uranyl ($[O=U=O]^{2+}$) species is well developed, as this dication is stable in aqueous media.[4] The stability of the uranyl fragment derives from relativistic effects, as the similar energies of the 5f, 6p, 6d and 7s orbitals mean they all contribute to the very short, strong U=O bonds. Like the lanthanides, uranium is Lewis acidic and coordinates with Lewis bases if there is space within the coordination sphere.

Of the five oxidation states known, the +6 state is prevalent in uranyl chemistry and the +4 state is the most common in organometallic chemistry. Uranium(V) complexes have attracted increasing interest in recent years as their tendency to disproportionate has given rise to some interesting redox activity and the formation of novel uranium-element multiple bonds.[12] However one of the largest topics of interest, activation of small molecules, has focused predominantly on uranium(IV) and uranium(III) complexes.[13] The latter has become increasingly important in recent decades, as the formal electrode potential of the U^{IV}/U^{III} redox couple is of a similar magnitude to the M^{+}/M couple in the alkali metals.[14] The reactivity of such complexes will be discussed further in Chapter 3.

1.3 Aromatic ligands in organouranium Chemistry

1.3.1 Five-membered carbocycles

1.3.1.1 Properties of cyclopentadienyl ligands

Cyclopentadienyl ligands are anionic and derive their aromaticity from six electrons lying in a delocalised, cyclic π-system. The molecular orbitals can be split into a single set of a-symmetry orbitals, and two sets of doubly degenerate e-symmetry orbitals with one and two nodes respectively (**Figure 1.1**).[1] These orbitals are able to overlap with the 6d and 5f orbitals of uranium, and the small size of the Cp ligand in comparison to the large uranium centre gives rise to predominantly σ- and π-interactions.

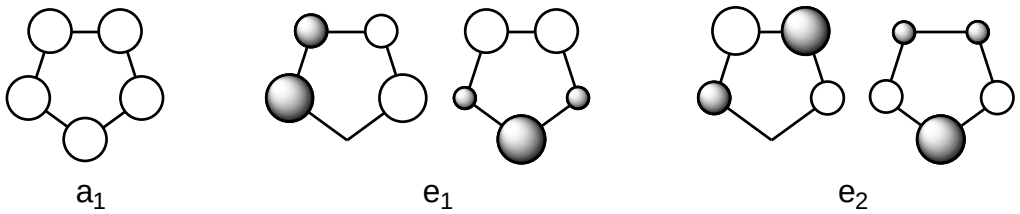

Figure 1.1 Molecular orbital combinations for cyclopentadienyl ligands.[1]

The electron-donating properties of cyclopentadienyl ligands can be modified by the addition of substituents. This has the added effect of providing steric stabilisation to the complex, which is especially important with larger metals.

1.3.1.2 Tetrakis(cyclopentadienyl)uranium complexes

[UCp_4] was first synthesised by Fischer in 1962, and other analogous actinide complexes soon followed.[15] The molecular structure of the complex illustrates η^5-

bonding for each ligand, which gives rise to pseudo-tetrahedral geometry (**Figure 1.2**).[16,17] This assignment was supported by photoelectron spectroscopy, however the dipole moment of this complex is non-zero, indicating a lower molecular symmetry than T_d.[18–21] DFT studies found the preference of pentahapto bonding is accounted for by electron donation into an almost equal mix of 6d- and 5f-orbitals, and that the ligand π-interaction results in a stronger bond, thereby stabilising the metal complex.[22]

An NMR study of a substituted version of this complex, $[U(Cp^{-PPh2})_4]$, found this species is dynamic in solution, and illustrates that the sterics of the diphenylphosphino substituents do not prevent the formation of this complex or significantly affect its structure.[23] Furthermore, this complex was found to react with the molybdenum complex, $[Mo(CO)_4(C_7H_8)]$, to yield a bimetallic complex bridged by two of the Cp^{-PPh2} ligands (**Figure 1.2**).

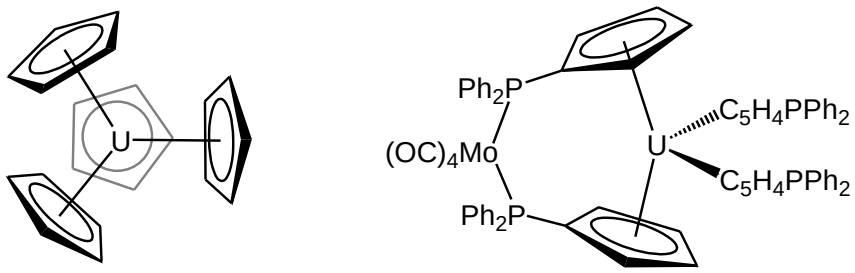

Figure 1.2 $[UCp_4]$ (left) and a molybdenum-uranium bimetallic complex with a $[U(Cp^{-PPh2})_4]$ unit (right).[15,23]

1.3.1.3 Tris(cyclopentadienyl)uranium complexes

The tris(cyclopentadienyl) motif has become prevalent in organouranium chemistry due to the steric stabilisation it imparts whilst accommodating substituents on the Cp^R rings and other ligands bound to the uranium centre. It is therefore unsurprising that this was the motif employed in the isolation of the first organometallic complex of uranium,

[Cp_3UCl], in 1956.[24] Since then, many [Cp_3UX] complexes have been synthesised, where X includes carbon, nitrogen, oxygen and halide based ligands and more unusual phosphido, azide and nitrosyl groups.[25–27]

DFT studies of [Cp_3UX] complexes illustrate pseudo-tetrahedral geometry, with a quasi-planar [UCp_3] arrangement.[22] The tris(cyclopentadienyl)uranium fragment exhibits similar bonding to [UCp_4], with additional stabilisation arising from the transfer of electron density from the a_2 ligand orbitals to the 5f-metal orbitals.[28] Studies of the U–X interaction reveal that when X is a hydride, the σ-bond has dominant 6d and weak 5f and 7s character.[22] When X is a chloride however, both σ- and π-interactions are observed with the latter being predominantly 6d in character and mainly localised on chlorine. It is also observed that the HOMOs of these complexes are lower in energy than [UCp_4], due to the decreased amount of ligand-to-metal donation when Cp is replaced by X. This was verified by electrochemical studies which found the potential of the U^{IV}/U^{III} reduction couple becomes less negative as the number of cyclopentadienyl ligands decreases.[29]

This motif has also been employed to stabilise other oxidation states. There are several examples of uranium(III) [$U(Cp^R)_3$] complexes, which can be synthesised *via* several routes.[30–35] These include reaction of a uranium trihalide with K[Cp^R], or by comproportionation of uranium metal with [UCp_4].[36] More interestingly, [$Cp_3U{\cdot}THF$] could be generated by photolytic cleavage of [Cp_3U-^{i}Pr] in THF.[37,38] This reaction proceeds *via* homolytic cleavage of the uranium–carbon bond, which contrasts to the β-hydride mechanism observed for the thorium analogue. The rationale for the different mechanisms is based on the An^{IV}/An^{III} reduction potentials for uranium and thorium. For [Cp_3UX] complexes, the U^{IV}/U^{III} reduction potential lies in the range of -1.6 to -2.6 V *vs* $[FeCp_2]^{+/0}$, whereas Th^{IV}/Th^{III} potentials are predicted to occur below -3.0 V.[29,39–42]

Tris(cyclopentadienyl)uranium(V) complexes were first reported over three decades ago, with the synthesis of the first uranium alkylidene and imido complexes (**Figure**

1.3).[43–47] These complexes paved the way for the synthesis of other uranium(V) complexes and illustrated interesting reactivity, including comproportionation in the presence of [U(Cp^{Me})$_3$(THF)] to give a dimeric complex with two imido bridges.[48]

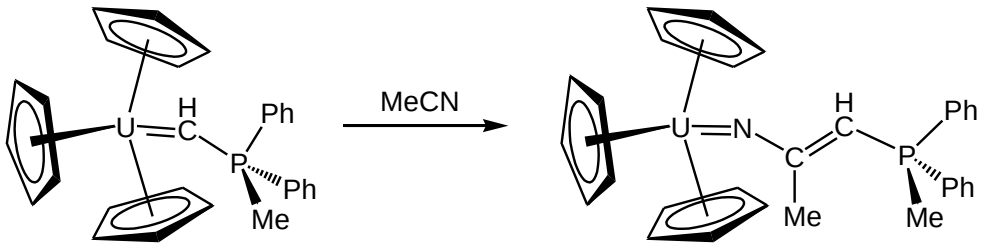

Figure 1.3 The first uranium alkylidene complex and synthesis of the resulting imido complex.[44,45]

Ionic complexes incorporating the tris(cyclopentadienyl)uranium fragment have been synthesised in several oxidation states. Reaction of uranium(IV) alkyl complexes with lithium alkyl reagents gave rise to concurrent reduction and alkylation to give uranium(III) Li[Cp_3UR] complexes.[49–51] An unusual hydrido-bridged uranium(III) complex was also synthesised by reaction of [(Cp^{SiMe3})$_3$U] with sodium hydride or by reaction of [(Cp^{SiMe3})$_3$UCl] with sodium hydride in the presence of sodium amalgam (**Figure 1.4**).[52,53]

Arguably one of the most notable ionic complexes of uranium is that of [K(crypt)][U(Cp^{SiMe3})$_3$], which was reported by Evans *et al.* in 2013 (**Figure 1.4**).[54] This formally uranium(II) complex was synthesised by reduction of the neutral uranium(III) complex in the presence of a cryptand ligand, and was verified as a uranium(II) species by comparison of electronic absorption spectra of this complex with an independently synthesised uranium(III) hydride anion. DFT studies of this complex

indicate a $5f^3 6d^1$ electronic configuration for the ground state, with predominantly $6d^1$ character for the HOMO that resembles a dz^2 orbital.

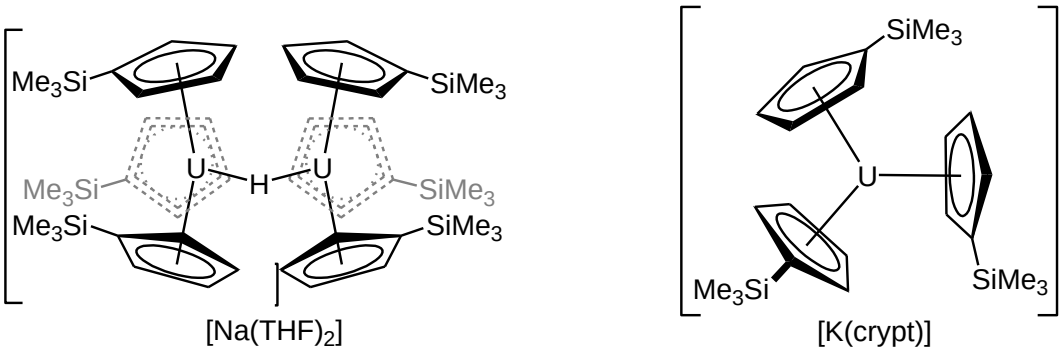

Figure 1.4 The anionic hydrido-bridged complex (left) and the uranium(II) anion (right).[52–54]

Cationic complexes of tris(cyclopentadienyl)uranium have also been synthesised, which have a metal-based counter ion. The first well-defined example of an organouranium cation was reported in 1983, when $[Cp_3UCl]$ reacted with traces of oxygen to give $[Cp_3U(NCMe)_2]_2[UO_2Cl_4]$ (**Figure 1.5**).[55] Uranium-metal bonds have also been synthesised using this motif. DFT studies of $[(Cp^R)_3U\text{-}Al(Cp^*)]$ indicate a covalent interaction between the two metals arising from charge transfer from the AlCp* unit onto uranium (**Figure 1.5**).[56] However, studies of the gallium analogue have shown predominantly ionic bonding which is composed of σ-type donation from the GaCp* unit to uranium.[57]

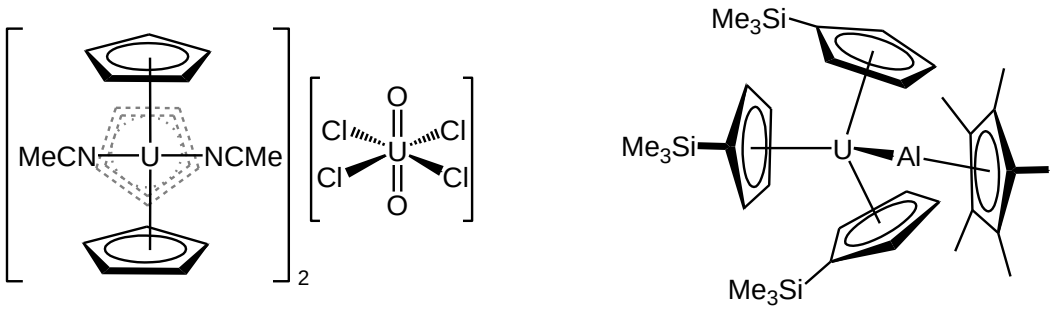

Figure 1.5 Two multimetallic complexes synthesised from $[(Cp^{R})_3UCl]$.[55,56]

1.3.1.4 Bis(cyclopentadienyl)uranium complexes

Bis(cyclopentadienyl)uranium(IV) complexes feature heavily in the literature and have been used to synthesise many novel fragments. Complexes with uranium(IV) centres typically feature two other supporting ligands, although some examples of dianionic ligand coordination have been reported. This is the case for two tri-*tert*-butylcyclopentadienyl (Cp^{tBu3}) complexes supporting oxo and imido fragments, $[(Cp^{tBu3})_2UO]$ and $[(Cp^{tBu3})_2UNMe]$ (**Figure 1.6**).[58,59] Reactivity and DFT studies of these complexes indicate uranium–nitrogen double bond character for the imido complex, but a stronger, polarised U^{+}–O^{-} bond for the oxo complex.[60] A uranium–sulfur double bond was also synthesised by cleavage of a thiolate ligand during the reduction of $[(Cp^*)_2U(S^tBu)_2]$ (**Figure 1.6**).[61]

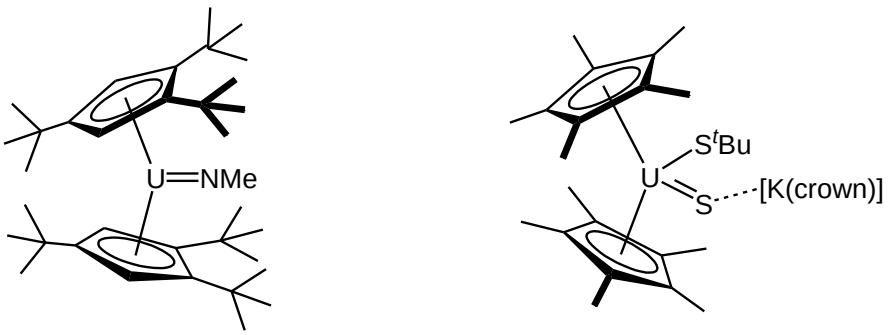

Figure 1.6 Uranium(IV) complexes featuring U=E bonds.[59,61]

Uranium(V) and uranium(VI) complexes featuring the $[(Cp^R)_2U]$ moiety have also been synthesised. The uranium(III) species, $[(Cp^*)_2UCl][NaCl]$, was found to reductively cleave azo or azido N=N bonds to give a uranium(VI) bis(imido) complex.[62] This species has been incorporated into a catalytic cycle, as reduction by dihydrogen forms two amide units, which can be replaced by further additions of azide (**Figure 1.7**).[63]

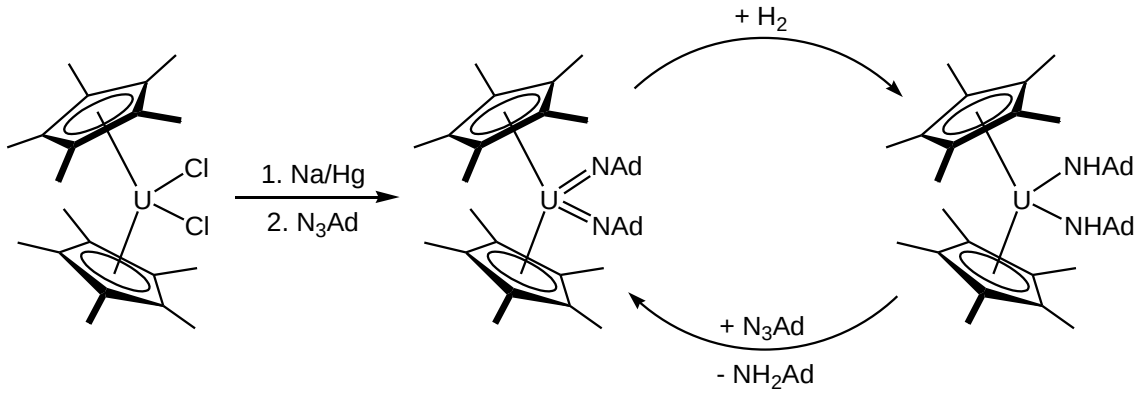

Figure 1.7 Synthesis of a uranium(VI) bis(imido) complex and the catalytic reduction of an imido moiety.[63]

Alternative complexes that mimic the $[(Cp^R)_2U]$ motif are uranium *ansa*-metallocenes. The first examples of such complexes were reported in 1976 by Marks, who synthesised a series of $[H_2C(Cp)_2U_2Cl_5][Li(THF)_2]$ complexes.[64] This was furthered in 1999 by Burns *et al.*, who synthesised analogous complexes using the preferred dimethylsilyl-bridged permethylated ligand (**Figure 1.8**).[65] The series has also been extended to include an ethyl-linked *ansa*-metallocene with a pendant pyridyl ring on each cyclopentadienyl ring, which also coordinates to the uranium centre (**Figure 1.8**).[66]

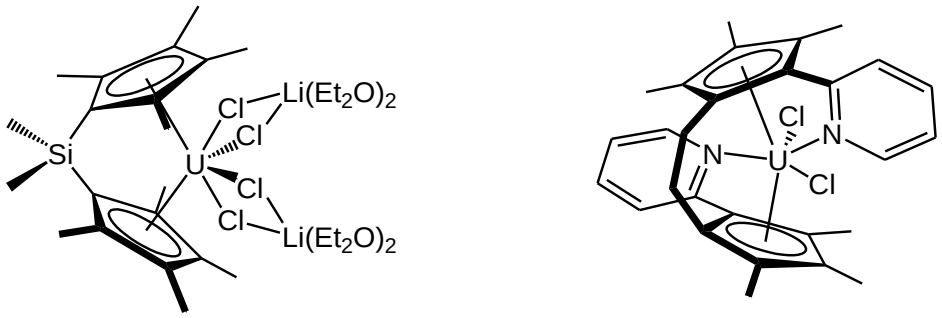

Figure 1.8 Examples of *ansa*-metallocenes.[64–66]

Although the bent bis(cyclopentadienyl)uranium configuration is preferred, linear ionic complexes have also been synthesised. These complexes feature five acetonitrile or cyanide molecules in a pentagonal planar arrangement around the equatorial axis of the molecule, whilst the two Cp* ligands occupy the axial positions (**Figure 1.9**).[67–69] DFT studies of the linear $[U(Cp^*)_2]$ fragment show these complexes have five 5f and two 6d non-bonding orbitals, of which five are in the equatorial plane.[70] These orbitals accept electrons from the cyanide or acetonitrile ligands whilst the remaining unpaired electrons occupy the out-of-plane non-bonding orbitals and one antibonding orbital.

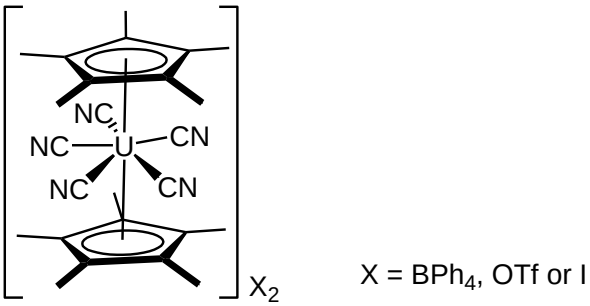

Figure 1.9 A linear $[U(Cp^*)_2(CN)_5]^{2+}$ complex.[69]

1.3.1.5 Electrochemical studies of bis(cyclopentadienyl)uranium complexes

Cyclic voltammetry has become a popular method for assessing the thermodynamic stability of complexes by measure of redox couples, as the change in Gibb's free energy is related to the electrode potential according to **Equation 1.1**.

$$\Delta G = -nFE$$

Equation 1.1 The change in Gibb's free energy as a function of electrode potential, where n is the number of electrons and F is the Faraday constant (9.65 x 10^4 $C \cdot mol^{-1}$).

Studies comparing families of complexes have therefore become especially prevalent, as this method ascertains the effect on ΔG of altering the electronic properties of the complexes.

$[(Cp^R)_2UX_2]$ complexes have been studied extensively using this method. Comparative studies of $[(Cp^*)_2UX_2]$ and $[Cp_3UX]$ complexes found a trend of electron donating ability by X ligands, whereby alkoxide ligands are more electron donating than alkyl and amide ligands, and halide ligands donate the least electron density.[41,42,71] Further studies investigating the effect of varying halides on $[(Cp^*)_2U\{N(SiMe_3)_2\}X]$ and $[(Cp^*)_2U(=NAr)X]$ complexes found that both the U^{IV}/U^{III} and U^{V}/U^{IV} reduction potentials become less negative descending the halogen group.[72,73]

Similar studies of $[(Cp^*)_2An(L)(L')]$ complexes have shown than when L and L' are σ-donors, a reversible metal-based process occurs between -1.8 and -2.9 V *vs* $[FeCp_2]^{+/0}$ corresponding to the U^{IV}/U^{III} redox process.[74–77] However, when one of the ligands can interact in both σ and π-modes due to a nitrogen lone pair and/or π-orbitals on the ligand, a second reversible wave is observed between -0.7 and +0.2 V *vs* $[FeCp_2]^{+/0}$. This corresponds to the U^{V}/U^{IV} redox process and further stabilisation of the higher

oxidation states can be observed in the formation of imide complexes, whereby the U^{V}/U^{IV} process is observed at -1.64 V *vs* $[FeCp_2]^{+/0}$, and the U^{VI}/U^{V} process is observed at -0.10 V (**Figure 1.10**).[78]

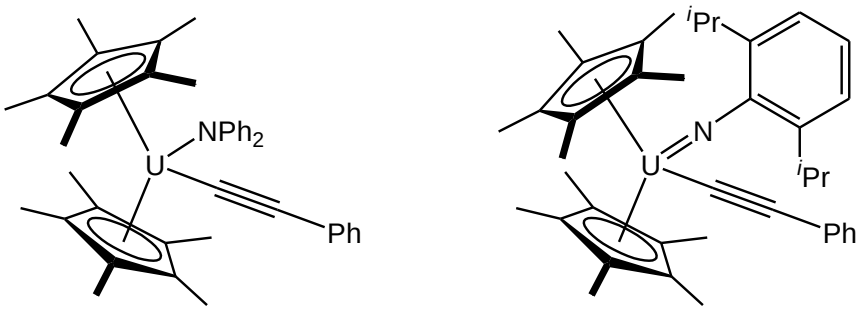

U^{IV}/U^{III} = -2.25 V
U^{V}/U^{IV} = -0.07 V

U^{V}/U^{IV} = -1.64 V
U^{VI}/U^{V} = -0.10 V

Figure 1.10 The observed redox potentials *vs* $[FeCp_2]^{+/0}$ for a uranium(IV) amide complex (left) and uranium(V) imide complex (right). [78]

The uranium(III) oxidation state can also be stabilised with use of appropriate ligands. Trimetallic actinide complexes containing either three uranium or two uranium and one thorium centre have been prepared alongside a monometallic uranium(IV) complex featuring tripyridine-based (tpy) bridging ligands.[79] These studies showed the U^{IV}/U^{III} potential to be appreciably less negative (-0.48 to -0.98 V *vs* $[FeCp_2]^{+/0}$) in comparison to other couples reported in the literature, which was attributed to U–tpy π-backbonding. These studies also illustrated covalent interactions between the metal 5f and 6d orbitals and the ligands, and DFT illustrates anti-ferromagnetic coupling between the metal centres which arises from effective π-overlap between the 5f orbitals and the nitrogen atoms.[80–82]

1.3.1.6 Mono(cyclopentadienyl)uranium complexes

In comparison to the number of bis- and tris(cyclopentadienyl)uranium complexes reported, there are few mono(cyclopentadienyl) species. The majority of these complexes, such as [CpU(BH_4)$_3$] and substituted variants, are synthesised as precursors to other complexes.[83–85] [Cp*UI_2(THF)$_3$] and [Cp*UI_2(py)$_3$] have also been synthesised and were found to be useful precursors to amide complexes as illustrated by their reactivity with K[N($SiMe_3$)$_2$] to yield [Cp*U(N{$SiMe_3$}$_2$)$_2$] (**Figure 1.11**).[86]

One of the reasons for employing a five-membered carbocycle is to impart the required steric and electronic properties that would not be achieved in a complex bearing non-carbocyclic ligands. For example, the synthesis of the first cyclopentadienyl complex of an uranyl fragment, whereby the Cp* ring forces the uranyl unit to adopt an unprecedented non-linear geometry (**Figure 1.11**).[87] It is anticipated that such fragments could lead to the development of a series of soluble uranium oxides, and have the potential to coordinate a second metal centre through the cyanide ligands.

Some cyclopentadienyl ligands also have coordinating substituents in order to enforce particular steric and electronic properties on a complex. One example, reported by Marks *et al.* in 2003, employs a Cp^R ring with an amide pendant in intramolecular catalytic hydroamination chemistry (**Figure 1.11**).[88–90] This species exhibits enhanced reactivity over [(Cp*)$_2$UMe_2] and the *ansa*-metallocene [(Me_2Si(Cp^{Me4})$_2$UMe_2], due to the open steric environment this ligand provides, without compromising the stability of the complex. The mechanism for hydroamination is proposed to proceed *via* C=C/C≡C insertion into a uranium-amide σ-bond, as this route is more kinetically viable than formation of an imido intermediate.

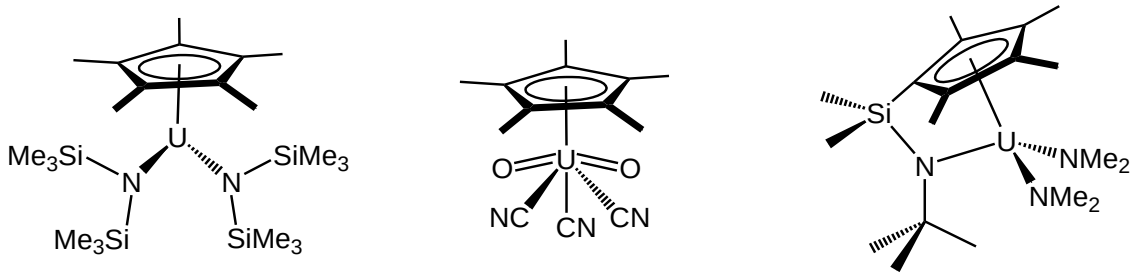

Figure 1.11 Examples of mono(cyclopentadienyl)uranium complexes.[86–88]

1.3.2 Five-membered heterocycles

1.3.2.1 Properties of heterocyclic ligands

Heterocyclic five-membered rings in which a carbon atom is replaced by a pnictogen exhibit some degree of aromaticity due to partial lone pair delocalisation with the diene unit.[91] However deprotonation of the ring to form the anion gives rise to a fully aromatic system with 6π electrons, in addition to the lone pair.[92] The lone pair is approximately perpendicular to the delocalised π-system and exhibits nucleophilic behaviour.

Incorporation of a heteroatom has a significant effect on the electronic properties of the heterocycle. This is rationalised by the electronegativities of the atoms, which for phosphorus and arsenic are 2.2, carbon is 2.5 and nitrogen is 3.0, according to the Pauling scale.[1] Therefore incorporation of nitrogen into the ring gives rise to partial localisation of the electron density on nitrogen, however the σ-donor/π-acceptor properties of phosphorus make phospholyl rings apolar and a suitable substitute for the cyclopentadienyl ligand.

A further effect of introducing a heteroatom is that the degeneracy of the e_1 and e_2 orbitals is broken. If the heteroatom is more electronegative than carbon, the orbitals with a coefficient on the heteroatom are lowered with respect to the cyclopentadienyl analogue and all other orbitals remain the same energy (**Figure 1.12**).[93–95] The opposite

is true however when the heteroatom is less electronegative than carbon, however the similar electronegativity values for carbon, phosphorus and arsenic give rise to smaller energy differences between the orbitals of the phospholide and arsolide anions than is observed for the pyrrolide. The consequences of removal of degeneracy have been observed in transition metal sandwich complexes, whereby redox potentials are anodically shifted (E values are more positive) relative to their Cp^R counterparts due to the smaller energy gap between the HOMO and the LUMO.

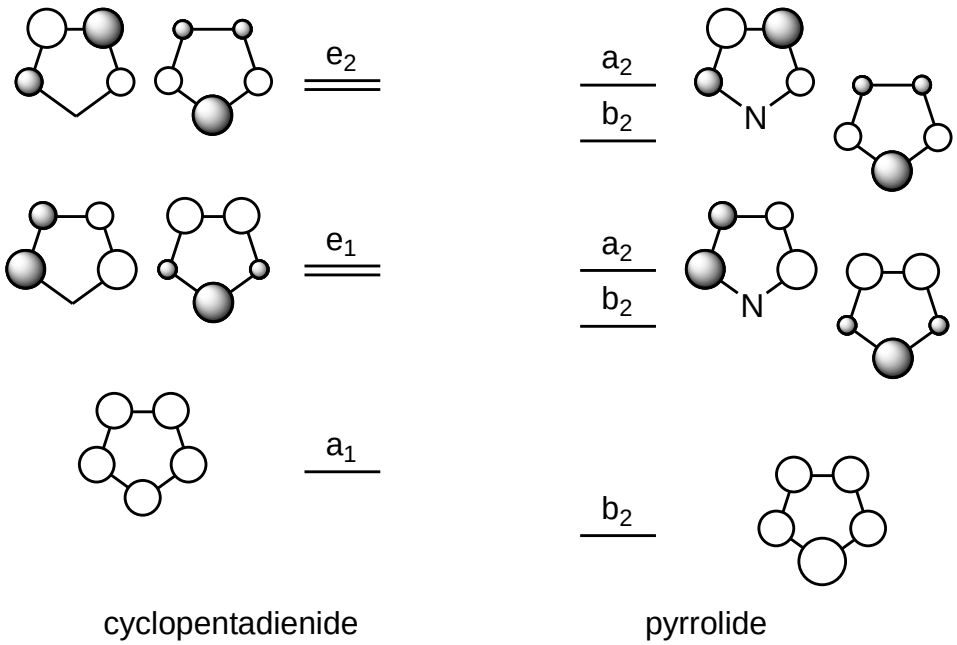

Figure 1.12 Splitting of the e_1 and e_2 orbitals in the pyrrolide anion as reported by Janiak *et al.*.[93] Energy levels are not drawn to scale.

1.3.2.2 Uranium heterocyclic complexes

In comparison to the wealth of research which details organoactinide complexes supported by Cp^R ligands, few reports have discussed complexes bearing heterocyclic

derivatives. Of these complexes the majority incorporate tetramethylphospholyl (Cp^{PMe4}) ligands as this moiety can be considered analogous with Cp*.

In 2008, Cloke *et al.* published the synthesis of tris(1,3-di-*tert*-butyl-1,2,4-triphospholyl)uranium, which to date is the only example of a homoleptic uranium complex employing heterocyclic ligands (**Figure 1.13**).[96] This complex features two η^5-bound phospholyl rings and one η^2-bound phospholyl ring, which reduces the steric crowding around the uranium centre.

Mixed-coordination modes have also been observed for uranium(IV) borohydride complexes. Ephritikhine observed that reduction of $[(Cp^{PMe4})_2U(BH_4)_2]$ gives rise to loss of one $[BH_4]^-$ ion and dimerisation of the complex *via* the phospholyl ring (**Figure 1.13**).[97–99] Coordination in this manner has been shown to retain the aromaticity of the phospholyl ring and, in the case of these particular complexes, is not shown to impart any steric constraints on the metrics within the molecular structure. It was also observed that η^1-coordination of the phosphorus lone pair to the second uranium centre is out of plane with the phospholyl ring, illustrating that the lone pair is not involved in the aromaticity of this ligand, and that the phospholyl rings coordinate in order to place the phosphorus atoms centrally between the two metal centres.

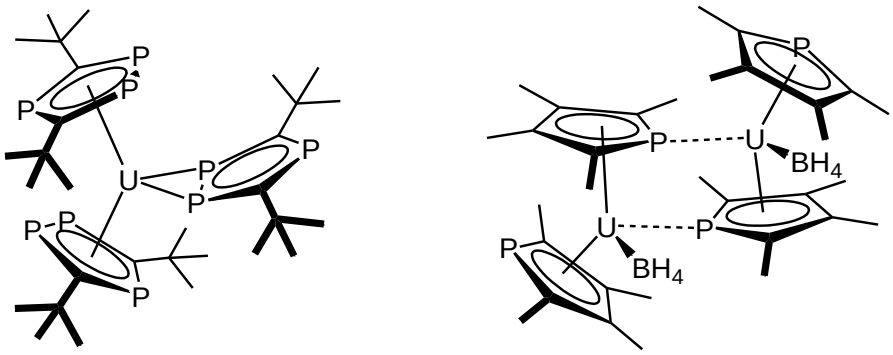

Figure 1.13 A homoleptic uranium complex featuring triphospholyl ligands (left) and a uranium borohydride dimer featuring bridging phospholyl ligands (right).[96,99]

Mixed-metal complexes have also been synthesised by exploiting the η^1:η^5-coordination modes of the tetramethylphospholyl ligand. In 1996 the syntheses of the trimetallic complex, $[Cl_2U(\mu\text{-}\eta^5\text{:}\eta^1\text{-}Cp^{PMe4})_2Ni(\mu\text{-}\eta^5\text{:}\eta^1\text{-}Cp^{PMe4})_2UCl_2]$, and the bimetallic complex, $[Cl_2U(\mu\text{-}\eta^5\text{:}\eta^1\text{-}Cp^{PMe4})_2RuH_2(PPh_3)_2]$, were reported (**Figure 1.14**). These complexes demonstrate that in uranium-transition metal complexes the phospholyl ring bonds exclusively to the uranium atoms *via* the aromatic ring and exclusively to the transition metal *via* the phosphorus lone pair.[100–102] The formation of a Ru···H···U bridge in the latter complex is proposed to arise from a lack of electron-density on the metal centre, which is not observed for the analogous borohydride complex, $[(BH_4)_2U(\mu\text{-}\eta^5\text{:}\eta^1\text{-}Cp^{PMe4})_2RuH_2(PPh_3)_2]$ as $[BH_4]^-$ is more electron donating than Cl^-.

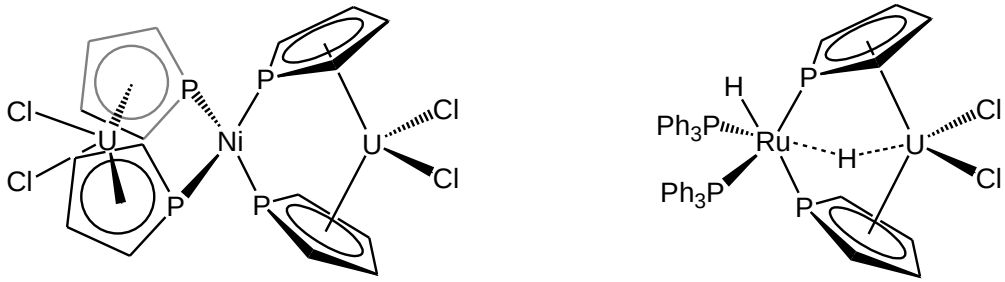

Figure 1.14 Mixed-metal complexes featuring η^5:η^1-coordinated phospholyl ligands. Methyl groups on the phospholyl rings have been omitted for clarity.

In a similar manner to the synthesis and studies of $[(Cp^R)_nUX_{(4-n)}]$ complexes, a range of uranium phospholyl complexes have been studied. Comparison of Cp* and Cp^{PMe4} complexes of $[(Cp^R)_nUCl_{(4-n)}]$ illustrate that Cp* donates more electron density to uranium than the phospholyl analogue, which makes coordinated THF more labile and stabilises sterically unsaturated complexes.[103] NMR studies of $[(Cp^R)_nU(BH_4)_{(4-n)}]$ complexes also found a correlation between electron density at the uranium(IV) centre

and chemical shift, whereby the ^{11}B resonance shifts downfield as the number of Cp^R rings increases and as the rings become more electron donating.[104]

Ephritikhine, Durand and colleagues studied bis- and tris(cyclopentadienyl)uranium(IV) halide and borohydride complexes by cyclic voltammetry and DFT and found a good correlation between the calculated electron affinities and the measured half-wave potentials.[39,40,105] Variation of Cp^R illustrated that increasing the number of electron-donating substituents resulted in an increasingly negative U^{IV}/U^{III} redox couple. In the case of Cp^{PMe4} however, it was found that the inductive effects from the methyl substituents are counteracted by the phosphorus atom, so that overall this ligand donates less electron density to the uranium centre than the unsubstituted cyclopentadienyl ligand. When the $E_{½}$ values are compared for $[(Cp^R)_2U(BH_4)_2]$ and $[(Cp^R)_3UCl]$ complexes, it was found that the phospholyl complexes have redox values that are more than 0.2 V less negative than Cp, illustrating the additional stabilisation of the +3 oxidation state relative to the +4 state.

The different electronic properties of phospholyl ligands in comparison to cyclopentadienyl ligands have led to the synthesis of some synthetically challenging fragments. $[(Cp^{PMe4})_3UCl]$ for example, can be synthesised in high yield and can undergo further reactivity to form hydride, alkyl and alkoxide complexes.[106] Synthesis of $[(Cp^*)_3UCl]$ however, was not achieved until eight years later.[107] Conversely, synthesis of $[(Cp^{PMe4})_2UCl_2]$ proved challenging and it could only be isolated in low yields.[106]

Despite the use of the phospholyl ligands as Cp^R alternatives, only two examples of simple uranium pyrrolyl ligands have been reported. In comparison to the phospholyl ligand, pyrrolyl complexes prefer to adopt the η^1-coordination mode, and can rapidly interconvert between η^5- and η^1-modes. However, Boncella and co-workers found increasing the sterics of the pyrrolyl ligand gives rise to η^5-coordination, presumably because the uranium centre no longer has access to the sterically protected lone pair.[108]

Pseudo-η^3-coordination of tetramethylpyrrolyl (Cp^{NMe4}) was also observed by Evans *et al.*, who found [$(Cp^*)_2U(Cp^{NMe4})$] exhibited coordination of the pyrrolyl ligand *via* the nitrogen lone pair, the α-ring carbon and its methyl group.[109]

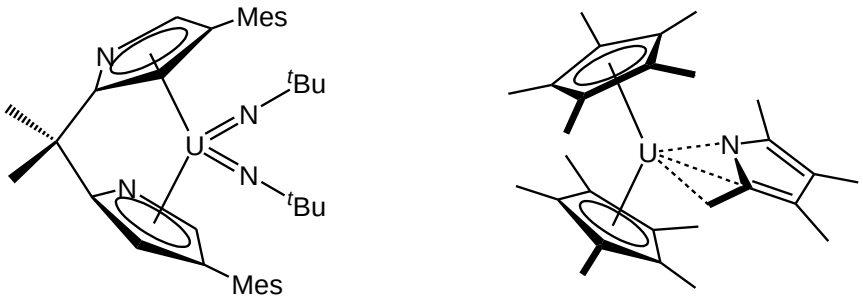

Figure 1.15 η^5-coordination of pyrrolyl ligands with bulky substituents (left) and η^3-coordination of Cp^{NMe4} in [$(Cp^*)_2U(Cp^{NMe4})$] (right).[108,109]

1.3.3 Six-membered carbocycles

1.3.3.1 Properties of arene ligands

Arene rings are aromatic when neutral, and have one additional molecular orbital combination than the cyclopentadienyl ligand: a singularly degenerate combination that has three nodes.[1] As such the lower energy orbitals (a and e_1) tend to be involved in σ- and π-bonding, whilst δ-interactions arise from the e_2 orbitals. Despite the lack of charge on arene ligands, uranium complexes have illustrated that these molecules can accept electron density and acceptance of four electrons generates an alternative 10π aromatic system.[110]

Although there are examples of pyridine- and phosphinine-based ligands in organouranium chemistry, all examples involve η^1-coordination through the lone pair.[111–113] Therefore a discussion of these complexes will not be included.

1.3.3.2 Terminal arene uranium complexes

The earliest report of uranium arene complexes appeared in 1971 and featured the synthesis of $[(C_6H_6)U(AlCl_4)_3]$ from UCl_4 using Friedel-Crafts methodology.[114] XRD analysis of similar complexes, $[U_2(C_6Me_6)_2Cl_7][AlCl_4]$ and $[(C_6Me_6)U(AlCl_4)_3]$, illustrates η^6-coordination of the arene ring, however, a model of the bonding in these complexes was not conducted.[115,116] Other variants of these complexes supported by borohydride ligands have since been published.[117,118]

With exception of the aforementioned tetrachloroaluminate and borohydride complexes, other terminal monoarene complex have supporting functional groups which bind to the uranium centre and bring the arene unit into bonding proximity of the metal.[119] Meyer has reported two such complexes: a tris(aryloxide) functionalised mesitylene ligand and a bis(diphenylmethyl)-substituted aryloxide ligand (**Figure 1.16**).[120,121] These complexes are supported by a neutral, η^6-bound arene ring, giving rise to uranium centres in the +3 oxidation state. DFT studies of these complexes illustrate the metal-arene bond is comprised of a δ-interaction whereby electrons are donated from the 5f-orbitals to the arene antibonding π-orbitals.

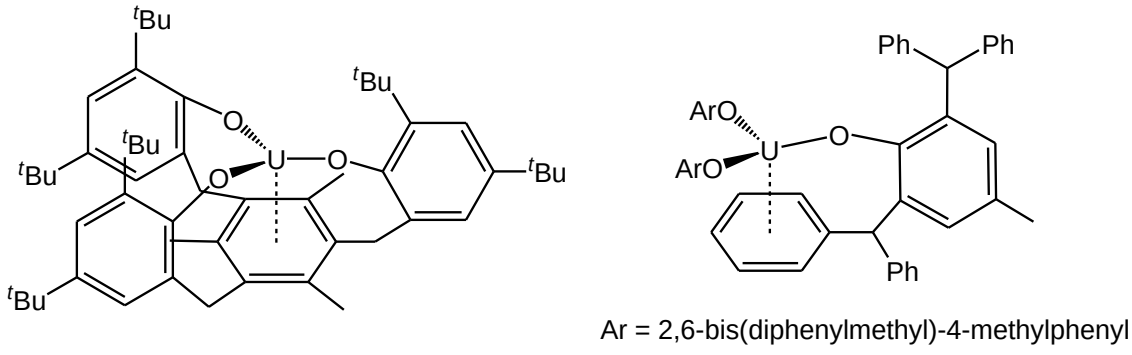

Figure 1.16 Uranium aryloxide complexes with supporting arene groups.[120,121]

The mesitylene-based complex has also been shown to undergo redox isomerisation in the presence of a reducing agent.[122] This proceeds *via* migration of a hydride from a CH_2 linker to the uranium centre to give a formal uranium(IV) complex with a U···H···M moiety and a reduced mesitylene unit (**Figure 1.17**). Further addition of a crown ether results in hydride insertion into the mesitylene ring. However, alternative use of a cryptand has illustrated that a uranium(II) monoarene complex can be synthesised.[123] Comparison of the molecular structure of this complex with the preceding uranium(III) species illustrates little variation in the core structure, and the planarity of the aromatic ring has been maintained. DFT studies of the uranium(II) complex describe the reduction as being predominantly metal centred and electrochemical studies have shown a quasi-reversible wave at -2.5 V *vs* $[FeCp_2]^{+/0}$ which is assigned to a formal U^{III}/U^{II} redox couple.

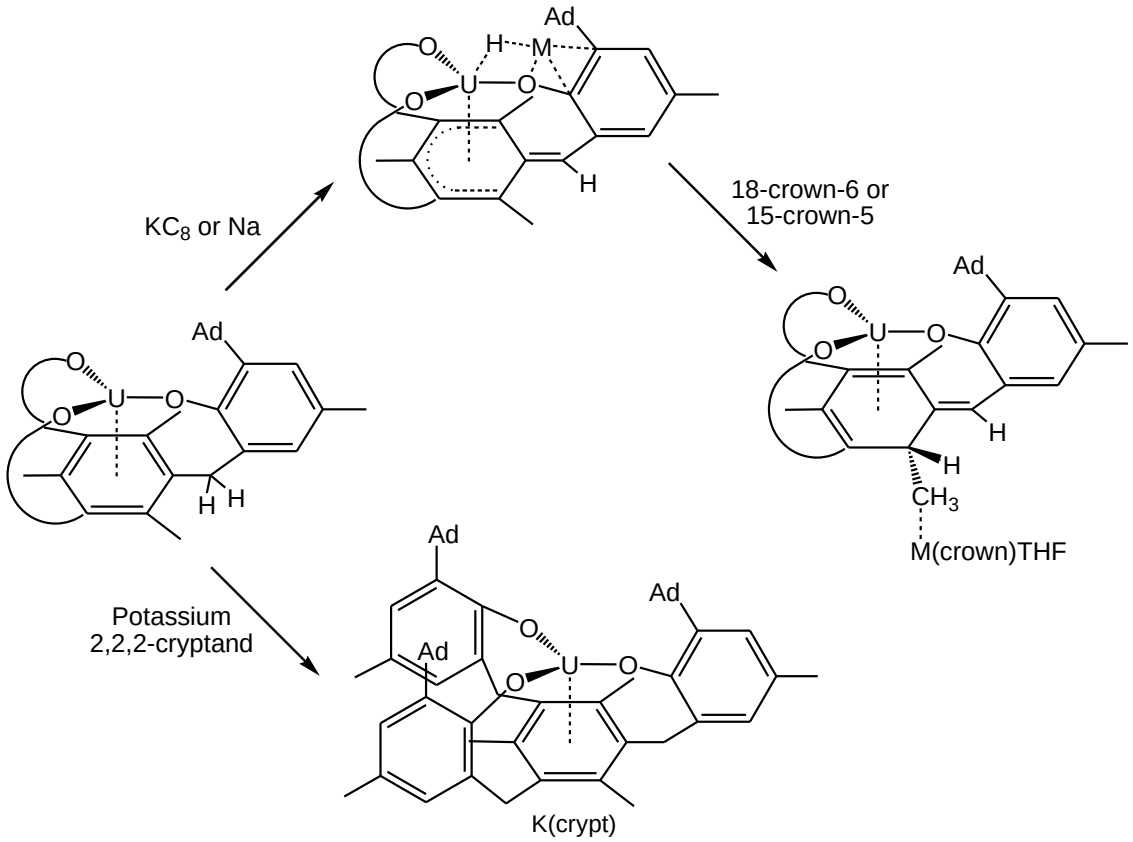

Figure 1.17 Reduction chemistry of a uranium monoarene complex.[122,123]

To date, no reports of bis(arene) sandwich complexes have been published due to the instability of a uranium complex in the zero oxidation state. Synthesis *via* Friedel-Crafts methodology has already been shown to be ineffective, and metal vapour synthesis techniques were unsuccessful.[124] DFT studies of bis(arene) complexes have shown that unlike transition metal complexes, actinide bis(arene) complexes would adopt a bent structure, unless sterically prohibited by bulky substituents.[125] However the feasibility of synthesising this type of complex is low, as the dissociation of the complex is thermodynamically favoured.[126]

1.3.3.3 Bridging arene complexes

Despite the small number of uranium arene complexes in the literature, in 2000 a new family of diuranium monoarene complexes was established with the publication of the first inverted sandwich complexes of benzene and toluene (**Figure 1.18**).[127] These complexes exhibit comparatively shorter U–C bond distances than the terminal arene complexes and exhibit η^6-coordination to both metal centres.

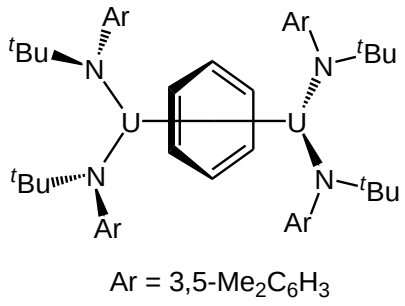

Figure 1.18 The first inverse sandwich complex of benzene.[127]

Assignment of the oxidation state of the metal and arene in these complexes is ambiguous. Formation of an inverted sandwich complex by reduction of a uranium(III)

species can give rise to several possibilities ranging from two uranium(II) centres with a neutral arene bridge to two uranium(IV) units with a tetraanionic arene ligand. Reactivity studies of these complexes suggest two uranium(II) centres due to the propensity for these complexes to behave as four-electron reductants.[127,128] Conversely, XANES spectroscopy has determined an effective electronic charge consistent with two uranium(III) centres. Evidence for an arene^{4-} ligand was however reported by Liddle, who observed that high valent uranium(V) inverse sandwich complexes can also be synthesised.[110,129]

DFT calculations of the low-valent 'uranium(III)' inverse sandwich complexes have suggested four electrons reside in uranium-based non-bonding orbitals, whilst another four electrons are stabilised predominantly by a covalent δ-interaction between 5f-orbitals and the arene LUMOs.[127] Further studies on an inverted arene complex stabilised by carbene ligands revealed the two δ-interactions consist of *ca.* 40% carbon (arene) 2p-orbitals, 40% 5f-orbitals and 10% 6d-orbitals.[130]

This family of complexes has since been extended to include other arene ligands, including naphthalene, biphenyl, *trans*-stilbene and *p*-terphenyl (**Figure 1.19**).[131,132] These complexes are supported by three ketimide ligands per uranium centre, and are synthesised as either the mono- or dianionic species. XRD studies illustrate that both uranium centres coordinate to the same arene ring in all instances, with coordination of the alkali-metal ion to another part of the complex. DFT studies have also illustrated that these ionic complexes exhibit the same bonding as their neutral counterparts in order to maintain the structure of the bridging unit, and that the charges are stabilised by the π-donor/acceptor properties of the ketimide ligands. [132]

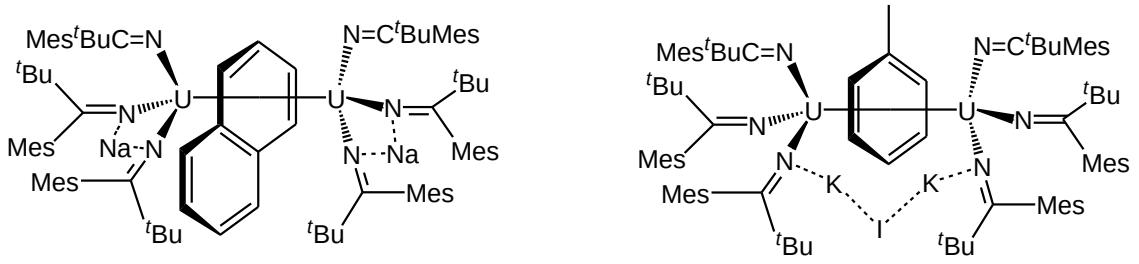

Figure 1.19 Examples of mono- and dianionic inverse sandwich complexes.[131,132]

Apart from their role as reducing agents, reactivity of these complexes includes cleavage of the dimeric unit by substitution of the arene with two anionic ligands.[133] This gives rise to two uranium(III) complexes supporting the assignment of two uranium(III) centres in the inverse sandwich complex. Other reactions include the borylation of the arene moiety, either by addition of the borane to the arene complex, or by addition of the borane during the synthesis of the inverse-arene complex (**Figure 1.20**).[134] The mechanism for this reaction is proposed to proceed *via* electrophilic aromatic substitution, and offers an alternative method for functionalising arenes.

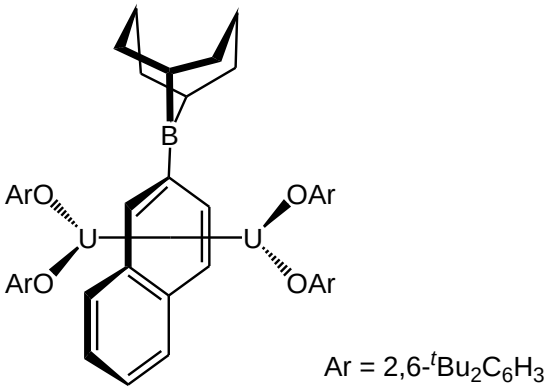

Figure 1.20 A borylated arene bridged between two uranium centres.[134]

1.3.4 Seven-membered carbocycles

1.3.4.1 Properties of cycloheptatrienyl ligands

The cycloheptatrienyl ligand is ambiguous in nature as it can be derived from cycloheptatriene by removal of a hydride to generate the $[C_7H_7]^+$ (tropylium) cation, which has 6π-electrons analogous to arene and cyclopentadienyl ligands. Alternatively, it can be doubly-reduced with loss of a proton to generate the $[C_7H_7]^{3-}$ trianion, which has 10π-electrons and is analogous to the cyclooctatetraenyl ligand.[1] In organoactinide chemistry, the latter mode is dominant as coordination of a tropylium ligand would suggest the formation of extremely low or negative oxidation states. The trianion has a set of a-symmetry orbitals and three sets of doubly degenerate e-symmetry orbitals which feature one, two and three nodes respectively.

1.3.4.2 Uranium cycloheptatriene complexes

Few cycloheptatriene complexes have been reported, partly due to the difficulty in functionalising this ligand. The first use of this ligand in organoactinide chemistry was published in 1994, and illustrates two examples of anionic inverted cycloheptatrienyl sandwich complexes with borohydride and amido ligands (**Figure 1.21**).[135,136] Both species exhibit planar $[C_7H_7]^{3-}$ units, indicating that the ligand is aromatic in these complexes and that both uranium centres are in the +5 oxidation state.

Following this publication, the first example of a bis(cycloheptatrienyl) uranium sandwich complex was reported (**Figure 1.21**).[137,138] This species, which is synthesised as $[K(18\text{-crown-6})][U(C_7H_7)_2]$, exhibits two staggered parallel rings giving rise to a dumbbell-shaped molecule with C_{2h} symmetry. In the synthesis of this complex uranium has undergone a one-electron oxidation to form the +5 oxidation state in order to allow coordination of two $[C_7H_7]^{3-}$ moieties.

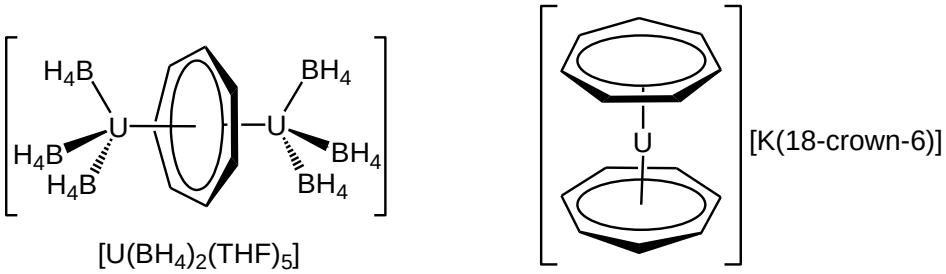

Figure 1.21 An inverse cycloheptatrienyl complex (left) and the cycloheptatrienyl sandwich complex (right).[135,137]

1.3.5 Eight-membered carbocycles

1.3.5.1 Properties of cyclooctatetraene ligands

Neutral cyclooctatetraene has 8π electrons and is most stable in the tub conformation. A two-electron reduction of this ligand however, generates the 10π-aromatic system. This ligand features a set of a-symmetry orbitals, three doubly degenerate e-symmetry orbitals sets and a set of b-symmetry orbitals, which features four nodes.[1] Of these orbitals, typically the lowest four are involved in bonding, and δ-interactions tend to be dominant due to the increased size of this ligand.

1.3.5.2 Uranocene

Uranocene, $[U(C_8H_8)_2]$, was the first organoactinide sandwich complex to be synthesised and was reported by Streitwieser and Müller-Westerhoff in 1968.[2] This complex exhibits parallel COT rings giving rise to a dumbbell shaped structure with D_{8h} symmetry and was the first f-element complex to resemble ferrocene.[139,140] Other studies of this complex found it to be thermodynamically stable, although it reacts violently with pure oxygen and decomposes in air.[141]

After this initial publication, several variations were reported with substituted COT rings,[142–148] including one example of a bridged uranocene,[149] and a biuranocenylene (**Figure 1.22**).[150] Some of these structures exhibit both staggered and eclipsed conformations in crystalline material, but analysis of dibenzouranocene and dicyclopentenouranocene suggests that the differing conformations are a result of packing within the lattice rather than steric constraints.[142,143] The presence of more than one conformation in the solid state also demonstrates the very small rotation barrier exhibited by these complexes.[151] However, silyl and *tert*-butyl substituted complexes show the sterics of these groups inhibit full rotation, which is illustrated by the static conformations observed by NMR spectroscopy at cooler temperatures.[145,152] Studies of 1,1'-dimesityluranocene have shown that the two mesityl moieties favour close contact, which is proposed to be due to van der Waals attraction.[148] This was determined by NMR studies which revealed a high separation barrier of 10 kcal·mol^{-1}.

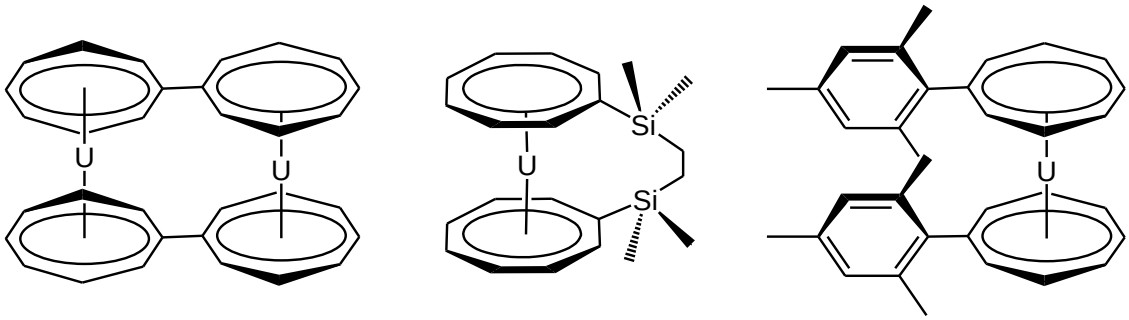

Figure 1.22 Examples of substituted uranocenes.[148–150]

The one exception to the usual structural motif of uranocene was reported in 2011 in the formation of a bent uranocene which incorporates two COT^{BIG} ($C_8H_6{}^{\{1,4\text{-}SiPh3\}2}$) ligands.[153] Despite the non-linear COT–U–COT angle, the U–C distances vary little from those of other uranocene complexes, illustrating that bending of the complex

allows the general features of uranocene to be maintained whilst accommodating four large substituents.

Analysis of the bonding in uranocenes found there is overlap between the 5f and the e_{2u} orbitals, and the 6d and e_{2g} orbitals, which stabilise the complex.[154,155] Due to relativistic effects, these contributions are comparable, however greater radial extension of the 6d orbitals also allows overlap with deeper ligand orbitals.[156] It was also observed that substituents cause little alteration in the spectra, indicating that they do not stabilise or destabilise the complex.[157,158] However, increasing levels of alkylation gives rise to increased 6d- and 5f-orbital involvement in the bonding.

Despite the thermodynamic stability of uranocene, reactions of these complexes have been reported. Early studies found uranocene could be reduced with potassium to yield potassium bis(cyclooctatetraenyl)uranium(III) and substituted derivatives.[159–161] These studies were supported by DFT which found uranocene to have a positive electron affinity, and demonstrates than a uranium(III) species with a $5f^3$ configuration is stable.[162] More recently, a novel bent uranocene was synthesised by reaction of $[U(C_8H_8)_2]$ with a cyanide ion (**Figure 1.23**).[163] This gave rise to coordination of cyanide to uranocene with a separated $[NR_4]^+$ cation.

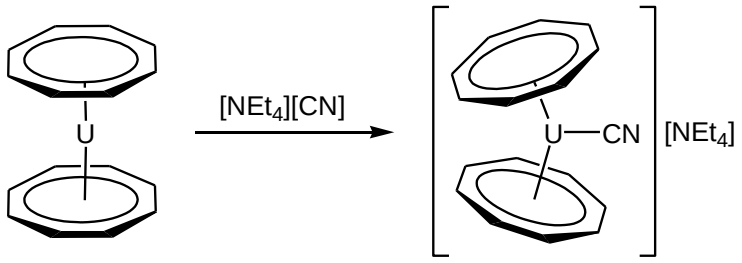

Figure 1.23 Synthesis of a bent uranocene.[163]

Infrared spectroscopy of this complex illustrates little backbonding and XRD studies found significant bending of the COT–U–COT angle. DFT studies of this complex have found 6d and 5f orbitals continue to participate in the metal-ligand bonding to all three ligands, giving rise to covalency in the U–CN bond.[164]

1.3.5.3 Monocyclooctatetraene uranium complexes

Despite the popularity of uranocene and the volume of research that has been conducted on these complexes, reactivity studies of these complexes are limited. However half-sandwich synthons incorporating only one COT ring have since been reported and offer a wealth of reactivity.

An early example is $[(C_8H_8)UCl_2(THF)_2]$, which could be synthesised by reduction of cyclooctatetraene with UCl_3, or by reaction of UCl_4, COT and sodium hydride.[165] The synthetic utility of this complex was demonstrated by its conversion to $[(C_8H_8)U\{N(SiMe_3)_2\}_2]$, however the analogue to this complex, $[(C_8H_8)U(NEt_2)_2(THF)]$, could not only be synthesised *via* $[(C_8H_8)UCl_2]$, but also from uranocene, $[U(NEt_2)_4]$ and UCl_4 (**Figure 1.24**).[166–168] Another useful synthon, $[U(COT)(OTf)_2(py)]$, could be synthesised directly from $[U(OTf)_4]$ and one equivalent $K_2[C_8H_8]$.[169,170]

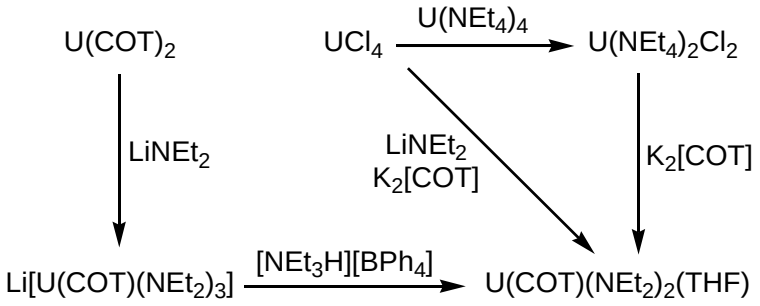

Figure 1.24 Synthetic routes to $[(C_8H_8)U(NEt_2)_2(THF)]$.[167,168]

Initial reactivity of $[(C_8H_8)U(NEt_2)_2(THF)]$ involved conversion of the complex into the ionic complex, $[(C_8H_8)U(NEt_2)(THF)_2][BPh_4]$, by protonolysis of the half-sandwich with $[NEt_3H][BPh_4]$.[171] From this complex a range of reactivity was observed which included addition, insertion and substitution reactions. More recently, this motif was used to synthesise dicationic uranium(IV) and cationic uranium(III) complexes.[172,173] Addition of a Lewis base during these reactions gave rise to separation of the ions to form discrete piano-stool uranium cations, which could be employed as precursors for the synthesis of other complexes (**Figure 1.25**). This was demonstrated by reaction of the uranium(III) cation with K[Cp*], which gave rise to displacement of two HMPA ligands in order to allow coordination of the five-membered ring.[174] Similarly, reaction of the uranium(IV) dication with $K[Cp^{PMe4}]$ gave rise to $[U(C_8H_8)(Cp^{PMe4})(HMPA)_2][BPh_4]$ which could be reduced to the uranium(III) complex with sodium amalgam.[175] Regeneration of the parent uranium(IV) cation could however be achieved by protonation of the Cp^{PMe4} ligand, illustrating the lability of this ligand in comparison to its cyclopentadienyl analogues.

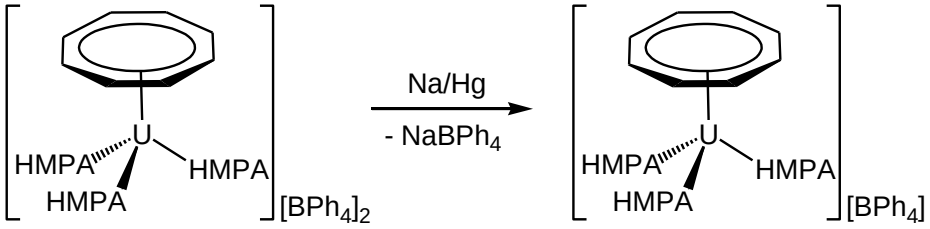

Figure 1.25 A uranium(IV) dication and uranium(III) cation, synthesised by protonolysis of $[(C_8H_8)U(BH_4)(HMPA)_3][BPh_4]$.[172,173]

The mixed-sandwich family of complexes with one cyclooctatetraenyl ligand and a five-membered ring began with the publication of [U(COT)(Cp*)(THF)] in 1993.[176] This complex, as with all uranium(III) and uranium(IV) mixed-sandwich complexes,

adopts a bent structure. The ability of these complexes to coordinate a Lewis base, or undergo a one-electron oxidation has given rise to a wide range of reactivity and has led to the formation of many new complexes (see Chapters 2 – 4).

1.3.5.4 Inverse cyclooctatetraene uranium complexes

Although there is a large array of literature for cyclooctatetraenyl rings in organoactinide chemistry, few inverse cyclooctatetraenyl uranium complexes have been published. The earliest report appeared in 1978 which proposed the formation of $[\{(Cp^*)_3U\}_2(C_8H_8)]$ by reaction of $[U(Cp^*)_3]$ with $K_2[C_8H_8]$.[177] In 1990, a second publication described the synthesis of $[(COT)U(BH_4)_2]$ from $[U(BH_4)_4]$ and uranocene, in which it was proposed that the inverse sandwich complex $[(BH_4)_3U(COT)U(BH_4)_3]$ was formed as an intermediate.[178]

Crystallographic evidence of an inverse cyclooctatetraene complex was not published until 2000, when Evans *et al.* reported the synthesis of $[\{(C_8H_8)(Cp^*)U\}_2(C_8H_8)]$ by a formal three-electron reduction of COT by $[U(Cp^*)_3]$.[179] The bridging C_8H_8 unit was found to be non-planar and bound in an η^3:η^3 fashion (**Figure 1.26**). Alternative methods of synthesising this complex have since been published and include reduction of COT by $[U(COT)(Cp^*)(THF)]$, $[U(Cp^*)_2H]_2$, and $[\{(C_8H_8)(Cp^*)U\}_2(C_6H_6)]$.[180,181]

A second inverted cyclooctatetraene complex was reported by Diaconescu and Cummins in 2002 *via* a bridged naphthalene complex (**Figure 1.26**).[131] This complex however exhibits η^8:η^8-bonding of the COT ring, which is proposed to be due to the lesser sterics around the metal centre in comparison to $[\{(C_8H_8)(Cp^*)U\}_2(C_8H_8)]$. Theoretical calculations of this complex also illustrate the bonding between the bridging ligand and the two metal centres is weaker than the analogous arene complexes due to poorer overlap of the ligand δ-orbitals and the 5f-orbitals.

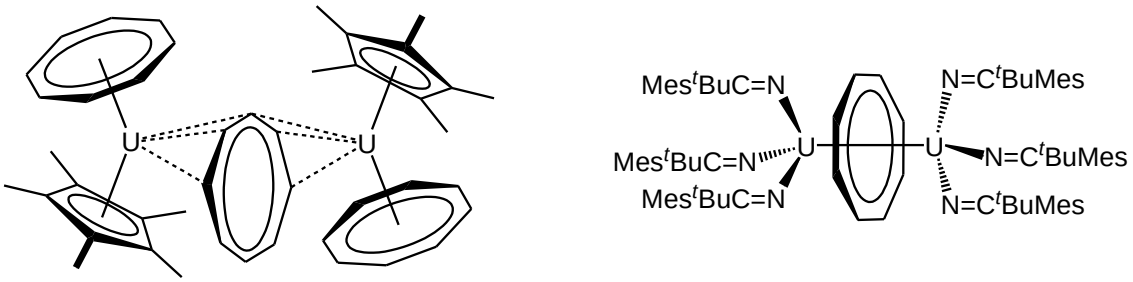

Figure 1.26 Two inverse COT complexes with η^3:η^3-bonding (left) and η^8:η^8-bonding (right).[131,179]

1.3.5.5 Properties of pentalene

An alternative eight-membered, dianionic aromatic ligand derives from pentalene, which is a bicyclic moiety composed of two fused-five-membered rings. The neutral, unsubstituted 8π-system is unstable above -196 °C and readily decomposes, however the stability of this species increases upon the addition of substituents. The aromatic pentalene dianion however is stable at ambient temperature and a growing number of organometallic complexes have now incorporated this ligand.[182]

The bonding modes of this ligand are more varied than those of COT, and whilst the ligand is viewed as a planar 10π-aromatic system, planar pentalene ligands tend to adopt η^5-coordination, giving rise to a Cp^R motif.[182] This has also led to the synthesis of a series of bimetallic complexes, which can be *anti*- or *syn*-facial, with the latter allowing the formation of metal-metal bonds.[182] Monometallic complexes however, tend to exhibit η^8-coordination of the ligand, which folds along the bridge with consequential loss of aromaticity. This latter coordination mode is prevalent in the organometallic chemistry of pentalene and is the only coordination mode observed in organoactinide complexes.

1.3.5.6 Uranium pentalene complexes

Uranium bis(pentalene) was first reported by Cloke and co-workers in 1999 and was shown to form in both the semi-eclipsed and staggered conformations.[183] Theoretical studies and photoelectron spectroscopy illustrate that the bonding in this complex is similar to the bonding in uranocene, with overlap of the 5f and 6d-orbitals with the pentalene HOMO. Studies of the ionisation energies of several complexes found the pentalene complex to have the lowest energies, therefore illustrating that this ligand donates more electron density to the metal centre than both Cp and COT.

An analogous complex was also synthesised a decade later with permethylpentalene ligands (**Figure 1.27**).[184] This complex was found to exist in one staggered and two eclipsed conformations in the solid state, which relate to one another by *ca.* 120° rotation around the *c*-axis. Electrochemical studies of this complex suggest access to the uranium(III) oxidation state is achievable, as demonstrated by a redox wave at -1.13 V relative to $[FeCp_2]^{+/0}$. However, these results are not in agreement with other U^{IV}/U^{III} reduction couples in the literature and it is instead proposed that the metal-based process occurs at *ca.* -2.3 V *vs* $[FeCp_2]^{+/0}$.

Half-sandwich uranium(III) pentalene complexes have also been synthesised with Cp* and Tp^{Me2} supporting ligands, which bear resemblance to the COT mixed-sandwich system (**Figure 1.27**).[185,186] DFT calculations on these two complexes illustrate that the Tp^{Me2} analogue is more reducing than its Cp* counterpart, but that the steric environment around the metal centre is more crowded, giving rise to less observed reactivity.

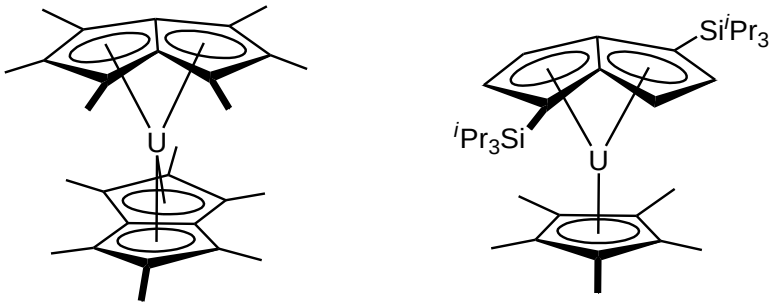

Figure 1.27 A uranium bis(pentalene) complex in the staggered conformation (left) and a uranium half-sandwich complex (right).[184,185]

1.4 Summary

The rich chemistry observed for uranium with aromatic ligands could not have been foreseen when this field first emerged over 50 years ago. However the range of complexes synthesised illustrates the applicability of these ligands in organometallic chemistry, with tuning of the steric and electronic properties in terms of charge, heteroatom incorporation and substituents available. This thesis extends this concept, with the specific aim of altering the steric and electronic properties of published complexes by changing the ligand substituents and incorporating heteroatoms into the five membered ring.

1.5 References

1 C. Elschenbroich, *Organometallics,* Wiley-VCH Verlag GmbH & Co. KGaA, Weinheim, Germany, 3rd edn., 2006.

2 A. Streitwieser and U. Müller-Westerhoff, *J. Am. Chem. Soc.*, 1968, **90**, 7364.

3 N. Kaltsoyannis and P. Scott, *The f elements*, Oxford University Press Inc., New York, 1999.

4 S. Cotton, *Lanthanide and Actinide Chemistry*, John Wiley & Sons Ltd., Chichester, England, 2006.

5 W. J. Evans, *J. Organomet. Chem.*, 2002, **647**, 2–11.

6 F. Nief, *Dalton Trans.*, 2010, **39**, 6589–6598.

7 P. C. Blake, M. F. Lappert, J. L. Atwood and H. Zhang, *J. Chem. Soc., Chem. Commun.*, 1986, 1148–1149.

8 J. S. Parry, F. G. N. Cloke, S. Coles and M. B. Hursthouse, *J. Am. Chem. Soc.*, 1999, **121**, 6867–6871.

9 P. C. Blake, N. M. Edelstein, P. B. Hitchcock, W. K. Kot, M. F. Lappert, G. V. Shalimoff and S. Tian, *J. Organomet. Chem.*, 2001, **636**, 124–129.

10 J. R. Walensky, R. L. Martin, J. W. Ziller and W. J. Evans, *Inorg. Chem.*, 2010, **49**, 10007–10012.

11 N. A. Siladke, C. L. Webster, J. R. Walensky, M. K. Takase, J. W. Ziller, D. J. Grant, L. Gagliardi and W. J. Evans, *Organometallics*, 2013, **32**, 6522–6531.

12 C. R. Graves and J. L. Kiplinger, *Chem. Commun.*, 2009, 3831–3853.

13 B. M. Gardner and S. T. Liddle, *Eur. J. Inorg. Chem.*, 2013, 3753–3770.

14 N. G. Connelly and W. E. Geiger, *Chem. Rev.*, 1996, **96**, 877–910.

15 E. O. Fischer and Y. Hristidu, *Z. Naturforsch B*, 1962, **17**, 275.

16 J. H. Burns, *J. Am. Chem. Soc.*, 1973, **95**, 3815–3817.

17 J. H. Burns, *J. Organomet. Chem.*, 1974, **69**, 225–233.

18 J. C. Green, M. R. Kelly, J. A. Long, B. Kanellakopulos and P. I. Yarrow, *J. Organomet. Chem.*, 1981, **212**, 329–340.

19 B. E. Bursten, M. Casarin, S. Di Bella, A. Fang and I. L. Fragalà, *Inorg. Chem.*, 1985, **24**, 2169–2173.

20 B. Kanellakopulos, R. Maier and J. Heuser, *J. Alloys and Compounds*, 1991, **176**, 89–96.

21 M. J. Tassell and N. Kaltsoyannis, *Dalton Trans.*, 2010, **39**, 6719–6725.

22 M. BenYahia, L. Belkhiri and A. Boucekkine, *J. Mol. Structure: THEOCHEM*, 2006, **777**, 61–73.

23 A. Dormond, P. Hepiégne, A. Hafid and C. Moise, *J. Organomet. Chem.*, 1990, **398**, C1–C5.

24 L. T. Reynolds and G. Wilkinson, *J. Inorg. Nucl. Chem.*, 1956, **2**, 246–253.

25 Paolucci, Gino, Rossetto, Gilberto, Zanella, Pierino and Fischer, R Dieter, *J. Organomet. Chem.*, 1985, **284**, 213–228.

26 N. A. Siladke, K. R. Meihaus, J. W. Ziller, M. Fang, F. Furche, J. R. Long and W. J. Evans, *J. Am. Chem. Soc.*, 2012, **134**, 1243–1249.

27 J.-C. Berthet, M. Lance, M. Nierlich, J. Vigner and M. Ephritikhine, *J. Organomet. Chem.*, 1991, **420**, C9–C11.

28 A. Gulino, E. Cillberto, S. Di Bella and I. L. Fragalà, *Organometallics*, 1992, **11**, 3248–3257.

29 D. C. Sonnenberger and J. G. Gaudiello, *Inorg. Chem.*, 1988, **27**, 2747–2748.

30 A. Zalkin, J. G. Brennan and R. A. Andersen, *Acta Cryst. Sect. C*, 1988, **C44**, 2104–2106.

31 M. del Mar Conejo, J. S. Parry, E. Carmona, M. Schultz, J. G. Brennan, S. M. Beshouri, R. A. Andersen, R. D. Rogers, S. Coles and M. B. Hursthouse, *Chem. Eur. J.*, 1999, **5**, 3000–3009.

32 J.-C. Berthet, J.-F. Le Maréchal, M. Lance, M. Nierlich, J. Vigner and M. Ephritikhine, *J. Chem. Soc. Dalton Trans.*, 1992, 1573–1577.

33 N. A. Siladke, J. W. Ziller and W. J. Evans, *Z. Anorg. Allg. Chem*, 2010, **636**, 2347–2351.

34 W. J. Evans, K. J. Forrestal and J. W. Ziller, *Angew. Chem. Int. Ed.*, 1997, **36**, 774–776.

35 H. J. Wasserman, A. J. Zozulin, D. C. Moody, R. R. Ryan and K. V. Salazar, *J. Organomet. Chem.*, 1983, **254**, 305–311.

36 B. Kanellakopulos, E. O. Fischer, E. Dornberger and F. Baumgärtner, *J. Organomet. Chem.*, 1970, **24**, 507–514.

37 M. Burton, H. Marquet-Ellis, G. Folcher and C. Giannotti, *J. Organomet. Chem.*, 1982, **229**, 21–28.

38 J. W. Bruno, D. G. Kalina, E. A. Mintz and T. J. Marks, *J. Am. Chem. Soc.*, 1982, **104**, 1860–1869.

39 C. Clappe, D. Leveugle, D. Hauchard and G. Durand, *J. Electroanal. Chem.*, 1998, **448**, 95–103.

40 A. Elkechai, Y. Mani, A. Boucekkine and M. Ephritikhine, *Inorg. Chem.*, 2012, **51**, 6943–6952.

41 A. Elkechai, A. Boucekkine, L. Belkhiri, M. Amarouche, C. Clappe, D. Hauchard and M. Ephritikhine, *Dalton Trans.*, 2009, 2843–2849.

42 F. Ossola, P. Zanella, P. Ugo and R. Seeber, *Inorg. Chim. Acta*, 1988, **147**, 123–126.

43 R. E. Cramer, R. B. Maynard, J. C. Paw and J. W. Gilje, *J. Am. Chem. Soc.*, 1981, **103**, 3589–3590.

44 R. E. Cramer, R. B. Maynard, J. C. Paw and J. W. Gilje, *Organometallics*, 1983, **2**, 1336–1340.

45 R. E. Cramer, K. Panchanetheswaran and J. W. Gilje, *J. Am. Chem. Soc.*, 1984, **106**, 1853–1854.

46 R. C. Stevens, R. Bau, R. E. Cramer, D. Afzal, J. W. Gilje and T. F. Koetzle, *Organometallics*, 1990, **9**, 694–697.

47 J. G. Brennan and R. A. Andersen, *J. Am. Chem. Soc.*, 1985, **107**, 514–516.

48 J. G. Brennan, R. A. Andersen and A. Zalkin, *J. Am. Chem. Soc.*, 1988, **110**, 4554–4558.

49 L. Arnaudet, G. Folcher, H. Marquet-Ellis, E. Klähne, K. Yünlü and R. D. Fischer, *Organometallics*, 1983, **2**, 344–346.

50 L. Arnaudet, P. Charpin, G. Folcher, M. Lance, M. Nierlich and D. Vigner, *Organometallics*, 1986, **5**, 270–274.

51 M. Foyentin, G. Folcher and M. Ephritikhine, *J. Organomet. Chem.*, 1987, **335**, 201–206.

52 J.-C. Berthet, C. Villiers, J.-F. Le Maréchal, B. Delavaux-Nicot, M. Lance, M. Nierlich, J. Vigner and M. Ephritikhine, *J. Organomet. Chem.*, 1992, **440**, 53–65.

53 J.-F. Le Maréchal, C. Villiers, P. Charpin, M. Lance, M. Nierlich, J. Vigner and M. Ephritikhine, *J. Chem. Soc., Chem. Commun.*, 1989, 308–310.

54 M. R. MacDonald, M. E. Fieser, J. E. Bates, J. W. Ziller, F. Furche and W. J. Evans, *J. Am. Chem. Soc.*, 2013, **135**, 13310–13313.

55 G. Bombieri, F. Benetollo, E. Klähne and R. D. Fischer, *J. Chem. Soc. Dalton Trans.*, 1983, 1115–1121.

56 S. G. Minasian, J. L. Krinsky, V. A. Williams and J. Arnold, *J. Am. Chem. Soc.*, 2008, **130**, 10086–10087.

57 B. Vlaisavljevich, P. Miró, C. J. Cramer, L. Gagliardi, I. Infante and S. T. Liddle, *Chem. Eur. J.*, 2011, **17**, 8424–8433.

58 G. Zi, L. Jia, E. L. Werkema, M. D. Walter, J. P. Gottfriedsen and R. A. Andersen, *Organometallics*, 2005, **24**, 4251–4264.

59 G. Zi, L. L. Blosch, L. Jia and R. A. Andersen, *Organometallics*, 2005, **24**, 4602–4612.

60 N. Barros, D. Maynau, L. Maron, O. Eisenstein, G. Zi and R. A. Andersen, *Organometallics*, 2007, **26**, 5059–5065.

61 L. Ventelon, C. Lescop, T. Arliguie, P. C. Leverd, M. Lance, M. Nierlich and M. Ephritikhine, *Chem. Commun.*, 1999, 659–660.

62 B. P. Warner, B. L. Scott and C. J. Burns, *Angew. Chem. Int. Ed.*, 1998, **37**, 959–960.

63 R. G. Peters, B. P. Warner and C. J. Burns, *J. Am. Chem. Soc.*, 1999, **121**, 5585–5586.

64 C. A. Secaur, V. W. Day, R. D. Ernst, W. J. Kennelly and T. J. Marks, *J. Am. Chem. Soc.*, 1976, **98**, 3713–3715.

65 R. C. Schnabel, B. L. Scott, W. H. Smith and C. J. Burns, *J. Organomet. Chem.*, 1999, **591**, 14–23.

66 L. Moisan, T. Le Borgne, C. Villiers, P. Thuéry and M. Ephritikhine, *Comptes Rendus Chimie*, 2007, **10**, 883–887.

67 J. Maynadié, J.-C. Berthet, P. Thuéry and M. Ephritikhine, *J. Am. Chem. Soc.*, 2006, **128**, 1082–1083.

68 J. Maynadié, J.-C. Berthet, P. Thuéry and M. Ephritikhine, *Organometallics*, 2006, **25**, 5603–5611.

69 J. Maynadié, J.-C. Berthet, P. Thuéry and M. Ephritikhine, *Organometallics*, 2007, **26**, 4585–4591.

70 J. Maynadié, N. Barros, J.-C. Berthet, P. Thuéry, L. Maron and M. Ephritikhine, *Angew. Chem. Int. Ed.*, 2007, **46**, 2010–2012.

71 A. Elkechai, S. Meskaldji, A. Boucekkine, L. Belkhiri, D. Bouchet, M. Amarouche, C. Clappe, D. Hauchard and M. Ephritikhine, *J. Mol. Structure: THEOCHEM*, 2010, **954**, 115–123.

72 R. K. Thomson, B. L. Scott, D. E. Morris and J. L. Kiplinger, *Comptes Rendus Chimie*, 2010, **13**, 790–802.

73 C. R. Graves, P. Yang, S. A. Kozimor, A. E. Vaughn, D. L. Clark, S. D. Conradson, E. J. Schelter, B. L. Scott, J. D. Thompson, P. J. Hay, D. E. Morris and J. L. Kiplinger, *J. Am. Chem. Soc.*, 2008, **130**, 5272–5285.

74 D. E. Morris, R. E. Da Re, K. C. Jantunen, I. Castro-Rodriguez and J. L. Kiplinger, *Organometallics*, 2004, **23**, 5142–5153.

75 J. L. Kiplinger, D. E. Morris, B. L. Scott and C. J. Burns, *Organometallics*, 2002, **21**, 3073–3075.

76 E. J. Schelter, P. Yang, B. L. Scott, J. D. Thompson, R. L. Martin, P. J. Hay, D. E. Morris and J. L. Kiplinger, *Inorg. Chem.*, 2007, **46**, 7477–7488.

77 E. J. Schelter, J. M. Veauthier, J. D. Thompson, B. L. Scott, K. D. John, D. E. Morris and J. L. Kiplinger, *J. Am. Chem. Soc.*, 2006, **128**, 2198–2199.

78 C. R. Graves, B. L. Scott, D. E. Morris and J. L. Kiplinger, *Organometallics*, 2008, **27**, 3335–3337.

79 E. J. Schelter, R. Wu, B. L. Scott, J. D. Thompson, D. E. Morris and J. L. Kiplinger, *Angew. Chem. Int. Ed.*, 2008, **47**, 2993–2996.

80 E. J. Schelter, R. Wu, J. M. Veauthier, E. D. Bauer, C. H. Booth, R. K. Thomson, C. R. Graves, K. D. John, B. L. Scott, J. D. Thompson, D. E. Morris and J. L. Kiplinger, *Inorg. Chem.*, 2010, **49**, 1995–2007.

81 S. Meskaldji, A. Zaiter, L. Belkhiri and A. Boucekkine, *Theor. Chem. Acc.*, 2012, **131**, 1151–1161.

82 T. Mehdoui, J.-C. Berthet, P. Thuéry, L. Salmon, E. Rivière and M. Ephritikhine, *Chem. Eur. J.*, 2005, **11**, 6994–7006.

83 D. Baudry, P. Charpin, M. Ephritikhine, G. Folcher, J. Lambard, M. Lance, M. Nierlich and J. Vigner, *J. Chem. Soc., Chem. Commun.*, 1985, 1553–1554.

84 D. Baudry, A. Dormond, A. Hafid and C. Raillard, *J. Organomet. Chem.*, 1996, **511**, 37–45.

85 D. Barbier-Baudry, O. Blacque, A. Hafid, A. Nyassi, H. Sitzmann and M. Visseaux, *Eur. J. Inorg. Chem.*, 2000, 2333–2336.

86 L. R. Avens, C. J. Burns, R. J. Butcher, D. L. Clark, J. C. Gordon, A. R. Schake, B. L. Scott, J. G. Watkin and B. D. Zwick, *Organometallics*, 2000, **19**, 451–457.

87 J. Maynadié, J.-C. Berthet, P. Thuéry and M. Ephritikhine, *Chem. Commun.*, 2007, 486–488.

88 B. D. Stubbert, C. L. Stern and T. J. Marks, *Organometallics*, 2003, **22**, 4836–4838.

89 B. D. Stubbert and T. J. Marks, *J. Am. Chem. Soc.*, 2007, **129**, 4253–4271.

90 B. D. Stubbert and T. J. Marks, *J. Am. Chem. Soc.*, 2007, **129**, 6149–6167.

91 K. B. Dillon, F. Mathey and J. F. Nixon, *Phosphorus: The Carbon Copy*, John Wiley & Sons Ltd., Chichester, 1998.

92 L. Nyulászi and Z. Benkõ, *Aromaticity in Heterocyclic Compounds*, Springer, Verlag Berlin Heidelberg, 2009.

93 N. Kuhn, G. Henkel, J. Kreutzberg, S. Stubenrauch and C. Janiak, *J. Organomet. Chem.*, 1993, **456**, 97–106.

94 M. D. Su and S. Y. Chu, *J. Phys. Chem.*, 1989, **93**, 6043–6051.

95 N. M. Kostić and R. F. Fenske, *Organometallics*, 1983, **2**, 1008–1013.

96 G. K. B. Clentsmith, F. G. N. Cloke, M. D. Francis, J. R. Hanks, P. B. Hitchcock and J. F. Nixon, *J. Organomet. Chem.*, 2008, **693**, 2287–2292.

97 D. Baudry, M. Ephritikhine, F. Nief, L. Ricard and F. Mathey, *Angew. Chem. Int. Ed.*, 1990, **29**, 1485–1486.

98 P. Gradoz, D. Baudry, M. Ephritikhine, F. Nief and F. Mathey, *J. Chem. Soc. Dalton Trans.*, 1992, 3047–3051.

99 P. Gradoz, M. Ephritikhine, M. Lance, J. Vigner and M. Nierlich, *J. Organomet. Chem.*, 1994, **481**, 69–73.

100 T. Arliguie, M. Ephritikhine, M. Lance and M. Nierlich, *J. Organomet. Chem.*, 1996, **524**, 293–297.

101 P. Desmurs, M. Visseaux, D. Baudry, A. Dormond, F. Nief and L. Ricard, *Organometallics*, 1996, **15**, 4178–4181.

102 D. Barbier-Baudry, A. Dormond and M. Visseaux, *J. Organomet. Chem.*, 2000, **609**, 21–28.

103 P. Gradoz, D. Baudry, M. Ephritikhine, M. Lance, M. Nierlich and J. Vigner, *J. Organomet. Chem.*, 1994, **466**, 107–118.

104 D. Baudry, A. Dormond and O. Lesprit, *Bull. Soc. Chim. Fr*, 1995, **132**, 183–187.

105 A. Elkechai, A. Boucekkine, L. Belkhiri, D. Hauchard, C. Clappe and M. Ephritikhine, *Comptes Rendus Chimie*, 2010, **13**, 860–869.

106 P. Gradoz, C. Boisson, D. Baudry, M. Lance, M. Nierlich, J. Vigner and M. Ephritikhine, *J. Chem. Soc., Chem. Commun.*, 1992, 1720–1721.

107 W. J. Evans, G. W. Nyce, M. A. Johnston and J. W. Ziller, *J. Am. Chem. Soc.*, 2000, **122**, 12019–12020.

108 D. L. Swartz II, L. P. Spencer, B. L. Scott, A. L. Odom and J. M. Boncella, *Dalton Trans.*, 2010, **39**, 6841–6846.

109 C. L. Webster, J. E. Bates, M. Fang, J. W. Ziller, F. Furche and W. J. Evans, *Inorg. Chem.*, 2013, **52**, 3565–3572.

110 D. Patel, F. Moro, J. McMaster, W. Lewis, A. J. Blake and S. T. Liddle, *Angew. Chem. Int. Ed.*, 2011, **50**, 10388–10392.

111 T. Mehdoui, J.-C. Berthet, P. Thuéry and M. Ephritikhine, *Dalton Trans.*, 2004, 579–590.

112 T. Arliguie, M. Doux, N. Mézailles, P. Thuéry, P. L. Floch and M. Ephritikhine, *Inorg. Chem.*, 2006, **45**, 9907–9913.

113 T. Mehdoui, J. Berthet, P. Thuéry and M. Ephritikhine, *Eur. J. Inorg. Chem.*, 2004, 1996–2000.

114 M. Cesari, U. Pedretti, A. Zazzetta, G. Lugli and W. Marconi, *Inorg. Chim. Acta*, 1971, **5**, 439–444.

115 F. A. Cotton and W. Schwotzer, *Organometallics*, 1985, **4**, 942–943.

116 F. A. Cotton and W. Schwotzer, *Organometallics*, 1987, **6**, 1275–1280.

117 A. V. Garbar, M. R. Leonov, L. N. Zakharov and Y. T. Struchkov, *Russ. Chem. Bull.*, 1996, **45**, 451–454.

118 D. Baudry, E. Bulot, P. Charpin, M. Ephritikhine, M. Lance, M. Nierlich and J. Vigner, *J. Organomet. Chem.*, 1989, **371**, 155–162.

119 W. G. Van Der Sluys, C. J. Burns, J. C. Huffman and A. P. Sattelberger, *J. Am. Chem. Soc.*, 1988, **110**, 5924–5925.

120 S. C. Bart, F. W. Heinemann, C. Anthon, C. Hauser and K. Meyer, *Inorg. Chem.*, 2009, **48**, 9419–9426.

121 S. M. Franke, B. L. Tran, F. W. Heinemann, W. Hieringer, D. J. Mindiola and K. Meyer, *Inorg. Chem.*, 2013, **52**, 10552–10558.

122 H. S. La Pierre, H. Kameo, D. P. Halter, F. W. Heinemann and K. Meyer, *Angew. Chem. Int. Ed.*, 2014, **53**, 7154–7157.

123 H. S. La Pierre, A. Scheurer, F. W. Heinemann, W. Hieringer and K. Meyer, *Angew. Chem. Int. Ed.*, 2014, **53**, 7158–7162.

124 F. G. N. Cloke, *Private Communication*.

125 J. Li and B. E. Bursten, *J. Am. Chem. Soc.*, 1999, **121**, 10243–10244.

126 G. Hong, F. Schautz and M. Dolg, *J. Am. Chem. Soc.*, 1999, **121**, 1502–1512.

127 P. L. Diaconescu, P. L. Arnold, T. A. Baker, D. J. Mindiola and C. C. Cummins, *J. Am. Chem. Soc.*, 2000, **122**, 6108–6109.

128 W. J. Evans, S. A. Kozimor, J. W. Ziller and N. Kaltsoyannis, *J. Am. Chem. Soc.*, 2004, **126**, 14533–14547.

129 D. Patel, F. Tuna, E. J. L. McInnes, J. McMaster, W. Lewis, A. J. Blake and S. T. Liddle, *Dalton Trans.*, 2013, **42**, 5224–5227.

130 D. P. Mills, F. Moro, J. McMaster, J. V. Slageren, W. Lewis, A. J. Blake and S. T. Liddle, *Nature Chemistry*, 2011, **3**, 454–460.

131 P. L. Diaconescu and C. C. Cummins, *J. Am. Chem. Soc.*, 2002, **124**, 7660–7661.

132 P. L. Diaconescu and C. C. Cummins, *Inorg. Chem.*, 2012, **51**, 2902–2916.

133 W. J. Evans, C. A. Traina and J. W. Ziller, *J. Am. Chem. Soc.*, 2009, **131**, 17473–17481.

134 P. L. Arnold, S. M. Mansell, L. Maron and D. Mckay, *Nature Chemistry*, 2012, **4**, 668–674.

135 T. Arliguie, M. Lance, M. Nierlich, J. Vigner and M. Ephritikhine, *J. Chem. Soc., Chem. Commun.*, 1994, 847–848.

136 T. Arliguie, M. Lance, M. Nierlich and M. Ephritikhine, *J. Chem. Soc. Dalton Trans.*, 1997, 2501–2504.

137 T. Arliguie, M. Lance, M. Nierlich, J. Vigner and M. Ephritikhine, *J. Chem. Soc., Chem. Commun.*, 1995, 183–184.

138 D. Gourier, D. Caurant, T. Arliguie and M. Ephritikhine, *J. Am. Chem. Soc.*, 1998, **120**, 6084–6092.

139 A. Zalkin and K. N. Raymond, *J. Am. Chem. Soc.*, 1969, **91**, 5667–5668.

140 A. Avdeef, K. N. Raymond, K. O. Hodgson and A. Zalkin, *Inorg. Chem.*, 1972, **11**, 1083–1088.

141 J. Streitwieser Andrew, U. Müller-Westerhoff, G. Sonnichsen, F. Mares, D. G. Morrell, K. O. Hodgson and C. A. Harmon, *J. Am. Chem. Soc.*, 1973, **95**, 8644–8649.

142 A. Zalkin, D. H. Templeton, W. D. Luke and A. Streitwieser, Jr., *Organometallics*, 1982, **1**, 618–622.

143 A. Streitwieser, R. Q. Kluttz, K. A. Smith and W. D. Luke, *Organometallics*, 1983, **2**, 1873–1877.

144 A. Streitwieser, D. Dempf, G. N. La Mar, D. G. Karraker and N. M. Edelstein, *J. Am. Chem. Soc.*, 1971, **93**, 7343–7344.

145 U. Kilimann, R. Herbst-Irmer, D. Stalke and F. T. Edelmann, *Angew. Chem. Int. Ed.*, 1994, **33**, 1618–1621.

146 C. Apostolidis, F. T. Edelmann, B. Kanellakopulos and U. Reiß mann, *Z. Naturforsch B*, 1999, **54b**, 960–962.

147 K. O. Hodgson, D. Dempf and K. N. Raymond, *Chem. Commun.*, 1971, 1592–1593.

148 A. Streitwieser, M. H. Lyttle, H.-K. Wang, T. R. Boussie, A. Weinländer and J. P. Solar, *J. Organomet. Chem.*, 1995, **501**, 245–249.

149 A. Streitwieser, M. T. Barros, H.-K. Wang and T. R. Boussie, *Organometallics*, 1993, **12**, 5023–5024.

150 M. J. Miller and A. Streitwieser, Jr., *J. Organomet. Chem.*, 1981, **209**, C52–C54.

151 K. O. Hodgson and K. N. Raymond, *Inorg. Chem.*, 1973, **12**, 458–466.

152 W. D. Luke and A. Streitwieser, Jr., *J. Am. Chem. Soc.*, 1981, **103**, 3241–3243.

153 V. Lorenz, B. M. Schmiege, C. G. Hrib, J. W. Ziller, A. Edelmann, S. Blaurock, W. J. Evans and F. T. Edelmann, *J. Am. Chem. Soc.*, 2011, **133**, 1257–1259.

154 D. B. Beach, K. D. Bomben, N. M. Edelstein, D. C. Eisenberg, W. L. Jolly, R. Shinomoto and A. Streitwieser, Jr., *Inorg. Chem.*, 1986, **25**, 1735–1737.

155 J. G. Brennan, J. C. Green and C. M. Redfern, *J. Am. Chem. Soc.*, 1989, **111**, 2373–2377.

156 W. Liu, M. Dolg and P. Fulde, *J. Chem. Phys.*, 1997, **107**, 3584–3591.

157 G. Bruno, E. Ciliberto, R. D. Fischer, I. L. Fragalà and A. W. Spiegl, *Organometallics*, 1982, **1**, 1060–1062.

158 J. C. Green, M. P. Payne and A. Streitwieser, Jr., *Organometallics*, 1983, **2**, 1707–1710.

159 F. Billiau, G. Folcher, H. Marquet-Ellis, P. Rigny and E. Saito, *J. Am. Chem. Soc.*, 1981, **103**, 5603–5604.

160 D. C. Eisenberg, A. Streitwieser and W. K. Kot, *Inorg. Chem.*, 1990, **29**, 10–14.

161 T. R. Boussie, D. C. Eisenberg, J. Rigsbee, A. Streitwieser and A. Zalkin, *Organometallics*, 1991, **10**, 1922–1928.

162 M. Dolg and P. Fulde, *Chem. Eur. J.*, 1998, **4**, 200–204.

163 J.-C. Berthet, P. Thuéry and M. Ephritikhine, *Organometallics*, 2008, **27**, 1664–1666.

164 C. Clavague and J.-P. Dognon, *Theor. Chem. Acc.*, 2011, **129**, 447–452.

165 T. R. Boussie, R. M. Moore, A. Streitwieser, A. Zalkin, J. G. Brennan and K. A. Smith, *Organometallics*, 1990, **9**, 2010–2016.

166 T. M. Gilbert, R. R. Ryan and A. P. Sattelberger, *Organometallics*, 1988, **7**, 2514–2518.

167 C. Boisson, J.-C. Berthet, M. Lance, J. Vigner, M. Nierlich and M. Ephritikhine, *J. Chem. Soc. Dalton Trans.*, 1996, 947–953.

168 J.-C. Berthet and M. Ephritikhine, *J. Chem. Soc., Chem. Commun.*, 1993, 1566–1567.

169 J.-C. Berthet, M. Nierlich and M. Ephritikhine, *Eur. J. Inorg. Chem.*, 2002, 850–858.

170 J.-C. Berthet, M. Lance, M. Nierlich and M. Ephritikhine, *Chem. Commun.*, 1998, 1373–1374.

171 C. Boisson, J.-C. Berthet, M. Ephritikhine, M. Lance and M. Nierlich, *J. Organomet. Chem.*, 1996, **522**, 249–257.

172 S. M. Cendrowski-Guillaume, M. Lance, M. Nierlich and M. Ephritikhine, *Organometallics*, 2000, **19**, 3257–3259.

173 S. M. Cendrowski-Guillaume, M. Nierlich and M. Ephritikhine, *Eur. J. Inorg. Chem.*, 2001, 1495–1498.

174 S. M. Cendrowski-guillaume, G. Le Gland, M. Nierlich and M. Ephritikhine, *Eur. J. Inorg. Chem.*, 2003, 1388–1393.

175 S. M. Cendrowski-Guillaume, M. Nierlich and M. Ephritikhine, *J. Organomet. Chem.*, 2002, **643-644**, 209– 213.

176 A. R. Schake, L. R. Avens, C. J. Burns, D. L. Clark, A. P. Sattelberger and W. H. Smith, *Organometallics*, 1993, **12**, 1497–1498.

177 G. R. Sienel, A. W. Spiegl and R. D. Fischer, *J. Organomet. Chem.*, 1978, **160**, 67–73.

178 D. Baudry, E. Bulot, M. Ephritikhine, M. Nierlich, M. Lance and J. Vigner, *J. Organomet. Chem.*, 1990, **388**, 279–287.

179 W. J. Evans, G. W. Nyce and J. W. Ziller, *Angew. Chem. Int. Ed.*, 2000, **39**, 240–242.

180 W. J. Evans, K. A. Miller, S. A. Kozimor, J. W. Ziller, A. G. DiPasquale and A. L. Rheingold, *Organometallics*, 2007, **26**, 3568–3576.

181 W. J. Evans, E. Montalvo, S. A. Kozimor and K. A. Miller, *J. Am. Chem. Soc.*, 2008, **130**, 12258–12259.

182 O. T. Summerscales and F. G. N. Cloke, *Coord. Chem. Rev.*, 2006, **250**, 1122–1140.

183 F. G. N. Cloke, J. C. Green and C. N. Jardine, *Organometallics*, 1999, **18**, 1080–1086.

184 F. M. Chadwick, A. E. Ashley, G. Wildgoose, J. M. Goicoechea, S. Randall and D. O'Hare, *Dalton Trans.*, 2010, **39**, 6789–6793.

185 F. G. N. Cloke and P. B. Hitchcock, *J. Am. Chem. Soc.*, 2002, **124**, 9352–9353.

186 J. H. Farnaby, F. G. N. Cloke, M. P. Coles, J. C. Green and G. Aitken, *Comptes Rendus Chimie*, 2010, **13**, 812–820.

CHAPTER 2: URANIUM(III) MIXED-SANDWICH COMPLEXES

2.1 Introduction

Sandwich complexes consist of a metal centre that is 'sandwiched' between two aromatic ligands and have been prevalent in the literature since the discovery of ferrocene by several research groups in 1951.[1–4] Over the ensuing decades this area of organometallic chemistry branched into half-sandwich complexes and complexes with two-or more metal centres such as multi-decker sandwich complexes, inverse sandwich complexes and double sandwich complexes (**Figure 2.1**). Mixed-sandwich systems, which have two non-identical aromatic ligands have also been synthesised.

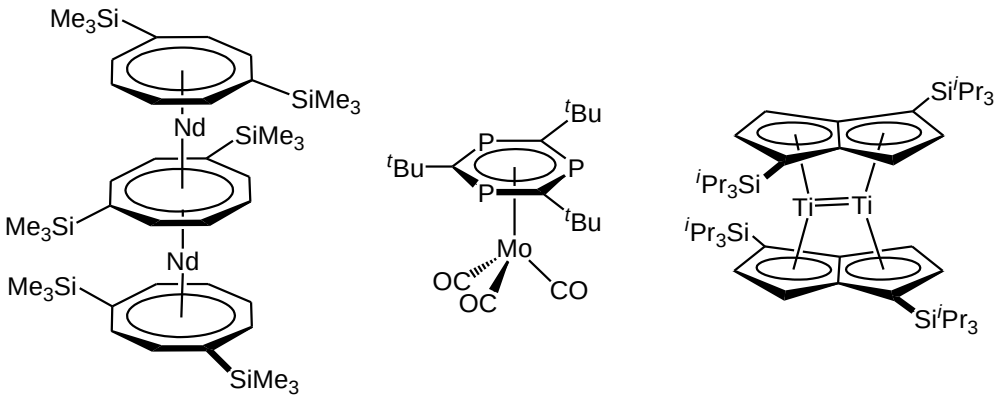

Figure 2.1 Examples of sandwich complexes: a neodymium triple-decker sandwich (left), molybdenum half-sandwich (centre) and titanium double sandwich (right).[5–7]

The sandwich framework has been widely used in organometallic chemistry, and has become a popular choice in catalyst design.[8] The aromatic ligands provide a suitable steric and energetic environment for the isolation of metal complexes in various oxidation states and tend to be innocent towards reactivity with the substrates. Recently however, researchers have reported the activation of C–H bonds within the substituents

of the ligands, which results in oxidation of the metal centre and the formation of an M–C σ-bond (see section 2.3.7).[9–20]

Previous work by Cloke and colleagues has included the use of a mixed-sandwich system in the synthesis of uranium(III) and uranium(IV) complexes. These complexes are composed of a substituted COT or pentalene ligand, and a substituted cyclopentadienyl ring (**Figure 2.2**), and demonstrate that the mixed-sandwich motif provides suitable kinetic stabilisation of the +3 oxidation state, without compromising the thermodynamic reactivity of the complexes with small molecules. As such further variations of this ligand system have been explored with alteration of the five-membered ring and COT substituents.[21,22]

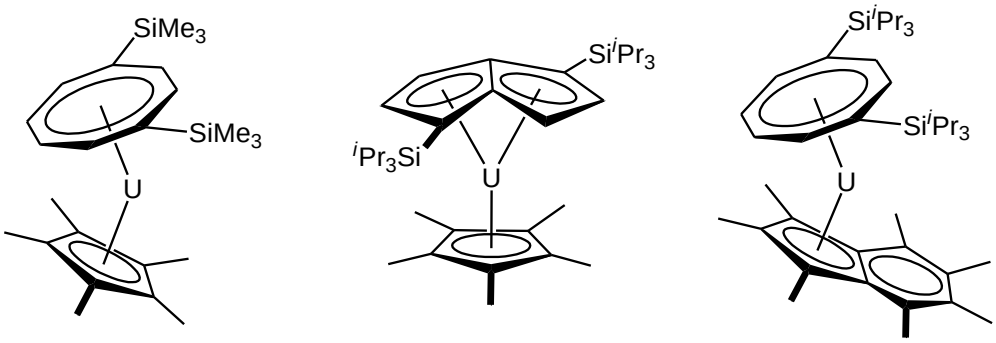

Figure 2.2 Examples of uranium(III) mixed-sandwich complexes synthesised by Cloke *et al.*.[21,23,24]

In order to further these studies and find trends regarding the electronic properties of these complexes with respect to the activation of small molecules, this thesis aims to synthesise a range of novel uranium(III) mixed-sandwich complexes, and analyse the properties of these complexes by cyclic voltammetry. In order to obtain objective comparisons, the [U(COT$^{(Si\mathit{i}Pr3)2}$)(Cp^R)] motif is utilised so that the only variation arises from the five-membered ring, either by alteration of the ring substituents or by heteroatom incorporation into the ring.

2.2 Synthesis and characterisation of cyclopentadienyl-based uranium(III) mixed-sandwich complexes

Synthetic routes to the previously synthesised mixed-sandwich complexes involved successive salt metathesis reactions of UI_3 or UCl_4 with the ligand salts.[21,25] The solubility of these starting materials precluded the use of non-coordinating solvents for these reactions but reasonable yields were obtained with ethereal solvents. The synthetic route for the synthesis of the new mixed-sandwich complexes was based on the published preparation of [U(COT$^{(Si\textit{i}Pr3)2}$)(Cp*)(THF)].[26]

2.2.1 Synthetic route to mixed-sandwich complexes

The synthesis of the mixed-sandwich complexes was achieved by successive addition of the ligand salts to UI_3 according to **Figure 2.3**. Full conversion of UI_3 to the [$UI_2(Cp^R)(THF)_n$] intermediate was observed over several hours by a gradual colour change from deep blue to green or purple. Subsequent work up removed residual UI_3 and KI and addition of a deficiency of K_2[COT$^{(Si\textit{i}Pr3)2}$] solution was required in order to minimise the formation of the substituted uranocene, [U(COT$^{(Si\textit{i}Pr3)2}$)$_2$].

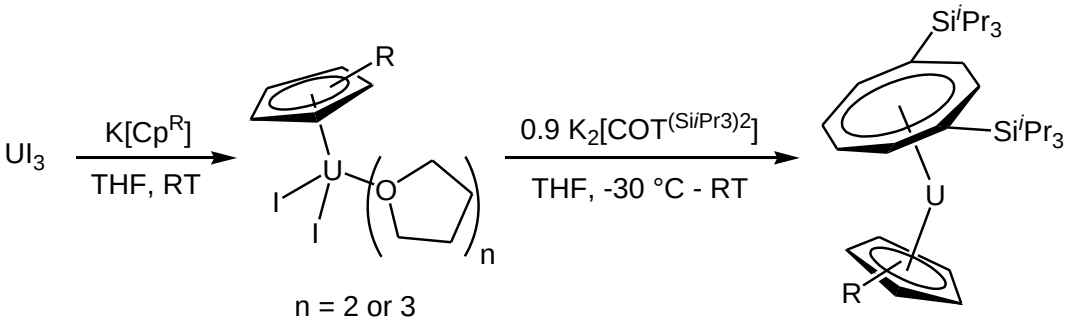

Figure 2.3 Synthesis of [U(COT$^{(Si\textit{i}Pr3)2}$)(Cp^R)], where R = ^{t}Bu (**2.1**), ^{t}Bu$_2$ (**2.2**), ^{t}Bu$_3$ (**2.3**) or (Si^{i}Pr$_3$)$_2$ (**2.4**).

Filtration of the mixed-sandwich complexes to remove KI and residual $[UI_2(Cp^R)(THF)_n]$ was ineffective for $[U(COT^{(Si\textit{i}Pr3)2})(Cp^{\textit{t}Bu})(THF)]$ (**2.1THF**) unless the mixture was first treated with pentane then stripped to dryness several times. This resulted in removal of coordinated THF to yield the base-free complex, $[U(COT^{(Si\textit{i}Pr3)2})(Cp^{\textit{t}Bu})]$ (**2.1**). Desolvation of complexes **2.2** – **2.4** however occurred as soon as THF was removed *in vacuo*.

Synthesis of $[U(COT^{(Si\textit{i}Pr3)2})(Cp^{\textit{t}Bu2})]$ (**2.2**) in adequate yield proved challenging as two additional products were observed in the ^{1}H NMR spectrum of the crude product mixture. Separation of these species by crystallisation revealed the side products to include $[\{U(Cp^{\textit{t}Bu2})_2\}_2(\mu\text{-}I)_2]$ (**6.1**) and $[U(Cp^{\textit{t}Bu2})_3]$ (**6.3**). The presence of these other complexes is rationalised by the increased solubility of $[UI_2(Cp^{\textit{t}Bu2})(THF)_n]$ in comparison to UI_3. However the yield of the desired complex could be improved by addition of $K[Cp^{\textit{t}Bu2}]$ as a powder instead of a suspension.

The synthesis of $[U(COT^{(Si\textit{i}Pr3)2})(Cp^{\textit{t}Bu3})]$ (**2.3**) was also modified to exclude work up of the intermediate as $[UI_2(Cp^{\textit{t}Bu3})(THF)_n]$was found to be insoluble in non-coordinating solvents. However adaptation of the synthetic route to a two-step, one-pot synthesis was successful in this instance and significantly improved the yield.

*2.2.2 NMR studies of mixed-sandwich complexes **2.1** - **2.4***

Despite the pitfalls of NMR spectroscopy for paramagnetic complexes which include loss of observable multiplicity, ambiguity in integration and in some cases, unobservable resonances, NMR has been an important tool in the characterisation of the uranium complexes synthesised in this thesis. A useful feature of paramagnetic complexes is that most obey the Curie law, whereby the chemical shifts of the resonances are inversely proportional to temperature. Therefore, in addition to characterisation of proton and heteronuclei resonances, variable temperature ^{1}H NMR

has been used to provide additional information on the properties of the complexes in solution.

Analysis of complexes **2.1** – **2.4** by variable temperature ^{1}H NMR has shown the *tert*-butyl substituted complexes have clearly defined resonances at room temperature and follow the Curie law between -80 and +100 °C (**Figure 2.4**). However, the *iso*-propyl and *tert*-butyl protons for **2.1** do not follow the Curie law, a feature which was also reported by Andersen and co-workers for [(Cp^{Me})$_3$U(C(O)^{t}Bu)] and was ascribed to a temperature-dependent conformational equilibrium.[27]

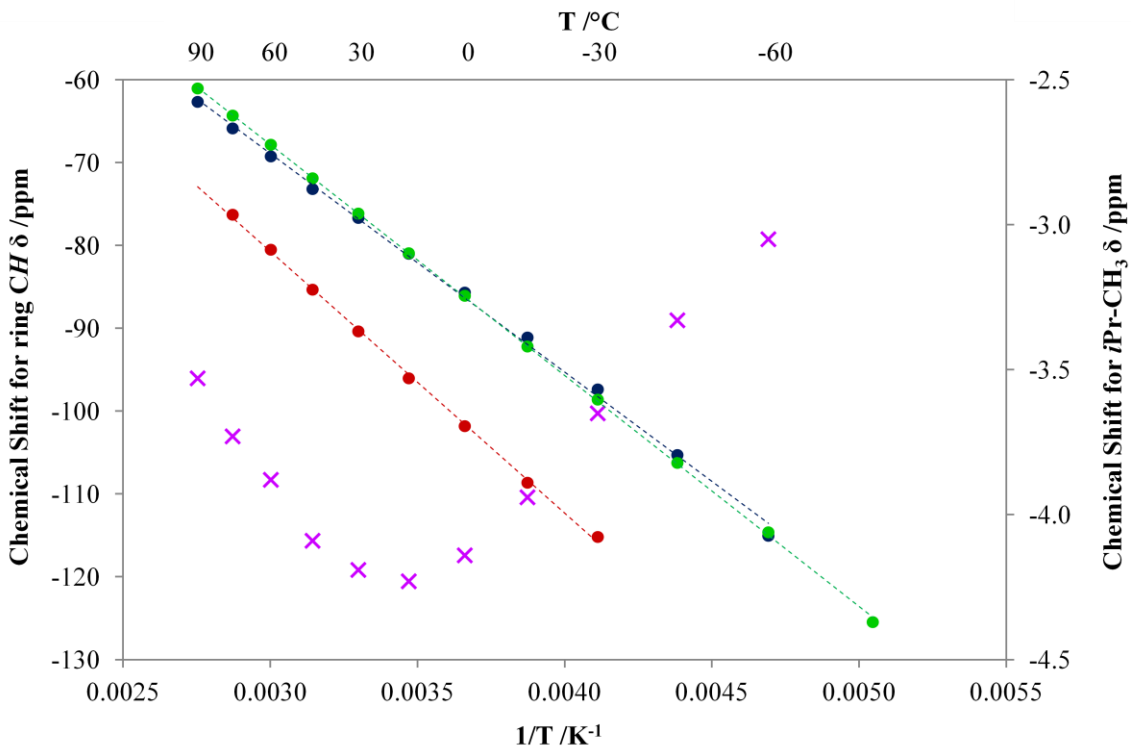

Figure 2.4 Chemical shift *vs* 1/T for a COT/Cp-C*H* resonance of **2.1** (blue, y = -26358x + 10.25, R^2 = 0.998), **2.2** (red, y = -31608x + 14.11, R^2 = 0.999) and **2.3** (green, y = -27885x +15.84, R^2 = 1.00) and chemical shift *vs* 1/T for an ^{i}Pr-C*H*$_3$ resonance of **2.1** (purple crosses).

In the case of **2.1**, it is the protons that are furthest from the metal centre that are most affected by conformational changes as rotation of both rings allows for variation in the interactions between the *tert*-butyl substituent and the *iso*-propyl groups. This feature was not observed in the NMR of **2.2** and **2.3** and it is postulated that this effect is minimised by the presence of additional *tert*-butyl groups which dictate that the *iso*-propyl groups always interact with one of the *tert*-butyl substituents.

The ^{1}H NMR spectrum of [U(COT$^{(SiiPr3)2}$)(Cp$^{(SiiPr3)2}$)] (**2.4**) at ambient temperature did not show any clearly defined resonances, and variable temperature ^{1}H NMR shows that this complex illustrates fluxional behaviour at this temperature (**Figure 2.5**).

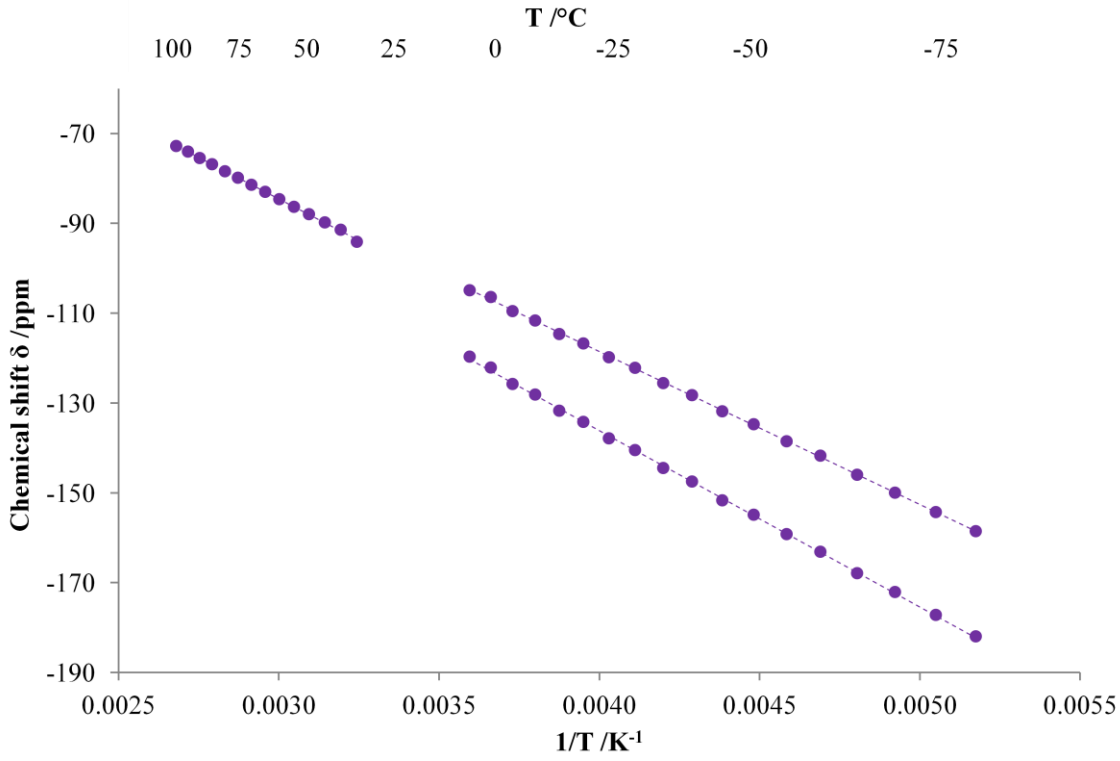

Figure 2.5 Plot of chemical shift *vs* 1/T for two COT ring proton resonances in **2.4**. Above 35 °C, the data fit the line y = -37117x + 26.77, R^2 = 0.9993. Below 5 °C the data fit the lines y = -34043x + 17.64, R^2 = 0.9998 (above) and y = -39253x + 20.87, R^2 = 0.9996 (below)

Below 5 °C, the ring protons resolve into nine separate resonances, indicating that this complex has C_1 symmetry on the timescale of the experiment. Between 5 and 35 °C these resonances begin to coalesce and are not observed in the spectra. Above 35 °C, five ring proton environments are observed, indicating that there is free movement of the rings on the timescale of the experiment, giving rise to C_s symmetry. The proton resonances of the *iso*-propyl groups overlap between -30 and 70 °C and a coalescence temperature could not therefore be determined. These data also illustrate that above and below the coalescence temperature, Curie-Weiss behaviour is observed.

*2.2.3 Molecular structure of [U(COT$^{(SiiPr3)2}$)(Cp^{tBu})(THF)] (**2.1THF**)*

Single crystals of **2.1THF** were obtained from slow cooling saturated pentane solutions to -35 °C and the structure was solved with two molecules in the unit cell (**Figure 2.6**). Comparison of **2.1THF** with previously synthesised uranium(III) mixed-sandwich complexes incorporating Cp*, Cp^{Me4} and Cp^{Me} ligands illustrates little variation in the U–COT centroid and U–Cp^R centroid distances (1.96(2) – 1.977(5) and 2.499(6) – 2.50(2) Å respectively).[28] The COT–U–Cp^R angle however varies by up to 5° and it was observed that the angle increases as the ligand size increases (139.8(5)° when R = Me, 141.8(2)° for R = Me_4, and 144.5(2)° for R = Me_5), giving rise to a larger pocket for the smaller complexes. Based on this trend, it is concluded that complex **2.1THF** is smaller than [U(COT$^{(SiiPr3)2}$)(Cp^{Me4})(THF)], and may therefore exhibit different reactivity. Further studies on the sterics of all the mixed-sandwich complexes are discussed in Chapter 5.

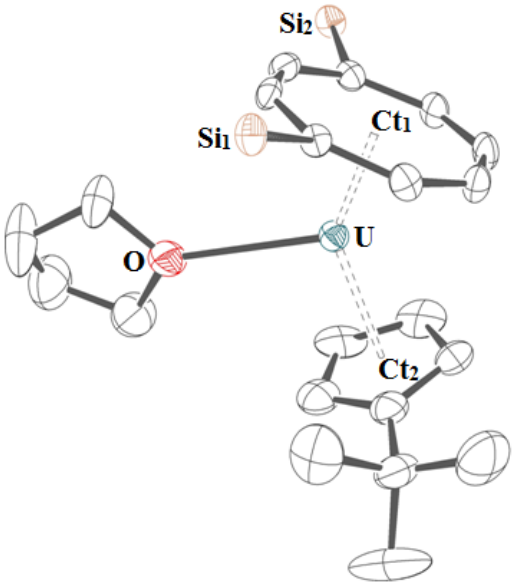

Figure 2.6 ORTEP view of **2.1THF** with thermal ellipsoids at 50% probability; hydrogen atoms and COT *iso*-propyl groups have been omitted for clarity. Selected bond distances (Å) and angles (°): U–Ct_1 1.9740(4), 1.9730(4); U–Ct_2 2.5061(4), 2.5046(4); U–O 2.673(6), 2.671(6); Ct_1–U–Ct_2 140.574(19), 140.768(19).

*2.2.4 Molecular structures of the desolvated mixed-sandwich complexes (**2.1** – **2.4**)*

Single crystals of all the mixed-sandwich complexes were obtained from slow cooling saturated pentane solutions to -35 °C (**Figure 2.7**). Selected data are presented in **Table 2.1**.

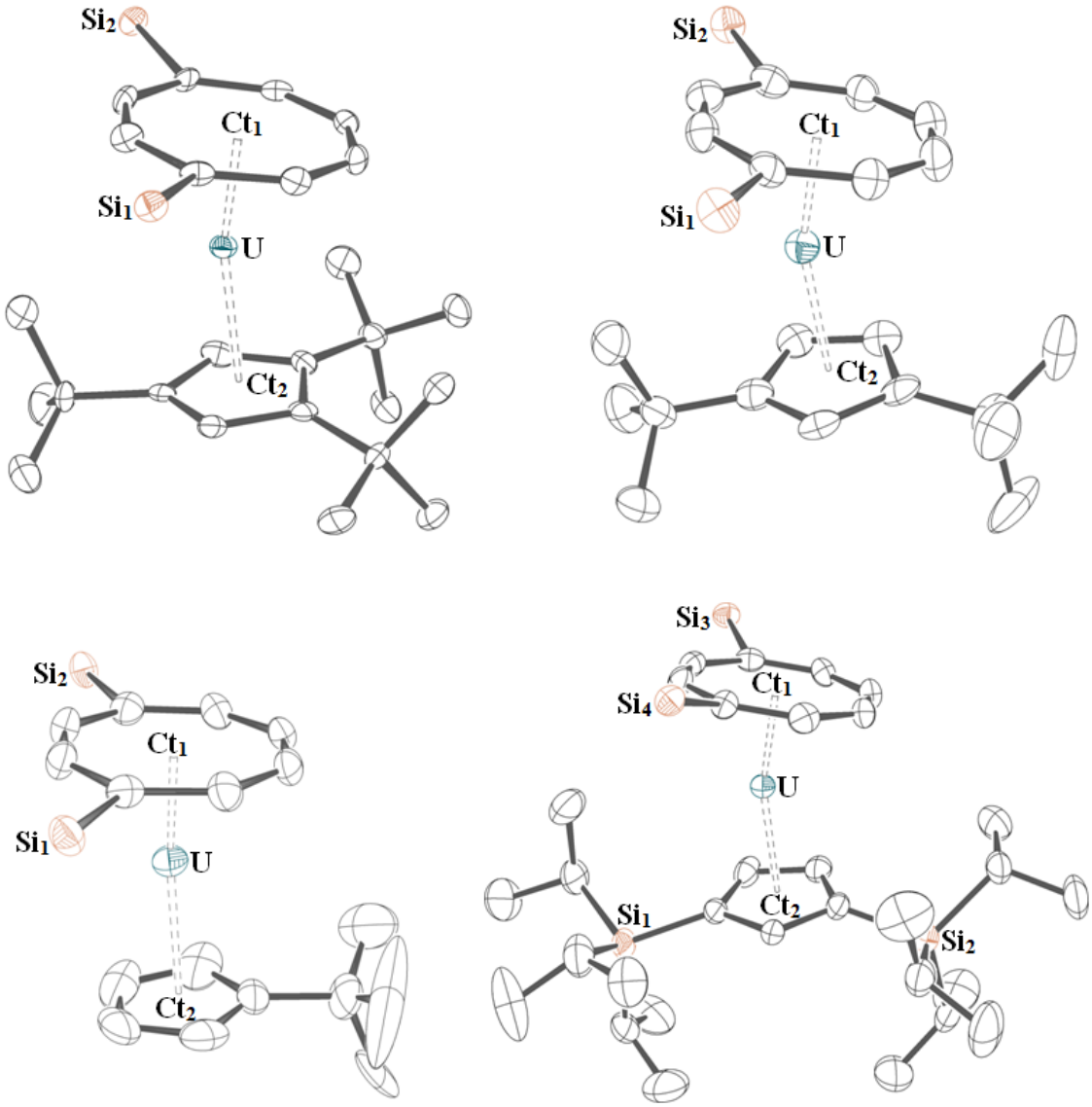

Figure 2.7 ORTEP views of **2.3** (top left), **2.2** (top right), **2.1** (bottom left), and **2.4** (bottom right) with thermal ellipsoids at 50% probability; hydrogen atoms and COT *iso*-propyl groups have been omitted for clarity.

Comparison of complexes **2.1** and **2.1THF** show that upon coordination of THF the U–Cp and U–COT distances increase. This is a minor difference for U–Cp (0.011 Å), but a more significant difference is observed for U–COT (0.085 Å). Trends relating to the U–Cp, U–COT and Cp–U–COT data are not apparent from analysis of these four complexes alone, but are discussed in depth in Chapter 5.

It has also been observed with all the mixed-sandwich complexes that there is a degree of ring slippage for the five-membered ring. This is marginal for **2.1** as observed by the U–C(Cp) distances which range from 2.766(11) – 2.776(13) Å, but is more significant for **2.3**, whose U–C(Cp) distances range from 2.724(6) – 2.823(6) Å. This gives rise to a pseudo η^3 U–Cp interaction with the two adjacent *tert*-butyl groups lying on the two carbon atoms that are furthest from the metal. Similarly, the two di-substituted complexes show a slight tilt of the two adjacent unsubstituted carbon atoms towards the metal centre, illustrating that these complexes allow tilting of the ligands in order to accommodate the sterically demanding groups.

Compound	**Distances (Å)**		**Angles (°)**
	Ct_1–U	**Ct_2–U**	**Ct_1–U–Ct_2**
[U(COT$^{(Si\textit{i}Pr3)2}$)(Cp$^{\textit{t}Bu}$)] (2.1)	1.8891(7)	2.4950(7)	174.66(4)
[U(COT$^{(Si\textit{i}Pr3)2}$)(Cp$^{\textit{t}Bu2}$)] (2.2)	1.9129(4) 1.9150(4)	2.4706(4) 2.4772(4)	161.09(2) 159.83(2)
[U(COT$^{(Si\textit{i}Pr3)2}$)(Cp$^{\textit{t}Bu3}$)] (2.3)	1.92263(18)	2.48047(18)	167.042(10)
[U(COT$^{(Si\textit{i}Pr3)2}$)(Cp$^{(Si\textit{i}Pr3)2}$)] (2.4)	1.9086(7)	2.4830(7)	161.79(4)

Table 2.1 Bond lengths, distances and angles for **2.1** – **2.4**. Ct_1 is the centroid for the COT$^{(Si\textit{i}Pr3)2}$ ligand and Ct_2 is the centroid for the Cp^R ligand.

2.2.5 Cyclic voltammetry of cyclopentadienyl mixed-sandwich complexes

Studies by Cloke *et al.* on several uranium(III) mixed-sandwich complexes have shown little variation in the U^{IV}/U^{III} redox potential when altering the substituents on the cyclopentadienyl ring.[22] As such it was anticipated that studies of complexes **2.1** – **2.4**

would give similar values for the U^{IV}/U^{III} redox couple. For the purpose of comparing redox values, all experiments were conducted under identical conditions as significant variations can occur when altering solvent and electrolyte. This is also the case for the *in situ* ferrocenium/ferrocene reference couple, and its decamethylferrocene analogue.[29] Comparison of the observed redox potentials can only therefore be conducted when identical conditions are used and conclusions about the results in reference to other systems or reference electrodes can only be made with a degree of caution.

Upon application of potential in the anodic direction, an oxidative half-wave is observed between -2.5 and -1.5 V *vs* $[FeCp_2]^{+/0}$ (process II, **Figure 2.8**). Scanning to a less negative potential gives rise to a second oxidative wave for all complexes (process III), a third wave for the *tert*-butyl-substituted complexes (process IV) and several more overlapping waves for **2.1**. Reverse scanning indicates these last processes in **2.1** are irreversible, but that processes II and III are quasi-reversible for all complexes. Process IV was found to be quasi-reversible for complex **2.3** but was ambiguous for the other *tert*-butyl complexes. Further scanning in the cathodic direction revealed a reductive half-wave (process I) close to the solvent breakdown, which was also found to be quasi-reversible for **2.3** but ambiguous for the other complexes. Scanning in both directions across the entire solvent window and across individual processes confirmed these processes to be reproducible for five cycles at varying scan rates (50 – 200 $mV \cdot s^{-1}$), although some changes were observed in the voltammogram of **2.1** which indicated that this complex was the least stable under the experimental conditions.

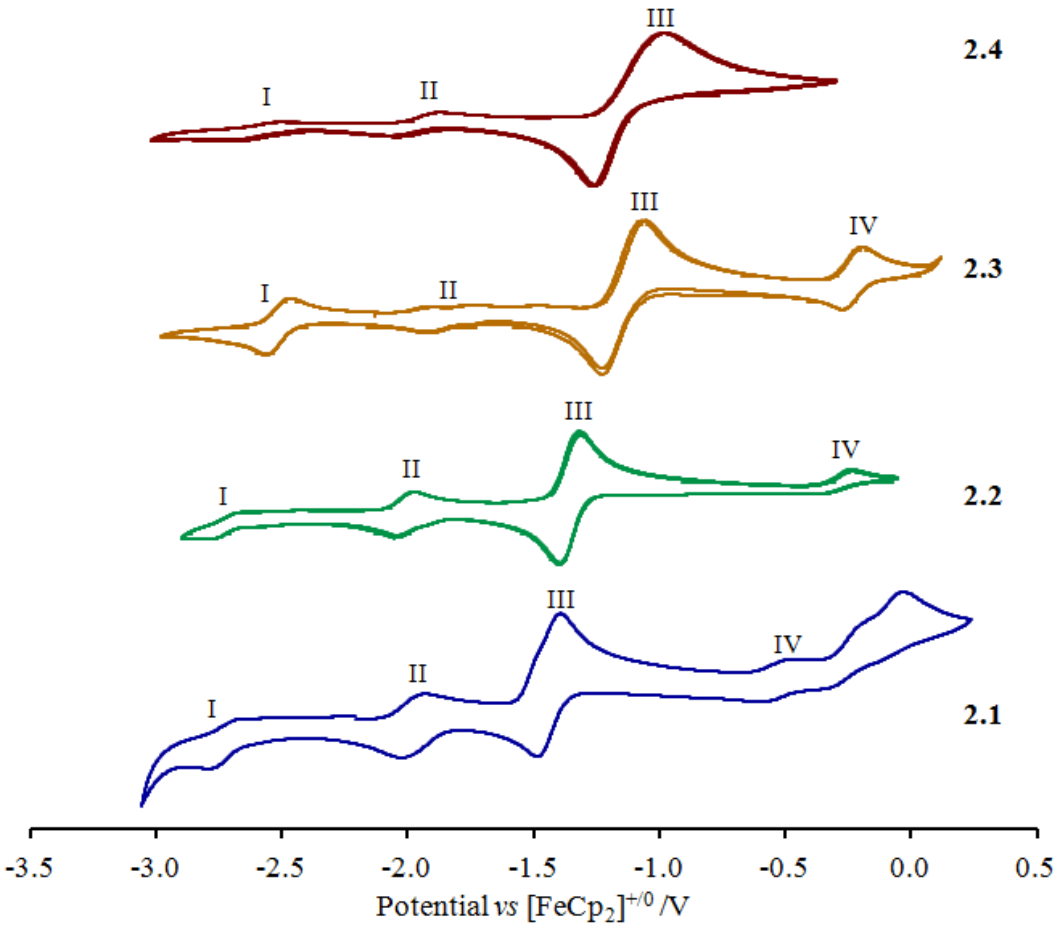

Figure 2.8 Cyclic voltammograms of 5-10 mM solutions of uranium(III) mixed-sandwich complexes in 0.05 M [^{n}Bu$_4$N][B(C$_6$F$_5$)$_4$]/THF at 100 mV·s^{-1}. A minimum of three cycles are shown for all complexes, except **2.1**, where only the first cycle is shown.

The $E_{½}$ values for process II are in the range of -2.01 and -1.83 V *vs* $[FeCp_2]^{+/0}$, and are assigned to the U^{IV}/U^{III} redox couples (**Table 2.2**). This is in general agreement with values quoted in the literature and with the data obtained for a uranium(IV) mixed-sandwich halide complex, [U(COT$^{(SiiPr3)2}$)(Cp^{tBu})Cl] (**3.5**), which has a U^{IV}/U^{III} reduction potential at -2.04 V *vs* $[FeCp_2]^{+/0}$ (see Chapter 3). Ideally, verification of this assignment would be derived from a uranium(IV) cation, [U(COT$^{(SiiPr3)2}$)(Cp^{R})]$^{+}$, as the presence of the halide gives rise to variation in the redox potentials. However, studies

by colleagues of the author on [U(COT$^{(SiiPr3)2}$)(Cp^{Me4Et})][B(C$_6$F$_5$)$_4$] found this complex to be highly reactive in THF and meaningful data could not be obtained.[30] The synthesis and electrochemical analysis of an alternative cation has therefore not been attempted.

The other observed processes (I, III and IV) have not been assigned and the electrochemical events to which they correspond can only be speculated upon. However, uranium(III) mixed-sandwich complexes have been proven to both activate C–H bonds within the substituents of the ligands and ring open THF (see section 2.3.7). The fact that several electrochemical events are observed is perhaps therefore unsurprising, given the highly reactive nature of these complexes. Further studies to definitively assign processes I, III and IV are however, beyond the scope of this thesis.

	$E_{½}$ values (V) *vs* [FeCp$_2$]$^{+/0}$			
	Process I	***Process II***	*Process III*	*Process IV*
[U(COT$^{(SiiPr3)2}$)(Cp$^{(SiiPr3)2}$)] (2.4)	-2.58	**-1.95**	-1.12	-
[U(COT$^{(SiiPr3)2}$)(Cp^{tBu3})] (2.3)	-2.51	**-1.83**	-1.14	-0.234
[U(COT$^{(SiiPr3)2}$)(Cp^{tBu2})] (2.2)	-2.72	**-2.01**	-1.36	-0.309
[U(COT$^{(SiiPr3)2}$)(Cp^{tBu})] (2.1)	-2.73	**-1.98**	-1.44	-0.527

Table 2.2 $E_{½}$ values (V) *vs* [FeCp$_2$]$^{+/0}$ for uranium(III) mixed-sandwich complexes. Process II has been assigned to the U^{IV}/U^{III} redox process.

Comparison of the values for the proposed U^{IV}/U^{III} redox couples reported here with those found by colleagues of the author illustrates the reducing ability of mixed-sandwich complexes incorporating COT$^{(SiiPr3)2}$ is as follows, where [U]^R denotes a

uranium(III) mixed-sandwich complex with R substituents on the cyclopentadienyl ligand:[30]

$$[U]^{tBu3} < [U]^{(SiiPr3)2} < [U]^{tBu} < [U]^{tBu2} < [U]^{Me4SiMe3} < [U]^{Me4} < [U]^{Me4iPr} < [U]^{Me4Et} < [U]^{Me5}$$

These complexes clearly demonstrate that addition of electron-donating groups to the cyclopentadienyl ring increases the electron density at the uranium centre and destabilises the uranium(III) oxidation state. However, [U(COT$^{(SiiPr3)2}$)(Cp^{tBu3})] (**2.3**), was an anomaly in the trend and the U^{IV}/U^{III} couple for this complex had the least negative potential. This is rationalised by the coordination of THF to the mixed-sandwich complexes in solution. All the complexes under study were shown to coordinate THF by observable shifting of the resonances in the ^{1}H NMR spectrum when this solvent was added to the solutions. However, this was not the case for **2.3**, and the absence of coordinated THF gives rise to less electron density at the metal centre, resulting in a less negative U^{IV}/U^{III} redox couple. Excluding the data obtained for **2.3** from the overall analysis shows that the total variation in potential is only 0.18 V (when comparing $[U]^{Me5}$ to $[U]^{(SiiPr3)2}$), illustrating that altering the substituents on the cyclopentadienyl ring has little effect on the redox properties of the complex.

Comparison of these values with the analogous pentalene complex, [U(Pn$^{(SiiPr3)2}$)(Cp*)] (-2.50 V *vs* $[FeCp_2]^{+/0}$), illustrates that exchange of the COT ring for the pentalene ring has a more substantial effect on the redox couple than varying the cyclopentadienyl substituents.[31] This value is 0.37 V more negative than the corresponding redox process for [U(COT$^{(SiiPr3)2}$(Cp*)], illustrating that the pentalene complex is more reducing than the COT variant. This is the rationale behind the activation of dinitrogen which occurs with the pentalene complex but not with the analogous COT complex.[24]

2.3 Synthesis and characterisation of heterocyclic uranium(III) mixed-sandwich complexes

Previous studies by Cloke *et al.* investigated the potential of heterocyclic ligands Cp^{EMe4} (E = P and As) in the synthesis of $[UI_2(Cp^{EMe4})]$ complexes.[32] Whilst the attempts to synthesise the base-free complexes were unsuccessful, these ligands formed $[UI_2(Cp^{EMe4})(THF)_3]$ species analogous to their cyclopentadienyl analogues. This offered the potential for these ligands to be used in the synthesis of mixed-sandwich complexes.

2.2.1 Synthetic route to heterocyclic mixed-sandwich complexes

Synthesis of the mixed-sandwich complexes used the two-step, one-pot methodology as the $[UI_2(Cp^{EMe4})(THF)_3]$ intermediates were found to be insoluble in hydrocarbon solvents (**Figure 2.9**). Removal of solvent resulted in complete desolvation of the mixed-sandwich complexes, which could be accelerated by heating the complex to 80 °C under high vacuum (10^{-6} mbar).

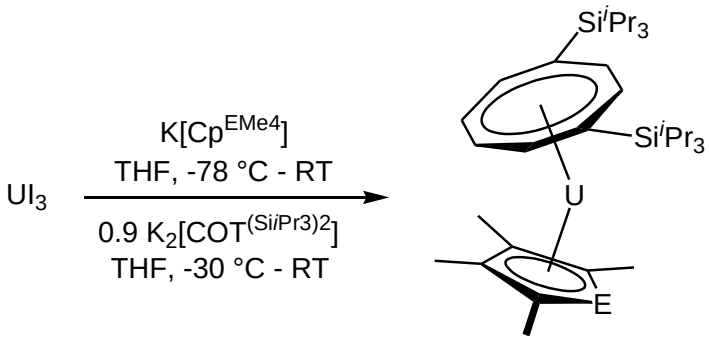

Figure 2.9 Synthesis of $[U(COT^{(SiiPr3)2})(Cp^{EMe4})]$, where E is N (**2.5**), P (**2.6**) or As (**2.7**).

Despite using a deficiency of $K_2[COT^{(SiiPr3)2}]$, the corresponding uranocene was a major side product in all reactions. Whilst this resulted in poor to moderate crystal yields (15 – 40%) of **2.6** and **2.7**, uranocene was the only product obtained in half of the syntheses of **2.5** conducted. In order to improve the reliability and yield of this reaction two alternative methods were attempted (**Figure 2.10**).

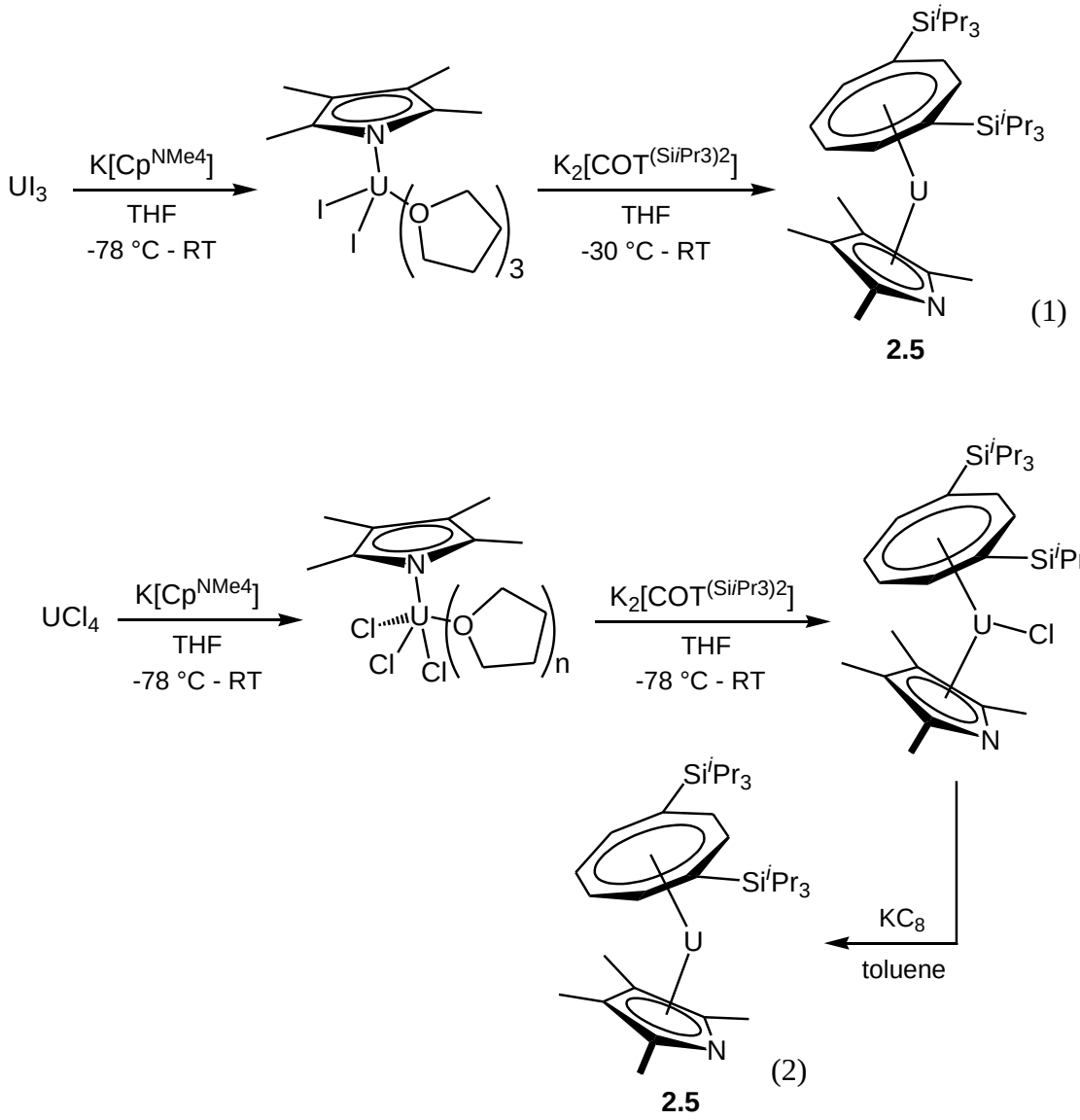

Figure 2.10 Alternative synthetic routes to **2.5.**

Method (1) aimed to isolate $[UI_2(Cp^{NMe4})(THF)_3]$ in order to ensure no residual UI_3 remained, and therefore reduce the formation of uranocene. However, whilst the intermediate was soluble in aromatic solvents, isolation of this complex did not improve the overall synthesis and uranocene was formed exclusively alongside brown intractable solids. Method (2) focused on the synthesis of the uranium(IV) mixed-sandwich chloride, which could then be reduced to **2.5**. However addition of $K_2[COT^{(SiiPr3)2}]$ to a solution of $[UCl_3(Cp^{NMe4})(THF)_n]$ also gave rise to a mixture of uranocene and brown intractable solids. The unsuccessful nature of these preliminary tests meant that these approaches were not explored further and other alternative syntheses were not attempted.

2.3.2 Characterisation of heterocyclic mixed-sandwich complexes

The phospholyl and arsolyl mixed-sandwich complexes were fully characterised by NMR spectroscopy. However, full characterisation of **2.5THF** was precluded as it was always present in equilibrium with **2.5**, preventing definitive assignment of the coordinated THF resonances. The presence of both species in solution and the differing pattern of proton resonances for the pyrrolyl complex in comparison to the phospholyl and arsolyl analogues gave rise to the hypothesis that **2.5** is dimeric in solution (**Figure 2.11**). Attempts to confirm this using DOSY NMR spectroscopy were inconclusive and cryoscopic molecular weight determination experiments were deemed unsuitable for this complex due to its limited solubility.

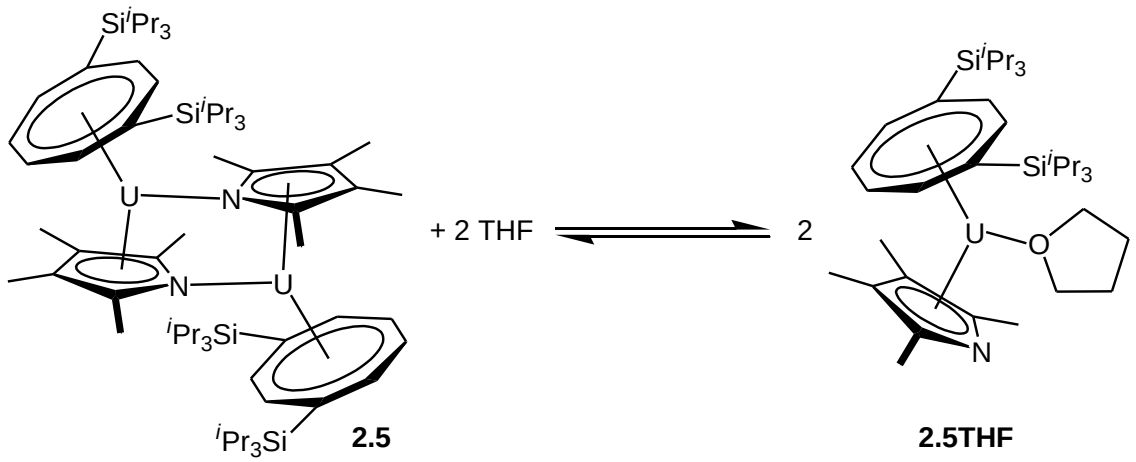

Figure 2.11 The proposed equilibrium between **2.5** and **2.5THF**.

To investigate the coordination of THF to **2.5** in solution, a series of samples with increasing concentrations of THF were analysed and independent integrals of the resonances of **2.5** and **2.5THF** were compared with an internal standard. This experiment illustrated exponential decrease of **2.5** with concurrent formation of **2.5THF** as the concentration of THF increased (**Figure 2.12**).

These data indicate that **2.5** remains present in solution until THF becomes the sole constituent of the solvent. However, preparation of samples in d_8-THF found there were traces (<2%) of **2.5** in solution. Addition of benzene to this solution gave rise to a gradual increase in the ratio of **2.5**:**2.5THF**, which is consistent with the proposed equilibrium in **Figure 2.11**. The data further illustrate that uranium is conserved in this process and that there are no unobservable intermediates in the conversion of **2.5** to **2.5THF** (**Figure 2.12**).

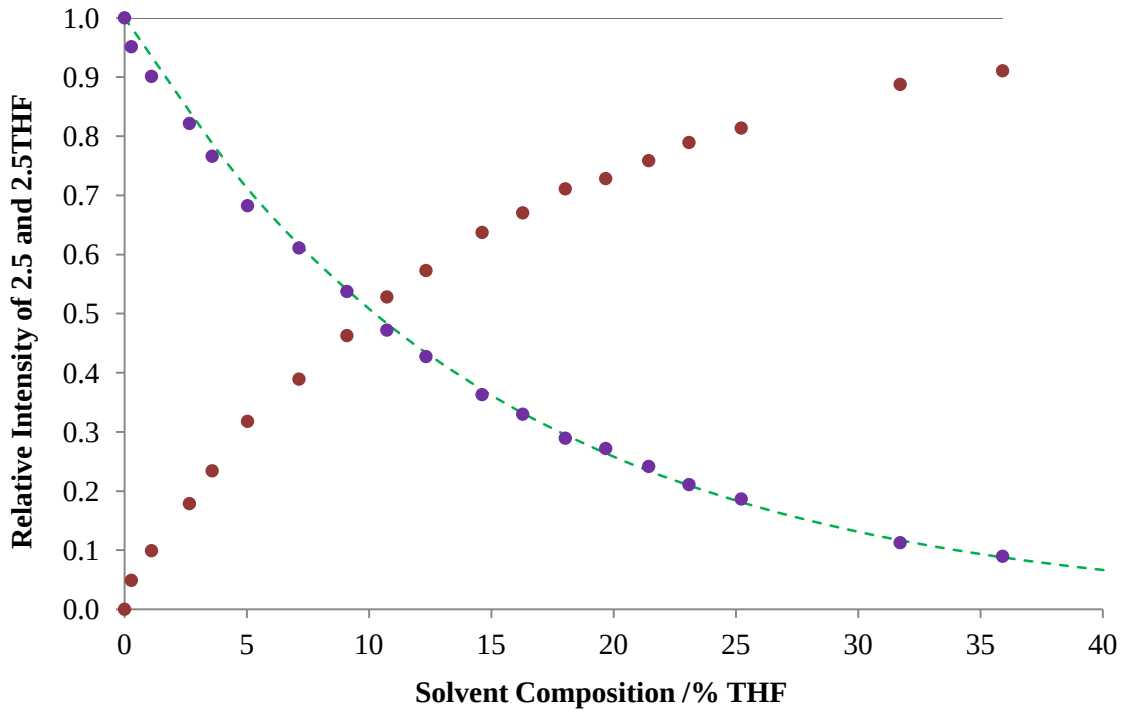

Figure 2.12 The change in relative intensity of **2.5** (purple) and **2.5THF** (red) with increasing concentration of THF in d_6-benzene. Green dashes represent the exponential fit for **2.5** according to y = exp(-0.0677x), R^2 = 0.999, and the black line illustrates that the total relative intensity remains constant as the ratio of THF:benzene varies.

Calculation of the equilibrium constant (**Equation 2.1**) and ΔG (**Equation 2.2**) from these data illustrates that the formation of **2.5THF** is not spontaneous. The first two data points gave anomalous results due to the errors associated with the measurements (see Appendix III). However the other data give a value for K_b of 3.02 x 10^{-2} kg·mol^{-1} (±5.99 x 10^{-3} kg·mol^{-1}) and a value of ΔG of 8.86 kJmol^{-1} (±0.47 kJ·mol^{-1}) at 30 °C.

$$K_b = \frac{(b_{2.5THF})^2}{(b_{2.5})(b_{THF})^2}$$

$$\Delta G = -RTLnK_b$$

Equation 2.1 (top) The equilibrium constant according to **Figure 2.11**; and **Equation 2.2** (bottom) Finding the change in Gibb's free energy from the equilibrium constant.

*2.3.3 Molecular structures of **2.5THF** – **2.7THF***

Despite the ease in which the heterocyclic mixed-sandwich complexes could be desolvated, single crystals of the base-free complexes could not be obtained for the phospholyl and arsolyl complexes. However, addition of THF to saturated pentane solutions yielded single crystals of **2.5THF** – **2.7THF** at -35 °C (**Figure 2.13**).

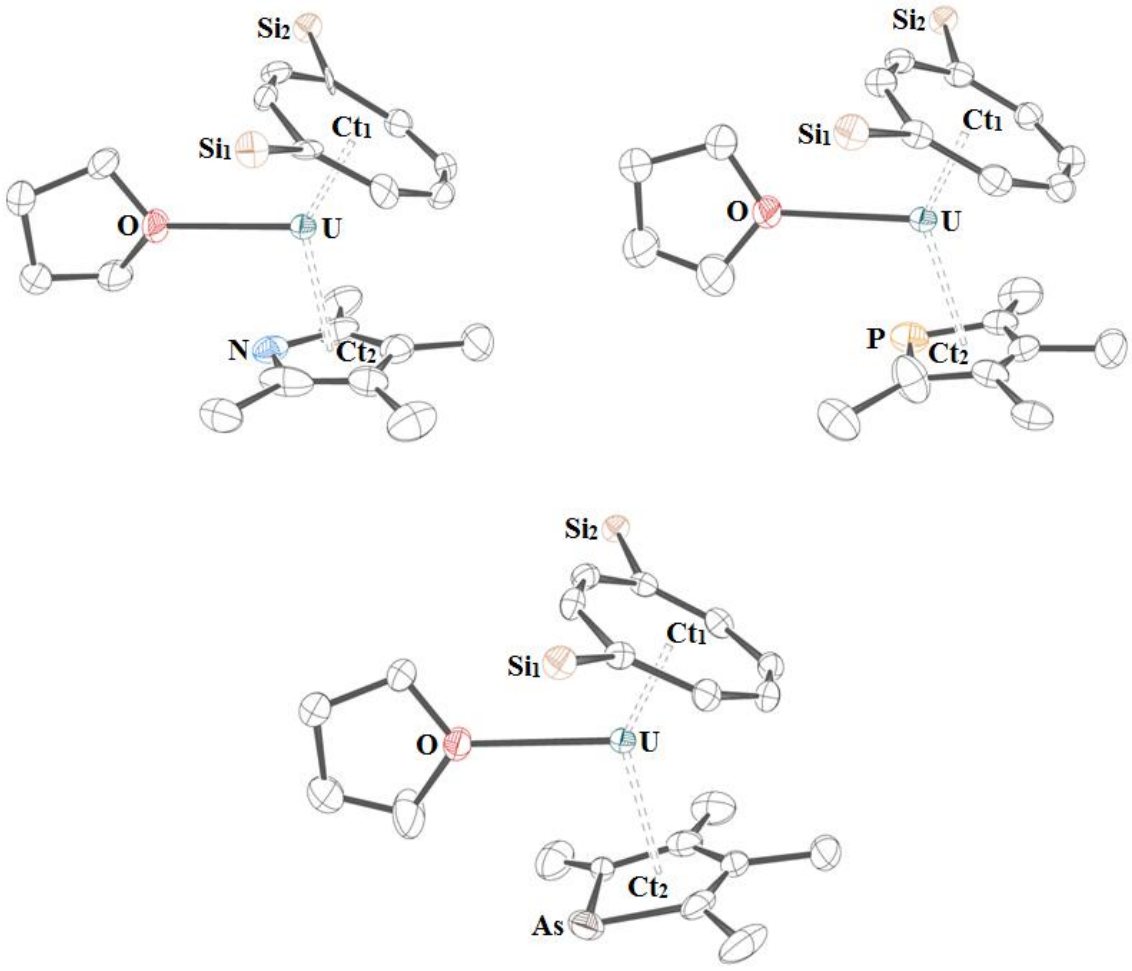

Figure 2.13 ORTEP views of **2.5THF** (top left), **2.6THF** (top right) and **2.7THF** (lower centre) with thermal ellipsoids at 50% probability; hydrogen atoms and COT *iso*-propyl groups have been omitted for clarity.

The data for **2.6THF** illustrate disorder of the five-membered ring over two positions, which has been modelled by splitting the phospholyl ring. Data for **2.5THF** however could only be obtained at low resolution and the data must therefore be treated with a degree of caution. Selected distances and angles are listed in **Table 2.3**.

Distances (Å) and Angles (°)	**Compound**		
	2.5THF	**2.6THF**	**2.7THF**
U–Ct$_1$	1.9649(3)	1.969(12)	1.9744(4)
U–Ct$_2$	2.4867(3)	2.54(9), 2.59(2)	2.5962(4)
U–C(Cp)	2.682(10) - 2.896(10)	2.859(19) - 2.905(6)	2.861(10) - 2.924(9)
U–E	2.595(8)	2.776(15), 2.9868(14)	3.0781(7)
U–O(THF)	2.651(7)	2.716(2)	2.726(4)
Ct$_1$–U–Ct$_2$	139.735(14)	135.8(15), 142.4(14)	141.482(16)

Table 2.3 Bond lengths, distances and angles for **2.5THF**, **2.6THF** and **2.7THF**. Ct_1 is the centroid for the $COT^{(SiiPr3)2}$ ligand and Ct_2 is the centroid for the Cp^{EMe4} ligand. Two values are given for some metrics of **2.6THF** as a result of splitting the phospholyl ring.

Comparison of the data from the three complexes illustrates that there is an increase in the U–Cp, U–COT and U–O(THF) distances as the pnictogen becomes larger, however this increase is most pronounced between the pyrrolyl and phospholyl complexes and only a marginal difference is observed between the phospholyl and arsolyl complexes.

In comparison to the cyclopentadienyl analogues, the molecular structures of these three complexes bear most resemblance to [U(COT$^{(SiiPr3)2}$)(Cp^{Me4})(THF)], however the U–Cp distances in **2.6THF** and **2.7THF** have been found to be the longest distances in all comparable [U(COT$^{(SiiPr3)2}$)(Cp^{R})(THF)] complexes (2.450(2) – 2.5061(4) Å).[26] It was also noted that whilst all mixed-sandwich complexes exhibit a small degree of ring slippage, this effect is more pronounced in the heterocyclic analogues due to the varying U–E distances. In complex **2.5THF**, the U–N distance is significantly shorter than the U–C distances, giving rise to a pseudo η^3-interaction. However in complexes **2.6THF** and **2.7THF**, the increased U–E distances give rise to longer U–C(Cp) distances. Whilst the U–C(Cp) distances are still within the range reported for the majority of published complexes (*ca.* 2.65 – 2.95 Å),[33,34] they are longer than average for the uranium(III) complexes synthesised by Cloke *et al.* (2.687(6) – 2.816(7) Å).[21,28,30]

Similar mixed-sandwich complexes incorporating pyrrolyl and phospholyl ligands have been synthesised for the lanthanides. Comparison of samarium and neodymium complexes with unsubstituted COT rings and bulky heterocyclic rings have illustrated an increase in the COT–M–Cp^{R} angle, which is postulated to be due to an overall decrease in the sterics around the metal centre.[35–37] Further comparison to a uranium mixed-sandwich borohydride complex, [U(COT)(Cp^{PMe4})(THF)(BH4)], shows a marginal increase in the U–COT and U–Cp distances (2.013(4) and 2.610(3) Å respectively), but a significant decrease in the U–O(THF) distance (2.527(7) Å).[38] The degree of ring slippage in all these complexes was found to be more pronounced than in **2.6THF** and **2.7THF** and this is speculated to be due to the different sterics around the metal centre.

*2.3.4 Molecular structure of [U(COT$^{(SiiPr3)2}$)(Cp^{NMe4})] (**2.5**)*

XRD data of single crystals of **2.5** illustrate a dimeric structure in the solid-state, with η^5:η^1-coordination of both pyrrolyl ligands (**Figure 2.14**). The steric environment is not predicted to be over-crowded around the uranium centres however, as the silyl groups on the COT ring are still observed to face towards the centre of the molecule.

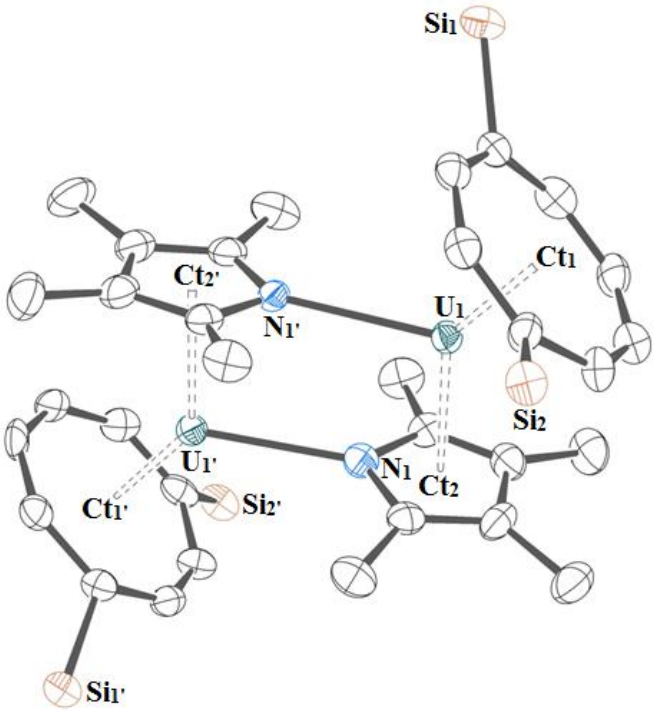

Figure 2.14 ORTEP view of **2.5** with thermal ellipsoids at 50% probability; hydrogen atoms and COT *iso*-propyl groups have been omitted for clarity. Selected distances (Å) and angles (°): U_1–Ct_1 1.968(3), 1.974(3); U_1–Ct_2 2.548(4), 2.568(4); U_1–N_1 2.680(5), 2.691(6); U_1–$N_{1'}$ 2.598(6), 2.615(5); Ct_1–U_1–Ct_2 138.66(11), 138.55(12); Ct_2–U_1–$N_{1'}$ 96.7(2), 96.36(19).

The averaged U–N bond distances are observed to be very similar to the U–O(THF) distances in the THF adducts, and are only 0.05 Å shorter than the U–O distances in

2.5THF. The U–Cp and U–COT distances in this complex are also found to be very similar to those in complexes **2.5THF** – **2.7THF**, and the degree of ring slippage is very similar to **2.5THF** such that this molecule can also be considered to have a pseudo η^3-pyrrolyl-uranium interaction.

Similar dimeric pyrrolyl complexes are prevalent in the literature and have recently been observed by Cloke *et al.* for desolvated ytterbium and samarium bis(2,5-di-*tert*-butylpyrrolyl) complexes.[39] However, the only other uranium complexes featuring this interaction were supported by a calix[4]tetrapyrrole ligand, which enforced a perpendicular orientation of the two uranium centres (**Figure 2.15**).[40] These complexes exhibit near identical U–Cp distances (2.547(3) – 2.611(4) Å) and U–N distances (2.609(5) – 2.696(7) Å) to **2.5**, but the scaffold and halide ligands dictate a wider Cp–U–Cp angle (151.45(16) – 153.87(11) °) and more acute Cp–U–N angles (80.38(18) - 83.01(17) °).

Other dimeric phospholyl and arsolyl complexes have also been reported and it is hypothesised that **2.6** and **2.7** may also be dimeric in the solid state. Phospholyl complexes in which this ligand adopts η^5:η^1-coordination include [{U(η^5-Cp^{PMe4})(μ-η^5:η^1-Cp^{PMe4})(BH_4)}$_2$] (**Figure 2.15**), which has similar U–Cp distances to **2.6THF** (2.56(1) and 2.54(1) Å), but expectedly longer U–P distances (2.945(3) and 2.995(3) Å) than the U–O(THF) and U–N distances discussed here.[41,42]

Evidence for the dimeric nature of [{U(η^5-Cp^{PMe4})(μ-η^5:η^1-Cp^{PMe4})(BH_4)}$_2$] in solution was also present in the $^{31}P\{^1H\}$ NMR spectrum, which exhibited two broad resonances at 727 and 3471 ppm for the terminal and bridging phospholyl rings respectively.[41,42] This contrasts to **2.6**, which has a broad resonance at 911 ppm, illustrating that there is no interaction between the phosphorus atom and the second uranium centre.

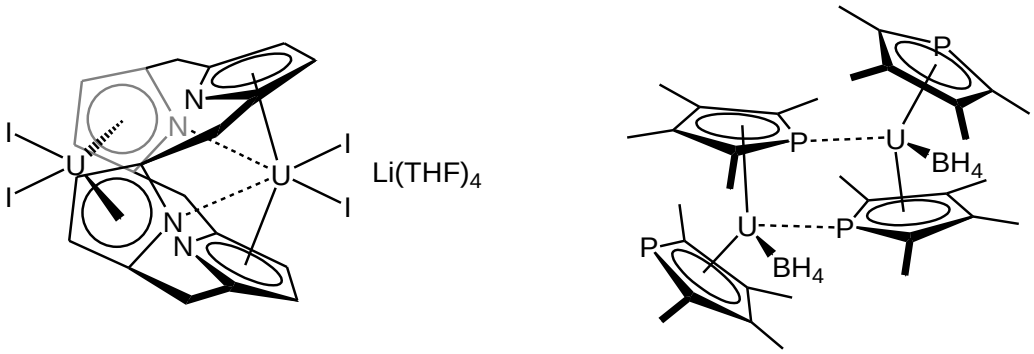

Figure 2.15 Published structures which feature η^5:η^1-bonding: A diuranium calix[4]tetrapyrrole complex (left) and a dimeric uranium phospholyl complex (right).[40,42]

The propensity for heterocyclic ligands to exchange between η^5 and η^1-coordination has been well documented (see Chapter 1) and accounts for the lability of these ligands in comparison to Cp^R ligands. This is demonstrated by reaction of **2.6THF** with K[Cp*], which gives rise to [U($COT^{(SiiPr3)2}$)(Cp*)(THF)], although the reverse reaction does not occur.

2.3.5 Cyclic voltammetry of heterocyclic mixed-sandwich complexes

As discussed in Chapter 1, studies of uranium, complexes with Cp^R and Cp^{PMe4} ligands illustrate that incorporation of a pnictogen into the five-membered ring reduces the electron density at the uranium centre giving rise to less negative redox couples.[43–45] It was therefore anticipated that the heterocyclic complexes **2.5THF** – **2.7THF** would exhibit U^{IV}/U^{III} redox potentials that are *ca.* 0.2 V less reducing than their carbocyclic counterparts. In order to obtain comparable results, the experiments were carried out under the same conditions as complexes **2.1** – **2.4**. The electrode potentials *vs* $[FeCp_2]^{+/0}$ are listed in **Table 2.4** and the cyclic voltammograms are shown in **Figure 2.16**.

Scanning in the anodic direction gave rise to a half-wave between -2.0 and -1.7 V *vs* $[FeCp_2]^{+/0}$ (process II), which has been assigned to the U^{IV}/U^{III} redox couple. This was followed by two additional waves (processes III – IV) for **2.6THF** and **2.7THF** and three additional waves (processes III – V) for **2.5THF**. Reverse scanning revealed processes III and IV to be quasi-reversible, however ambiguity in the analysis of the voltammetric responses was found descending the group from Cp^{NMe4} to Cp^{AsMe4}. An additional reductive process (process I) was also observed for **2.5THF** bordering the solvent breakdown (-2.5 V), which was not seen in the other two voltammograms. As was the case for complexes **2.1** – **2.4**, the additional redox processes (I, III – V) could not be assigned.

	$E_{½}$ values (V) *vs* $[FeCp_2]^{+/0}$		
	Process II	*Process III*	*Process IV*
$[U(COT^{(SiiPr3)2})(Cp^{AsMe4})(THF)]$ (2.7THF)	**-1.8**	-1.3	-0.78
$[U(COT^{(SiiPr3)2})(Cp^{PMe4})(THF)]$ (2.6THF)	**-1.8**	-1.3	-0.81
$[U(COT^{(SiiPr3)2})(Cp^{NMe4})(THF)]$ (2.5THF)	**-1.9**	-1.4	-0.62

Table 2.4 $E_{½}$ values (V) *vs* $[FeCp_2]^{+/0}$ for the heterocyclic mixed-sandwich complexes.

Comparison of these results to those of the carbocyclic mixed-sandwich complexes found the U^{IV}/U^{III} redox couple to be 0.2 – 0.3 V less negative than the comparable redox couple for $[U(COT^{(SiiPr3)2})(Cp^{Me4})(THF)]$ (-2.08 V). This is in agreement with the other published results.[30,43–48] However, the error that arises in the values of $E_{½}$ due to the distortion in the half-waves precludes comparison between the three complexes.

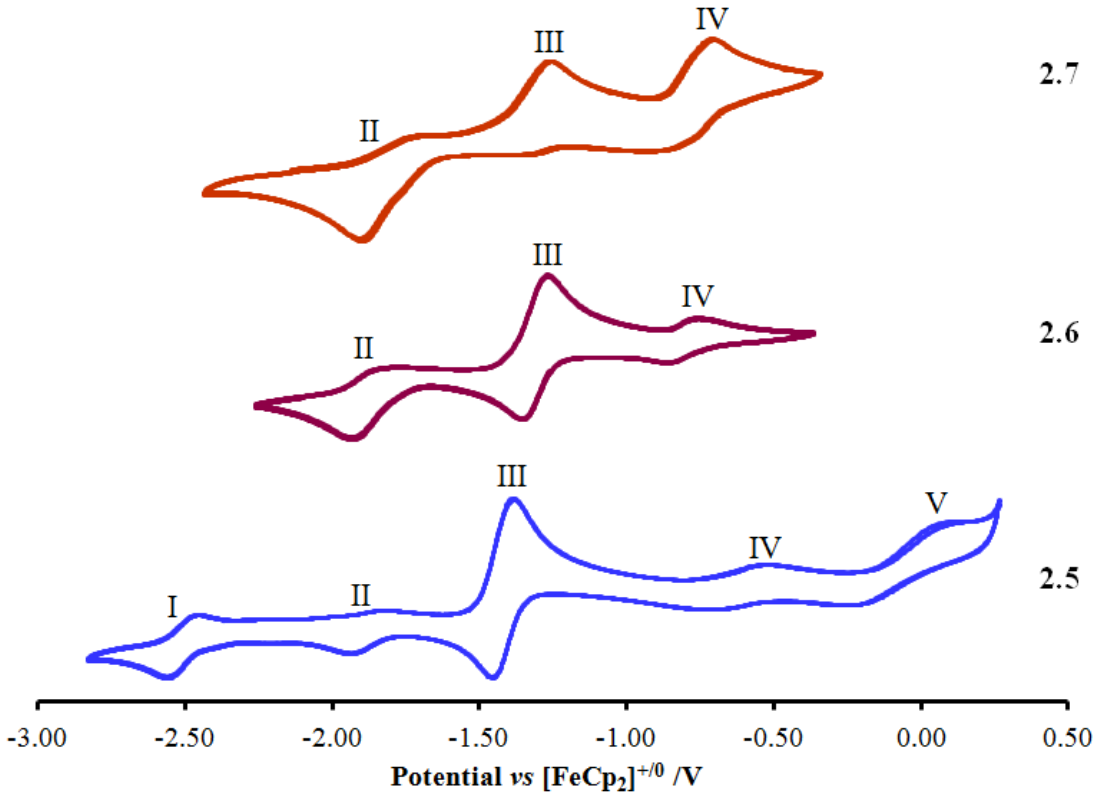

Figure 2.16 Cyclic voltammograms of 5-10 mM solutions of **2.5THF** – **2.7THF** in 0.05 M [^{n}Bu$_4$N][B(C$_6$F$_5$)$_4$]/THF at 100 mV·s^{-1}. Two cycles are shown for all complexes.

2.3.6 Identification and characterisation of side products

2.3.6.1 Characterisation of [U(COT$^{1,4\text{-Si}i\text{Pr3}}$)(COT$^{1,3\text{-Si}i\text{Pr3}}$)] (**2.8**)

Although uranocene was the predominant side product in the synthesis of **2.5** – **2.7**, another species precipitated from all three reaction mixtures. This complex was identified as [U(COT$^{1,4\text{-Si}i\text{Pr3}}$)(COT$^{1,3\text{-Si}i\text{Pr3}}$)] (**Figure 2.17**), a novel uranocene in which one of the silyl groups has migrated to give 1,3-substitution. XRD data illustrated the connectivity of this complex, however full refinement was precluded due to twinning. Comparison with the major uranocene side product, [U(COT$^{1,4\text{-Si}i\text{Pr3}}$)$_2$], was therefore not attempted.

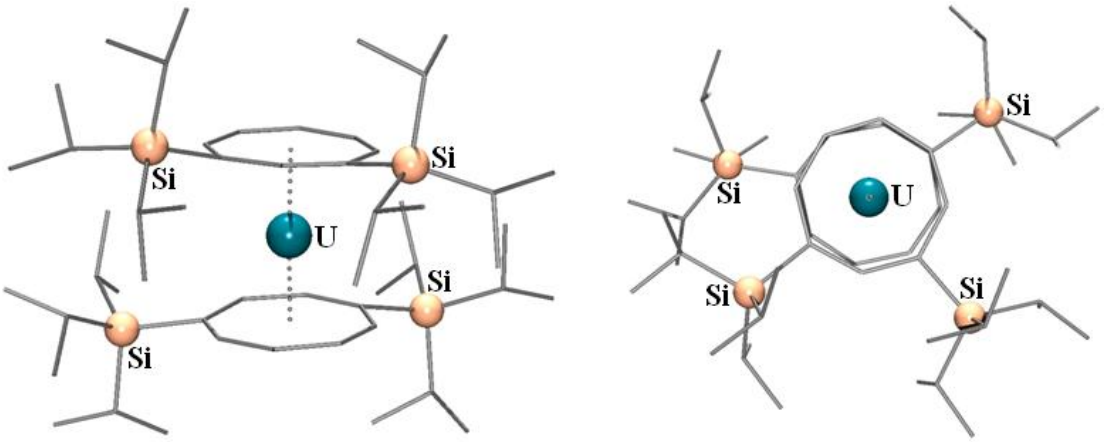

Figure 2.17 POV-Ray views of **2.8** from the side (left) and the top (right).

Substituent redistribution on COT rings has been previously observed by Evans and Edelmann who synthesised a bent cerocene anion with two migrated COT^{BIG} ($C_8H_6^{1,4\text{-}SiPh3}$) ligands.[49] Oxidation of this complex resulted in silyl migration on both rings to generate the linear cerocene with two $C_8H_6^{1,3\text{-}SiPh3}$ ligands in order to relieve steric congestion around the metal centre. Similarly, Edelmann reported silyl group migration in the synthesis of a holmium triple-decker sandwich complex which did not occur for the corresponding neodymium, cerium and samarium analogues due to the larger radii of these lanthanide metals.[50]

2.3.6.2 Characterisation of [U($COT^{(Si\mathit{i}Pr3)2}$)(Cp^{AsMe4})I] (**2.9**)

During attempts to obtain analytically pure samples of [U($COT^{(Si\mathit{i}Pr3)2}$)(Cp^{AsMe4})(THF)], single crystals of a second species were obtained. XRD studies revealed the complex to be the uranium(IV) mixed-sandwich iodide (**Figure 2.18**), which was partially characterised by NMR spectroscopy. Due to the very low yields (<5%) of this complex however, characterisation remains incomplete.

Comparison of **2.9** to the uranium(III) analogue **2.7THF** shows minimal variation in the mixed-sandwich fragment. Similarly, the related complex [U(COT$^{(SiiPr3)2}$)(Cp*)Cl], has an almost identical U–COT bond distance (1.9142(15) Å) and Ct_1–U–Ct_2 angle (139.85(8)°), although the U–Cp distance is shorter (2.465(2) Å).[51] This is postulated to be due to the smaller radius of the chloride compared to the iodide as Cp^{AsMe4} and Cp* are similar in size. The U–I bond distance is typical of uranium(IV) complexes with terminal iodide ligands which fall in the range of 2.942(3) – 3.1119(5) Å.[15,52–58]

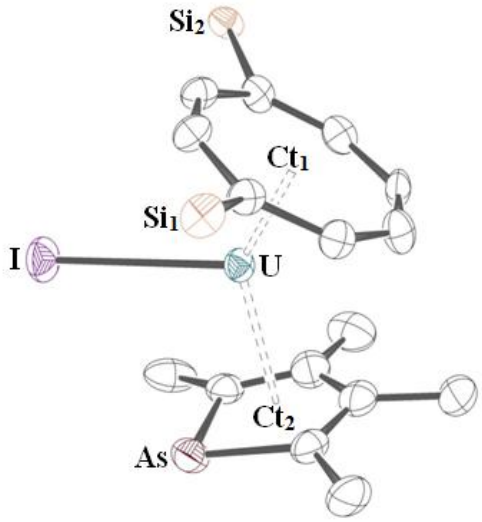

Figure 2.18 ORTEP view of **2.9** with thermal ellipsoids at 50% probability; hydrogen atoms and COT *iso*-propyl groups have been omitted for clarity. Selected bond distances (Å) and angles (°): U–Ct_1 1.9120(5); U–Ct_2 2.5386(5); U–I 3.0526(6); Ct_1–U–Ct_2 139.58(2).

2.3.7 Thermolysis of mixed-sandwich complexes

Studies by Cloke *et al.* on [U(COT$^{(SiiPr3)2}$)(Cp*)(THF)] revealed the formation of a 'tuck-in' complex, [U(COT$^{(SiiPr3)2}$)(η^5:η^1-$C_5Me_4CH_2$)], by activation of a Cp* methyl group at elevated temperatures.[19] In order to test for analogous reactivity, thermolysis

reactions of the heterocyclic mixed-sandwich complexes were conducted. Heating solutions of **2.5THF** – **2.7THF** at 70 °C for seven days yielded three analogous complexes, which were identified as the *n*-butoxide complexes [U(COT$^{(Si\textit{i}Pr3)2}$)(Cp^{EMe4})(O^{n}Bu)] (**2.10** – **2.12** for E = P, As and N respectively), formed by ring-opening THF. Mass spectrometry confirmed the formulation, and full characterisation of the *n*-butoxide resonances was achieved by comparison of the ^{1}H NMR spectra with those for [U(COT$^{(Si\textit{i}Pr3)2}$)(Cp*)(OR)] (R = Me, Et, and ^{n}Bu), synthesised by Cloke and co-workers.[51,59]

In order to find the optimum reaction conditions, the reaction was repeated with varying concentrations of THF at different temperatures for [U(COT$^{(Si\textit{i}Pr3)2}$)(Cp^{PMe4})(THF)]. Results from these studies illustrated that excess THF was required in order to avoid prolonged heating and decomposition, but that using THF as the solvent increased the concentration of impurities. Similarly, heating the complex to a high temperature caused degradation, and overall it was concluded that the reaction proceeds with fewest side reactions when carried out at 75 °C over ten days (**Figure 2.19**).

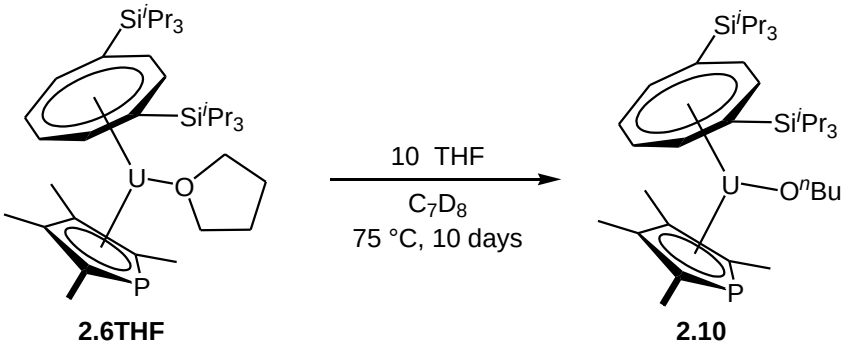

2.6THF **2.10**

Figure 2.19 Synthetic route to the *n*-butoxide uranium(IV) mixed-sandwich complex, **2.10** under optimum conditions.

The phospholyl and arsolyl *n*-butoxide complexes (**2.10** and **2.11** respectively) were the only paramagnetic species obtained from the parent uranium(III) complexes. However, thermolysis of [U(COT$^{(Si\textit{i}Pr3)2}$)(Cp^{NMe4})] (**2.5**) in the presence of THF yielded a second, minor species. This was identified crystallographically as a 'tuck-in tuck-over' complex [(COT$^{(Si\textit{i}Pr3)2}$)U(μ-η^5:η^1-NC$_4$Me$_3$CH)U(COT$^{(Si\textit{i}Pr3)2}$)(Cp^{NMe4})] (**2.13**), formed by activation of one methyl group on the pyrrolyl ring (**Figure 2.20**). This results in oxidation of the two uranium centres to uranium(IV) and loss one molecule of dihydrogen for every reacted molecule of **2.5**.

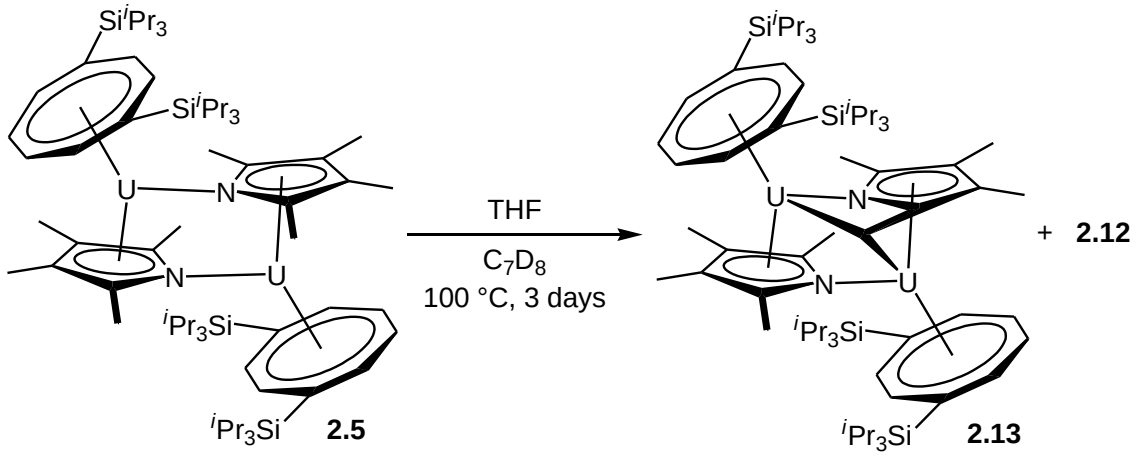

Figure 2.20 Activation of C-H to form the 'tuck-in tuck-over' complex, **2.13**.

Full characterisation of this complex by NMR spectroscopy was precluded, due to the *ca.* 4:1 ratio of *n*-butoxide (**2.12**) to **2.13**. This contrasts to the results obtained by Cloke *et al.*, which yielded an equal mixture of the 'tuck-in' complex and the *n*-butoxide complex.[51] Attempts to obtain **2.13** by thermolysis of **2.5** in the absence of THF gave rise to no reactivity or decomposition of the mixed-sandwich complex, even after 14 days at 100 °C.

The molecular structure of **2.13** (**Figure 2.21**) illustrates that activation of the methyl group has resulted in the formation of two new U–C bonds, evidenced by the observed bond lengths in **Table 2.5**. Comparison of these values with those stated in the literature for alkyl and silyl 'tuck-in' and 'tuck-over' complexes reveal the U_1–C_1 bond to be of average distance, whereas the U_2–C_1 distance lies within the lower limits of the literature values (**Figure 2.22**).[9–20] A decrease is also observed in the U–N distances compared to those in [U(COT$^{(Si\textit{i}Pr3)2}$)(Cp^{NMe4})] and it is postulated that these constraints give rise to the short 'tuck-over' bond. It is also worth noting that the C_1–C_2 bond length has not changed as a consequence of activation, and still lies within the range of the other C_{ring}–CH_3 distances.

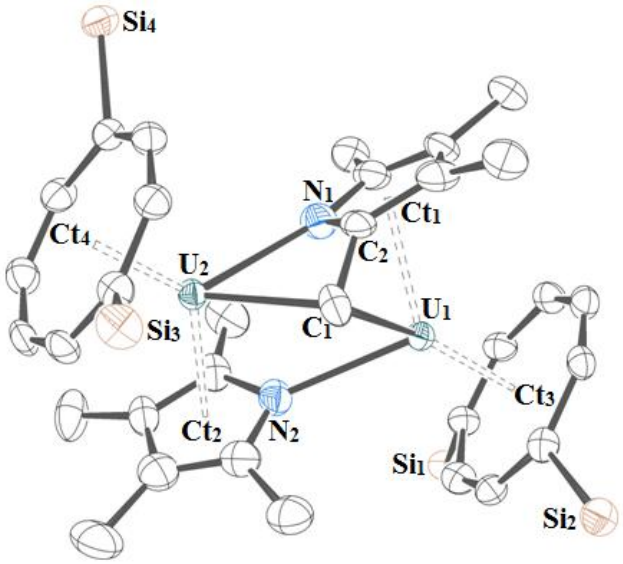

Figure 2.21 ORTEP view of **2.13** with thermal ellipsoids at 50% probability; hydrogen atoms and COT *iso*-propyl groups have been omitted for clarity.

Comparison of **2.13** with **2.5** also illustrates a marginal increase in the U–COT distances and the non-activated U–Cp distance, but that the activated pyrrolyl ring is now closer to the uranium centre. The latter is perceived to be another effect of the constraints introduced by the activated methyl substituent, and it is postulated that the other three

U–Ct distances have increased in order to counteract the increase in sterics as a consequence of the shorter U–Cp and U–N contacts.

Distances (Å)					
Ct_1–U_1	2.4623(4)	**Ct_2–U_2**	2.5953(4)	**Ct_3–U_1**	1.9869(4)
Ct_4–U_2	2.0025(4)	**U_1–N_2**	2.573(7)	**U_2–N_1**	2.525(7)
U_1–C_1	2.553(9)	**U_2–C_1**	2.388(9)	**C_1–C_2**	1.474(12)
Angles (°)					
Ct_1–U_1–Ct_3	134.318(19)	**Ct_2–U_2–Ct_4**	130.868(18)	**Ct_1–C_2–C_1**	151.9(9)
U_1–C_1–U_2	102.5(3)	**U_1–C_1–C_2**	69.6(5)	**U_2–C_1–C_2**	89.8(6)

Table 2.5 Bond lengths, distances and angles for **2.13**. Ct_1 and Ct_2 are the centroids for the pyrrolyl ligands and Ct_3 and Ct_4 are the centroids for the $COT^{(SiiPr3)2}$ ligands.

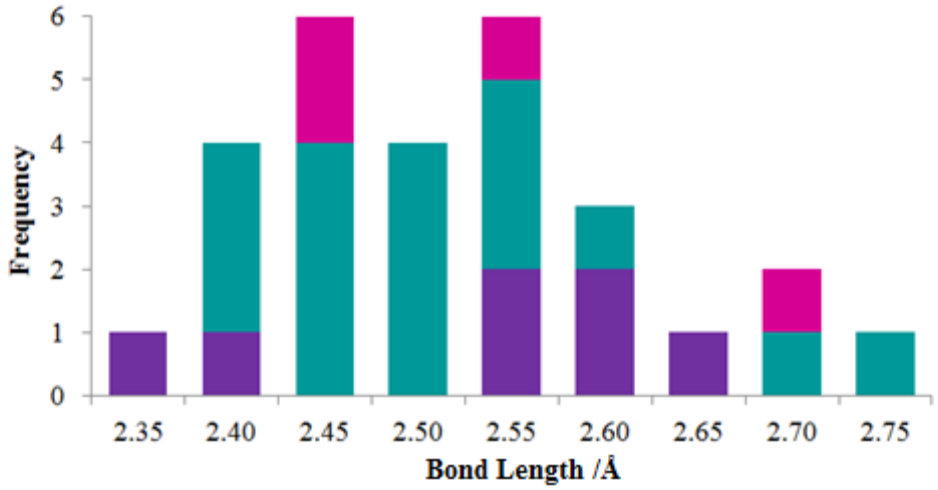

Figure 2.22 Published U–C bond lengths for silyl 'tuck-in' complexes (teal), alkyl 'tuck-in' complexes (purple) and 'tuck-over' complexes (pink).[9–20]

2.4 Summary

Seven novel mixed-sandwich complexes featuring substituted cyclopentadienyl or heterocyclic ligands have been synthesised. Analysis of the carbocyclic analogues by cyclic voltammetry reveals the U^{IV}/U^{III} redox couple is not significantly affected by the substituents and that the potential for this process occurs at *ca.* -2.0 V *vs* $[FeCp_2]^{+/0}$. Comparative studies of the heterocyclic derivatives illustrate that incorporation of a pnictogen lessens the reducing power of these complexes and that their synthesis is complicated by the formation of multiple side products. The complexes are also thermally sensitive in the presence of coordinating solvents giving rise to ring-opening of THF and formation of a novel 'tuck-in tuck-over' complex.

2.5 Experimental details for chapter 2

*2.5.1 Synthesis of [U(COT$^{(SiiPr3)2}$)(Cp^{tBu})(THF)] (**2.1THF**)*

A solution of K[Cp$^{t\text{Bu}}$] (0.3025 g, 1.89 mmol) in THF (30 mL) was added *via* cannula to a solution of UI_3 (1.176 g, 1.90 mmol) in THF (100 mL), and stirred overnight to give a teal solution of [UI_2(Cp$^{t\text{Bu}}$)(THF)$_n$] and KI precipitate. The solvent was removed *in vacuo* and the residue dissolved in toluene. The green solution was filtered and dried *in vacuo* and the yield of the green residue recorded. The complex was dissolved in THF and a solution of K_2[COT$^{(SiiPr3)2}$] (0.758 g, 1.53 mmol, 0.80 equivalents) in THF (20 mL) was added dropwise over 40 minutes at -35 °C. A brown solution with a pale precipitate formed after 10 minutes and upon warming to room temperature the solvent was immediately removed *in vacuo* leaving a brown residue. The product was filtered in pentane through a Celite frit to give a green solution from which dark green crystals were obtained at -20 °C.

Yield: 0.554 g (6.53 mmol), 34% based on UI_3.

Anal. calc (found) for $C_{39}H_{69}OSi_2U$: C 55.23 (55.20), H 8.20 (7.76)%.

MS (EI): *m/z* = 115 (100%), 776 (19%, M^+ - THF).

^{1}H NMR (d_8-toluene, 303 K): δ 5.6 (s, br, 2H, Cp/COT-C*H*), 4.9 (s, br, 2H, Cp/COT-C*H*), 1.5 (s, br, 4H, THF), 0.7 (s, br, 4H, THF), -2.8 (s, br, 6H, ^{i}Pr-C*H*), -4.0 (s, br, 18H, ^{i}Pr-CH_3), -4.1 (s, br, 2H, Cp/COT-C*H*), -5.7 (s, br, 18H, ^{i}Pr-CH_3), -12.8 (s, br, 9H, ^{t}Bu-CH_3), -58.2 (s, br, 2H, Cp/COT-C*H*), -74.8 (s, br, 2H, Cp/COT-C*H*).

^{29}Si{^{1}H} NMR (d_8-toluene, 303 K): δ -134.3 (Si^iPr$_3$).

*2.5.2 Synthesis of [U(COT$^{(SiiPr3)2}$)(Cp^{tBu})] (**2.1**)*

A solution of **2.1THF** in pentane (20 mL) was thoroughly dried under reduced pressure (10^{-2} mbar). The residue was dissolved in pentane and filtered through a Celite frit. Removal of solvent under reduced pressure resulted in quantitative yield of green powder. Crystals were obtained from a saturated pentane solution at -35 °C.

^{1}H NMR (d_8-toluene, 303 K): δ 10.8 (s, br, 2H, Cp/COT-C*H*), 5.8 (s, br, 2H, Cp/COT-C*H*), 0.0 (s, br, 2H, Cp/COT-C*H*), -4.6 (s, br, 6H, ^{i}Pr-C*H*), -6.8 (s, br, 18H, ^{i}Pr-CH_3), -9.0 (s, br, 18H, ^{i}Pr-CH_3), -17.9 (s, br, 9H, ^{t}Bu-CH_3), -54.7 (s, br, 2H, Cp/COT-C*H*), -76.8 (s, br, 2H, Cp/COT-C*H*).

^{29}Si{^{1}H} NMR (d_8-toluene, 303 K): δ -126.7 (Si^iPr$_3$).

*2.5.3 Synthesis of [U(COT$^{(SiiPr3)2}$)(Cp^{tBu2})] (**2.2**)*

To a stirring solution of UI_3 (0.900 g, 1.45 mmol) in THF (50 mL), was added K[Cp^{tBu2}] powder (0.310 g, 1.45 mmol) to give [UI_2(Cp^{tBu2})(THF)$_n$] and KI precipitate after 12

hours. The solvent was removed *in vacuo* leaving white solids and purple residue, which was dissolved in toluene. The dark pink solution was filtered *via* filter cannula and stripped to dryness leaving green powder and the yield of this complex recorded. Dissolution in THF and cooling to -35 °C yielded a teal solution, to which a solution of $K_2[COT^{(SiiPr3)2}]$ (0.51 g, 1.0 mmol, 0.71 equivalents) in THF (20 mL) was added dropwise *via* cannula over 40 minutes. A brown solution with a pale precipitate formed after 10 minutes and upon warming to room temperature the solvent was immediately removed *in vacuo* leaving a brown residue. The product was taken up in pentane and filtered through a Celite frit to give a green solution from which a dark green powder was obtained.

Yield: 0.425 g (0.511 mmol), 35% based on UI_3.

Anal. calc (found) for $C_{39}H_{69}Si_2U$: C 55.72 (56.29), H 8.48 (8.36)%.

MS (EI): *m/z* = 373 (100%), 831 (5%, M^+).

^{1}H NMR (d_8-toluene, 303 K): δ 20.2 (s, br, 2H, Cp/COT-C*H*), 10.6 (s, br, 1H, Cp-C*H*), -2.6 (s, br, 6H, ^{i}Pr-C*H*), -4.4 (s, br, 18H, ^{i}Pr-CH_3) -6.6 (s, br, 18H, ^{i}Pr-CH_3), -14.7 (s, br, 2H, Cp/COT-C*H*), -17.0 (s, br, 18H, ^{t}Bu-CH_3), -58.1 (s, br, 2H, Cp/COT-C*H*), -90.4 (s, br, 2H, Cp/COT-C*H*).

^{29}Si{^{1}H} NMR (d_8-toluene, 303 K): δ -122.5 (Si^iPr_3).

*2.5.4 Synthesis of [U(COT$^{(SiiPr3)2}$)(Cp^{tBu3})] (**2.3**)*

A suspension of K[Cp^{tBu3}] (0.630 g, 2.32 mmol) in THF (30 mL) was added *via* cannula to a solution of UI_3 (1.44 g, 2.33 mmol) in THF (100 mL), and stirred overnight to give a purple solution of $[UI_2(Cp^{tBu3})(THF)_n]$ and KI precipitate. To this, a solution of $K_2[COT^{(SiiPr3)2}]$ (0.98 g, 1.98 mmol, 0.85 equivalents) in THF (30 mL) was added dropwise at -35 °C over 30 minutes. Upon warming, the solution became brown with a

pale precipitate and was stirred overnight at room temperature. The solvent was removed *in vacuo* to give a brown residue which was dissolved in pentane and filtered through a Celite frit to give a green solution from which crystals were obtained.

Yield: 1.34 g (1.51 mmol), 64.8% based on UI_3.

Anal. calc (found) for $C_{43}H_{77}Si_2U$: C 58.14 (57.95), H 8.74 (8.81)%.

MS (EI): *m/z* = 888 (100%, M^+).

^{1}H NMR (d_8-toluene, 303 K): δ 2.8 (s, br, 2H, Cp/COT-C*H*), -3.1 (overlapping, br, 24H, ^{i}Pr-C*H*$_3$, ^{i}Pr-C*H*), -4.7 (overlapped, br, 20H, ^{i}Pr-C*H*$_3$, Cp/COT-C*H*), -7.8 (s, br, 18H, ^{t}Bu-C*H*$_3$), -24.3 (s, br, 9H, ^{t}Bu-C*H*$_3$), -50.4 (s, br, 2H, Cp/COT-C*H*), -76.1 (s, br, 2H, Cp/COT-C*H*).

^{29}Si{^{1}H} NMR (d_8-toluene, 303 K): δ -116.6 (*Si*^{i}Pr$_3$).

*2.5.5 Synthesis of [U(COT$^{(SiiPr3)2}$)(Cp$^{(SiiPr3)2}$)] (**2.4**)*

A solution of K[Cp$^{(SiiPr3)2}$] (0.65 g, 1.6 mmol) in THF (20 mL) was added *via* cannula to a deep blue solution of UI_3 (0.97 g, 1.7 mmol) in THF (100 mL), and stirred overnight to give a purple solution of [UI_2(Cp$^{(SiiPr3)2}$)(THF)$_n$] and KI precipitate. The solvent was removed *in vacuo* leaving white solids in a green residue, which was dissolved in pentane. The solution was filtered and the green residue dried *in vacuo*. The yield was recorded. The residue was dissolved in THF and to this was added a solution of K_2[COT$^{(SiiPr3)2}$] (0.67 g, 1.4 mmol, 0.87 equivalents) in THF (30 mL) at -30 °C over 30 minutes. Upon warming to room temperature the solvent was immediately removed *in vacuo* leaving a green residue, which dissolved in pentane. The solution was filtered through a Celite frit to give a green solution from which dark green crystals were obtained.

Yield: 0.848 g (0.822 mmol), 52% based on UI_3.

Anal. calc (found) for $C_{49}H_{93}Si_4U$: C 56.99 (56.702), H 9.08 (8.693)%.

MS (EI): *m/z* = 157 (100%, $[Si^iPr_3]^+$), 1032 (6%, M^+).

^{1}H NMR (d_8-toluene, 373 K): δ 19.0 (s, br, 2H, Cp/COT-C*H*), 8.1 (s, br, unassigned), 7.7 (s, br, unassigned), -1.6 (s, br, 6H, ^{i}Pr-C*H*), -2.0 (s, br, 18H, ^{i}Pr-CH_3), -3.3 (s, br, 18H, ^{i}Pr-CH_3), -4.0 (s, br, 18H, ^{i}Pr-CH_3), -4.2 (s, br, 18H, ^{i}Pr-CH_3), -5.8 (s, br, 6H, ^{i}Pr-C*H*), -46.5 (s, br, 2H, Cp/COT-C*H*), -72.8 (s, br, 2H, Cp/COT-C*H*).

^{29}Si{^{1}H} NMR (d_8-toluene, 373 K): δ -96.8 (Si^iPr_3), -98.0 (Si^iPr_3).

^{29}Si{^{1}H} NMR (d_8-toluene, 228 K): δ -106.5 (Si^iPr_3), -136.2 (Si^iPr_3), -159.6 (Si^iPr_3), -212.6 (Si^iPr_3).

2.5.6 Synthesis of [U(COT$^{(SiiPr3)2}$)(Cp^{NMe4})] (**2.5**)

To a dry mixture of UI_3 (1.240 g, 2.000 mmol) and K[Cp^{NMe4}] (0.335 g, 2.08 mmol) was added THF (150 mL) at -78 °C. The mixture was slowly warmed to room temperature and stirred for 24 hours. The blue/black solution was cooled to –38 °C and to this was added a solution of K_2[COT$^{(SiiPr3)2}$] (0.865 g, 1.75 mmol) in THF (50 mL) dropwise over 35 minutes. The reaction mixture was warmed to room temperature and the solvent removed *in vacuo* to give a dark green/brown residue. Residual THF was removed by addition of pentane (20 mL) and subsequent drying *in vacuo*. Dissolution in pentane and filtration through a Celite frit gave a brown solution from which brown solids were obtained at -35 °C.

Yield: 0.243 g (0.311 mmol), 16% based on UI_3.

Anal. calc (found) for $C_{34}H_{60}NSi_2U$: C 52.55 (52.73), N 1.80 (1.85), H 7.78 (7.77)%.

MS (EI): *m/z* = 157 (100%), 776 (9%, M^+).

^{1}H NMR (d_8-toluene, 303 K): δ 1.7 (s, br, 18H, ^{i}Pr-CH_3), 1.1 (s, br, 6H, ^{i}Pr-C*H*), -0.5 (s, br, 18H, ^{i}Pr-CH_3), -5.5 (s, br, 2H, COT-C*H*), -6.4 (s, br, 6H, Cp-CH_3), -43.9 (s, br, 2H, COT-C*H*), -60.4 (s, br, 2H, COT-C*H*), -60.9 (s, br, Cp-CH_3).

^{29}Si{^{1}H} NMR (d_8-toluene, 303 K): δ -139.6 ($Si^{i}Pr_3$).

*2.5.7 Characterisation of [U(COT$^{(SiiPr3)2}$)(Cp^{NMe4})(THF)] (**2.5THF**)*

To a saturated solution of [U(COT$^{(SiiPr3)2}$)(Cp^{NMe4})] in d_8-toluene was added THF (0.5 mL) to give a mixture of **2.5THF** and **2.5** in a 1:2 ratio.

^{1}H NMR (d_8-toluene, 303 K): δ 8.4 (s, br, 2H, COT-C*H*), 3.4 (s, br, Cp-CH_3), 3.2 (s, br, 4H, THF), -1.3 (s, br, 4H, THF), -1.1 (s, br, 6H, ^{i}Pr-C*H*), -2.2 (br, 24H, ^{i}Pr-CH_3), -4.0 (s, br, 18H, ^{i}Pr-CH_3), -34.9 (s, br, Cp-CH_3), -75.0 (s, br, 2H, COT-C*H*), -91.4 (s, br, 2H, COT-C*H*).

^{29}Si{^{1}H} NMR (d_8-toluene, 303 K): δ -141.6 ($Si^{i}Pr_3$).

*2.5.8 Synthesis of [U(COT$^{(SiiPr3)2}$)(Cp^{PMe4})(THF)] (**2.6THF**)*

To a solution of UI_3 (0.618 g, 0.999 mmol) in THF (30 mL) was added a solution of K[Cp^{PMe4}] (0.178 g, 0.998 mmol) in THF (20 mL) and the mixture was stirred overnight. The green solution was cooled to -45 °C and to this was added a solution of K_2[COT$^{(SiiPr3)2}$] (0.430 g, 0.869 mmol) in THF (20 mL) dropwise over 20 minutes. The reaction mixture was warmed to room temperature and the solvent removed *in vacuo* to give a dark brown residue. Dissolution in pentane and filtration through a Celite frit gave a brown solution. Purple needles were obtained at -35 °C from a saturated pentane solution with 0.5 ml THF added.

Yield: 0.281 g (0.324 mmol), 32% based on UI_3.

MS (EI): *m/z* = 157 (100%, $[Si^{i}Pr_3]^+$), 794 (5%, M^+ - THF).

^{1}H NMR (d_8-toluene, 303 K): δ 14.9 (s, br, 2H, COT-C*H*), 1.8 (s, br, 4H, THF), 0.8 (s, br, 4H, THF), -1.8 (s, br, 6H, ^{i}Pr-C*H*), -3.0 (br, 24H, ^{i}Pr-CH_3, Cp-CH_3), -4.8 (s, br, 18H, ^{i}Pr-CH_3), -25.7 (s, br, Cp-CH_3), -73.0 (s, br, 2H, COT-C*H*), -83.4 (s, br, 2H, COT-C*H*).

^{29}Si{^{1}H} NMR (d_8-toluene, 303 K): δ -127.5 ($Si^{i}Pr_3$).

^{31}P{^{1}H} NMR (d_8-toluene, 303K): δ 846.2 (br, $w_{½}$ = 411 Hz, P-'ring').

2.5.9 Synthesis of [U(COT$^{(SiiPr3)2}$)(Cp^{PMe4})] ***(2.6)***

Method A:

Solids of [U(COT$^{(SiiPr3)2}$)(Cp^{PMe4})(THF)] were heated at 80 °C under reduced pressure (10^{-6} mbar) for 45 minutes. The residue was dissolved in d_8-toluene and was used for later reactions.

Method B:

A pre-weighed sample of [U(COT$^{(SiiPr3)2}$)(Cp^{PMe4})(THF)] was dissolved in 3 mL toluene in a Young's tube. The solvent was slowly evaporated under reduced pressure at 50 °C to leave a purple residue, which could be used for later reactions.

Anal. calc (found) for $C_{34}H_{60}Si_2PU$: C 51.43 (51.57), H 7.62 (7.69)%.

^{1}H NMR (d_8-toluene, 303 K): δ 34.3 (s, br, 2H, COT-C*H*), -1.7 (s, br, 6H, ^{i}Pr-C*H*), -4.6 (s, br, 18H, ^{i}Pr-CH_3), -8.1 (s, br, 18H, ^{i}Pr-CH_3), -13.4 (s, br, 6H, Cp-CH_3), -35.4 (s, br, Cp-CH_3), -72.5 (s, br, 2H, COT-C*H*), -106.8 (s, br, 2H, COT-C*H*).

^{29}Si{^{1}H} NMR (d_8-toluene, 303 K): δ -120.3 ($Si^{i}Pr_3$).

^{31}P{^{1}H} NMR (d_8-toluene, 303K): δ 910.6 (br, $w_{½}$ = 1433 Hz, P-'ring').

*2.5.10 Synthesis of [U(COT$^{(SiiPr3)2}$)(Cp^{AsMe4})] (**2.7**)*

To a dry mixture of UI_3 (0.592 g, 0.956 mmol) and K[Cp^{AsMe4}] (0.213 g, 0.958 mmol) was added THF (80 mL) at -78 °C. The mixture was slowly warmed to room temperature and stirred for 24 hours. The green solution was cooled to -40 °C and to this was added a solution of K_2[COT$^{(Si\textit{i}Pr3)2}$] (0.370 g, 0.747 mmol) in THF (30 mL) over 30 minutes. The reaction mixture was warmed to room temperature and the solvent removed *in vacuo* to give a brown residue. Residual THF was removed by addition of pentane (20 mL) and subsequent drying *in vacuo*. Dissolution in pentane and filtration through a Celite frit gave a brown solution from which solids were obtained at -35 °C.

Yield: 0.320 g (0.381 mmol), 40% based on UI_3.

Anal. calc (found) for $C_{34}H_{60}Si_2AsU$: C 48.73 (48.29), H 7.22 (7.33)%.

MS (EI): *m/z* = 115 (100%, [Si^{i}Pr$_2$]$^+$), 837 (20%, M$^+$).

^{1}H NMR (d_8-toluene, 303 K): δ 35.3 (s, br, 2H, COT-C*H*), -1.6 (s, br, 6H, ^{i}Pr-C*H*), -4.2 (s, br, 18H, ^{i}Pr-C*H*$_3$), -7.6 (s, br, 18H, ^{i}Pr-C*H*$_3$), -13.9 (s, br, 6H, Cp-C*H*$_3$), -41.0 (s, br, Cp-C*H*$_3$), -71.7 (s, br, 2H, COT-C*H*), -105.8 (s, br, 2H, COT-C*H*).

^{29}Si{^{1}H} NMR (d_8-toluene, 303 K): δ -116.3 (*Si*^{i}Pr$_3$).

*2.5.11 Synthesis of U(COT$^{(SiiPr3)2}$)(Cp^{AsMe4})(THF) (**2.7THF**)*

To a saturated solution of [U(COT$^{(Si\textit{i}Pr3)2}$)(Cp^{AsMe4})] in pentane was added 0.5 mL THF. Crystals were obtained at -35 °C.

^{1}H NMR (d_8-toluene, 303 K): δ 15.4 (s, br, 2H, COT-C*H*), 8.4 (s, br, 4H, THF), -1.7 (s, br, 6H, ^{i}Pr-C*H*), -2.8 (br, 24H, ^{i}Pr-C*H*$_3$), -3.2 (s, br, Cp-C*H*$_3$) -4.6 (s, br, 18H, ^{i}Pr-C*H*$_3$), -16.5 (s, br, 4H, THF), -28.7 (s, br, Cp-C*H*$_3$), -72.6 (s, br, 2H, COT-C*H*), -80.5 (s, br, 2H, COT-C*H*).

^{29}Si{^{1}H} NMR (d_8-toluene, 303 K): δ -126.5 (*Si*^{i}Pr$_3$).

*2.5.12 Characterisation of [U(COT$^{1,4\text{-SiiPr3}}$)(COT$^{1,3\text{-SiiPr3}}$)] (**2.8**)*

After crystals of **2.6** had been obtained, the remaining pentane solution was allowed to evaporate at room temperature. The residue was dissolved in equal parts toluene and THF then cooled to -35 °C to yield microcrystalline solids of **2.8**.

MS (EI): *m/z* = 115 (100%, [Si^{i}Pr$_2$]$^{+}$), 1071 (5%, M^{+} + H).

^{1}H NMR (d_8-toluene, 303 K): δ -1.7 (s, br, 18H, ^{i}Pr-C*H*$_3$), -1.9 (s, br, 18H, ^{i}Pr-C*H*$_3$), -2.2 (s, br, 18H, ^{i}Pr-C*H*$_3$), -4.1 (s, br, 18H, ^{i}Pr-C*H*$_3$), -4.5 (s, br, 6H, ^{i}Pr-C*H*), -5.5 (s, br, 6H, ^{i}Pr-C*H*), -18.3 (s, br, 1H, COT-C*H*), -26.9 (s, br, 2H, COT-C*H*), -28.2 (s, br, 2H, COT-C*H*), -36.2 (s, br, 2H, COT-C*H*), -39.3 (s, br, 2H, COT-C*H*), -42.5 (s, br, 2H, COT-C*H*), -47.6 (s, br, 1H, COT-C*H*).

^{29}Si{^{1}H} NMR (d_8-toluene, 303 K): δ -72.8 (*Si*^{i}Pr$_3$), -93.4 (*Si*^{i}Pr$_3$).

*2.5.13 Characterisation of [U(COT$^{(SiiPr3)2}$)(Cp^{AsMe4})I] (**2.9**)*

Crystals of **2.9** were obtained at -35 °C amongst the desolvated powder of [U(COT$^{(Si\textit{i}Pr3)2}$)(Cp^{AsMe4})].

^{1}H NMR (d_8-toluene, 303 K): δ -73.8 (s, br, 2H, COT-C*H*), 9.0 (s, br, Cp-C*H*$_3$), 7.3 (s, br, Cp-C*H*$_3$), -6.5 (s, br, 6H, ^{i}Pr-C*H*), -7.4 (s, br, 18H, ^{i}Pr-C*H*$_3$), -8.6 (s, br, 18H, ^{i}Pr-C*H*$_3$), -90.2 (s, br, 2H, COT-C*H*), -101.5 (s, br, 2H, COT-C*H*).

^{29}Si{^{1}H} NMR (d_8-toluene, 303 K): δ -74.3 (*Si*^{i}Pr$_3$).

*2.5.14 Synthesis of [U(COT$^{(SiiPr3)2}$)(Cp^{PMe4})(O^{n}Bu)] (**2.10**)*

To a solution of [U(COT$^{(SiiPr3)2}$)(Cp^{PMe4})] (28.7 mg, 3.61 x 10^{-5} mol) in d_8-toluene was added 10 equivalents THF (30 μL). The solution was heated to 75 °C for ten days to quantitatively form **2.10**.

MS (EI): *m/z* = 728 (100%), 867 (15%, M^+).

^{1}H NMR (d_8-toluene, 303 K): δ 159.0 (m, br, 2H, OCH_2CH$_2$CH$_2$CH$_3$), 133.2 (m, br, 2H, COT-C*H*), 62.6 (s, br, 2H, OCH$_2$CH_2CH$_2$CH$_3$), 34.8 (s, br, 2H, OCH$_2$CH$_2$CH_2CH$_3$), 18.7 (s, br, 3H, OCH$_2$CH$_2$CH$_2$CH_3), -7.7 (m, 6H, ^{i}Pr-C*H*/Cp-CH_3), -7.9 (m, 18H, ^{i}Pr-CH_3), -15.0 (m, 6H, ^{i}Pr-C*H*/Cp-CH_3), -15.7 (s, br, 18H, ^{i}Pr-CH_3), -18.5 (m, 6H, ^{i}Pr-C*H*/Cp-CH_3), -31.8 (m, br, 2H, COT-C*H*), -107.7 (m, br, 2H, COT-C*H*).

^{29}Si{^{1}H} NMR (d_8-toluene, 303 K): δ -143.3 (*Si*^{i}Pr$_3$).

^{31}P{^{1}H} NMR (d_8-toluene, 303 K): δ 51.2 (m, *P-ring*).

*2.5.15 Synthesis of [U(COT$^{(SiiPr3)2}$)(Cp^{AsMe4})(O^{n}Bu)] (**2.11**)*

To a solution of [U(COT$^{(SiiPr3)2}$)(Cp^{AsMe4})] (15.9 mg, 1.90 x 10^{-5} mol) in d_8-toluene was added two drops THF. The solution was heated to 100 °C for three days to quantitatively form **2.11**.

MS (EI): *m/z* = 28 (100%), 919 (9%, M^+).

^{1}H NMR (d_8-toluene, 303 K): δ 161.8 (s, br, 2H, OCH_2CH$_2$CH$_2$CH$_3$), 135.5 (s, br, 2H, COT-C*H*), 63.2 (s, br, 2H, OCH$_2$CH_2CH$_2$CH$_3$), 35.1 (s, br, 2H, OCH$_2$CH$_2$CH_2CH$_3$), 18.9 (s, br, 3H, OCH$_2$CH$_2$CH$_2$CH_3), -7.7 (m, 6H, ^{i}Pr-C*H*/Cp-CH_3), -7.8 (m, 18H, ^{i}Pr-CH_3), -15.7 (s, br, 18H, ^{i}Pr-CH_3), -16.5 (m, 6H, ^{i}Pr-C*H*/Cp-CH_3), -18.6 (m, 6H, ^{i}Pr-C*H*/Cp-CH_3), -31.1 (s, br, 2H, COT-C*H*), -110.1 (s, br, 2H, COT-C*H*).

^{29}Si{^{1}H} NMR (d_8-toluene, 303 K): δ -144.3 (*Si*^{i}Pr$_3$).

*2.5.16 Synthesis of [U(COT$^{(SiiPr3)2}$)(Cp^{NMe4})(O^{n}Bu)] (**2.12**) and [(COT$^{(SiiPr3)2}$)U(μ-η^5:η^1-NC$_4$Me$_3$CH)U(COT$^{(SiiPr3)2}$)(NC$_4$Me$_4$)] (**2.13**)*

To a solution of [U(COT$^{(SiiPr3)2}$)(Cp^{NMe4})] (31.1 mg, 4.00 x 10^{-5} mol) in d_8-toluene was added one drop THF. The solution was heated to 75 °C for 14 days to completely consume the starting material. NMR analysis showed **2.12** and **2.13** were present in *ca.* 4:1 ratio. The residue was dried *in vacuo* then dissolved in pentane and filtered through a filter pipette to give a brown solution from which crystals of **2.13** were obtained at -35 °C.

Characterisation of [U(COT$^{(SiiPr3)2}$)(Cp^{NMe4})(O^{n}Bu)] (**2.12**)

MS (EI): *m/z* = 59 (100%), 850 (20%, M^+).

^{1}H NMR (d_8-toluene, 303 K): δ 153.1 (s, br, 2H, OC*H*$_2$CH$_2$CH$_2$CH$_3$), 122.9 (s, br, 2H, COT-C*H*), 60.4 (s, br, 2H, OCH$_2$C*H*$_2$CH$_2$CH$_3$), 34.6 (s, br, 2H, OCH$_2$CH$_2$C*H*$_2$CH$_3$), 18.0 (t, $^3J_{HH}$ = 6.5 Hz, 3H, OCH$_2$CH$_2$CH$_2$C*H*$_3$), -5.0 (s, br, 6H, ^{i}Pr-C*H*/Cp-C*H*$_3$), -7.6 (d, $^3J_{HH}$ = 6.5 Hz, 18H, ^{i}Pr-C*H*$_3$), -12.7 (s, br, 6H, ^{i}Pr-C*H*/Cp-C*H*$_3$), -15.6 (d, $^3J_{HH}$ = 5.5 Hz, 18H, ^{i}Pr-C*H*$_3$), -18.4 (s, br, 6H, ^{i}Pr-C*H*/Cp-C*H*$_3$), -33.8 (s, br, 2H, COT-C*H*), -100.3 (s, br, 2H, COT-C*H*).

^{29}Si{^{1}H} NMR (d_8-toluene, 303 K): δ -140.6 (*Si*^{i}Pr$_3$).

Characterisation of [(COT$^{(SiiPr3)2}$)U(μ-η^5:η^1-NC$_4$Me$_3$CH)U(COT$^{(SiiPr3)2}$)(NC$_4$Me$_4$)] (**2.13**)

Yield: 6.9 mg (4.4 x 10^{-6} mol), 22% based on [U(COT$^{(SiiPr3)2}$)(Cp^{NMe4})].

MS (EI): *m/z* = 775 (100%), 1550 (4%, M^+).

^{1}H NMR (d_6-benzene, 303 K): δ 24.0 (s, br, 3H, Cp-CH_3), 17.9 (s, br, 6H), 12.3 (s, br, 1H, COT-C*H*), 10.9 (s, br, 1H, COT-C*H*), 0.0 (br), -1.6 (s, br, 18H, ^{i}Pr-CH_3), -2.9 (s, br, 6H), -10.9 (s, br, 6H), -18.6 (s, br, 6H), -24.3 (s, br, 6H), -24.5 (s, br, 6H), -106.8 (s, br, 6H).

2.6 References

1 G. Wilkinson, M. Rosenblum, M. C. Whiting and R. B. Woodward, *J. Am. Chem. Soc.*, 1952, **74**, 2125–2126.

2 S. A. Miller, J. A. Tebboth and J. F. Tremaine, *J. Chem. Soc.*, 1952, 632–635.

3 T. J. Kealy and P. L. Pauson, *Nature*, 1951, **168**, 1039–1040.

4 V. E. O. Fischer and W. Pfab, *Z. Naturforsch B*, 1952, **7b**, 377–378.

5 V. Lorenz, S. Blaurock, C. G. Hrib and F. T. Edelmann, *Organometallics*, 2010, **29**, 4787–4789.

6 A. F. R. Kilpatrick, J. C. Green, F. G. N. Cloke and N. Tsoureas, *Chem. Commun.*, 2013, **49**, 9434–9436.

7 C. W. Tate, P. B. Hitchcock, G. A. Lawless, Z. Benkõ, L. Nyulászi and J. F. Nixon, *Comptes Rendus Chimie*, 2010, **13**, 1063–1072.

8 C. Elschenbroich, *Organometallics*, Wiley-VCH Verlag GmbH & Co. KGaA, Weinheim, Germany, 3rd edn., 2006.

9 E. Montalvo, K. A. Miller, J. W. Ziller and W. J. Evans, *Organometallics*, 2010, **29**, 4159–4170.

10 O. Bénaud, J.-C. Berthet, P. Thuéry and M. Ephritikhine, *Inorg. Chem.*, 2011, **50**, 12204–12214.

11 R. Boaretto, P. Roussel, A. J. Kingsley, I. J. Munslow, C. J. Sanders, N. W. Alcock and P. Scott, *Chem. Commun.*, 1999, 1701–1702.

12 R. Boaretto, P. Roussel, N. W. Alcock, A. J. Kingsley, I. J. Munslow, C. J. Sanders and P. Scott, *J. Organomet. Chem.*, 1999, **591**, 174–184.

13 W. J. Evans, N. A. Siladke and J. W. Ziller, *Chem. Eur. J.*, 2010, **16**, 796–800.

14 M. K. Takase, N. A. Siladke, J. W. Ziller and W. J. Evans, *Organometallics*, 2011, **30**, 458–465.

15 C. R. Graves, E. J. Schelter, T. Cantat, B. L. Scott and J. L. Kiplinger, *Organometallics*, 2008, **27**, 5371–5378.

16 S. W. Hall, J. C. Huffman, M. M. Miller, L. R. Avens, C. J. Burns, D. S. J. Arney, A. F. England and A. P. Sattelberger, *Organometallics*, 1993, **12**, 752–758.

17 O. Bénaud, J.-C. Berthet, P. Thuéry and M. Ephritikhine, *Inorg. Chem.*, 2010, **49**, 8117–8130.

18 W. J. Evans, K. A. Miller, A. G. DiPasquale, A. L. Rheingold, T. J. Stewart and R. Bau, *Angew. Chem. Int. Ed.*, 2008, **47**, 5075–5078.

19 J. A. Higgins, F. G. N. Cloke and S. M. Roe, *Organometallics*, 2013, **32**, 5244–5252.

20 E. Montalvo, J. W. Ziller, A. G. DiPasquale, A. L. Rheingold and W. J. Evans, *Organometallics*, 2010, **29**, 2104–2110.

21 N. Tsoureas, O. T. Summerscales, F. G. N. Cloke and S. M. Roe, *Organometallics*, 2013, **32**, 1353–1362.

22 N. Tsoureas, L. Castro, A. F. R. Kilpatrick, F. G. N. Cloke and L. Maron, *Chem. Sci.*, 2014, **5**, 3777–3788.

23 O. T. Summerscales, F. G. N. Cloke, P. B. Hitchcock, J. C. Green and N. Hazari, *Science*, 2006, **311**, 829–831.

24 F. G. N. Cloke and P. B. Hitchcock, *J. Am. Chem. Soc.*, 2002, **124**, 9352–9353.

25 J. H. Farnaby, F. G. N. Cloke, M. P. Coles, J. C. Green and G. Aitken, *Comptes Rendus Chimie*, 2010, **13**, 812–820.

26 O. T. Summerscales, F. G. N. Cloke, P. B. Hitchcock, J. C. Green and N. Hazari, *J. Am. Chem. Soc.*, 2006, **128**, 9602–9603.

27 M. Weydert, J. G. Brennan, R. A. Andersen and R. G. Bergman, *Organometallics*, 1995, **14**, 3942–3951.

28 O. T. Summerscales, DPhil Thesis, University of Sussex, 2007.

29 I. Noviandri, K. N. Brown, D. S. Fleming, P. T. Gulyas, P. A. Lay, A. F. Masters and L. Phillips, *J. Phys. Chem. B*, 1999, **103**, 6713–6722.

30 A. F. R. Kilpatrick, F. G. N. Cloke, N. Tsoureas and A. S. P. Frey, *Unpublished Results*.

31 A. F. R. Kilpatrick, DPhil Thesis, University of Sussex, 2014.

32 C. P. Larch, DPhil Thesis, University of Sussex, 2006.

33 F. H. Allen, *Acta Cryst. Sect. B*, 2002, **B58**, 380–388.

34 I. J. Bruno, J. C. Cole, P. R. Edgington, M. Kessler, C. F. Macrae, P. McCabe, J. Pearson and R. Taylor, *Acta Cryst. Sect. B*, 2002, **B58**, 389–397.

35 C. C. McComas, J. W. Ziller and D. L. Van Vranken, *Organometallics*, 2000, **19**, 2853–2857.

36 M. Visseaux, F. Nief and L. Ricard, *J. Organomet. Chem.*, 2002, **647**, 139–144.

37 S. M. Cendrowski-guillaume, G. Le Gland, M. Nierlich and M. Ephritikhine, *Eur. J. Inorg. Chem.*, 2003, 1388–1393.

38 S. M. Cendrowski-Guillaume, M. Nierlich and M. Ephritikhine, *J. Organomet. Chem.*, 2002, **643-644**, 209– 213.

39 Mostame, MChem Dissertation, University of Sussex, 2012.

40 I. Korobkov, S. Gambarotta, G. P. A. Yap, L. Thompson and P. J. Hay, *Organometallics*, 2001, **20**, 5440–5445.

41 D. Baudry, M. Ephritikhine, F. Nief, L. Ricard and F. Mathey, *Angew. Chem. Int. Ed.*, 1990, **29**, 1485–1486.

42 P. Gradoz, M. Ephritikhine, M. Lance, J. Vigner and M. Nierlich, *J. Organomet. Chem.*, 1994, **481**, 69–73.

43 A. Elkechai, A. Boucekkine, L. Belkhiri, D. Hauchard, C. Clappe and M. Ephritikhine, *Comptes Rendus Chimie*, 2010, **13**, 860–869.

44 A. Elkechai, Y. Mani, A. Boucekkine and M. Ephritikhine, *Inorg. Chem.*, 2012, **51**, 6943–6952.

45 C. Clappe, D. Leveugle, D. Hauchard and G. Durand, *J. Electroanal. Chem.*, 1998, **448**, 95–103.

46 K. J. Chase, R. F. Bryan, M. K. Woode and R. N. Grimes, *Organometallics*, 1991, **10**, 2631–2642.

47 P. Lemoine, M. Gross, P. Braunstein, F. Mathey, B. Deschamps and J. H. Nelson, *Organometallics*, 1984, **3**, 1303–1307.

48 A. J. Ashe III, S. Muhmoud, C. Elschenbroich and M. Wünsch, *Angew. Chem. Int. Ed. Engl.*, 1987, **26**, 229–230.

49 V. Lorenz, B. M. Schmiege, C. G. Hrib, J. W. Ziller, A. Edelmann, S. Blaurock, W. J. Evans and F. T. Edelmann, *J. Am. Chem. Soc.*, 2011, **133**, 1257–1259.

50 A. Edelmann, V. Lorenz, C. G. Hrib, L. Hilfert, S. Blaurock and F. T. Edelmann, *Organometallics*, 2013, **32**, 1435–1444.

51 J. A. Higgins, DPhil Thesis, University of Sussex, 2014.

52 J. Rebizant, *Acta Cryst. Sect. C*, 1991, **C47**, 854–856.

53 A. E. Enriquez, B. L. Scott and M. P. Neu, *Inorg. Chem.*, 2005, **44**, 7403–7413.

54 W. J. Evans, S. A. Kozimor, J. W. Ziller, A. A. Fagin and M. N. Bochkarev, *Inorg. Chem.*, 2005, **44**, 3993–4000.

55 W. J. Evans, J. R. Walensky and J. W. Ziller, *Organometallics*, 2010, **29**, 101–107.

56 M. J. Monreal and P. L. Diaconescu, *Organometallics*, 2008, **27**, 1702–1706.

57 P. C. Blake, M. F. Lappert, R. G. Taylor, J. L. Atwood, W. E. Hunter and H. Zhang, *J. Chem. Soc. Dalton Trans.*, 1995, 3335–3342.

58 J. Maynadié, J.-C. Berthet, P. Thuéry and M. Ephritikhine, *Organometallics*, 2006, **25**, 5603–5611.

59 A. S. P. Frey, F. G. N. Cloke, M. P. Coles, L. Maron and T. Davin, *Angew. Chem. Int. Ed.*, 2011, **50**, 6881–6883.

CHAPTER 3: ACTIVATION OF CARBON OXIDES BY URANIUM(III) MIXED-SANDWICH COMPLEXES WITH SUBSTITUTED CYCLOPENTADIENYL LIGANDS

3.1 Binding and activation of small molecules by uranium complexes

Reactive transformations of small molecules have been of considerable interest for many years. The prospect of controlled synthesis of biologically, pharmaceutically and industrially important species in a manner that is cost-effective, scalable and safe has profound implications, and could ultimately lead to better products and a cleaner environment. Uranium is an element that has recently come into the foreground of this area of research due to its ability to promote challenging transformations under mild reaction conditions. A summary of the chemistry reported within the last few decades is detailed below.

3.1.1 Dinitrogen

3.1.1.1 Features and applications of dinitrogen activation by uranium(III) complexes

Dinitrogen activation has been a prominent area of research for decades due to its significance in the synthesis of industrially useful molecules and important biological functions. The Haber-Bosch process, which employs iron and ruthenium catalysts to convert dinitrogen and dihydrogen into ammonia is an important example.[1] This process produces in excess of one hundred million tons of ammonia each year; however the conditions for the conversion are not trivial and require temperatures and pressures reaching 550 °C and 350 bar respectively.[2] This is a stark contrast to biological systems which, under ambient conditions, employ nitrogenase enzymes to facilitate the same transformation.

Whilst the availability of dinitrogen does not present any problems, its high bond dissociation energy (945 kJmol^{-1}), large HOMO-LUMO gap (*ca.* 23 eV) and its apolarity make it thermodynamically and kinetically difficult to break the triple bond.[3] The mechanisms nitrogenase enzymes employ to complete the transformation from dinitrogen to ammonia are still uncertain, but research has found that active sites incorporating transition metals play an active role in this process. Using nature as a model, it has been proposed that using the correct combination of metal(s) and ancillary ligands can significantly weaken the triple bond, allowing transformations to occur under mild conditions. As such, work to date on dinitrogen activation has looked at the binding and reduction of dinitrogen at metal centres within an organometallic complex. As a weak σ-donor/π-acceptor ligand, dinitrogen can bind either end-on or side-on, as a terminal or bridging ligand. Side-on binding has been reported for several trivalent lanthanide complexes as this coordination mode enables effective π-backbonding and reduction of the triple bond.[4]

The degree to which activation has occurred can be assessed by study of the N–N bond length and the N–N stretching frequency. As a coordinated, side-on ligand, dinitrogen is classed as a neutral ligand with a characteristic triple bond and high frequency N–N IR absorption band (*ca* 1.1 Å and 2331 cm^{-1} respectively). Upon reduction however, the bond length is seen to increase and the stretching frequency decrease (*ca* 1.24 Å and 1440 cm^{-1} for the N_2^{2-} ligand and 1.4 Å and 1110 cm^{-1} for the N_2^{4-} ligand).[5,6] Although most reductions of this nature are two-electron processes, the synthesis of an N_2^{3-} radical ligand bridging two dysprosium centres was reported in 2009, a study which has since been extended to other lanthanides (**Figure 3.1**).[7–11]

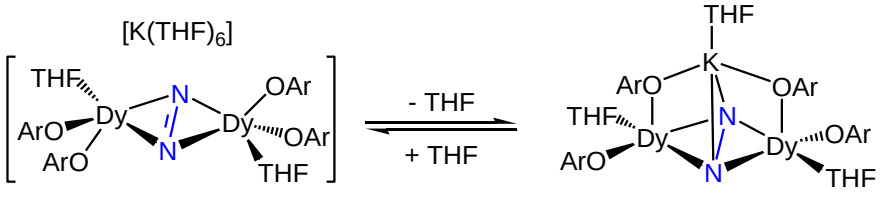

Figure 3.1 The dysprosium complexes featuring the N_2^{3-} ligand.[7]

3.1.1.2 Coordination of dinitrogen

Coordination of dinitrogen to a uranium(III) centre was first reported in 1998 by Roussel and Scott, who reported the reversible coordination of N_2 to a uranium(III) triamidoamine complex (**Figure 3.2**).[12] Subsequent removal of the dinitrogen ligand could be achieved by freeze-thaw degassing the solution, which regenerated the parent uranium complex without decomposition. Crystals of the dinitrogen complex however were stable under an argon atmosphere for several months.

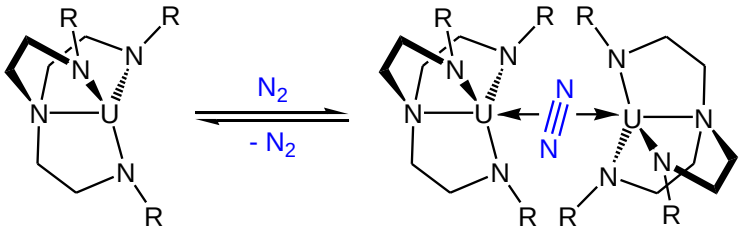

Figure 3.2 Reversible binding of dinitrogen to a uranium(III) triamidoamine complex.[12]

Magnetic susceptibility studies of the dinitrogen complex indicated that uranium had not undergone a change in oxidation state upon binding, and XRD studies illustrated side-on coordination of dinitrogen with negligible lengthening of the N–N bond.[12,13] At the time of publication the binding was proposed to consist of σ-donation by the π_p orbital to the uranium centre, however subsequent theoretical work has suggested the interaction to be predominantly backbonding from the 5f orbitals into the antibonding π_g orbital.[14]

In 2003 Evans and co-workers reported the first example of an end-on bound dinitrogen uranium complex, formed from $[U(Cp^*)_3]$ under 80 psi dinitrogen (**Figure 3.3**).[15] Studies of $[(Cp^*)_3U(\eta^1\text{-}N_2)]$ revealed the dinitrogen fragment retains the properties of a neutral N_2 ligand and binds perpendicularly to the $[U(Cp^*)_3]$ plane. The formation of this complex is also reversible and regenerates the trivalent uranium starting material without decomposition when the pressure is lowered to one atmosphere.

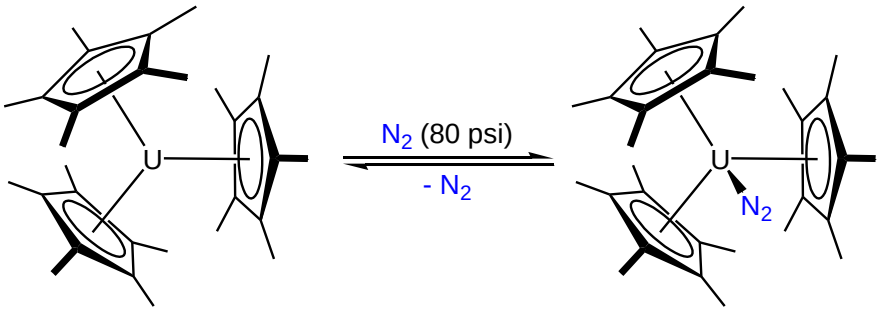

Figure 3.3 Synthesis of $[(C_5Me_5)_3U(\eta^1\text{-}N_2)]$.[15]

3.1.1.3 Reductive activation of dinitrogen

The earliest report of dinitrogen reduction by a uranium complex was published in 1998 by Cummins and co-workers, who synthesised a uranium/molybdenum bimetallic complex with an end-on bound dinitrogen bridge (**Figure 3.4**).[16] Initial reactivity studies found that the uranium(III) complex, [U(N-*tert*-butylanilide)$_3$], was unreactive towards dinitrogen. However, in the presence of a stoichiometric quantity of [Mo(N{^{t}Bu}Ph)$_3$], the dinitrogen bridged complex was synthesised quantitatively. This is rationalised by initial formation of [(N$_2$)Mo(N{^{t}Bu}Ph)$_3$] which is subsequently trapped by the uranium complex. Infrared and XRD data illustrate a two-electron reduction of dinitrogen with concurrent one-electron oxidations for uranium and molybdenum.

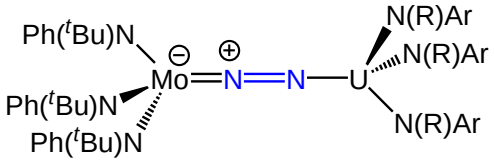

N(R)Ar = N-*tert*-butylanilide

Figure 3.4 A heterobimetallic dinitrogen complex featuring an end-on bound N_2^{2-} ligand.[16]

More recently, Cloke and co-workers reported the reduction of dinitrogen by a uranium(III) pentalene complex to yield a bridged species with a μ-η^2:η^2-N_2^{2-} fragment (**Figure 3.5**).[17] This complex exhibits a N=N bond length consistent with a two-electron reduction, and a slight fold within the [U_2N_2] core away from the pentalene ligands. This is postulated to be due to the sterics of the complex and it is believed that this is the cause of the facile regeneration of the uranium(III) pentalene complex under reduced pressure. Computational studies on this complex confirmed that a two-electron reduction of dinitrogen had occurred and found the core to be composed of uranium 5f orbitals and a set of N_2 π_g orbitals which point towards the uranium atoms.[18]

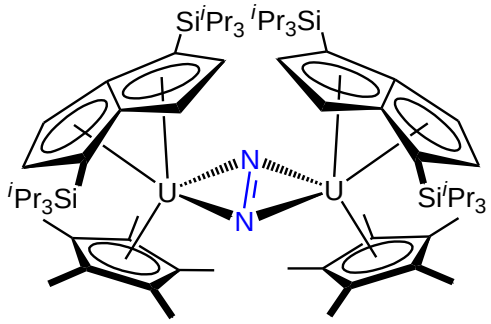

Figure 3.5 [U(Pn$^{(SiiPr3)2}$)(Cp*)]$_2$(μ-η^2:η^2-N_2) as synthesised by Cloke *et al*..[17]

In 2011, Arnold and co-workers reported the activation of dinitrogen during the synthesis of a uranium(III) trisaryloxide complex (**Figure 3.6**).[19] The complex, [(TtbpO)$_3$U(N_2)U(OTtbp)$_3$] (OTtbp = 2,4,6-^{t}Bu$_3$C$_6$H$_2$), was found to be more kinetically stable than the preceding dinitrogen complexes and only regenerated the starting complex when heated to 80 °C. Analogous complexes supported by siloxide ancillary ligands have also been reported and the stability of these and the aryloxide complexes is assigned to the steric environment supporting the N_2^{2-} fragment.[20]

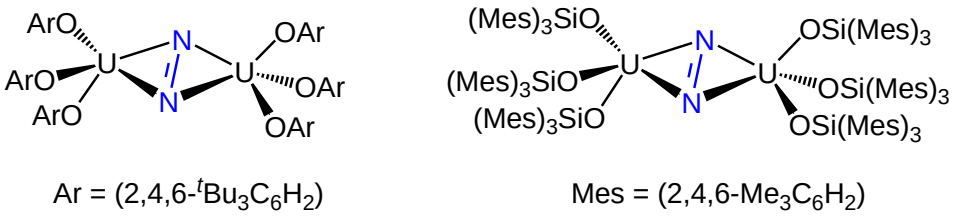

Ar = (2,4,6-^{t}Bu$_3$C$_6$H$_2$) Mes = (2,4,6-Me$_3$C$_6$H$_2$)

Figure 3.6 Dinitrogen complexes of uranium supported by TtbpO aryloxide ligands (left) and siloxide ligands (right).[19,20]

3.1.2 Carbon monoxide

3.1.2.1 Properties and applications of carbon monoxide

Carbon monoxide has become increasingly important over the last few decades for its use as a C_1 feedstock. Fischer-Tropsch processes, which convert carbon monoxide and dihydrogen into hydrocarbons and oxygenates, have seen more attention, especially as the finite resources of fossil fuels decline.[21,22] The scope for this chemistry is broad, with the synthesis of alcohols, carbonyl, aromatic and aliphatic compounds available. The majority of this chemistry employs transition metal catalysts, but forcing conditions are often required. Low Temperature Fischer-Tropsch (LTFT) reactions for example, require temperatures exceeding 180 °C and typically use syngas pressures above 10 bar.[23]

Carbon monoxide is ubiquitous as a ligand in transition metal chemistry, whereas lanthanide and actinide carbonyl complexes are contrastingly rare. As a σ-donor/π-acceptor ligand, CO interacts favourably with transition metals, with back-donation from the metal d-orbitals to the carbonyl π*-orbitals the main stabilising factor.[24] The f-orbitals however, are less suited to this role and consequently most f-element carbonyl complexes have only been observed by matrix isolation. Carbon monoxide can bind to metals in several modes (**Figure 3.7**), with characteristic infrared bands for each, allowing facile structural characterisation of the complexes.

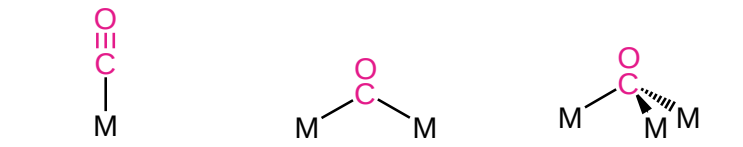

1850-2120 cm^{-1} 1750-1850 cm^{-1} 1620-1730 cm^{-1}

Figure 3.7 The binding modes of CO with infrared stretching frequencies.[24]

Reactivity of carbon monoxide at the metal centre is also of key importance. With a bond dissociation energy of 1076.5 $kJmol^{-1}$, cleavage of the C≡O bond is not trivial. However, the polarity of the bond gives rise to a wealth of reactivity which is not seen for isoelectronic dinitrogen.[25]

3.1.2.2 Carbonyl complexes

The earliest examples of uranium carbonyl compounds were observed by matrix isolation. In 1971, Sheline and Slater reported the synthesis of uranium carbonyl species by condensing uranium metal vapour into a dilute carbon monoxide-argon matrix at 4 K.[26] Infrared studies of the matrix identified over six carbonyl species, however, later studies found that pulsed laser evaporated uranium atoms have sufficient energy to insert into the C≡O bond upon condensation, giving rise to a series of C···U···O species.[27,28] These complexes were found to be the dominant product over the carbonyl species. Other carbon monoxide matrix isolation studies carried out on UF_4 show a blue-shifted carbonyl band, consistent for σ-donation to the metal centre, and little or no π-interaction.[29]

The first organometallic uranium carbonyl complex, $[(Cp^{SiMe3})_3UCO]$, was reported in 1986 by Andersen and co-workers, however this complex underwent reversible extrusion of carbon monoxide under reduced pressure.[30] The first isolable uranium

carbonyl complex was not reported until 1995, when the cyclopentadienyl rings were altered from Cp^{SiMe3} to Cp^{Me4}, providing the ideal steric and electronic environment to stabilise the uranium-carbonyl fragment.[31] The M–CO stretching frequencies of both complexes are red-shifted in comparison to carbon monoxide, indicating significant π-backbonding into the antibonding orbitals of the carbonyl moiety.

Studies on analogous complexes gave a total of five $[(Cp^{R})_3UCO]$ complexes. All these species exhibit reversible coordination of carbon monoxide and only $[(Cp^{Me4})_3UCO]$ and $[(Cp^*)_3UCO]$ (**Figure 3.8**) were crystallographically characterised.[32] Comparison of these structures shows that both complexes have a linear U–C–O unit, but have varying geometries as $[(Cp^{Me5})_3UCO]$ is too bulky to adopt a pseudo tetrahedral geometry in order to relieve steric strain. Infrared studies also illustrate that the frequency of the carbonyl stretch is lowered as more electron donating groups are added to the cyclopentadienyl ring.[32,33] $[(Cp^*)_3UCO]$ however, has a higher stretching frequency than $[(Cp^{Me4})_3UCO]$, which is assigned to the long U–CO bond in $[(Cp^*)_3UCO]$ due to steric crowding.[32]

When CO was added to $[(Cp^*)_3Nd]$ and $[(Cp^*)_3Sm]$ however, a carbonyl complex was not the product obtained. Instead two molecules of CO inserted into the M–C(Cp) bonds to give a carbonium ion complex with a positive charge on the reacted cyclopentadienyl ring and a negative charge on the metal centre (**Figure 3.8**).[32,34] The size similarity of Nd^{3+} and Sm^{3+} (112.3 and 109.8 ppm respectively) make the analogous reactivity unsurprising.[35] However, the varied reactivity for uranium illustrates that the reaction outcome is not governed by sterics alone, and highlights the differences in reactivity between the 4f- and 5f-elements.

Computational studies on the uranium carbonyl complexes found back-donation of electron density to originate from the $U–Cp^{R}$ bonding fπ and dπ orbitals.[36] This rationalises why $[Ln(Cp^{R})_3]$ complexes do not form carbonyl complexes as the radial

extension of the 4f and 5d orbitals is significantly smaller than the 5f and 6d, and cannot therefore engage in transfer of π-electron density.

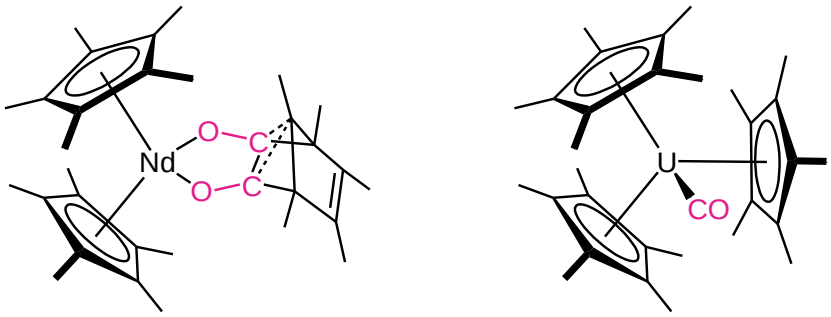

Figure 3.8 $[(Cp^{Me5})_2Nd(O_2C_7Me_5)]$ (left) and $[(Cp^{Me5})_3UCO]$ (right).[32]

3.1.2.3 Insertion chemistry

Due to the apparent instability of uranium carbonyl complexes it is not surprising that the earliest forms of reactivity involved insertion of CO into uranium-element σ-bonds. The majority of the literature on this subject centres on uranium-carbon and uranium-nitrogen bond reactivity. Unsurprisingly, the high affinity of uranium for oxygen implies that the uranium-oxygen bond is too strong to be broken by CO and no insertion reactions of this type have been reported. Insertion of carbon monoxide into other uranium-element bonds has also received little attention.

Early examples of CO insertion include the synthesis of η^2-acyl and η^2-carbamoyl complexes from $[Cp_3UR]$ and $[Cp_3UNR_2]$, which was found to be reversible with gentle heating under a dinitrogen atmosphere.[37] η^2-Coordination was confirmed by the presence of an infrared band between 1490 and 1505 cm^{-1} and the absence of a band between 1630 and 1680 cm^{-1}. Carbamoyl complexes of uranium and thorium synthesised by Fagan also exhibited distinct η^2-carbonyl frequencies, which were lower

in energy than analogous transition metal carbamoyls due to the actinides higher affinity for oxygen.[38]

Hoffmann and co-workers investigated the orbital interactions of η^2-acyl ligands with transition metal and actinide complexes of d^0 electronic configuration.[39] These calculations revealed that there are two energy minima for the complexes corresponding to O-inside coordination and O-outside coordination (**Figure 3.9**). These minima only differ by 0.03 eV, which rationalises the coexistence of both configurations in $[(Cp^*)_2An(CONR_2)Cl]$ complexes.[38] Further studies found that despite the small energy difference, uranium complexes with two acyl moieties such as $[Cp_2U(COCH_3)_2]$ favour O-outside, O-outside coordination, which is the most stable of the three possible configurations.[38–40] These results agree with the observed geometry of $[(Cp^*)_2U(CONMe_2)_2]$ which also favours this configuration (**Figure 3.9**).

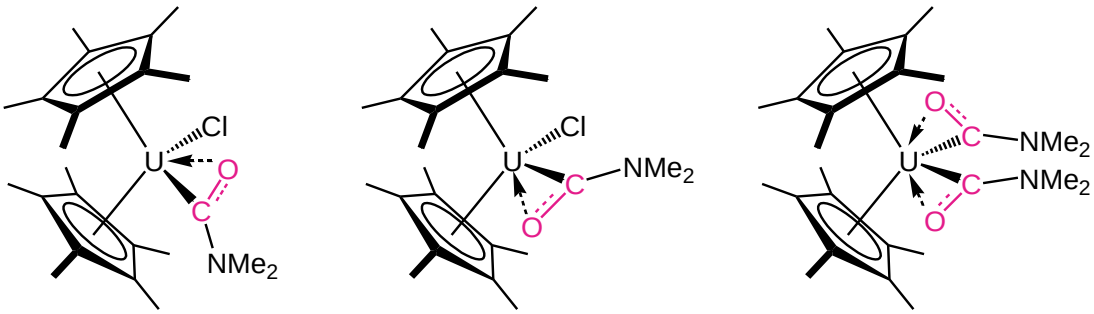

Figure 3.9 The O-inside configuration (left) and the O-outside configuration (centre) for $[(Cp^*)_2U(CONMe_2)Cl]$. The O-outside, O-outside configuration is illustrated by $[Cp^*_2U(CONMe_2)_2]$ (right).[38,40]

It has also been observed that reaction of carbon monoxide with uranium and thorium dialkyls gives rise to double CO insertion and coupling of the two acyl carbons to form an enediolate moiety.[41] These products are monomeric when the alkyl groups are large,

but have been found to dimerise when smaller alkyls are used. The enediolate fragment can be characterised by infrared spectroscopy and exhibits bands corresponding to *ν*C=C and *ν*C-O. Calculations by Hoffmann and co-workers rationalised the formation of the enediolate complex by finding that this species is 2.9 eV lower in energy than the acyl complex.[40]

Insertion of carbon monoxide into uranium metallacycles also gives rise to the formation of a C=C bond. A recent example reported by Bénaud found CO insertion gave rise to expansion of the ring by one atom with formation of an enolate fragment by migration of the silyl moiety (**Figure 3.10**).[42]

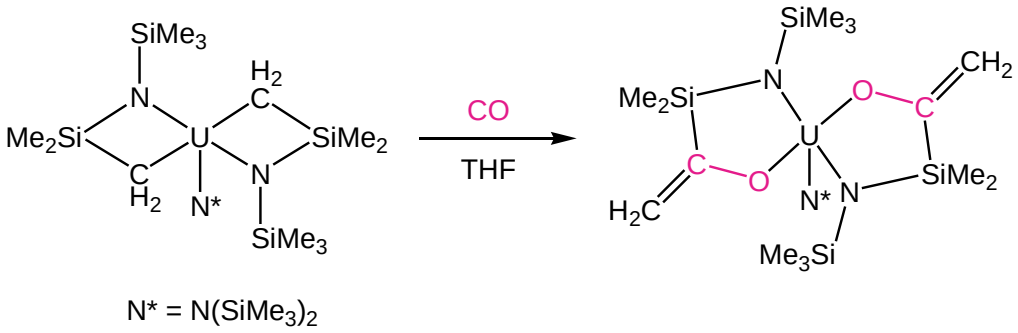

Figure 3.10 Formation of an enolate complex by double CO insertion.[42]

An analogous metallacycle was reported by Arnold and co-workers, who proposed carbon monoxide insertion occurs following thermally induced C-H activation.[43] This was rationalised to proceed according to the mechanism outlined in **Figure 3.11**, however attempts to isolate the C-H activated complex by thermolysis under partial static vacuum failed to produce the four-membered metallacycle intermediate. This reactivity indicates that the tethered carbene is sufficiently labile to allow approach of CO to the metal centre, however the reducing capability of the complex is insufficient to facilitate reductive coupling of carbon monoxide.

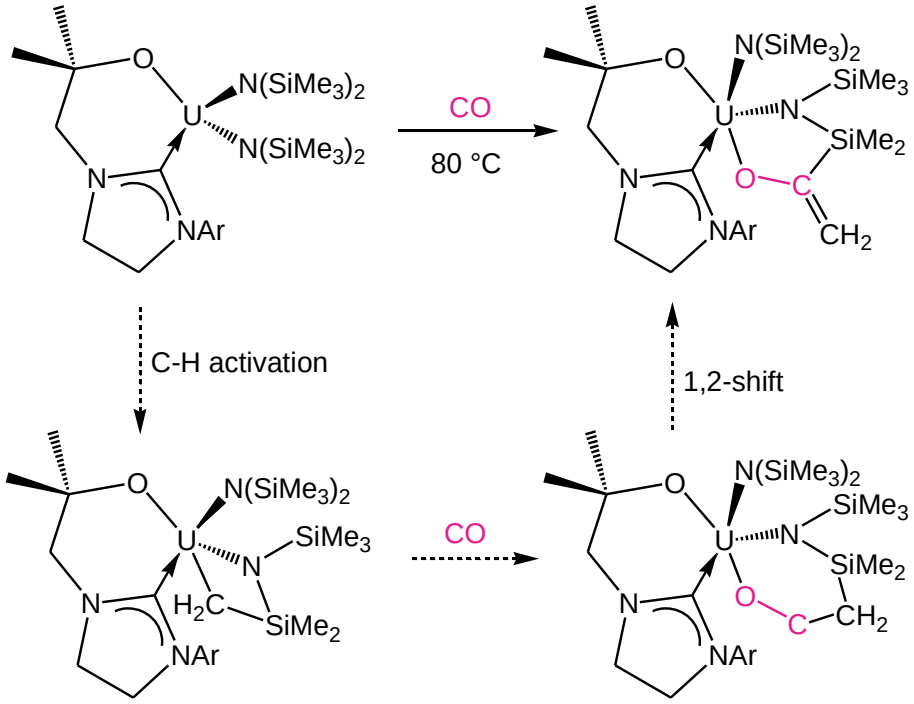

Figure 3.11 Formation of a five-membered metallacycle *via* C-H activation.[43]

Insertion reactions have also been reported for uranium-carbon multiple bonds. In 1982 Cramer and Gilje demonstrated that carbon monoxide insertion into a U=C(ylid) bond gives rise to an η^2-acyl complex with a C=C bond that is delocalised over the η^2-β-ketoylide fragment.[44] This study was furthered by reaction of [Cp_3U=CHPMe_2Ph] with [CpMn$(CO)_3$], which resulted in the insertion of one of the carbonyl ligands into the uranium–carbon double bond (**Figure 3.12**). The resulting bimetallic complex is observed to have similar delocalisation to the η^2-β-ketoylide complex, such that the bonding in the structure lies between an enolate and a Fischer carbene complex.[45]

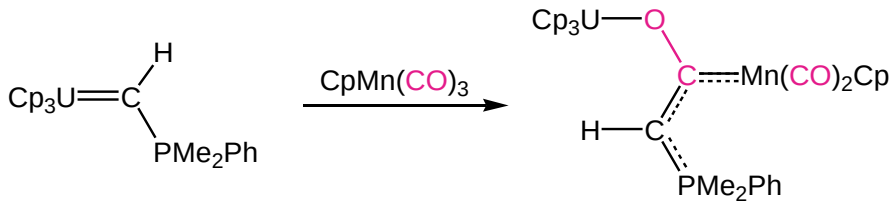

Figure 3.12 Insertion of a carbonyl ligand into a uranium-carbon multiple bond.[45,46]

Further studies found that the carbon-oxygen bond can be thermolytically cleaved giving rise to a novel manganese complex with a zwitterionic phosphonium acetylide ligand and a uranium hydroxo complex. This reactivity demonstrates that coordination of the oxygen atom to uranium weakens the carbon-oxygen bond, facilitating cleavage (**Figure 3.13**).[47] A related study found that reaction of [Cp_3U=CHPMe_2Ph] with tungsten hexacarbonyl gives rise to the analogous bimetallic complex. However thermolysis of this species results in rearrangement, leaving the C–O bond intact.[48]

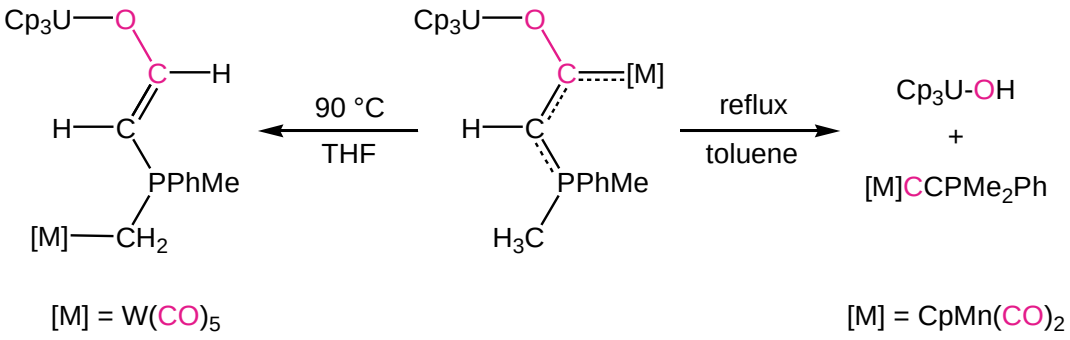

Figure 3.13 Thermolysis of the uranium-molybdenum and uranium-tungsten heterobimetallic complexes.[47,48]

3.1.2.4 Activation of CO

Whilst carbon monoxide insertion has been present in the literature for over forty years, reductive activation of carbon monoxide has only been reported recently. A novel example, published by Meyer and co-workers, is the one electron reduction of carbon monoxide by a uranium(III) tacn complex to form a uranium(III)/uranium(IV) mixed valence bimetallic complex with a μ:η^1:η^1-CO bridge.[49] Carbon monoxide has also been observed to serve as a reducing agent for a uranium(V) imido complex with the tacn ligand system to yield an isocyanate complex (**Figure 3.14**).[50] This results in the one-

electron reduction of the uranium centre, and coupling of the two trimethylsilyl fragments.

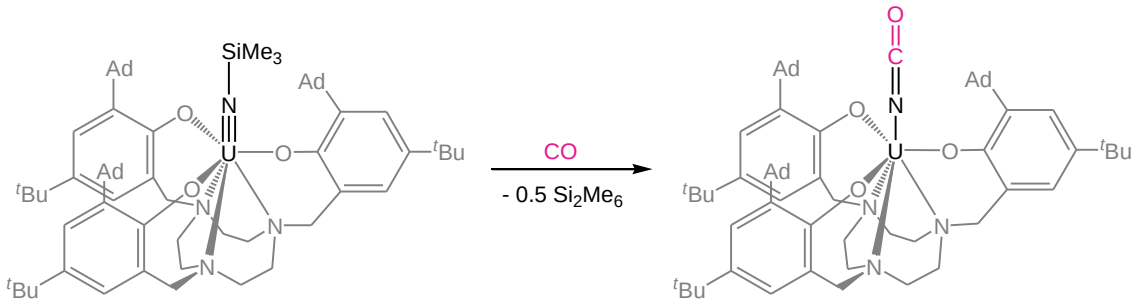

Figure 3.14 Reactivity of a uranium(V) imido complex with CO.[50]

Cloke and colleagues first reported the reductive activation of carbon monoxide by uranium(III) mixed-sandwich complexes in 2006 with the synthesis of the bimetallic deltate complex.[51] This was followed by the publication of the analogous squarate and ynediolate complexes and further investigations illustrated that the homologised CO-derived fragment obtained is dependent on the sterics of the ligands (**Figure 3.15**).[52,53] In addition, reactivity studies on this system found the final products to be unreactive towards dihydrogen, however a methoxide complex could be synthesised by reacting the uranium(III) complex with a mixture of CO and H_2.[54] Other gaseous mixtures also proved fruitful with the synthesis of cyanate and oxo complexes from a mixture of CO and NO.[55]

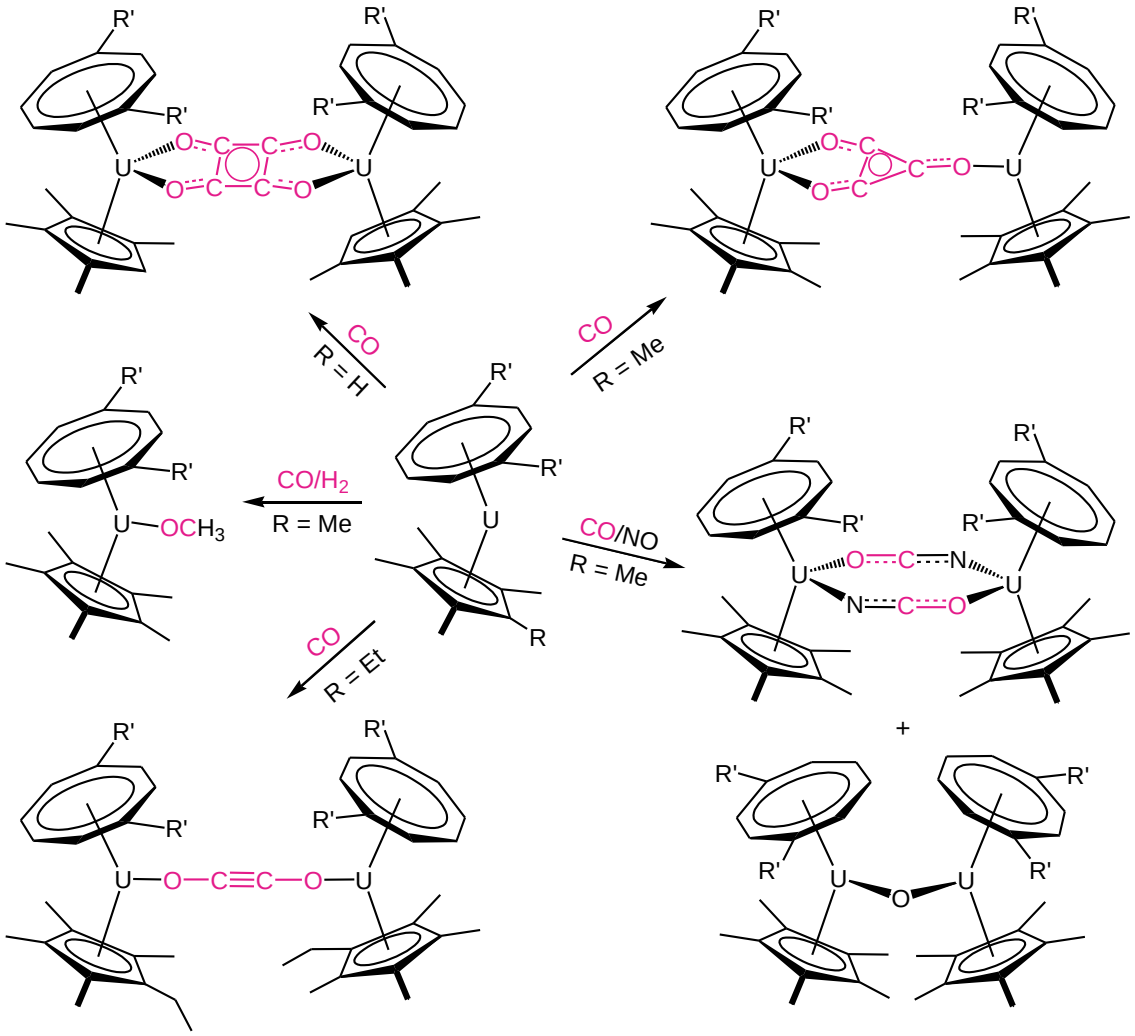

Figure 3.15 Reactivity of uranium(III) mixed-sandwich complexes with CO (R' = Si^iPr_3 except for the ynediolate complex where R' = $SiMe_3$).[51–55]

Ynediolate complexes have also been synthesised by other research groups. Arnold *et al.* reported the synthesis of this fragment from $[U(N\{SiMe_3\}_2)_3]$ under mild conditions regardless of CO stoichiometry.[56] This complex was also unreactive towards dihydrogen, however, underwent insertion of the ynediolate fragment into a C–H bond to form an asymmetrical enediolate complex when heated (**Figure 3.16**). Liddle and colleagues also reported subsequent reaction of the ynediolate fragment in a uranium complex bearing amido ligands.[57] In this case the ynediolate fragment inserts into the

N–Si bond, and a new oxo bridge is formed between the two metal centres by reaction of the complex with an unidentified oxygen source.

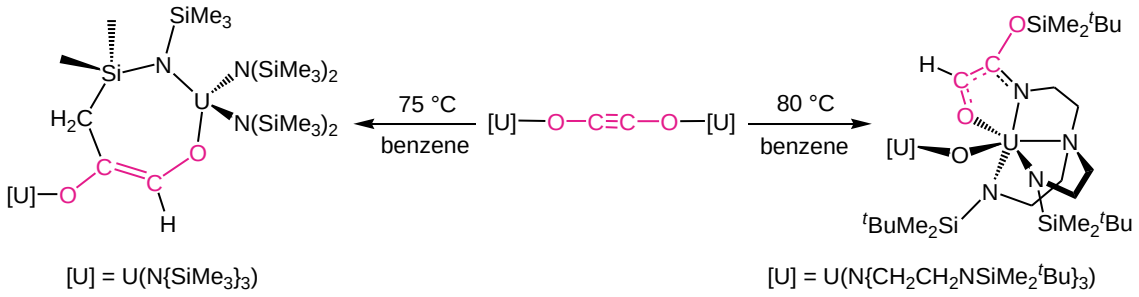

Figure 3.16 Thermolysis reactions of uranium ynediolate complexes.[56,57]

3.1.3 Carbon dioxide

3.1.3.1 Properties and coordination of carbon dioxide

Interest in carbon dioxide has become prominent over the last few decades, due in part to declining fossil fuel reserves and due to its contribution to climate change. Carbon dioxide is therefore not only desirable in terms of its use as a C_1 feedstock, but also as a recyclable gas that could be extracted from the atmosphere. Carbon dioxide is a linear molecule with two strong (532.2 $kJmol^{-1}$) polar C=O bonds giving rise to an overall apolar molecule.[25]

There are several modes of coordination for carbon dioxide to one or two metal centres (**Figure 3.17**) and several transition metal adducts have been reported.[58–60] Only Meyer and colleagues however, have reported the coordination of carbon dioxide to a uranium centre.[61,62] Coordination to [(($^{t\text{Bu,Ad}}$ArO)$_3$tacn)U] was accompanied by a one-electron reduction of CO_2 to give a linear η^1-OCO radical anion bound to a uranium(IV) centre.

This rare form of coordination occurs due to the cylindrical shape of the reactive pocket, which is encompassed by the adamantyl substituents.

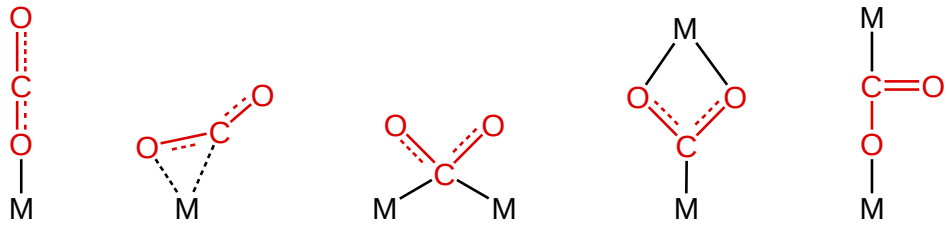

Figure 3.17 Coordination modes of carbon dioxide to one or two metal centres.

3.1.3.2 Insertion chemistry

Insertion of carbon dioxide into uranium-element bonds is a common occurrence and has proved useful for the synthesis of novel uranium complexes and fragments. Coordination of the fragment can be mono- or bidentate and can coordinate to one or two metal centres (**Figure 3.18**). For actinide complexes, it is generally expected that the fragment will coordinate in a bidentate fashion due to the large coordination sphere of the metal, unless the sterics of other ancillary ligands preclude this.

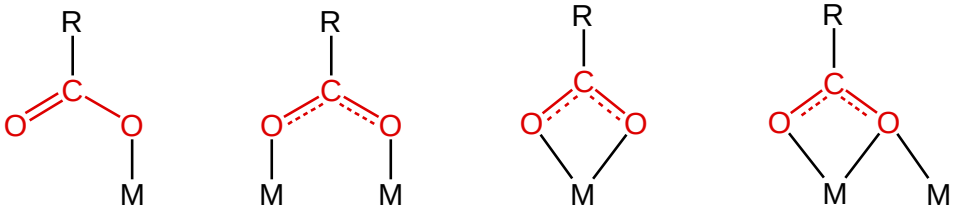

Figure 3.18 Coordination modes of carbon dioxide insertion fragments.

Variation in coordination mode was recently observed by Bart and Meyer in uranium(IV) tacn carbamate complexes, [((^{tBu,R}ArO)$_3$tacn)U(O$_2$CNHMes)], where the sterics of the R substituent dictate the bonding mode.[63] When R is *tert*-butyl, the coordination pocket is larger allowing for a shorter U–O contact and η^1-coordination. When R is adamantyl however, the binding pocket is smaller and prevents close contact between the oxygen atoms and uranium. This results in bidentate bonding with two longer U–O bonds. Interestingly, when the analogous uranium(V) imide complexes are exposed to carbon dioxide, insertion does not occur. Instead a [2+2] cycloaddition reaction yields a uranium(V) oxo complex with formation of mesityl isocyanate (**Figure 3.19**). However, alteration of the imide substituent from mesityl to phenyl results in a double [2+2] cycloaddition reaction, which forms the uranium(V) oxo complex and a uranium(V) diphenyl ureate complex.

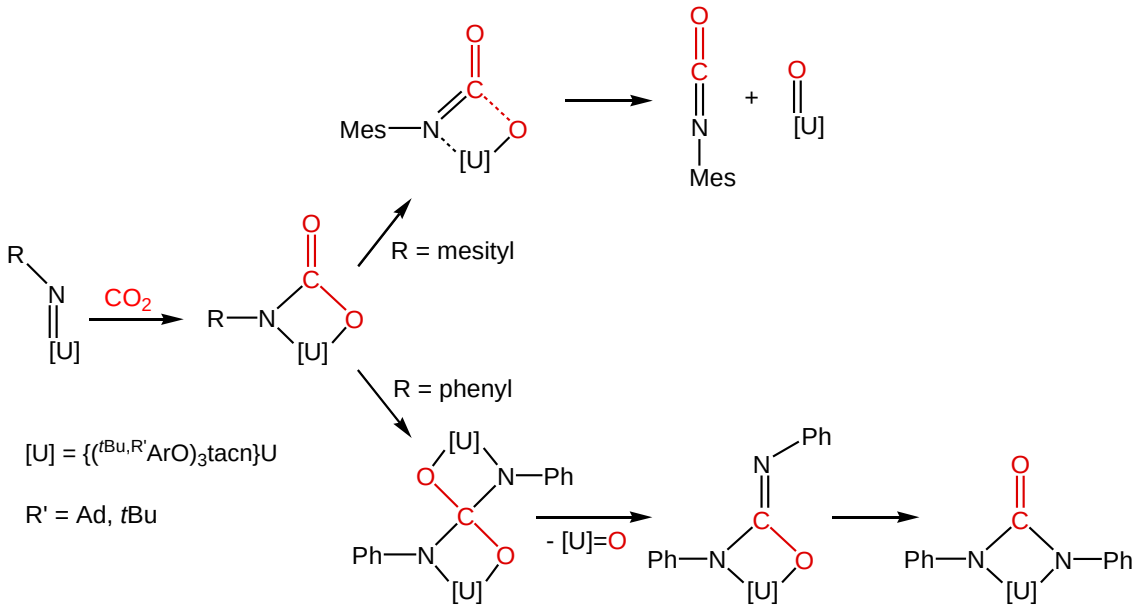

Figure 3.19 Observed reactivity of carbon dioxide with uranium(V) imide complexes.[63]

Insertion of carbon dioxide into uranium–carbon bonds was first reported by Moloy and Marks in 1985 with the sequential insertion of CO_2 into uranium–methyl fragments in the complexes $[Cp_2UMe_2]$ and $[(Cp^*)_2UMe_2]$.[64] These results also highlight the influence of sterics on coordination mode as it was found the smaller, unsubstituted cyclopentadienyl complex formed a dimeric product, whereas the Cp* complex remained monomeric. Evans has also shown that U–C insertion chemistry is not limited to uranium alkyls, by successful reaction of uranium alkynyl and allyl complexes with carbon dioxide.[65,66]

Although uranium hydride complexes are less common, they have also been shown to insert carbon dioxide to yield formate complexes.[67] In the case of $[U(Cp^{SiMe3})_3H]$, the resulting formate can then be converted to a dioxymethylene complex by reaction with the hydride starting complex (**Figure 3.20**) giving rise to a reduced carbon dioxide moiety.[68]

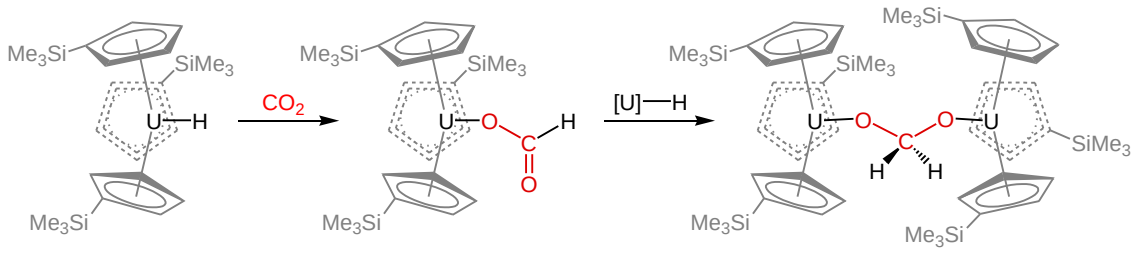

Figure 3.20 Synthesis of a dioxymethylene complex by reaction of a uranium hydride complex with carbon dioxide.[68]

CO_2 insertion into a uranium–sulfur bond was first reported in 1996 with the reversible synthesis of $[Cp_3UO_2CS^iPr]$.[69] $[(Cp^*)_2U(SR)_2]$ complexes however, have more stable insertion products and $[(Cp^*)_2U(O_2CS^tBu)_2]$ was the first crystallographically characterised complex of this type.[70] Similar reactivity was also observed with carbon

disulfide, which formed a novel trithiocarbonate complex, $[(Cp^*)_2U(S_2CS^tBu)(S^tBu)]$. More recently, Meyer and co-workers reported the insertion of CO_2, COS and CS_2 into uranium–sulfur and uranium–selenium bonds to give mixed-carbonate fragments bridging two uranium centres.[71] These complexes have proved to be stable and are not reactive towards hydrolysing, silylating or reducing reagents.

Whilst insertion reactivity has typically involved uranium(IV) complexes, Bart and co-workers published the first uranium(III) carboxylate and dithiocarboxylate complexes in 2011.[72,73] Interestingly, whilst the delocalisation of the carboxylate fragment is observed in the molecular structure, the dithiocarboxylate structure exhibits a U–S single bond and a U–S dative bond, as evidenced by infrared studies.

In recent years Meyer has investigated the derivatisation of 1,2-ketones by CO_2 insertion (**Figure 3.21**).[74] Reaction of the diketone with two mole equivalents uranium complex yielded a dinuclear dienolate complex, which inserted carbon dioxide to form a new C–C bond. The CO_2 unit is bidentate with delocalised charge whereas the diketone fragment shows distinct C–O single and double bonds. In contrast the mononuclear enolate complex, formed by stoichiometric reaction of the diketone with the starting complex, was shown to be unreactive towards carbon dioxide.

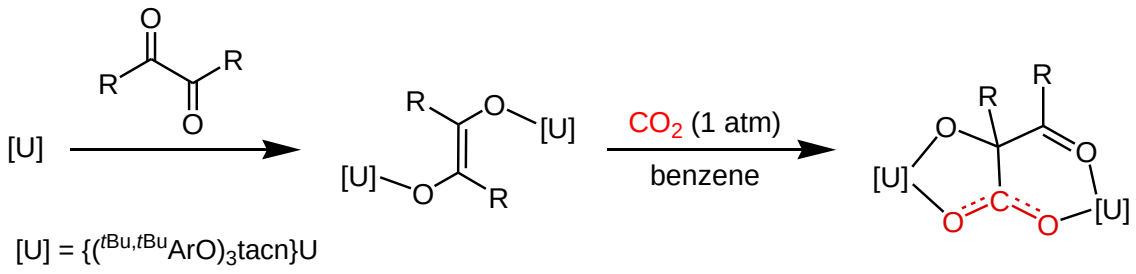

Figure 3.21 Functionalisation of diketones by carbon dioxide insertion.[74]

3.1.3.3 Reduction of carbon dioxide by uranium complexes

An area of research currently receiving a lot of attention is the reductive activation of carbon dioxide. One reductive transformation that can occur is a two electron reduction of CO_2 to the oxo dianion and CO. Formation of uranium complexes with bridging-oxo ligands by this method was first reported in 1991 by Ephritikhine and co-workers in the reaction of $[U(Cp^{SiMe3})_3]$ with CO_2 (**Figure 3.22**).[75] The resulting complex, $[\{(Cp^{SiMe3})_3U\}_2(\mu\text{-}O)]$, which can also be prepared by reaction of $[U(Cp^{SiMe3})_3]$ with N_2O, has S_6 symmetry, with the bridging oxygen atom lying on the inversion centre. The U–O–U bond angle is linear, minimising electrostatic repulsions between the cyclopentadienyl rings, and the short U–O distances indicate a possible bond order greater than one from a π-interaction between the oxygen and uranium atoms. The analogous sulfide complex however, formed by reaction of $[U(Cp^{SiMe3})_3]$ with COS, does not have this feature, and the minimised electrostatic repulsion caused by a greater U–U distance gives rise to a bent U–S–U fragment.[76]

Despite the being isoelectronic with carbon dioxide, reaction of $[U(Cp^{SiMe3})_3]$ with carbon disulfide resulted in the formation of a bridging adduct, $[\{(Cp^{SiMe3})_3U\}_2(\mu\text{-}\eta^1\text{:}\eta^2\text{-}CS_2)]$.[77] It was postulated that the formation of the oxo complex proceeds *via* the analogous CO_2 complex, however the oxophilicity of uranium, coupled with the thermodynamic stability of CO, favours extrusion of carbon monoxide to yield the observed product. Similar reactivity has also been observed by Cloke and Kilpatrick for a bis(pentalene) dititanium complex, which forms a kinetically unstable CO_2 adduct prior to formation of an oxo complex.[78–80] Similarly, reactivity of COS gives rise to an unstable COS adduct, which decomposes to sulfide and carbonyl complexes, however the CS_2 adduct is stable and undergoes no further reactivity.

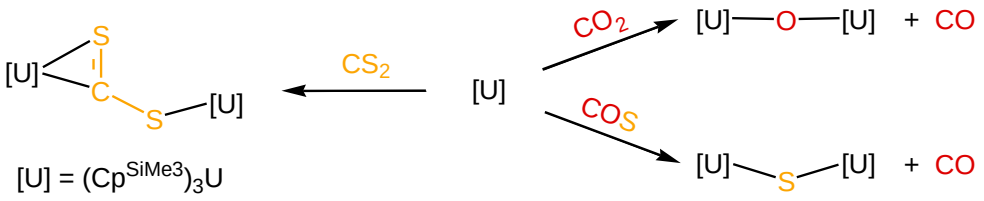

Figure 3.22 Comparative reactivity of [U(Cp^{SiMe3})$_3$] complex with CO_2, COS and CS_2.[75–77]

A more recent example of bridging oxo formation was reported by Meyer who found reaction of a uranium(III) tacn complex with carbon dioxide gave rise to the bridging oxo complex *via* a fleeting, colourless intermediate.[49] This species is proposed to be a carbon dioxide bridged diuranium species, however could not be isolated as rapid removal of solvent under vacuum only yielded the starting complex.

3.1.3.4 Reductive disproportionation

Uranium complexes have also facilitated the reductive disproportionation of two CO_2 molecules to give a carbonate dianion and CO. This was first reported by Cloke *et al.* in 2008, whereby reaction of the mixed-sandwich complex, [U($COT^{(SiiPr3)2}$)(Cp^{Me4})(THF)] with carbon dioxide yielded the bridging carbonate complex, [{U($COT^{(SiiPr3)2}$)(Cp^{Me4})}$_2$(μ-η^1:η^2-CO_3)].[81] Furthermore, if the stoichiometry of the reaction was adjusted to give 25% molar excess of the mixed-sandwich, the carbon monoxide side product was reductively coupled by the remaining complex to give the bridging squarate anion, making this the first synthesis of an oxocarbon fragment from CO_2.

Meyer and co-workers also observed similar reactivity with [({^{R}ArO}$_3$N)U] systems bearing resemblance to the tacn complexes.[82] Exposure of these species to excess carbon dioxide resulted in the formation of uranium(IV) bridging carbonate complexes,

where the mode of coordination is dependent on the ligand substituents (**Figure 3.23**). The formation of the carbonate complexes, which was not observed in the tacn ligand system, is explained by the increased flexibility of the aryloxide ligands, and it was suggested that smaller substituents on the tacn ligand would lead to similar reactivity. This proved to be the case and resulted in the formation of a μ-κ^2:κ^2-carbonate complex.[83] However, unlike the two carbonate complexes previously synthesised in this series, [[({^{Neop,Me}ArO}$_3$tacn)U]$_2$(μ-κ^2:κ^2-CO_3)] reacts cleanly and almost quantitatively with potassium graphite to regenerate the starting uranium(III) complex, illustrating the potential of optimised uranium systems for catalytic processes.

Mechanistic studies of these reactions found carbonate formation proceeds *via* an oxo intermediate which can be isolated by reaction of [({^{Neop,Me}ArO}$_3$tacn)U] with N_2O.[82,84] This has also led to the synthesis of the first uranium sulfite complex, [[({^{Neop,Me}ArO}$_3$tacn)U]$_2$(μ-κ^1:κ^2-SO_3)] by insertion of SO_2 into the uranium-oxo fragment.[85] The mixed-sandwich analogue however, was computed to form the carbonate complex *via* a concerted mechanism, as formation of an initial bridging oxo complex was found to be kinetically less accessible.[86]

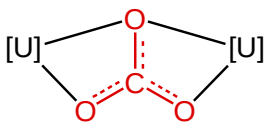

[U] = [({^{tBu}ArO}$_3$N)U]

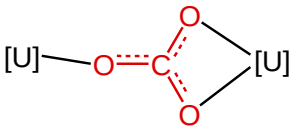

[U] = [({^{Ad}ArO}$_3$N)U]

Figure 3.23 Coordination modes of the carbonate fragment in [({^{R}ArO}$_3$N)U] complexes.[82]

3.1.3.5 Reductive coupling reactions

Until last year, reports of reductive coupling reactions by uranium complexes were limited to the synthesis of a tetrathiooxalate complex from [({^{Ad}ArO}$_3$N)U] and carbon disulfide.[87,88] The μ-κ^2:κ^2-C_2S_4 fragment, which bridges two uranium centres to form two four-membered metallacycles (**Figure 3.24**) was the major product from the reaction, with formation of the trithiocarbonate complex as a minor product. The preference for the formation of the tetrathiooxalate complex can be rationalised by the requirement to form CS in the synthesis of the trithiocarbonate complex. DFT studies of the formation of the sulfide complex from carbon disulfide show this step is endogonic (+2.6 kcal·mol^{-1}), unlike the CO_2 analogue, illustrating the favourable formation of CO *vs* CS. As a consequence, the trithiocarbonate is formed in low yields, as the thermodynamic gain from the formation of this species is reduced with respect to the tetrathiooxalate complex.

The tetrathiooxalate unit exhibited delocalisation over each CS_2 fragment, however the C–C bond was found to be single, and the unit exhibited a perpendicular twist along the C–C axis (**Figure 3.24**). Further studies on this complex found it could be reduced with sodium amalgam to yield the ethylenetetrathiolate complex. This fragment has a different bonding mode to its precursor, and bridges the two uranium centres to form two five-membered metallacycles (**Figure 3.24**). The bonding within the fragment also showed elongation of the C–S bonds with formation of a C=C bond.

Calculations by Maron and co-workers also suggested that the formation of the analogous oxalate species was more thermodynamically favourable than formation of the carbonate complex.[84] However, the synthesis of this complex was only recently observed, due to the higher activation barrier required for its formation. It was suggested however, that changes to the ligand substituents may lower the activation energy and facilitate its formation. This proved to be the case, and the oxalate complex was isolated from reaction of [({^{Ad}ArO}$_3$N)U] with a mixture of CO_2 and KC_8.[85] This is

rationalised by formation of the kinetically favoured carbonate complex, which is instantly reduced to the starting material by potassium graphite, allowing formation of the oxalate in modest yield.

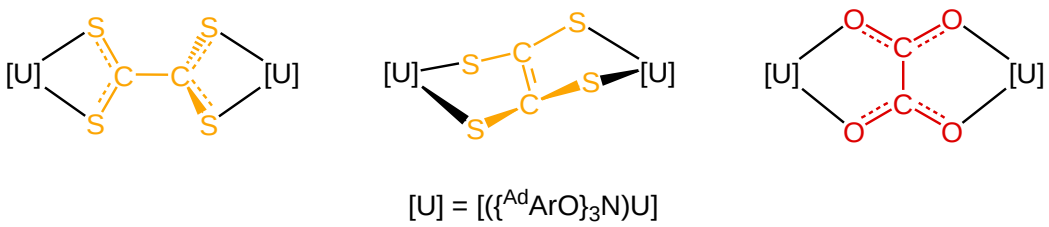

[U] = [({^{Ad}ArO}$_3$N)U]

Figure 3.24 The tetrathiooxalate (left), ethylenetetrathiolate (centre) and oxalate fragments (right) bridging two uranium centres.[85,87,88]

Cloke *et al.* also reported the synthesis of three oxalate complexes by reaction of uranium(III) mixed-sandwich complexes with carbon dioxide.[86] DFT studies of these reactions show the oxalate species to be thermodynamically more stable than the carbonate and oxo complexes, but kinetically more challenging under the reaction conditions employed. The difference in activation energy required however, is small accounting for the formation of both species.

3.1.4 Scope for Chapter 3

The wealth of small molecule reactivity reported in the literature illustrates the scope for uranium complexes to make unusual or otherwise inaccessible fragments under mild reaction conditions. The mixed-sandwich system, which has already been proven to facilitate challenging reductive transformations, has been thoroughly investigated, and illustrates the importance of the steric environment on the activation of small molecules.

Further studies of this nature using the *tert*-butyl and tri-*iso*-propylsilyl cyclopentadienyl ligands, were therefore conducted.

3.2 Activation of carbon monoxide

Activation of CO by mixed-sandwich complexes has seen the formation of the squarate, deltate and ynediolate fragments by reductive homologation of four, three and two CO molecules respectively.[51–53,89] The croconate and rhodizonate fragments, however, have not been observed despite the increased stability of these fragments with respect to the deltate and squarate moieties.[90] [U(COT$^{(SiiPr3)2}$)(Cp^{tBu})] (**2.1**) is a suitable candidate for the synthesis of one of these larger fragments due to the ability of the *tert*-butyl moiety to be positioned away from the COT silyl groups, allowing for a larger reactivity pocket. The rhodizonate fragment however, is thermodynamically unstable with respect to the croconate unit and would therefore only be formed if the increased steric stabilisation of the complex offset this energy. Previous studies by Cloke and the author for an undergraduate project found the largest three complexes, **2.2** – **2.4**, did not react with CO and the details of these experiments are not discussed.[91]

*3.2.1 Reactivity of [U(COT$^{(SiiPr3)2}$)(Cp^{tBu})] (**2.1**) with carbon monoxide*

Exposure of a solution of **2.1** to ^{13}CO resulted in a rapid colour change from green/brown to red/brown. NMR spectroscopy illustrated a multitude of proton resonances and no isotopically labelled carbon resonance, precluding characterisation of the resulting species. Repetition of the experiment with varying stoichiometries of CO (0.5 to 3.5 equivalents) for both the base-free complex (**2.1**) and THF adduct (**2.1THF**) consistently yielded the same result within minutes of gas addition. Other experiments conducted with a mixture of ^{13}CO and H_2 also gave rise to unassignable ^{1}H and ^{13}C{^{1}H} NMR spectra and it was therefore concluded that the decreased steric environment

around the uranium centre was unable to stabilise the croconate or rhodizonate fragments or the methoxide moiety observed by Cloke and Frey.[54]

However, red crystalline needles were obtained from saturated pentane solutions of both the CO and CO/H_2 reaction mixtures after several weeks. In both cases the crystals corresponded to a bimetallic uranium oxo species $[\{U(COT^{(SiiPr3)2})(Cp^{tBu})\}_2(\mu\text{-}O)]$ (**3.1**, **Figure 3.25**), formed by decomposition of the mixed-sandwich complex in the presence of CO. Comparison of the NMR spectra of the reaction mixtures after CO addition with the crude spectrum of **3.1** found that this species is not present within the first week after gas addition. It is therefore concluded that **3.1** is formed by slow reactivity between the decomposition products in solution.

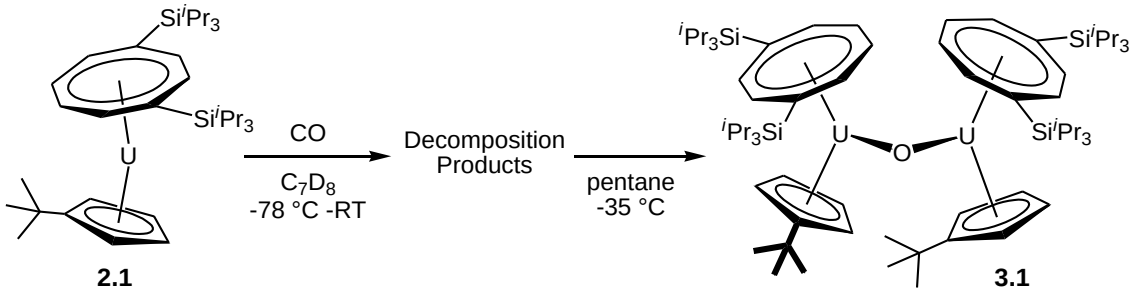

Figure 3.25 Reactivity of $[U(COT^{(SiiPr3)2})(Cp^{tBu})]$ with CO.

*3.2.2 Alternative synthesis of $[\{U(COT^{(SiiPr3)2})(Cp^{tBu})\}_2(\mu\text{-}O)]$ (**3.1**)*

In order to fully characterise **3.1**, an alternative synthetic route was required. Nitrous oxide has been shown to react with various uranium complexes to give bridging oxo species, including other mixed-sandwich complexes.[75,92–94] Addition of N_2O to a solution of **2.1** yielded **3.1** exclusively, which was characterised by a silicon resonance at -85.7 ppm (**Figure 3.26**). However the ^{1}H NMR spectrum precluded full assignment due to the presence of broad overlapping resonances between -6 and +5 ppm.

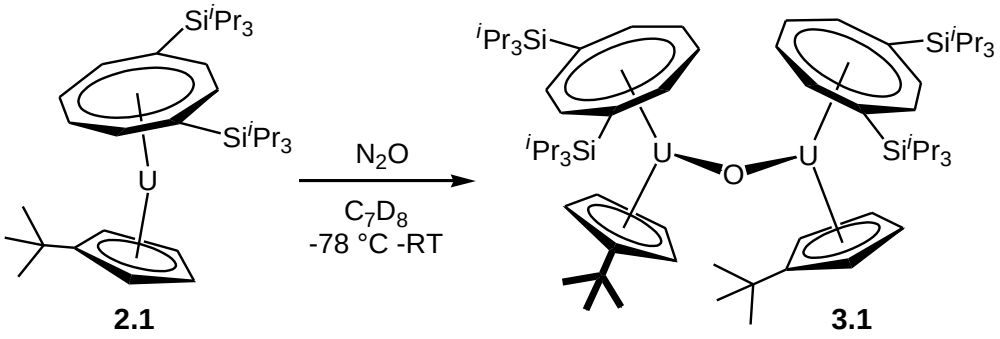

2.1 **3.1**

Figure 3.26 Synthesis of [{U(COT$^{(Si\mathit{i}Pr3)2}$)(Cp$^{\mathit{t}Bu}$)}$_2$(μ-O)] (**3.1**)

Comparison of the molecular structure of **3.1** (**Figure 3.27**, **Table 3.1**) with other oxo complexes in the literature which have no other bridging fragments to constrain the U–O–U unit shows that there is a wide variation in the U–O–U angle, ranging from 154.5(3) to 180.0°.[95,96] However with the exception of the reported mixed-sandwich oxo complexes, [{U(COT$^{(Si\mathit{i}Pr3)2}$)(Cp*)}$_2$(μ-O)] and [{U(COT$^{(SiMe3)2}$)(Cp*)}$_2$(μ-O)], which have U–O–U angles of 154.5(3) and 159.6(3)° respectively, all the other complexes have near linear angles, illustrating that **3.1** has the most acute U–O–U angle.[86,97] The U–O distances in the bridging oxo complexes however are similar (2.104(4) – 2.117(5) Å), resulting in a slight shortening of the U–U distances for the three mixed-sandwich complexes in comparison to other bridging oxo complexes.

Comparison of the mixed-sandwich fragments shows the COT–U–Cp angles in **3.1** are much more acute than **2.1** and *ca.* 5° more acute than **2.1THF** due to increased sterics caused by dimerisation. The U–COT and U–Cp distances vary marginally from the starting complexes and are found to lie between those of **2.1** and **2.1THF**.

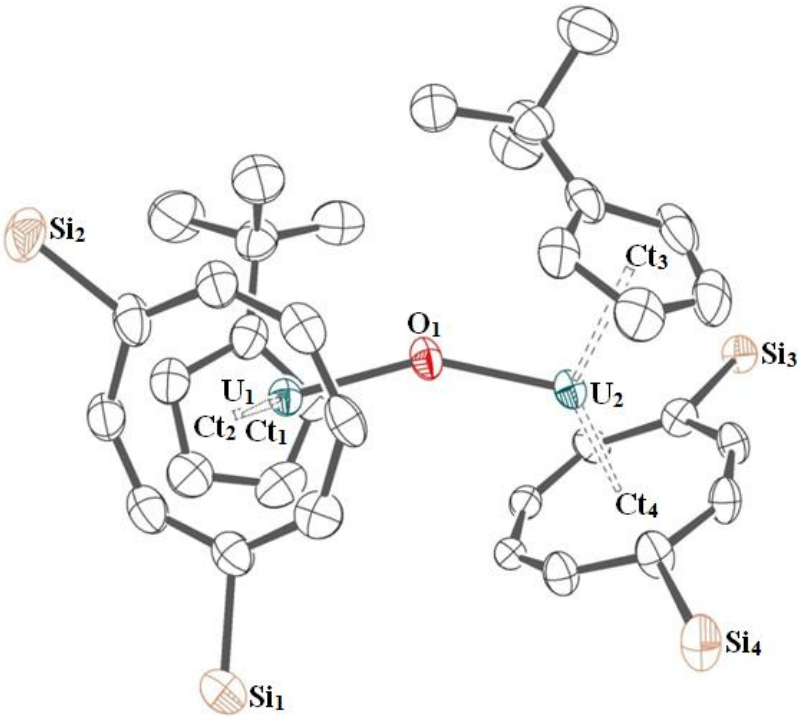

Figure 3.27 ORTEP view of **3.1** with thermal ellipsoids at 50% probability; hydrogen atoms and COT *iso*-propyl groups have been omitted for clarity.

The mixed-sandwich fragments are also similar to those in [{U(COT$^{(Si\textit{i}Pr3)2}$)(Cp*)}$_2$(μ-O)] and [{U(COT$^{(SiMe3)2}$)(Cp*)}$_2$(μ-O)] which have COT–U–Cp angles of 139.6(3) – 140.7(3)°, U–Cp distances of 2.501(9) – 2.538(4) Å, and U–COT distances of 1.955(4) – 2.003(9) Å. Variation is however found in the COT–U–U–COT and Cp–U–U–Cp torsion angles which are almost perpendicular for the Cp* complexes (*ca.* 80 – 95 °). This is postulated to be due to the increased size and symmetrical shape of the Cp* ligand in comparison to Cp$^{t\text{Bu}}$, and arises in order to avoid unfavourable contacts between the ligands.

Distances (Å)					
Ct_1–U_1	2.4932(2)	**Ct_2–U_1**	1.9708(2)	**Ct_3–U_2**	2.4959(2)
Ct_4–U_2	1.9732(2)	**U_1–O_1**	2.117(5)	**U_2–O_1**	2.110(4)
U_1–U_2	4.0871(7)				
Angles (°)					
Ct_1–U_1–Ct_2	135.327(9)	**Ct_3–U_2–Ct_4**	136.724(10)	**U_1–O_1–U_2**	150.4(3)
Ct_1–U_1–U_2–Ct_3	136.2508(16)	**Ct_2–U_1–U_2–Ct_4**	108.549(2)		

Table 3.1 Bond lengths, distances and angles for **3.1**. Ct_1 and Ct_3 are the centroids for the Cp^{tBu} ligands and Ct_2 and Ct_4 are the centroids for the $COT^{(SiiPr3)2}$ ligands.

3.3 Activation of carbon dioxide

The observed products from the reductive activation of carbon dioxide have been shown to be dependent on the sterics of the mixed-sandwich complexes.[81,86] It was anticipated that the largest mixed-sandwich complexes would therefore give rise to a bridging oxo complex, whereas [U($COT^{(SiiPr3)2}$)(Cp^{tBu})] would yield a carbonate and/or oxalate complex.

*3.3.1 Synthesis and characterisation of uranium(IV) oxo complexes (**3.2** and **3.3**)*

Exposure of solutions of [U($COT^{(SiiPr3)2}$)(Cp^{tBu3})] (**2.3**) and [U($COT^{(SiiPr3)2}$)($Cp^{(SiiPr3)2}$)] (**2.4**) to $^{13}CO_2$ gave rise to conversion of the complexes to [{U($COT^{(SiiPr3)2}$)(Cp^{tBu3})}$_2$(μ-O)] (**3.2**) and [{U($COT^{(SiiPr3)2}$)($Cp^{(SiiPr3)3}$)}$_2$(μ-O)] (**3.3**) respectively over several hours at room temperature. In both cases, $^{13}C\{^1H\}$ NMR spectra of the reaction mixture

showed no incorporation of ^{13}C-enriched carbon into the uranium complex, and the only labelled carbon resonance observed was assigned to ^{13}CO at 184.5 ppm. Whilst ^{1}H NMR spectra illustrated that only one uranium species was present in the mixture, impurities were observed that indicated some decomposition was occurring.

To support the hypothesis that **3.2** and **3.3** are both uranium(IV) bridging oxo complexes, the reactions were repeated with N_2O (**Figure 3.28**). In both cases the same products were observed to form quantitatively by NMR. However, verification of the identity of the complexes by XRD, microanalysis and mass spectrometry was precluded due to the thermal lability of the complexes and difficulty in obtaining analytically pure samples.

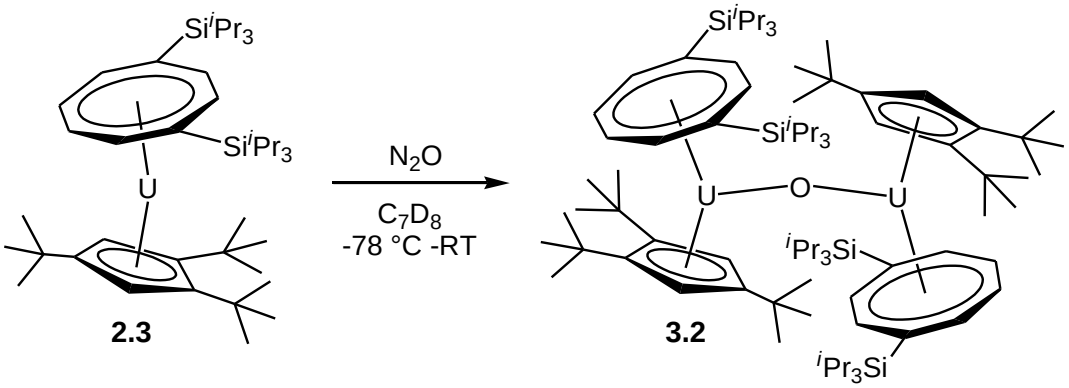

Figure 3.28 Synthesis of [{U(COT$^{(SiiPr3)2}$)(Cp^{tBu3})}$_2$(μ-O)] (**3.2**)

*3.3.2 Synthesis and characterisation of [{U(COT$^{(SiiPr3)2}$)(Cp^{tBu})}$_2$(μ-η^1:η^2-CO$_3$)] (**3.4**)*

Addition of $^{13}CO_2$ to [U(COT$^{(SiiPr3)2}$)(Cp^{tBu})] gave rise to the immediate formation of one product, **3.4**, that was crystallographically identified as a bridging carbonate complex (**Figure 3.29**). This reaction was reproducible with **2.1THF** and with varying stoichiometries of carbon dioxide. It was also observed that the oxo complex, **3.1**, was not formed when 0.5 mole equivalents CO_2 were used.

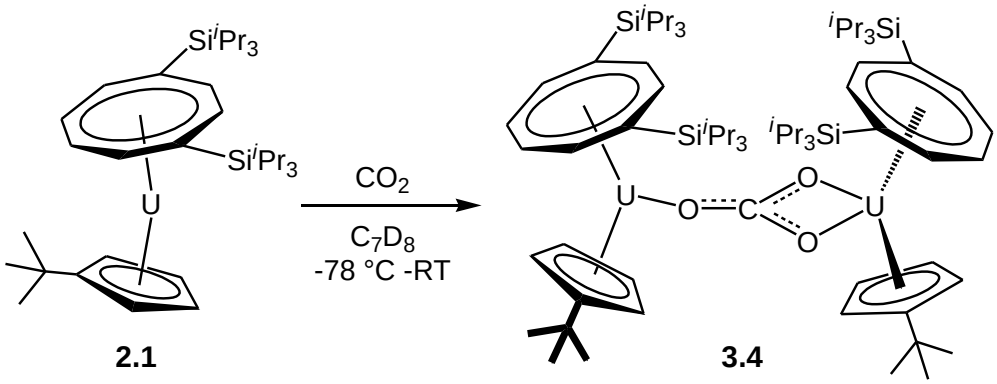

Figure 3.29 Synthesis of [{U(COT$^{(Si\textit{i}Pr3)2}$)(Cp$^{t\text{Bu}}$)}$_2$(μ-η^1:η^2-CO_3)] (**3.4**).

The $^{13}C\{^1H\}$ NMR spectrum displayed one broad resonance at 195.4 ppm ($w_{½}$ = 375 Hz), consistent with a fluxional carbonate environment at 30 °C (**Figure 3.30**). Variable temperature $^{13}C\{^1H\}$ NMR of the complex illustrated that the linewidth decreased as the complex was heated ($w_{½}$ = 44 Hz at 90 °C) and cooled ($w_{½}$ = 239 Hz at -60 °C) suggesting that it is possible to freeze out the fluxionality at low temperatures and encourage an averaged environment at higher temperatures. However, it was not possible to calculate the Gibb's energy of activation for this process, as broadening of all the carbon resonances was observed as the temperature was lowered.

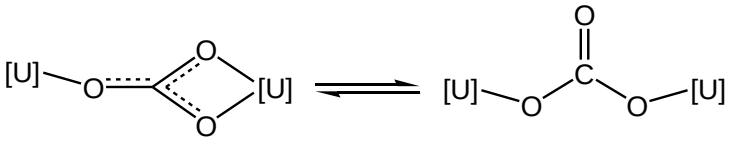

Figure 3.30 Proposed fluxionality of the carbonate fragment in **3.4**.

Single crystals of **3.4** were obtained from a saturated pentane solution and contained a molecule of pentane in the unit cell (**Figure 3.31**). Comparison of **3.4** with four related complexes synthesised by Cloke and colleagues ([{U(COT$^{(Si\textit{i}Pr3)2}$)(Cp*)}$_2$(μ-η^1:η^2-

CO_3)] and [{U($COT^{(SiMe3)2}$)(Cp^{Me4R})}$_2$(μ-η^1:η^2-CO_3)] (R = Et, ^{i}Pr, ^{t}Bu)) shows all the complexes except **3.4** feature Cp–U–U–Cp and COT–U–U–COT torsion angles of *ca.* 180°, and that [{U($COT^{(SiiPr3)2}$)(Cp*)}$_2$(μ-η^1:η^2-CO_3)] also features a centre of inversion.[81,86] This is justified by the asymmetrical shape of Cp^{tBu}, which gives rise to a near perpendicular twist to the uranium centres (**Table 3.2**). Despite this difference, the U–Ct distances and the COT–U–Cp angles are similar in all complexes, and the subtle variations can be explained by differing substituents on both rings.

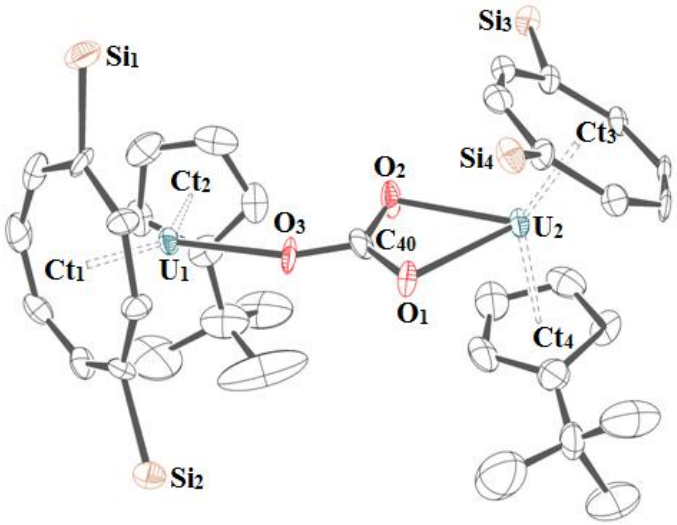

Figure 3.31 ORTEP view of **3.4** with thermal ellipsoids at 50% probability; hydrogen atoms and COT *iso*-propyl groups have been omitted for clarity.

Comparison of the carbonate fragment in **3.4** with the other mixed-sandwich carbonate complexes illustrate that the difference between the U_1–O_3 distance and the U_2–O_1 and U_2–O_2 distances is less pronounced in **3.4** (*ca.* 0.15 Å). The U_1–O_3–C_{40} angle is also more acute than in the analogous complexes (174.2(8) – 175.3(14)°), whereas the U_2–O_1–C_{40} and U_2–O_2–C_{40} angles are similar (93.2(3) – 95.3(9)°). Further variation between the complexes is seen within the carbonate unit itself whereby the three C–O bonds in **3.4** are similar, giving rise to a symmetrical carbonate fragment (**Figure 3.32**).

Distances (Å)					
Ct_1–U_1	1.9071(5)	**Ct_2–U_1**	2.4651(5)	**Ct_3–U_2**	1.9627(5)
Ct_4–U_2	2.5021(5)	**U_1–O_3**	2.229(7)	**U_2–O_1**	2.383(7)
U_2–O_2	2.387(7)	**C_{40}–O_1**	1.274(13)	**C_{40}–O_2**	1.280(14)
C_{40}–O_3	1.277(13)	**U_2–C_{40}**	2.778(11)		
Angles (°)					
Ct_1–U_1–Ct_2	136.55(2)	**Ct_3–U_2–Ct_4**	136.85(2)	**U_1–O_3–C_{40}**	158.5(8)
U_2–O_1–C_{40}	93.6(7)	**U_2–O_2–C_{40}**	94.0(7)	**O_1–C_{40}–O_2**	117.9(10)
O_1–C_{40}–O_3	121.6(11)	**O_2–C_{40}–O_3**	120.5(10)		
Ct_1–U_1–U_2–Ct_3	77.6564(6)			**Ct_2–U_1–U_2–Ct_4**	71.4376(5)

Table 3.2 Bond lengths, distances and angles for **3.4**. Ct_1 and Ct_3 are the centroids for the $COT^{(SiiPr3)2}$ ligands and Ct_2 and Ct_4 are the centroids for the Cp^{tBu} ligands.

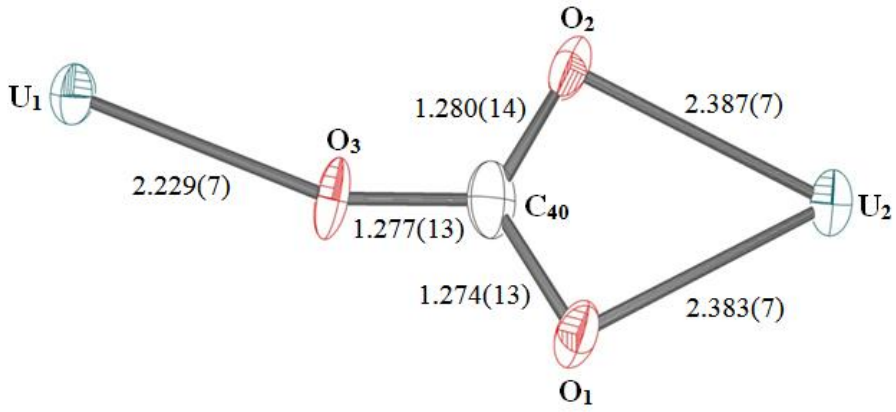

Figure 3.32 ORTEP view of the U-CO_3-U fragment in **3.4** with bond lengths.

*3.3.3 Cyclic voltammetry of [{U(COT$^{(SiiPr3)2}$)(Cp^{tBu})}$_2$(μ-η^1:η^2-CO$_3$)] (**3.4**)*

In order to compare the electronic properties of the carbonate complex with its uranium(III) precursor and other mixed-sandwich carbonate complexes, cyclic voltammetry was performed on **3.4**. Application of potential in the cathodic direction gives rise to two quasi-reversible waves at -2.07 and -2.80 V *vs* $[FeCp_2]^{+/0}$, which have been assigned to a single electron reduction of each uranium centre (**Figures 3.33** and **3.34**). A small wave (assigned to impurities at -2.47 V *vs* $[FeCp_2]^{+/0}$) is also observed between these two processes. No other reducing processes were observed in the solvent window. The separation between the two processes ($\Delta E_{½}$ = 0.73 V) is slightly larger than $\Delta E_{½}$ values obtained for [{U(COT$^{(SiMe3)2}$)(Cp^{Me4R})}$_2$(μ-η^1:η^2-CO$_3$)] (R = ^{i}Pr (0.67 V) and ^{t}Bu (0.67 V)), illustrating increased interaction between the two uranium centres in the mixed valence [U^{III}-U^{IV}]$^-$ state.[86]

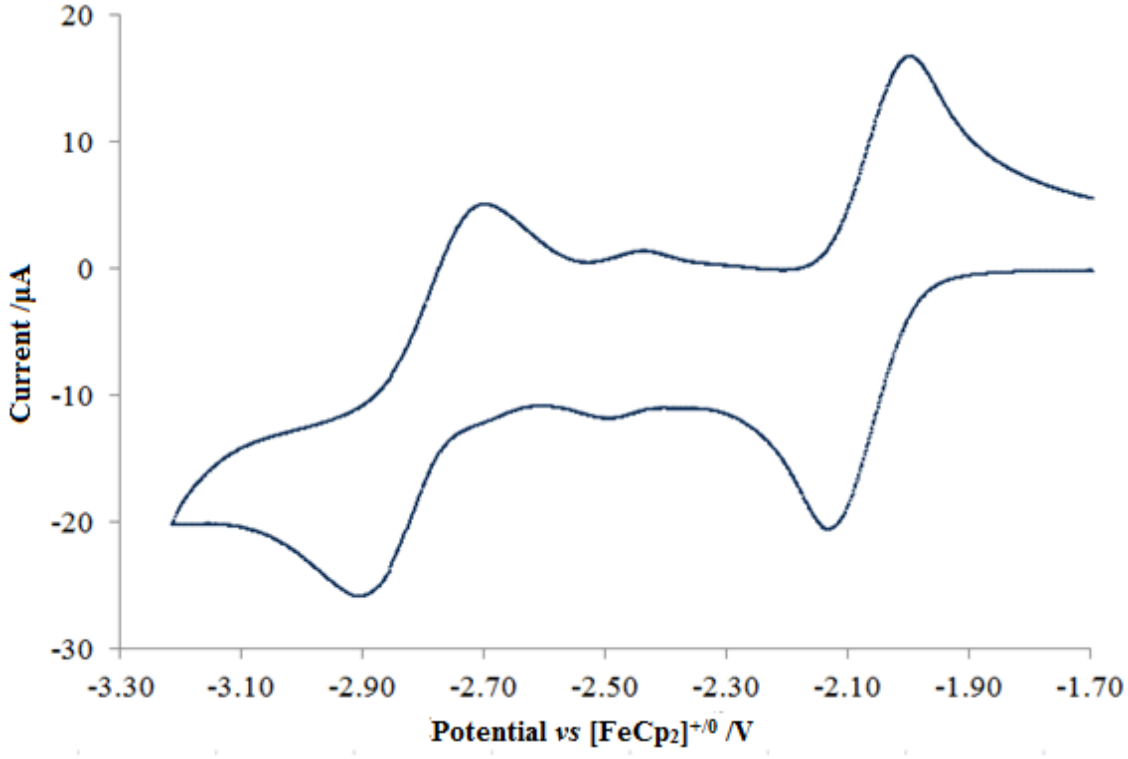

Figure 3.33 Cyclic voltammogram of a 5.6 mM solution of [{U(COT$^{(SiiPr3)2}$)(Cp^{tBu})}$_2$(CO$_3$)] in 0.1 M [^{n}Bu$_4$N][PF$_6$]/THF at 100 mV·s^{-1}.

$$[U^{III}\text{-}U^{III}]^{2-} \underset{\textit{Process I}}{\overset{-e^-}{\rightleftharpoons}} [U^{III}\text{-}U^{IV}]^{-} \underset{\textit{Process II}}{\overset{-e^-}{\rightleftharpoons}} [U^{IV}\text{-}U^{IV}]$$

-2.80 V *-2.07 V*

Figure 3.34 $E_{½}$ values (V) *vs* $[FeCp_2]^{+/0}$ for $[\{U(COT^{(Si\textit{i}Pr3)2})(Cp^{\textit{t}Bu})\}_2(\mu\text{-}\eta^1\text{:}\eta^2\text{-}CO_3)]$.

3.3.4 Extraction of the carbonate fragment

Whilst the activation of small molecules at metal centres is, independently, an area of interest, for any process to show catalytic potential the starting material must be regenerated. Research with this theme has already been published for other uranium mixed-sandwich complexes by Cloke and co-workers for the methoxide complex, whereby the uranium(III) mixed-sandwich is regenerated *via* the uranium(IV) triflate complex (**Figure 3.35**).[54]

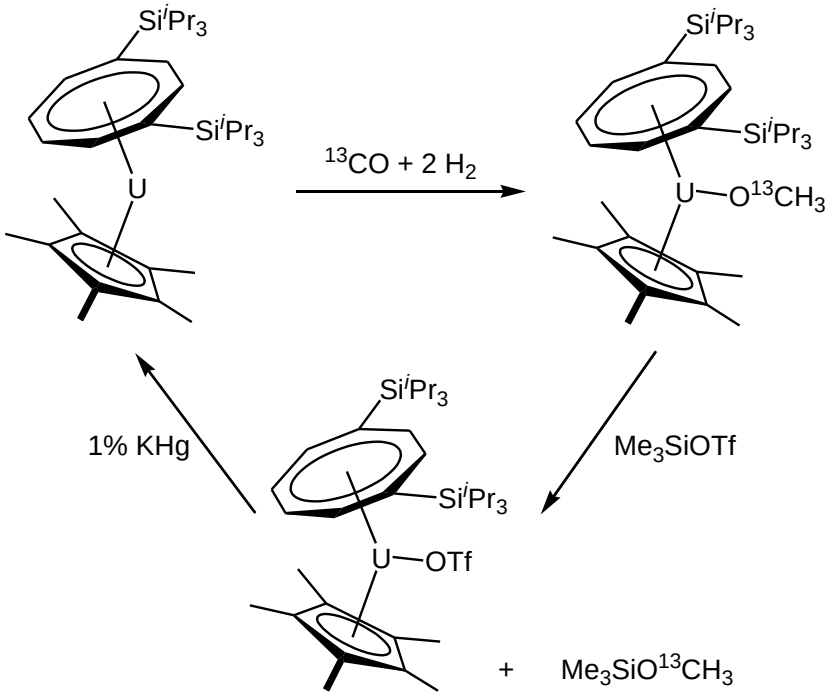

Figure 3.35 Activation of syngas to form a uranium(IV) methoxide complex, from which the uranium(III) mixed-sandwich is regenerated.[54]

Previous work by Cloke and Farnaby included extensive studies on the cleavage of oxocarbon fragments from the uranium centre using a variety of SiR_3X reagents (R = alkyl, X = halide or triflate).[98] These studies found mixed results, and in some instances the mixtures required heating in order for the reaction to reach completion. In order to avoid repetition of this work, only TMSCl was used to extract the carbonate fragment from **3.4**. The reasons for this were two-fold: reactivity of **3.4** with TMSCl would allow some comparison with previous work; and a mixed-sandwich halide was desired for cyclic voltammetry studies in order to validate the results obtained for the uranium(III) complexes (see Chapter 2).

The reaction of **3.4** with excess TMSCl was slow to progress at ambient temperature, however heating the mixture to 75 °C resulted in complete consumption of the carbonate complex within 24 hours. NMR spectroscopy revealed residual TMSCl and two paramagnetic species in equal ratio (**Figure 3.36**). One of these complexes was the uranium(IV) mixed-sandwich chloride [U(COT$^{(Si\textit{i}Pr3)2}$)(Cp$^{t\text{Bu}}$)Cl] (**3.5**), however the second complex could not be identified as crystals and analytically pure samples could not be obtained.

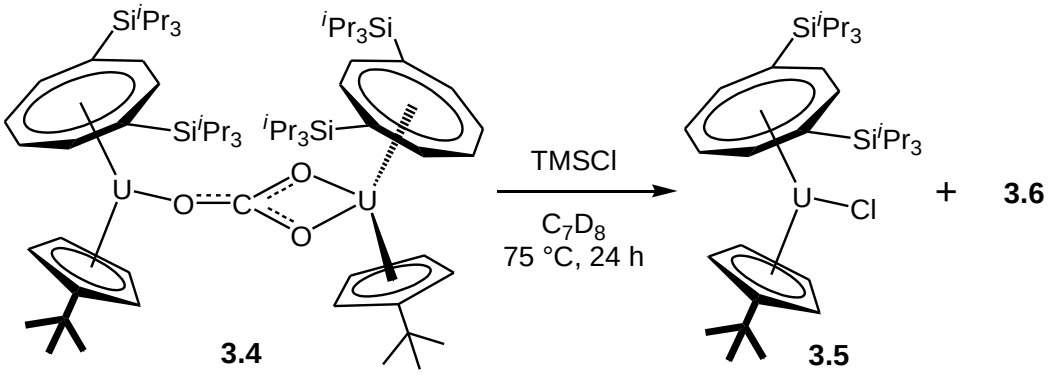

Figure 3.36 Reactivity of [{U(COT$^{(Si\textit{i}Pr3)2}$)(Cp$^{t\text{Bu}}$)}$_2$(μ-η^1:η^2-CO_3)] with TMSCl.

NMR characterisation of the unidentified complex (**3.6**) illustrated resonances corresponding to the mixed-sandwich fragment and an additional broad resonance which integrated to nine protons. However, the presence of only one silicon resonance for this complex at -136.4 ppm led to the conclusion that the nine additional protons do not derive from a TMS group. What is more, the only ^{13}C-enriched resonance observed corresponded to carbon dioxide, indicating that CO_2 is extruded from one of the species during the reaction. Further studies to characterise this species were not conducted as detailed work into the functionalisation of **3.4** is beyond the scope of this thesis.

*3.3.5 Alternative synthesis of [U(COT$^{(SiiPr3)2}$)(Cp^{tBu})Cl] (**3.5**)*

Due to the formation of **3.6** in the synthesis of **3.5** from the crude carbonate complex, crystalline material could only be obtained in low yields. An alternative synthesis of **3.5** by reaction of [U(COT$^{(SiiPr3)2}$)(Cp^{tBu})(THF)] with ^{t}BuCl was therefore conducted (**Figure 3.37**), and yielded sufficient material for full characterisation.

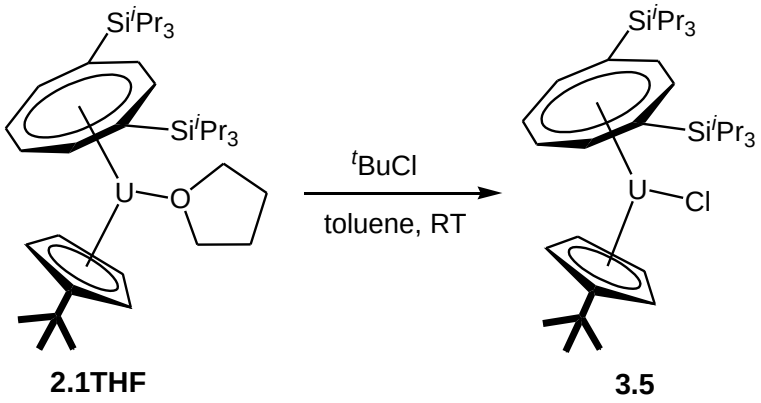

Figure 3.37 Synthesis of [U(COT$^{(SiiPr3)2}$)(Cp^{tBu})Cl] (**3.5**).

XRD data show the mixed-sandwich unit in **3.5** (**Figure 3.38**) is comparable to [{U(COT$^{(Si\mathit{i}Pr3)2}$)(Cp$^{\mathit{t}Bu}$)}$_2$(μ-η^1:η^2-CO_3)]. Both complexes exhibit marginally shorter U–COT and U–Cp bond lengths than [U(COT$^{(Si\mathit{i}Pr3)2}$)(Cp$^{\mathit{t}Bu}$)(THF)], and both complexes have a COT–U–Cp angle that is more acute than the uranium(III) complex by *ca.* 4°. Whilst this can be justified in the carbonate complex by the additional sterics from the second mixed-sandwich fragment, **3.5** is less sterically congested than [U(COT$^{(Si\mathit{i}Pr3)2}$)(Cp$^{\mathit{t}Bu}$)(THF)]. Comparison of **3.5** with [U(COT$^{(Si\mathit{i}Pr3)2}$)(Cp*)Cl] illustrates the complexes have almost identical bond distances (U–COT 1.9142(15) Å, U–Cp 2.465(2) Å and U–Cl (2.6496(15) Å) although the COT–U–Cp angle in **3.5** is more acute (139.85(8)°). This can be explained by the absence of the other four substituents on the cyclopentadienyl ring which allows additional bending to occur.

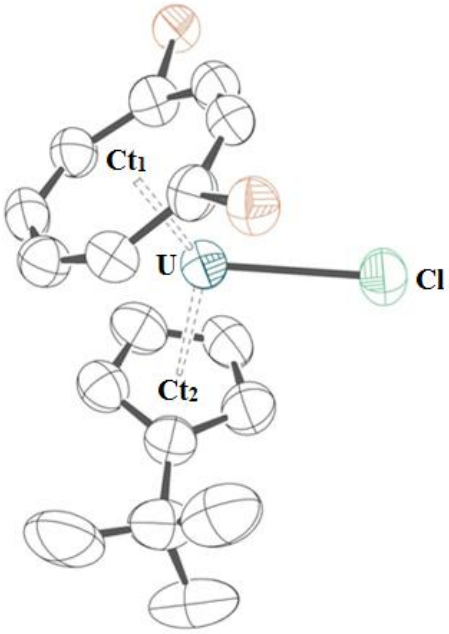

Figure 3.38 ORTEP view of **3.5** with thermal ellipsoids at 50% probability; hydrogen atoms and COT *iso*-propyl groups have been omitted for clarity. Selected bond distances (Å) and angles (°): U–Ct_1 1.9126(3), U–Ct_2 2.4522(4), U–Cl 2.647(2), Ct_1–U–Ct_2 136.233(15).

*3.3.6 Cyclic voltammetry of [U(COT$^{(SiiPr3)2}$)(Cp^{tBu})Cl] (**3.5**)*

In order to validate the electrochemical results obtained for the uranium(III) mixed-sandwich complexes in Chapter 2, cyclic voltammetry was conducted on **3.5**. Application of potential in the cathodic direction gave rise one quasi-reversible wave at -2.04 V *vs* $[FeCp_2]^{+/0}$, which has been assigned to the U^{IV}/U^{III} redox couple (**Figure 3.39**). Two additional processes were also observed to flank the main process, but these have not been assigned. The potential at which the U^{IV}/U^{III} reductive process occurs is consistent with the results obtained for [U(COT$^{(SiiPr3)2}$)(Cp^{tBu})(THF)] (**2.1THF**, -1.98 V *vs* $[FeCp_2]^{+/0}$), supporting the assignment that the U^{IV}/U^{III} redox processes for all the mixed-sandwich complexes occur between -1.8 and -2.1 V *vs* $[FeCp_2]^{+/0}$.

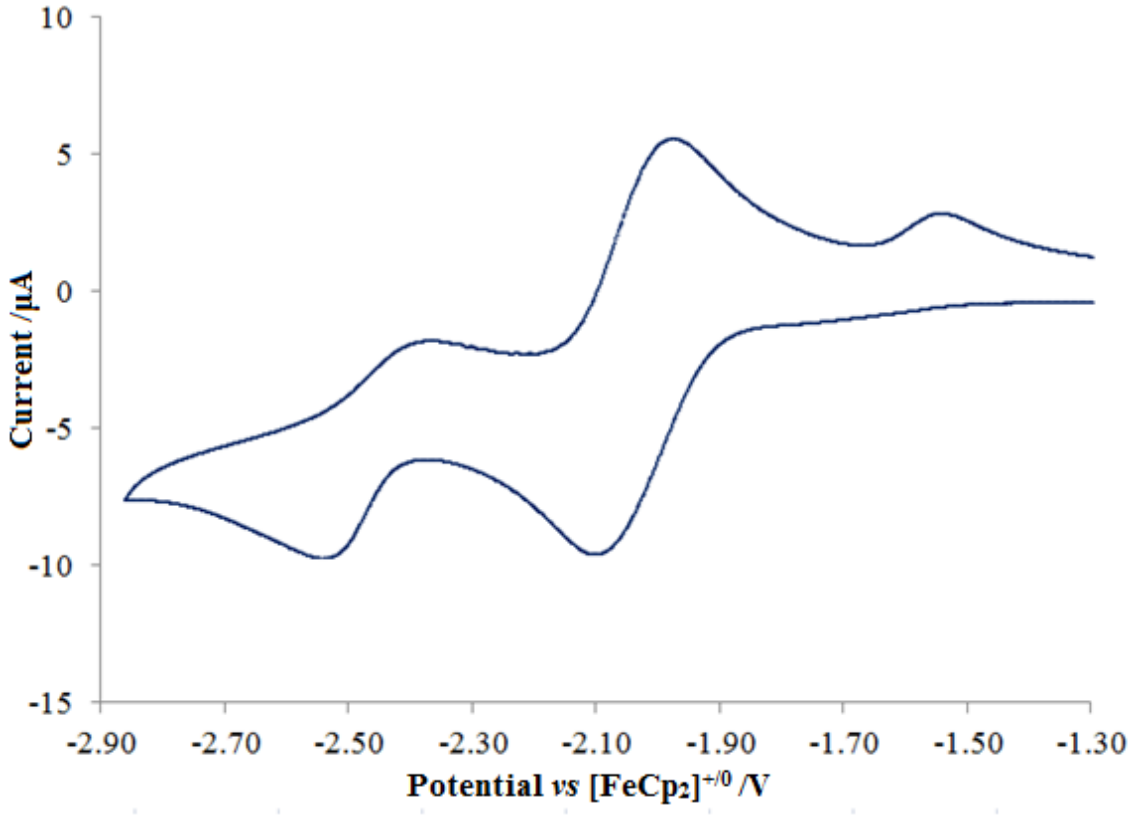

Figure 3.39 Cyclic Voltammogram of a 5.0 mM solution of [U(COT$^{(SiiPr3)2}$)(Cp^{tBu})Cl] in 0.1 M [^{n}Bu$_4$N][PF$_6$]/THF at 100 mV·s^{-1}.

*3.3.7 Regeneration of **2.1** by reduction of [U(COT$^{(SiiPr3)2}$)(Cp^{tBu})Cl]*

In order to complete the cycle of reactivity for this mixed-sandwich system, a stoichiometric quantity of potassium graphite was added to a solution of **3.5**. This achieved the desired result and reduced the uranium(IV) mixed-sandwich chloride to the uranium(III) mixed-sandwich complex.

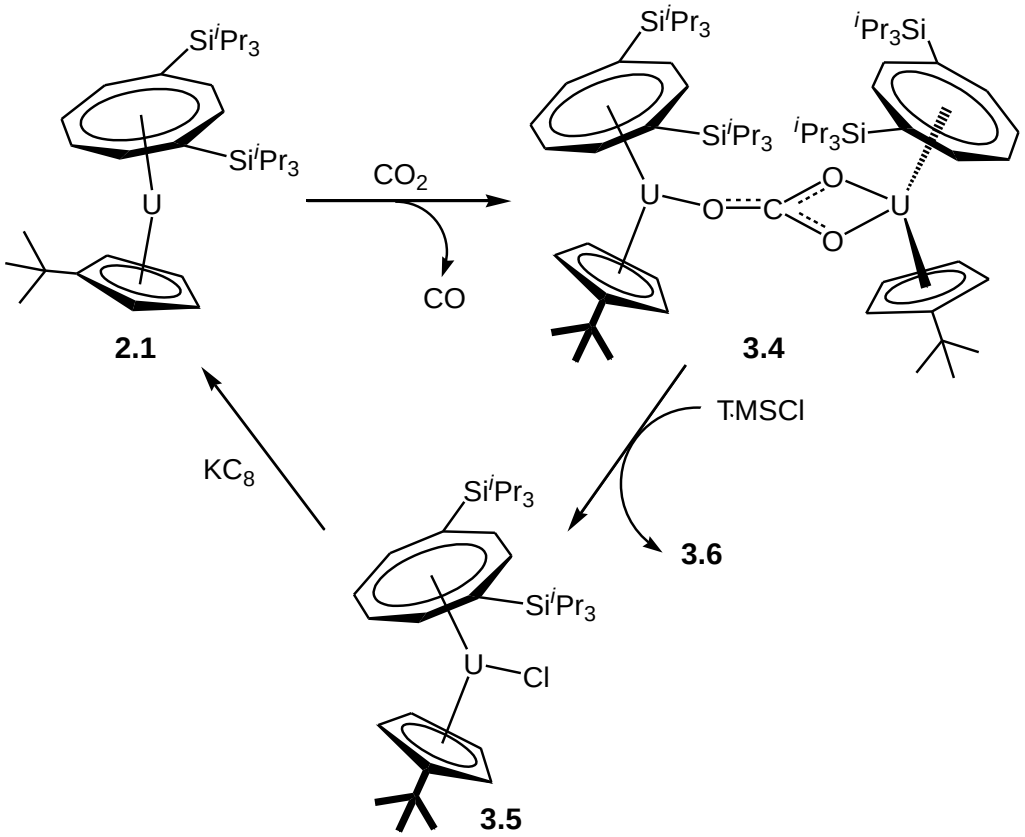

Figure 3.40 Reactive cycle of **2.1** with carbon dioxide.

3.4 Summary

Carbon monoxide reactivity studies of the cyclopentadienyl-based mixed sandwich complexes have illustrated that the steric environment in [U(COT$^{(SiiPr3)2}$)(Cp^{tBu})] is insufficient to stabilise an oxocarbon fragment. However it was observed that this

complex reacts with carbon dioxide to yield the carbonate complex from which the uranium(III) precursor can be obtained *via* [U(COT$^{(Si\textit{i}Pr3)2}$)(Cp$^{t\text{Bu}}$)Cl]. [U(COT$^{(Si\textit{i}Pr3)2}$)(Cp$^{t\text{Bu3}}$)] and [U(COT$^{(Si\textit{i}Pr3)2}$)(Cp$^{(Si\textit{i}Pr3)2}$)] are observed to react with carbon dioxide or nitrous oxide to yield bridging oxo complexes and carbon monoxide.

3.5 Experimental details for Chapter 3

*3.5.1 Synthesis of [{U(COT$^{(SiiPr3)2}$)(Cp^{tBu})}$_2$(μ-O)] (**3.1**)*

To a frozen, degassed solution of [U(COT$^{(Si\textit{i}Pr3)2}$)(Cp$^{t\text{Bu}}$)(THF)] (90.6 mg, 1.07 x 10^{-4} mol) in toluene (5 mL) was added excess N_2O at -78 °C. Upon thawing, an immediate colour change from green/brown to red/brown was observed. The mixture was stirred for 24 hours then the solvent removed *in vacuo.* The residue was dissolved in pentane and filtered. Slow evaporation of the solvent at -35 °C yielded red crystalline needles.

Yield: 37.9 mg (2.42 x 10^{-5} mol), 45.2% based on [U(COT$^{(Si\textit{i}Pr3)2}$)(Cp$^{t\text{Bu}}$)].

Anal. calc (found) for $C_{70}H_{122}OSi_4U_2$: C 53.62 (52.44), H 7.84 (7.51)%.

^{1}H NMR (d_6-benzene, 303 K): δ 115.6 (s, br, 2H, Cp/COT-C*H*), 2.1 (br), -0.4 (m, br, 18H, ^{i}Pr-CH_3), -0.5 (m, br, 18H, ^{i}Pr-CH_3), -1.39 (br), -5.0 (br), -10.6 (s, br, 9H, ^{t}Bu-CH_3).

^{29}Si{^{1}H} NMR (d_6-benzene, 303 K): δ -85.7 (*Si*^{i}Pr$_3$).

*3.5.2 Synthesis of [{U(COT$^{(SiiPr3)2}$)(Cp^{tBu3})}$_2$(μ-O)] (**3.2**)*

To a frozen, degassed solution of [U(COT$^{(Si\textit{i}Pr3)2}$)(Cp$^{t\text{Bu3}}$)] (280 mg, 3.15 x 10^{-4} mol) in pentane was added a stoichiometric amount of N_2O at -196 °C. Thawing the solid to room temperature resulted in a colour change from olive green to red/brown. **3.2** was obtained quantitatively by NMR.

^{1}H NMR (d_8-toluene, 303 K): δ 39.2 (s, br, 2H, Cp/COT-C*H*), 11.7 (s, br, 9H, ^{t}Bu-CH_3), -0.5 (s, br, 18H, ^{i}Pr-CH_3), -2.3 (s, br, 2H, Cp/COT-C*H*), -4.1 (s, br, 18H, ^{i}Pr-CH_3), -5.0 (s, br, 6H, ^{i}Pr-C*H*), -9.5 (s, br, 18H, ^{t}Bu-CH_3), -37.5 (s, br, 2H, Cp/COT-C*H*).

^{29}Si{^{1}H} NMR (d_8-toluene, 303 K): δ -73.3 (*Si*^{i}Pr$_3$)

*3.5.3 Synthesis of [{U(COT$^{(SiiPr3)2}$)(Cp$^{(SiiPr3)2}$)}$_2$(μ-O)] (**3.3**)*

To a frozen, degassed solution of [U(COT$^{(SiiPr3)2}$)(Cp$^{(SiiPr3)2}$)] (226 mg, 2.18 x 10^{-4} mol) in pentane was added a stoichiometric amount of N_2O at -196 °C. Thawing the mixture to room temperature resulted in a colour change from green to red/brown. **3.3** was obtained quantitatively by NMR.

^{1}H NMR (d_8-toluene, 303 K): δ 37.6 (s, br, 2H, Cp/COT-C*H*), 5.2 (s, br, 18H, ^{i}Pr-CH_3), 4.6 (s, br, 6H, ^{i}Pr-C*H*), 4.3 (s, br, 18H, ^{i}Pr-CH_3), -2.1 (s, br, 18H, ^{i}Pr-CH_3), -5.2 (s, br, 18H, ^{i}Pr-CH_3), -6.6 (s, br, 6H, ^{i}Pr-C*H*), -22.9 (s, br, 2H, Cp/COT-C*H*), -38.5 (s, br, 2H, Cp/COT-C*H*), -39.7 (s, br, 2H, Cp/COT-C*H*).

^{29}Si{^{1}H} NMR (d_8-toluene, 303 K): δ -40.7 (*Si*^{i}Pr$_3$), -52.6 (*Si*^{i}Pr$_3$).

*3.5.4 Synthesis of [{U(COT$^{(SiiPr3)2}$)(Cp^{tBu})}$_2$(μ:η^1:η^2-CO$_3$)] (**3.4**)*

To a frozen degassed solution of [U(COT$^{(SiiPr3)2}$)(Cp$^{t\text{Bu}}$)] (85.0 mg, 1.09 x 10^{-4} mol) in pentane was added three equivalents of CO_2 at -196 °C. Thawing of the solution caused a colour change from green to red/brown over several minutes. Reduction of solvent volume to 50% and addition of three drops toluene gave rise to crystals at -35 °C.

Yield: 39.9 mg (2.47 x 10^{-5} mol), 45% based on [U(COT$^{(SiiPr3)2}$)(Cp$^{t\text{Bu}}$)].

Anal. calc (found) for $C_{71}H_{122}O_3Si_4U_2$: C 52.90 (52.44), H 7.63 (7.51)%.

MS (EI): *m/z* = 115 (100%, $[Si^{i}Pr_2]^+$), 1613 (19%, M^+).

^{1}H NMR (d_6-benzene, 303 K): δ 33.7 (s, br, 2H, Cp/COT-C*H*), 9.7 (s, br, 2H, Cp/COT-C*H*), -4.8 (d, $^3J_{HH}$ = 6.8 Hz, 18H, ^{i}Pr-CH_3), -6.4 (d, $^3J_{HH}$ = 6.6 Hz, 18H, ^{i}Pr-CH_3), -8.3 (s, br, 6H, ^{i}Pr-C*H*),-13.3 (s, br, 9H, ^{t}Bu-CH_3), -15.7 (s, br, 2H, Cp/COT-C*H*), -21.7 (s, br, 2H, Cp/COT-C*H*), -44.7 (s, br, 2H, Cp/COT-C*H*).

^{13}C{^{1}H} NMR **(3.4)-^{13}CO$_3$** (d_6-benzene, 303 K): δ 195.4 (br, $w_{½}$ = 375 Hz).

^{29}Si{^{1}H} NMR (d_6-benzene, 303 K): δ -100.8 ($Si^{i}Pr_3$).

*3.5.5 Synthesis of [U(Cp^{tBu})(COT$^{(SiiPr3)2}$)Cl] (**3.5**)*

Method A:

To a cooled, degassed solution of [U(COT$^{(Si\textit{i}Pr3)2}$)(Cp$^{t\text{Bu}}$)] (48.9 mg, 6.30 x 10^{-5} mol) in d_8-toluene was added 0.86 bar $^{13}CO_2$ at -78 °C. Warming the solution resulted in a colour change from olive to red/brown. After 24 hours the solution was degassed and two drops TMSCl were added. The mixture was heated to 75 °C for 24 hours to yield **3.5** and **3.6** in equal quantity. The mixture was stripped to dryness then dissolved in pentane and filtered. Slow cooling a saturated diethyl ether solution to -35 °C yielded red crystals of **3.5**.

Yield: 5.6 mg (6.9 x 10^{-6} mol), 11% based on [U(COT$^{(Si\textit{i}Pr3)2}$)(Cp$^{t\text{Bu}}$)].

Method B:

To a stirring solution of [U(COT$^{(Si\textit{i}Pr3)2}$)(Cp$^{t\text{Bu}}$)(THF)] (101.7 mg, 1.20 x 10^{-4} mol) in toluene (5 mL) was added 13 μL ^{t}BuCl (1.20 x 10^{-4} mol) *via* microsyringe. The mixture was stirred at ambient temperature and a colour change from olive to red was observed. The mixture was stirred for several hours then stripped to dryness. The residue was

dissolved in pentane and filtered then dried *in vacuo*. Red crystals were obtained at -35 °C from a saturated diethyl ether solution.

Yield: 67.9 mg (8.37 x 10^{-5} mol), 69.7% based on [U(COT$^{(Si\textit{i}Pr3)2}$)(Cp$^{\textit{t}Bu}$)(THF)].

Anal. calc (found) for $C_{35}H_{61}ClSi_2U$: C 51.80 (52.30), H 7.58 (7.59)%.

MS (EI): *m/z* = 157 (100%), 811 (22%, M^+).

^{1}H NMR (d_8-toluene, 303 K): δ 52.5 (s, br, 2H, Cp/COT-C*H*), 36.7 (s, br, 2H, Cp/COT-C*H*), 4.6 (s, br, 2H, Cp/COT-C*H*), -5.9 (s, br, 18H, $^{\textit{i}}$Pr-CH_3), -6.4 (s, br, 6H, $^{\textit{i}}$Pr-C*H*), -6.9 (s, br, 18H, $^{\textit{i}}$Pr-CH_3), -10.0 (s, br, 9H, $^{\textit{t}}$Bu-CH_3), -67.4 (s, br, 2H, Cp/COT-C*H*), -86.9 (s, br, 2H, Cp/COT-C*H*).

^{29}Si{^{1}H} NMR (d_8-toluene, 303 K): δ -80.7 (*Si*$^{\textit{i}}$Pr$_3$).

3.5.6 Characterisation of ***3.6***

^{1}H NMR (d_8-toluene, 303 K): δ 108.7 (s, br, 2H, Cp/COT-C*H*), 37.4 (s, br, 9H, unassigned), 8.7 (s, br, 2H, Cp/COT-C*H*), -6.7 (s, br, 18H, $^{\textit{i}}$Pr-CH_3), -13.7 (s, br, 18H, $^{\textit{i}}$Pr-CH_3), -16.5 (s, br, 6H, $^{\textit{i}}$Pr-C*H*), -26.1 (s, br, 9H, unassigned), -29.6 (s, br, 2H, Cp/COT-C*H*), -62.2 (s, br, 2H, Cp/COT-C*H*), -96.2 (s, br, 2H, Cp/COT-C*H*).

^{29}Si{^{1}H} NMR (d_8-toluene, 303 K): δ -136.4 (*Si*$^{\textit{i}}$Pr$_3$).

3.6 References

1 R. Schlögl, *Angew. Chem. Int. Ed.*, 2003, **42**, 2004–2008.

2 R. R. Schrock, *Nature Chemistry*, 2011, **3**, 95–96.

3 F. A. Cotton, C. A. Murillo, M. Bochmann and G. Wilkinson, *Advanced Inorganic Chemistry*, John Wiley & Sons Ltd., New York, 6th edn., 1999.

4 S. Demir, S. E. Lorenz, M. Fang, F. Furche, G. Meyer, J. W. Ziller and W. J. Evans, *J. Am. Chem. Soc.*, 2010, **132**, 11151–11158.

5 P. J. Chirik, *Nature Chemistry*, 2009, **1**, 520–522.

6 B. A. Mackay and M. D. Fryzuk, *Chem. Rev.*, 2004, **104**, 385–401.

7 W. J. Evans, M. Fang, G. Zucchi, F. Furche, J. W. Ziller, R. M. Hoekstra and J. I. Zink, *J. Am. Chem. Soc.*, 2009, **131**, 11195–11202.

8 M. Fang, J. E. Bates, S. E. Lorenz, D. S. Lee, D. B. Rego, J. W. Ziller, F. Furche and W. J. Evans, *Inorg. Chem.*, 2011, **50**, 1459–1469.

9 M. Fang, D. S. Lee, J. W. Ziller, R. J. Doedens, J. E. Bates, F. Furche and W. J. Evans, *J. Am. Chem. Soc.*, 2011, **133**, 3784–3787.

10 J. D. Rinehart, M. Fang, W. J. Evans and J. R. Long, *Nature Chemistry*, 2011, **3**, 538–542.

11 J. D. Rinehart, M. Fang, W. J. Evans and J. R. Long, *J. Am. Chem. Soc.*, 2011, **133**, 14236–14239.

12 P. Roussel, N. D. Tinker and P. Scott, *J. Alloys and Compounds*, 1998, **271-273**, 150–153.

13 P. G. Wilkinson and N. B. Houk, *J. Chem. Phys.*, 1956, **24**, 528–534.

14 N. Kaltsoyannis and P. Scott, *Chem. Commun.*, 1998, 1665–1666.

15 W. J. Evans, S. A. Kozimor and J. W. Ziller, *J. Am. Chem. Soc.*, 2003, **125**, 14264–14265.

16 A. L. Odom, P. L. Arnold and C. C. Cummins, *J. Am. Chem. Soc.*, 1998, **120**, 5836–5837.

17 F. G. N. Cloke and P. B. Hitchcock, *J. Am. Chem. Soc.*, 2002, **124**, 9352–9353.

18 F. G. N. Cloke, J. C. Green and N. Kaltsoyannis, *Organometallics*, 2004, **23**, 832–835.

19 S. M. Mansell, N. Kaltsoyannis and P. L. Arnold, *J. Am. Chem. Soc.*, 2011, **133**, 9036–9051.

20 S. M. Mansell, J. H. Farnaby, A. I. Germeroth and P. L. Arnold, *Organometallics*, 2013, **32**, 4214–4222.

21 C.-C. Chang, *Inorg. Chim. Acta*, 1984, **94**, 259–262.

22 Q. Zhang, W. Deng and Y. Wang, *J. Energy Chem.*, 2013, **22**, 27–38.

23 O. O. James, B. Chowdhury, M. A. Mesubi and S. Maity, *RSC Adv.*, 2012, **2**, 7347–7366.

24 C. Elschenbroich, *Organometallics*, Wiley-VCH Verlag GmbH & Co. KGaA, Weinheim, Germany, 3rd edn., 2006.

25 B. deB Darwent, *Bond Dissociation Energies in Simple Molecules*, National Bureau of Standards, 1970.

26 J. L. Slater, R. K. Sheline, K. C. Lin and W. Weltner, *J. Chem. Phys.*, 1971, **55**, 5129–5130.

27 R. K. Sheline and J. L. Slater, *Angew. Chem. Int. Ed.*, 1975, **14**, 309–313.

28 T. J. Tague Jr., L. Andrews and R. D. Hunt, *J. Phys. Chem.*, 1993, **97**, 10920–10924.

29 K. R. Kunze, R. H. Hauge, D. F. Hamill and J. L. Margrave, *J. Phys. Chem*, 1977, **81**, 1664–1667.

30 J. G. Brennan, R. A. Andersen and J. L. Robbins, *J. Am. Chem. Soc.*, 1986, **108**, 335–336.

31 J. S. Parry, E. Carmona, S. Coles and M. B. Hursthouse, *J. Am. Chem. Soc.*, 1995, **117**, 2649–2650.

32 W. J. Evans, S. A. Kozimor, G. W. Nyce and J. W. Ziller, *J. Am. Chem. Soc.*, 2003, **125**, 13831–13835.

33 M. del Mar Conejo, J. S. Parry, E. Carmona, M. Schultz, J. G. Brennan, S. M. Beshouri, R. A. Andersen, R. D. Rogers, S. Coles and M. B. Hursthouse, *Chem. Eur. J.*, 1999, **5**, 3000–3009.

34 W. J. Evans, K. J. Forrestal and J. W. Ziller, *J. Am. Chem. Soc.*, 1995, **117**, 12635–12636.

35 S. Cotton, *Lanthanide and Actinide Chemistry*, John Wiley & Sons Ltd., Chichester, England, 2006.

36 L. Maron, O. Eisenstein and R. A. Andersen, *Organometallics*, 2009, **28**, 3629–3635.

37 Paolucci, Gino, Rossetto, Gilberto, Zanella, Pierino, Yünlü, Kenan and Fischer, R Dieter, *J. Organomet. Chem.*, 1984, **272**, 363–383.

38 P. J. Fagan, J. M. Manriquez, S. H. Vollmer, C. S. Day, V. W. Day and T. J. Marks, *J. Am. Chem. Soc.*, 1981, **103**, 2206–2220.

39 K. Tatsumi, A. Nakamura, P. Hofmann, P. Stauffert and R. Hoffmann, *J. Am. Chem. Soc.*, 1985, **107**, 4440–4451.

40 K. Tatsumi, A. Nakamura, P. Hofmann, R. Hoffmann, K. G. Moloy and T. J. Marks, *J. Am. Chem. Soc.*, 1986, **108**, 4467–4476.

41 J. M. Manriquez, P. J. Fagan, T. J. Marks, C. S. Day and V. W. Day, *J. Am. Chem. Soc.*, 1978, **100**, 7112–7114.

42 O. Bénaud, J.-C. Berthet, P. Thuéry and M. Ephritikhine, *Inorg. Chem.*, 2010, **49**, 8117–8130.

43 P. L. Arnold, Z. R. Turner, A. I. Germeroth, I. J. Casely, G. S. Nichol, R. Bellabarba and R. P. Tooze, *Dalton Trans.*, 2013, **42**, 1333–1337.

44 R. E. Cramer, R. B. Maynard, J. C. Paw and J. W. Gilje, *Organometallics*, 1982, **1**, 869–871.

45 R. E. Cramer, K. T. Higa and J. W. Gilje, *J. Am. Chem. Soc.*, 1984, **106**, 7245–7247.

46 J. W. Gilje and R. E. Cramer, *Inorg. Chim. Acta*, 1987, **139**, 177–181.

47 R. E. Cramer, K. T. Higa and J. W. Gilje, *Organometallics*, 1985, **4**, 1140–1141.

48 R. E. Cramer, J. H. Jeong and J. W. Gilje, *Organometallics*, 1986, **5**, 2555–2557.

49 I. Castro-Rodriguez and K. Meyer, *J. Am. Chem. Soc.*, 2005, **127**, 11242–11243.

50 I. Castro-Rodriguez, H. Nakai and K. Meyer, *Angew. Chem. Int. Ed.*, 2006, **45**, 2389–2392.

51 O. T. Summerscales, F. G. N. Cloke, P. B. Hitchcock, J. C. Green and N. Hazari, *Science*, 2006, **311**, 829–831.

52 O. T. Summerscales, F. G. N. Cloke, P. B. Hitchcock, J. C. Green and N. Hazari, *J. Am. Chem. Soc.*, 2006, **128**, 9602–9603.

53 N. Tsoureas, O. T. Summerscales, F. G. N. Cloke and S. M. Roe, *Organometallics*, 2013, **32**, 1353–1362.

54 A. S. P. Frey, F. G. N. Cloke, M. P. Coles, L. Maron and T. Davin, *Angew. Chem. Int. Ed.*, 2011, **50**, 6881–6883.

55 C. E. Kefalidis, A. S. P. Frey, S. M. Roe, F. G. N. Cloke and L. Maron, *Dalton Trans.*, 2014, **43**, 11202–11208.

56 P. L. Arnold, Z. R. Turner, R. M. Bellabarba and R. P. Tooze, *Chem. Sci.*, 2011, **2**, 77–79.

57 B. M. Gardner, J. C. Stewart, A. L. Davis, J. McMaster, W. Lewis, A. J. Blake and S. T. Liddle, *PNAS*, 2012, **109**, 9265–9270.

58 R. Alvarez, E. Carmona, E. Gutiérrez-puebla, J. M. Marin, A. Monge and M. L. Povedaa, *J. Chem. Soc., Chem. Commun.*, 1984, 1326–1327.

59 R. Alvarez, E. Carmona, M. L. Poveda and R. Sãnchez-Delgado, *J. Am. Chem. Soc.*, 1984, **106**, 2731–2732.

60 R. Alvarez, E. Carmona, J. M. Marin, M. L. Poveda, E. Gutiérrez-Puebla and A. Monge, *J. Am. Chem. Soc.*, 1986, **108**, 2286–2294.

61 I. Castro-Rodriguez, H. Nakai, L. N. Zakharov, A. L. Rheingold and K. Meyer, *Science*, 2004, **305**, 1757–1759.

62 I. Castro-Rodriguez and K. Meyer, *Chem. Commun.*, 2006, 1353–1368.

63 S. C. Bart, C. Anthon, F. W. Heinemann, E. Bill, N. M. Edelstein and K. Meyer, *J. Am. Chem. Soc.*, 2008, **130**, 12536–12546.

64 K. G. Moloy and T. J. Marks, *Inorg. Chim. Acta*, 1985, **110**, 127–131.

65 W. J. Evans, J. R. Walensky and J. W. Ziller, *Organometallics*, 2010, **29**, 945–950.

66 C. L. Webster, J. W. Ziller and W. J. Evans, *Organometallics*, 2012, **31**, 7191–7197.

67 J. A. Higgins, F. G. N. Cloke and S. M. Roe, *Organometallics*, 2013, **32**, 5244–5252.

68 M. Ephritikhine, *J. Alloys and Compounds*, 1994, **213-214**, 15–19.

69 P. C. Leverd, M. Ephritikhine, M. Lance, J. Vigner and M. Nierlich, *J. Organomet. Chem.*, 1996, **507**, 229–237.

70 C. Lescop, T. Arliguie, M. Lance, M. Nierlich and M. Ephritikhine, *J. Organomet. Chem.*, 1999, **580**, 137–144.

71 O. P. Lam, S. M. Franke, F. W. Heinemann and K. Meyer, *J. Am. Chem. Soc.*, 2012, **134**, 16877–16881.

72 E. M. Matson, P. E. Fanwick and S. C. Bart, *Organometallics*, 2011, **30**, 5753–5762.

73 E. M. Matson, W. P. Forrest, P. E. Fanwick and S. C. Bart, *J. Am. Chem. Soc.*, 2011, **133**, 4948–4954.

74 S. J. Zuend, O. P. Lam, F. W. Heinemann and K. Meyer, *Angew. Chem. Int. Ed.*, 2011, **50**, 10626–10630.

75 J.-C. Berthet, J.-F. Le Maréchal, M. Nierlich, M. Lance, J. Vigner and M. Ephritikhine, *J. Organomet. Chem.*, 1991, **408**, 335–341.

76 J. G. Brennan, R. A. Andersen and A. Zalkin, *Inorg. Chem.*, 1986, **25**, 1761–1765.

77 J. G. Brennan, R. A. Andersen and A. Zalkin, *Inorg. Chem.*, 1986, **25**, 1756–1760.

78 A. F. R. Kilpatrick and F. G. N. Cloke, *Unpublished Results*.

79 A. F. R. Kilpatrick and F. G. N. Cloke, *Chem. Commun.*, 2014, **50**, 2769–2771.

80 A. F. R. Kilpatrick, DPhil Thesis, University of Sussex, 2014.

81 O. T. Summerscales, A. S. P. Frey, F. G. N. Cloke and P. B. Hitchcock, *Chem. Commun.*, 2009, 198–200.

82 O. P. Lam, S. C. Bart, H. Kameo, F. W. Heinemann and K. Meyer, *Chem. Commun.*, 2010, **46**, 3137–3139.

83 A.-C. Schmidt, A. V. Nizovtsev, A. Scheurer, F. W. Heinemann and K. Meyer, *Chem. Commun.*, 2012, **48**, 8634–8636.

84 L. Castro, O. P. Lam, S. C. Bart, K. Meyer and L. Maron, *Organometallics*, 2010, **29**, 5504–5510.

85 A.-C. Schmidt, F. W. Heinemann, C. E. Kefalidis, L. Maron, P. W. Roesky and K. Meyer, *Chem. Eur. J.*, 2014, **20**, 13501–13506.

86 N. Tsoureas, L. Castro, A. F. R. Kilpatrick, F. G. N. Cloke and L. Maron, *Chem. Sci.*, 2014, **5**, 3777–3788.

87 O. P. Lam, F. W. Heinemann and K. Meyer, *Angew. Chem. Int. Ed.*, 2011, **50**, 5965–5968.

88 O. P. Lam, L. Castro, B. Kosog, F. W. Heinemann, L. Maron and K. Meyer, *Inorg. Chem.*, 2012, **51**, 781–783.

89 A. S. P. Frey, F. G. N. Cloke, P. B. Hitchcock, I. J. Day, J. C. Green and G. Aitken, *J. Am. Chem. Soc.*, 2008, **130**, 13816–13817.

90 O. T. Summerscales, DPhil Thesis, University of Sussex, 2007.

91 R. J. Kahan and F. G. N. Cloke, MChem Dissertation, University of Sussex, 2011.

92 W. B. Tolman, *Angew. Chem. Int. Ed.*, 2010, **49**, 1018–1024.

93 D.-H. Lee, B. Mondal and K. D. Karlin, in *Activation of Small Molecules: Organometallic and Bioinorganic Perspectives (ed W. B. Tolman)*, Wiley-VCH Verlag GmbH & Co. KGaA, Weinheim, Germany, 2006.

94 F. G. N. Cloke and N. Tsoureas, *Unpublished Results*.

95 F. H. Allen, *Acta Cryst. Sect. B*, 2002, **B58**, 380–388.

96 I. J. Bruno, J. C. Cole, P. R. Edgington, M. Kessler, C. F. Macrae, P. McCabe, J. Pearson and R. Taylor, *Acta Cryst. Sect. B*, 2002, **B58**, 389–397.

97 A. S. P. Frey, F. G. N. Cloke, M. P. Coles and P. B. Hitchcock, *Chem. Eur. J.*, 2010, **16**, 9446–9448.

98 J. H. Farnaby, DPhil Thesis, University of Sussex, 2011.

CHAPTER 4: ACTIVATION OF SMALL MOLECULES BY HETEROCYCLIC MIXED-SANDWICH COMPLEXES

4.1 Introduction

As discussed in Chapter 3, the steric properties of the mixed-sandwich complexes are important in determining the outcome of small molecule reactivity. The heterocyclic complexes [U(COT$^{(Si\textit{i}Pr3)2}$)(Cp^{EMe4})] (E = N (**2.5**), P (**2.6**) and As (**2.7**)) have similar steric properties to their Cp^{Me4} and Cp* analogues, both of which have shown interesting reactivity with small molecules.[1–5] It is therefore concluded that the steric environment of the three heterocyclic mixed-sandwich complexes should be favourable with respect to activation of small molecules.

Studies of **2.5THF** – **2.7THF** by cyclic voltammetry (Chapter 2) showed a shift in the U^{IV}/U^{III} redox potential from *ca.* -2.1 V *vs* $[FeCp_2]^{+/0}$ for the Cp^R complexes to *ca.* -1.8 – -1.9 V for the heterocyclic complexes. These values indicate that complexes **2.5THF** – **2.7THF** are thermodynamically less reactive than their all-carbon counterparts. However, these values are comparable with the redox potential for [U(COT$^{(Si\textit{i}Pr3)2}$)(Cp$^{\textit{t}Bu3}$)] (**2.3**, -1.83 V) and therefore should reductively activate the small molecules under study.

As both the steric and thermodynamic properties of the heterocyclic mixed-sandwich complexes imply favourable reactivity with small molecules, it was concluded that the Cp^{EMe4} fragment was an appropriate choice for exploratory reactions with carbon monoxide and carbon dioxide. These gases were chosen due to their industrial and environmental importance (see Chapter 3). However, in order to gain better understanding of the reactivity, analogous molecules such as isonitriles and heteroallenes of the type S=C=X (X = O and S) were also explored.

4.2 Activation of carbon monoxide

Reactivity of CO with uranium(III) mixed-sandwich complexes has to date been limited to reductive activation, although insertion of carbon monoxide has been observed for uranium(IV) alkyl, amide and hydride complexes.[6] Despite the literature presence of heterocyclic uranium complexes, there have to date been no reports of small molecule activation by these species.

4.2.1 Reactivity of [U(COT$^{(SiiPr3)2}$)(Cp^{PMe4})] with carbon monoxide

Addition of excess CO to a cold solution of [U(COT$^{(SiiPr3)2}$)(Cp^{PMe4})] (**2.6**) resulted in a colour change from purple to red upon warming. NMR studies of the mixture revealed the initial formation of **4.1**, which decomposed over several days to give a mixture of species in solution and brown intractable solids (**Figure 4.2**). However, in the presence of a coordinating solvent, **4.1** persisted in solution, even though the solvent molecules do not coordinate to this complex. **4.1** was identified by XRD studies as a mixed-sandwich complex with an oxy-phosphinine ligand, formed by insertion of CO into the P–C bond of the phospholyl ligand (**Figure 4.1**).

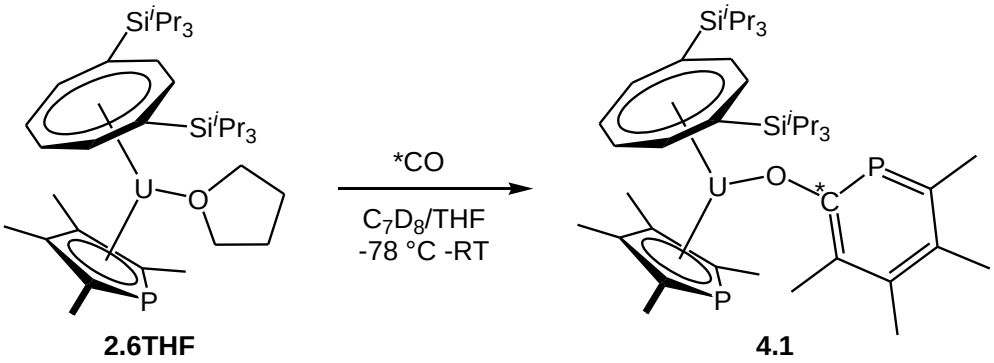

Figure 4.1 Reactivity of [U(COT$^{(SiiPr3)2}$)(Cp^{PMe4})(THF)] with *CO.

Decomposition of **4.1** in the absence of coordinating solvent occurred above -20 °C, even if the solution was degassed shortly after CO addition. Two of the decomposition products observed were diamagnetic, and their stoichiometry in solution was determined by the addition of an internal standard (**Figure 4.2**). The first species was identified as $COT^{(Si\textit{i}Pr3)2}$, which was often observed in trace amounts in other gas reaction mixtures. However, accurate comparison of the integrals of this species with the resonances of **2.6** was precluded by overlap of the ligand *iso*-propyl resonances and significant line-broadening of the ring proton resonances.

The second species was found to incorporate isotopically labelled carbon when ^{13}CO was used. This species was identified crystallographically as [bis(2,3,4,5-tetramethylphospholyl)acetylene] (**4.2**), a detailed characterisation of which is discussed below. This species was formed quantitatively, and $^{13}C\{^{1}H\}$ NMR spectroscopy revealed that no other ^{13}C-enriched species were formed in this reaction.

Analyses of the brown solids were difficult due to their insolubility in all hydrocarbon and ethereal solvents and attempted characterisation by infrared spectroscopy did not reveal any notable absorptions. Further attempts to characterise the solids by powder diffraction and mass spectrometry were unsuccessful, however microanalysis revealed low carbon and hydrogen content, indicating a cluster or polymeric species of approximate composition $[(COT^{(Si\textit{i}Pr3)2})U_8O_8]$.

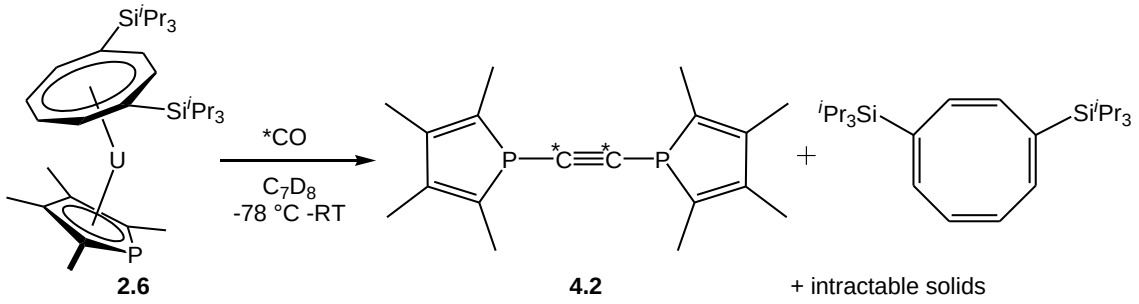

Figure 4.2 Reactivity of $[U(COT^{(Si\textit{i}Pr3)2})(Cp^{PMe4})]$ with *CO in the absence of THF.

Similar decomposition products were observed by Ephritikhine *et al.*, for the reaction of [Cp_3UR] with carbon monoxide.[7] This reaction involved insertion of CO into the U–R bond to yield the acyl complex which subsequently decomposed into an unidentified uranium oxo species and a substituted arene (**Figure 4.3**). Analogous reactivity was also reported by Andersen for uranium(IV) alkyl complexes and Cloke *et al.* for a uranium(IV) hydride.[8,9] Studies by Cramer and Gilje also demonstrate that η^1-coordination of the CO-oxygen to uranium weakens the triple bond facilitating cleavage.[10]

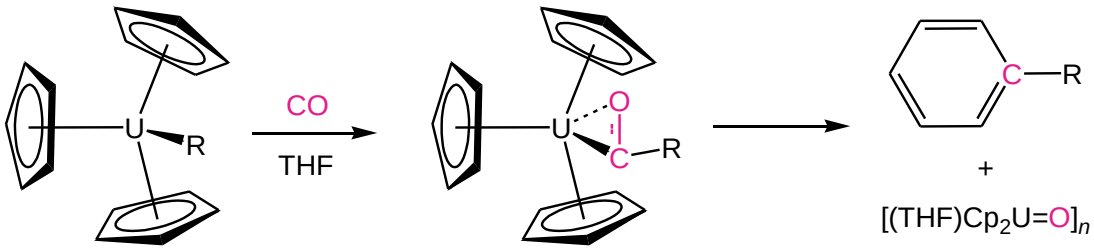

Figure 4.3 Synthesis and decay of [$Cp_3U(CO)R$].[7]

4.2.1.1 Characterisation of [$U(COT^{(SiiPr3)2})(Cp^{PMe4})(2\text{-}O\text{-}PC_5Me_4)$] (**4.1**)

After work-up of the reaction mixture, **4.1** is stable without the presence of a coordinating solvent and is found to persist for several weeks in hydrocarbon solvents. Mass spectrometry supported crystallographic data for **4.1** (**Figure 4.4**, **Table 4.1**) and NMR analysis illustrated the coupling between the phosphinine-phosphorus (191.4 ppm) and the ^{13}C-enriched carbon atom (423.1 ppm, $^1J_{CP}$ = 33 Hz).

Comparison of the mixed-sandwich fragment in **4.1** with **2.6THF** shows a slight contraction of the U–Ct distances and increased bending of the Cp–U–COT unit, which is caused by shortening of the U–O distance upon creation of a formal U–O bond.

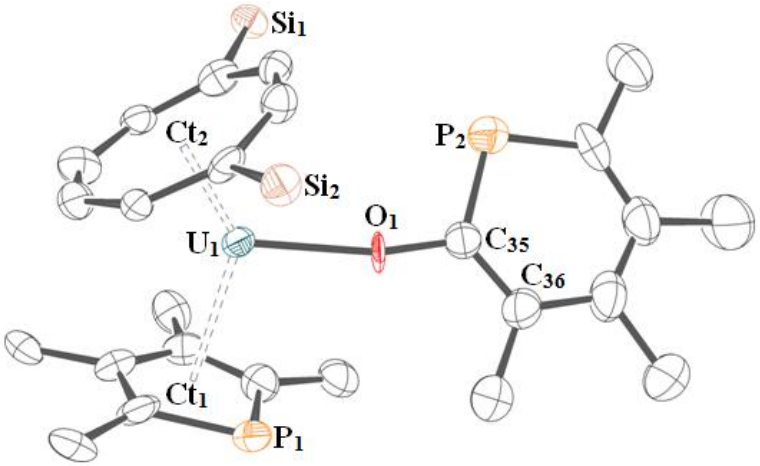

Figure 4.4 ORTEP view of **4.1** with thermal ellipsoids at 50% probability; *iso*-propyl groups and hydrogen atoms have been omitted for clarity.

Distances (Å)			
U_1–Ct_1	2.58768(5), 2.57980(6)	**U_1–Ct_2**	1.91936(3), 1.91819(4)
U_1–O_1	2.146(7), 2.120(6)	**O_1–C_{35}**	1.347(14), 1.376(12)
C_{35}–C_{36}	1.382(18), 1.358(16)	**C_{36}–C_{37}**	1.418(19), 1.446(17)
C_{37}–C_{38}	1.40(2), 1.40(2)	**C_{38}–C_{39}**	1.39(2), 1.357(19)
C_{39}–P_2	1.721(14), 1.752(12)	**P_2–C_{35}**	1.759(13), 1.755(12)
Angles (°)			
Ct_1–U_1–Ct_2	135.2974(10), 136.7744(9)	**U_1–O_1–C_{35}**	166.9(8), 168.4(7)
O_1–C_{35}–P_2	114.5(9), 113.4(8)	**O_1–C_{35}–C_{36}**	121.1(12), 121.5(10)

Table 4.1 Bond lengths, distances and angles for **4.1**. Ct_1 is the centroid for the Cp^{PMe4} ligand and Ct_2 is the centroid for the $COT^{(SiiPr3)2}$ ligand.

The 2-oxyphosphinine moiety has very similar metrics to three analogous ligands in the literature (C–C distances of 1.362(10) – 1.439(2) Å and P–C distances of 1.700(7) – 1.7793(17) Å).[11–13] However, these ligands exhibit different coordination modes, whereby η^6-coordination is observed for two chromium carbonyl complexes and phosphorus-based η^1-coordination is observed for a tungsten complex (**Figure 4.5**). **4.1** is therefore not only the first uranium complex featuring a phosphinine ligand, but also the first organometallic complex with an oxygen-bound oxy-phosphinine moiety. The C–O distance in this complex short, indicative of oxygen lone pair delocalisation into the aromatic ring, giving rise to partial double bond character. The bond angles around C_{35} and the C–C and P–C distances within the ring further illustrate the aromaticity of the unit.

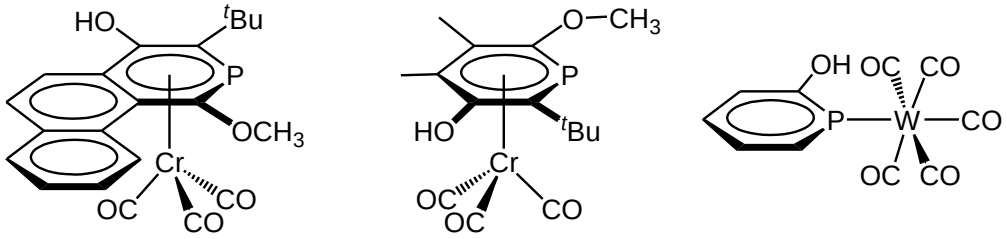

Figure 4.5 Oxy-phosphinine ligands in organometallic chemistry.[11–13]

4.2.1.2. Infrared studies of the reaction of [U(COT$^{(Si\textit{i}Pr3)2}$)(Cp^{PMe4})] with CO

In situ solution phase IR studies were carried out for the reaction of [U(COT$^{(Si\textit{i}Pr3)2}$)(Cp^{PMe4})] with ^{12}CO from -52 to 27 °C. As the mixture warmed, two absorption bands assigned to **4.1** were observed at 2178 and 2015 cm^{-1}. However, above -10 °C, the intensity of these bands diminished, illustrating that decomposition was occurring. The frequencies of these absorptions are high with respect to U–CO complexes in the literature, which have absorption bands in the range of 1817 to

1976 cm^{-1} for terminal U–CO stretches and 1429 to 1600 cm^{-1} for η^2-carbonyl complexes.[8,14–23] A complex which exhibits a carbonyl absorption band that is closer in value to the frequencies reported here however, is (tacn)U–CO–U(tacn), whose ^{12}CO stretching frequency lies at 2092 cm^{-1}.[24]

Repetition of the reaction with ^{13}CO illustrated an isotopic shift of both absorption bands (**Figure 4.6**, **Table 4.2**), however the isotopic ratio *R* for these absorptions is not consistent with the calculated values using the reduced mass ratio for carbon monoxide ($\mu(^{12}CO)/\mu(^{13}CO)$ = 0.9777).[25] It is therefore proposed that the bands correspond to O–C–P/O–C–C stretches, as analogous –C=C=O, –N=C=O and –N=C=S bands typically fall in the region of 2260 to 2020 cm^{-1}.[26] The absence of a typical M–CO stretching frequency suggests that this species only occurs transiently and is not observed on the timescale of the experiment. The infrared spectrum of analytically pure **4.1** also exhibits the same absorption bands and supports the assignment.

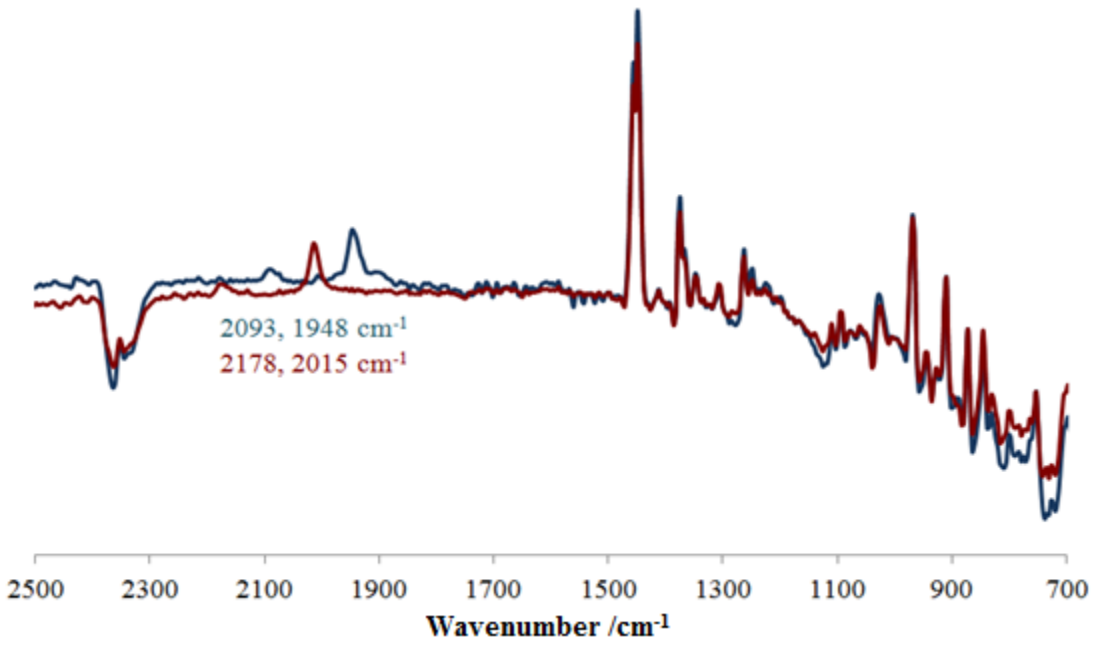

Figure 4.6 Overlaid *in situ* infrared spectra at -20 °C for the reaction of [U(COT$^{(Si\mathit{i}Pr3)2}$)(Cp^{PMe4})] with ^{12}CO (red) and ^{13}CO (blue).

Band	$\nu(^{12}CO)$	$\nu(^{13}CO)$ (*obs*)	$\nu(^{13}CO)$ (*calc*)	$\Delta\nu$	*R*
(1)	2178	2093	2129	36	0.9610
(2)	2015	1948	1970	22	0.9667

Table 4.2 Frequency values (cm^{-1}) and the calculated isotopic shifts *R* [$\nu(^{12}CO)/\nu(^{13}CO)$] at -20 °C for both absorption bands. $\Delta\nu$ is the frequency difference between the calculated and observed values for $\nu(^{13}CO)$.

4.2.1.3 Characterisation of [bis(2,3,4,5-tetramethylphospholyl)acetylene] (**4.2**)

Analysis of **4.2** by ^{1}H NMR spectroscopy shows a singlet at 1.5 ppm corresponding to the methyl groups in the 3- and 4-ring positions, and a doublet at 2.0 ppm for the methyl groups in the 2- and 5-ring positions ($^{3}J_{PH}$ = 10.9 Hz, **Figure 4.7**). The $^{31}P\{^{1}H\}$ spectrum shows a singlet at -19.4 ppm which splits into a doublet of doublets ($^{1}J_{CP}$ = 16.7 Hz, $^{2}J_{CP}$ = 15.3 Hz) when the acetylenic carbons are ^{13}C-enriched. The corresponding doublet of doublets was also observed in the $^{13}C\{^{1}H\}$ spectrum at 103.1 ppm. This is due to an AA'XX' system, which gives rise to both one-bond and two-bond coupling, illustrating that each phosphorus atom is magnetically inequivalent.

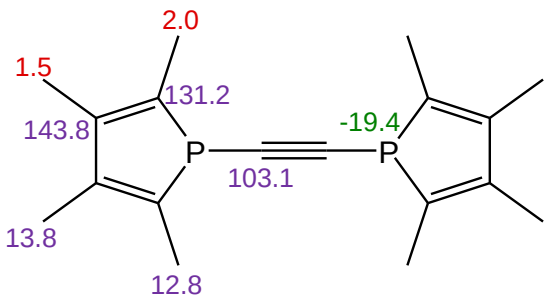

Figure 4.7 NMR assignments (δ) of **4.2**. Proton resonances are shown in red, carbon resonances are shown in blue and the phosphorus resonance is shown in green.

The molecular structure of **4.2** has a gauche-conformation, a feature which is seen to a lesser extent in other reported structures with a P–C≡C–P unit.[27–29] This conformation gives rise to partial overlap between the phosphorus lone pair and the π* system in the acetylenic unit. As a result, the P–C single bond is *ca*. 0.05 Å shorter than typical P–C bonds (*ca.* 1.83 – 1.86 Å) and the C≡C bond is *ca*. 0.02 Å longer than non-conjugated C≡C bonds (*ca.* 1.18 Å, **Table 4.3**).[30] These metrics agree with the other published structures with the P–C≡C–P unit, which have similar short P–C bonds and long C≡C bonds (1.753(7) – 1.789(9) and 1.198(12) – 1.211(11) Å respectively).[27–29]

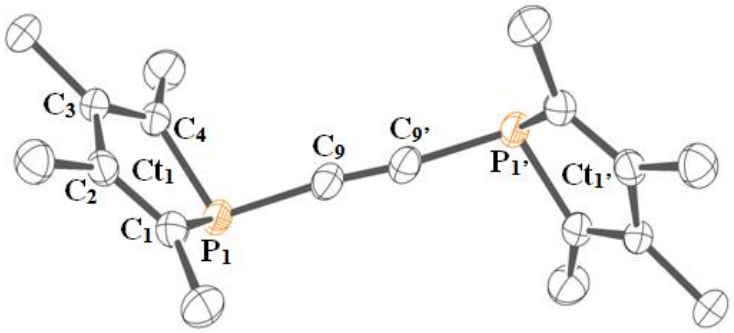

Figure 4.8 ORTEP view of **4.2** with thermal ellipsoids at 50% probability; hydrogen atoms have been omitted for clarity.

The P–C–C bond angle in **4.2** falls within the range of the literature values for analogous complexes (170.2(8) – 175.792(7)°), but the Ct–P–C angle is less acute than in analogous phosphorus(III) (*ca.* 105 – 111°) and phosphorus(V) molecules (*ca.* 111 - 115°). This cannot be attributed to steric parameters, as the molecules reported in the literature have varied sterics around the phosphorus atom. It is therefore concluded that the obtuse angle is due to packing of the molecules within the lattice in order to enable staggered overlap of the phosphole rings due to dipolar interactions (**Figure 4.9**).

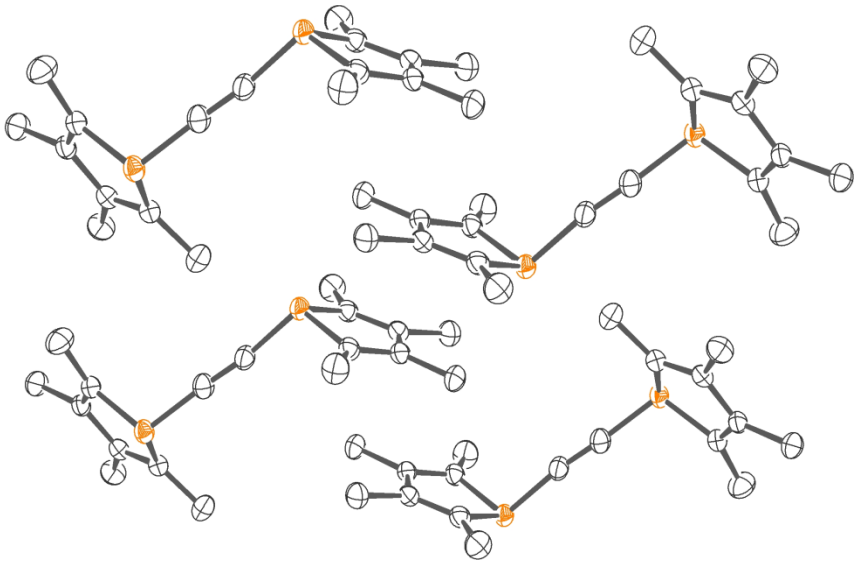

Figure 4.9 The molecular structure of **4.2** illustrating the partial overlap of the phosphole rings in the solid-state.

Distances (Å)					
C_1–C_2	1.353(2)	**C_2–C_3**	1.481(2)	**C_3–C_4**	1.352(2)
C_4–P_1	1.8009(15)	**P_1–C_1**	1.8047(15)	**P_1–C_9**	1.7673(16)
C_9–$C_{9'}$	1.209(3)				
Angles (°)					
P_1–C_9–$C_{9'}$	172.67(15)	**Ct_1–P_1–C_9**	115.12(6)	**Ct_1–P_1–$P_{1'}$–$Ct_{1'}$**	96.08(7)

Table 4.3 Selected bond lengths and angles for **4.2.** Ct_1 and $Ct_{1'}$ are the centroids for the phosphole fragments.

4.2.1.4 Synthesis of [{U(COT$^{(Si\mathit{i}Pr3)2}$)}$_2$(μ-O)(μ-η^1:η^1-O_2SOCF_3)$_2$] (**4.3**)

Prior to the successful isolation of **4.1**, attempts were made to trap this species before decomposition occurred. Maintaining the solution of [U(COT$^{(Si\mathit{i}Pr3)2}$)(Cp^{PMe4})] and ^{13}CO at -40 °C for 1 hour after gas addition gave rise to full conversion to **4.1** without significant decomposition, at which point TMSOTf was added.

NMR analysis of the solution revealed a mixture of species, one of which was identified as [{U(COT$^{(Si\mathit{i}Pr3)2}$)}$_2$(μ-O)(μ:η^1:η^1-O_2SOCF_3)$_2$] (**4.3**) by XRD and mass spectrometry (**Figure 4.10**). Attempts to further characterise this species have proved difficult due to its high solubility in hydrocarbon and silane solvents and consequential difficulty in obtaining an analytically pure sample. Mass spectrometry also revealed a peak which corresponds to [Me_4C_4P-$COSiMe_3$]. However, the number of resonances present in the NMR spectra of the reaction mixture precluded the estimation of a yield or further characterisation of either species.

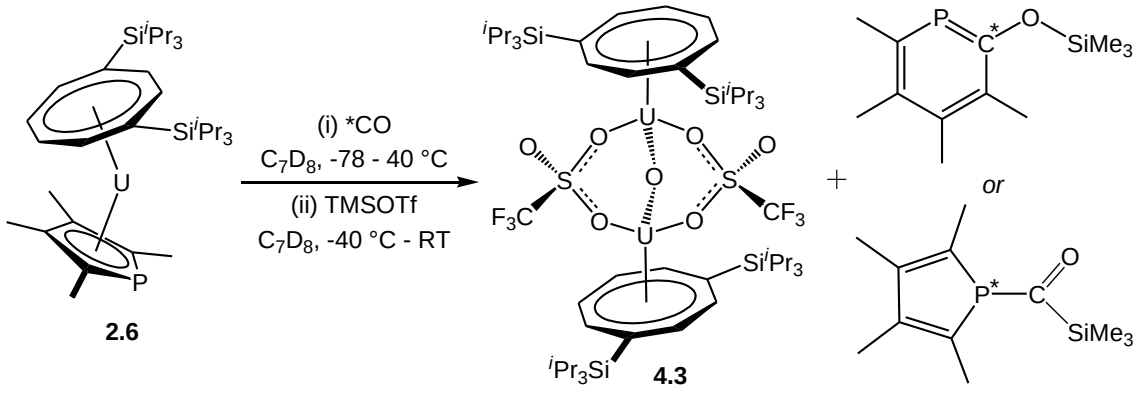

Figure 4.10 The synthesis of **4.3** *via* the reaction of [U(COT$^{(Si\mathit{i}Pr3)2}$)(Cp^{PMe4})] with *CO.

4.2.1.5 Molecular structure of [{U(COT$^{(SiiPr3)2}$)}$_2$(μ-O)(μ:η^1:η^1-O_2SOCF_3)$_2$] (**4.3**)

Crystals of **4.3** were obtained by slow evaporation of a pentane/$SiMe_4$ solution at -35 °C. However, XRD studies revealed a disordered structure with a mirror plane, illustrated in **Figure 4.11**.

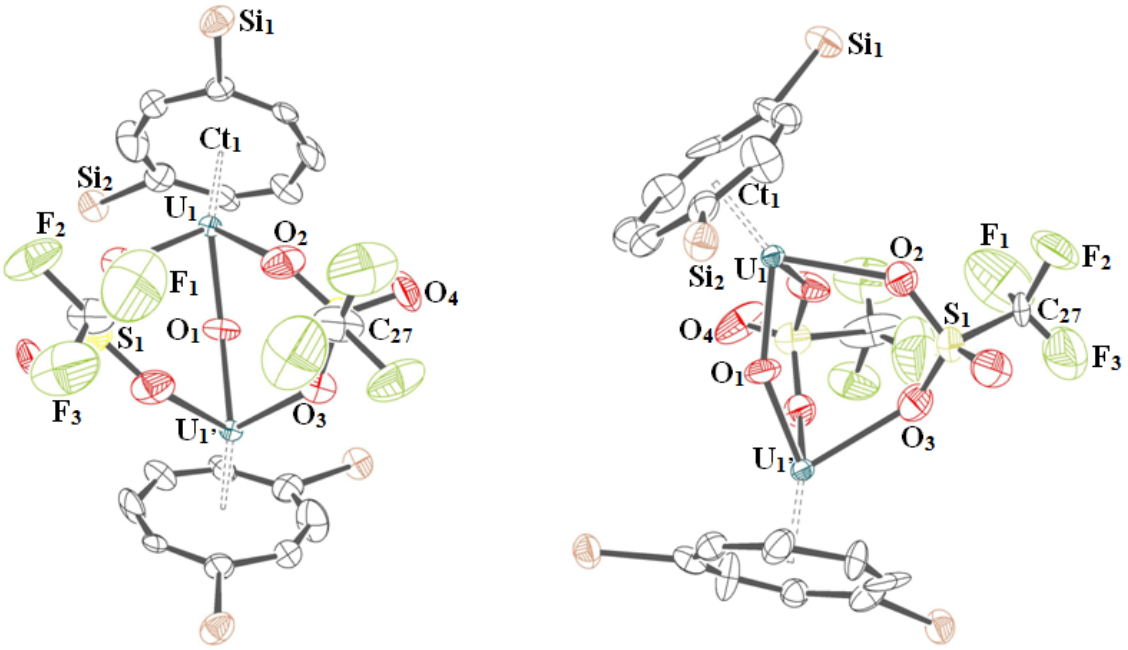

Figure 4.11 Two ORTEP views of **4.3** with thermal ellipsoids at 50% probability; hydrogen atoms and COT *iso*-propyl groups have been omitted for clarity.

To date, only two other bimetallic uranium complexes with analogous bridging triflate and oxo fragments have been published, and feature longer U–O bonds and more obtuse U–O–U angles than **4.3** (2.0987(16) – 2.115(4) Å and 158.7(2) – 159.2(5)° respectively).[31,32] Comparison of the triflate metrics however, reveal that the U–O and O–S distances in **4.3** show more similarity to terminal triflate complexes (U–O distances lie in the range of 2.36(1) – 2.485(9) Å), whereas the U–O–S angles are typical of bridging triflate complexes (121.6(3) – 156.8(3)°).[33,34]

Distances (Å)					
U_1–O_1	2.087(6)	**U_1–O_2**	2.425(18)	**U_1'–O_3**	2.381(16)
S_1–O_2	1.471(19)	**S_1–O_3**	1.485(17)	**S_1–O_4**	1.36(2)
S_1–C_{27}	1.95(4)	**U_1–Ct_1**	1.901(9)	**U_1–U_1'**	4.0028(9)
Angles (°)					
O_2–S_1–C_{27}	101.5(15)	**O_3–S_1–C_{27}**	102.1(12)	**O_4–S_1–C_{27}**	104.9(16)
O_2–S_1–O_3	111.2(10)	**O_2–S_1–O_4**	114.9(12)	**O_3–S_1–O_4**	119.3(13)
U_1–O_2–S_1	139.0(10)	**U_1'–O_3–S_1**	136.0(11)	**U_1–O_1–U_1'**	147.0(12)

Table 4.4 Bond lengths, distances and angles for **4.3**. Ct_1 is the centroid for the $COT^{(Si\mathit{i}Pr3)2}$ ligand.

4.2.2. Reactivity of [U($COT^{(SiiPr3)2}$)(Cp^{AsMe4})] with carbon monoxide

Reaction of [U($COT^{(Si\mathit{i}Pr3)2}$)(Cp^{AsMe4})(THF)] (**2.7THF**) with carbon monoxide in THF/toluene resulted in the formation of several species, including the analogue to **4.1** [U($COT^{(Si\mathit{i}Pr3)2}$)(Cp^{AsMe4})(2-O-AsC_5Me_4)] in 43% yield (**4.4**). This species was characterised by a distinctive ^{13}C-resonance at 428.0 ppm and it was observed that the ^{1}H NMR spectrum for this complex closely resembled that of **4.1**. However, further characterisation of this complex was not achieved as an analytically pure sample could not be obtained. In the absence of coordinating solvent, the yield of **4.4** was reduced (*ca.* 8%), illustrating analogous reactivity to the phospholyl complex. A second diamagnetic species was also observed in low yields (29%), which was identified as [2,2'-bis(3,4,5,6-tetramethylarsenine)], formed by coupling of two cleaved arsenine units (**Figure 4.12**).

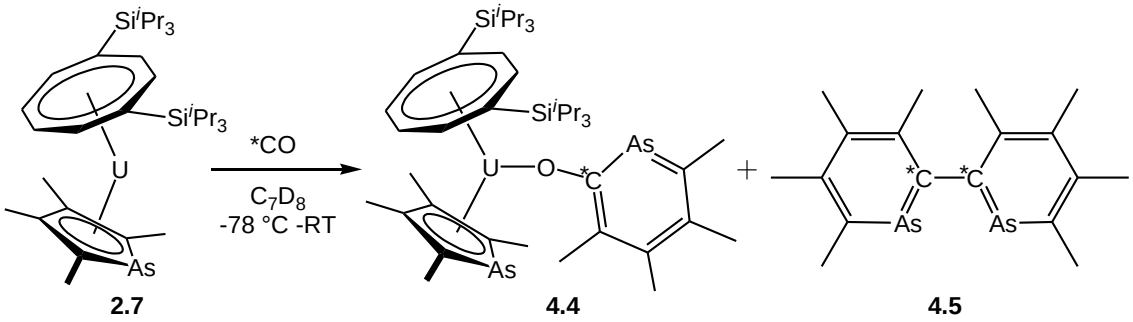

2.7 **4.4** **4.5**

Figure 4.12 Reactivity of [U(COT$^{(SiiPr3)2}$)(Cp^{AsMe4})] with *CO.

In situ solution phase infrared studies for this reaction illustrated the appearance of an absorption band at 1964 cm^{-1}, which shifted to 1923 cm^{-1} when ^{13}CO was used (**Figure 4.13**). These values are consistent with a uranium monocarbonyl complex, such as those synthesised from [(Cp^R)$_3$U] complexes (1880 – 1976 cm^{-1}).[16] The isotopic shift of 41 cm^{-1} is also within error of the calculated value using the reduced mass ratio (1920 cm^{-1} for ^{13}CO), and supports the assignment of a uranium-carbonyl frequency.[25]

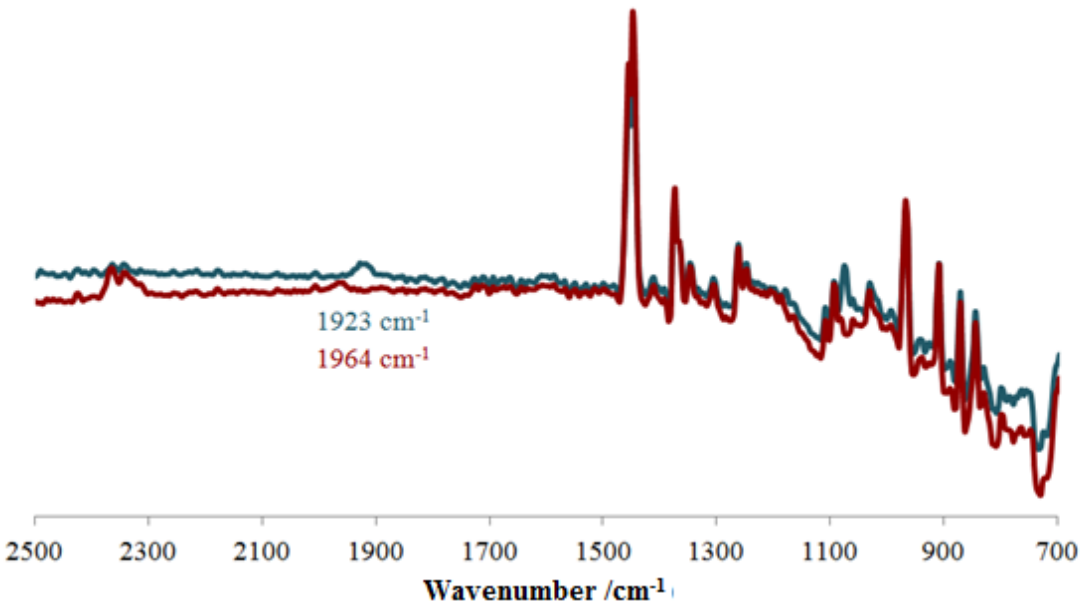

Figure 4.13 Overlaid *in situ* infrared spectra at -32 °C for the reaction of [U(COT$^{(SiiPr3)2}$)(Cp^{AsMe4})] with ^{12}CO (red) and ^{13}CO (blue).

These absorption bands diminished upon warming, however the two anticipated bands for **4.4** were not observed in solution. This is postulated to be due to the very low yields of **4.4** in the absence of THF. However a solid-state infrared spectrum did reveal two bands at 2123 and 1921 cm^{-1} assigned to O–C–As/O–C–C stretching frequencies.

4.2.2.1 Characterisation of [2,2'-bis(3,4,5,6-tetramethylarsenine)] (**4.5**)

Crystals of **4.5** were obtained in low yields due to the number of decomposition products present in the crude solution. This was demonstrated by the addition of an internal standard, which showed the formation of **4.5** in 29% yield, and **4.4** in 15% yield. As a consequence, **4.5** could only be partially characterised. The ^{1}H NMR spectrum showed four methyl proton environments between 2.5 and 1.7 ppm. Five carbon environments corresponding to the methyl carbons (25.0 – 14.6 ppm) and the ^{13}C-enriched carbon atom from ^{13}CO (185.7 ppm) were also identified, however the other aromatic carbon resonances could not be definitively assigned.

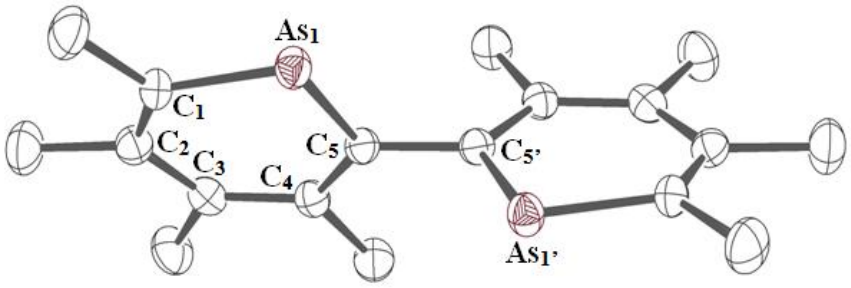

Figure 4.14 ORTEP view of **4.5** with thermal ellipsoids at 50% probability; hydrogen atoms have been omitted for clarity. Selected bond distances (Å) and angles (°): aromatic C–C 1.39678(7) – 1.41803(10), C_5–$C_{5'}$ 1.495(6), C–As_1 1.85512(13) – 1.86145(9), As_1–C_5–$C_{5'}$–$As_{1'}$ 63.672(6).

XRD data of the crystals (**Figure 4.14**) showed that aromaticity is maintained within the six-membered rings as shown by the ring C–C bond lengths. The C_5–$C_{5'}$ bond that links the two rings is however significantly longer and is more consistent with a single bond. The twist observed between the rings, illustrated by the 63° torsion angle, is due to repulsion of the methyl substituents at C_4.

Few structures have been published which contain the arsenine unit, and only two exhibit a six-membered ring linked by a C–C bond α to arsenic.[35,36] These structures also show a twist in the torsion angle of 45.6(3) and 37.32(2)°, which is less pronounced due to the repulsion arising from proton substituents at C_4 rather than methyl groups.

4.2.3. Reactivity of [U(COT$^{(SiiPr3)2}$)(Cp^{PMe4})(THF)] with isonitriles

During the course of reactivity studies with carbon monoxide, isoelectronic reagents were also considered. Whilst awaiting identification of **4.1** and **4.4**, it was proposed that an alternative steric environment would allow the synthesis of a stable analogue to these complexes, which could be isolated in higher yields. Isonitriles are isoelectronic with carbon monoxide, but the variety of R substituents available allows the sterics to be tuned in order increase product stability.

Reaction of methyl isonitrile with **2.6THF** resulted in decomposition of the complex, however the larger variant, *tert*-butyl isonitrile yielded the adduct [U(COT$^{(Si\mathit{i}Pr3)2}$)(Cp^{PMe4})(CN^{t}Bu)] (**4.6**, **Figure 4.15**). *In situ* infrared studies illustrated that adduct formation occured instantaneously upon addition of the isonitrile by the appearance of a *ν*CN absorption band at 2152 cm^{-1} (+14 cm^{-1} *vs* CN^{t}Bu). The small shift of free *vs* coordinated isonitrile has been observed previously, and the direction of the shift is dependent upon the bonding within the complex.[16] The positive shift in **4.6** illustrates weak π back-donation, so that ligand-to-metal σ-donation is the main bonding interaction.

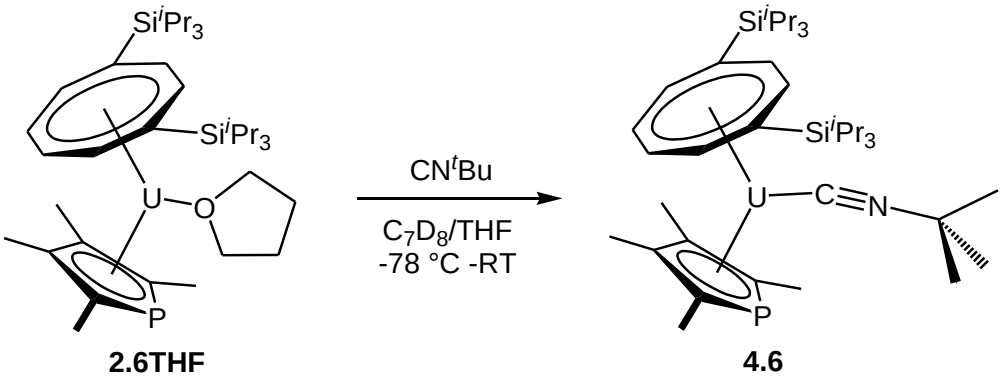

2.6THF **4.6**

Figure 4.15 Reactivity of [U(COT$^{(Si\textit{i}Pr3)2}$)(Cp^{PMe4})(THF)] with *tert*-butyl isonitrile.

4.2.3.1 Molecular structure of [U(COT$^{(Si\textit{i}Pr3)2}$)(Cp^{PMe4})(CN^{t}Bu)] (**4.6**)

Comparison of the molecular structure of **4.6** (**Figure 4.16**) with **2.6THF** illustrates the U–Cp and U–COT distances have contracted slightly upon adduct formation, and the increased Cp–U–COT angle arises from the decreased sterics of the isonitrile ligands in comparison to THF.

The isonitrile fragment maintains the C≡N bond, which is also observed for other uranium isonitrile complexes in the literature.[16,22,37–41] Comparison of **4.6** with [U(COT$^{(Si\textit{i}Pr3)2}$)(Tp^{Me2})(CNMe)] and [U(COT$^{(Si\textit{i}Pr3)2}$)(η^2-dmpz)(CNMe)], illustrates **4.6** has a shorter U–C bond (2.675(3) and 2.660(4) Å) and a longer C–N bond (1.140(3) and 1.142(5) Å), implying **4.6** exhibits more backbonding.[42,43] This was also inferred by the infrared data, which illustrate the *ν*CN band for **4.6** is *ca*. 20 cm^{-1} lower in frequency than the other two complexes.

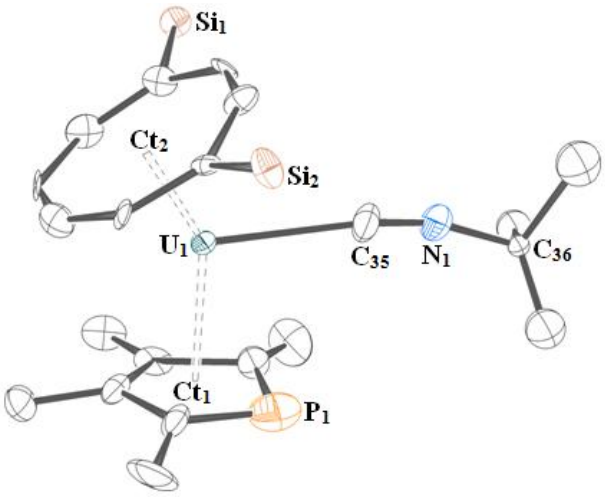

Figure 4.16 ORTEP view of **4.6** with thermal ellipsoids at 50% probability; hydrogen atoms and iso-propyl groups have been omitted for clarity. Selected bond distances (Å) and angles (°):U_1–Ct_1 2.52807(14); U_1–Ct_2 1.9459(2); U_1–C_{35} 2.626(6); C_{35}–N_1 1.156(8); N_1–C_{36} 1.515(14), 1.442(16); Ct_1–U_1–Ct_2 146.882(17); U_1–C_{35}–N_1 173.2(10); C_{35}–N_1–C_{36} 173(3), 165.0(14).

4.3 Activation of carbon dioxide

Due to the observed insertion reactivity of carbon monoxide with the heterocyclic mixed-sandwich complexes, it was anticipated that this reactivity might also occur with carbon dioxide. Insertion of CO_2 has been observed for uranium(IV) mixed-sandwich complexes, with the formation of carboxyl, carbamate and formate complexes from the respective alkyl, amide and hydride species.[6,9] However, it was anticipated that oxidation of the uranium(III) complexes would also occur, resulting in a mixture of reduction and insertion reactivity.

4.3.1 Reactivity of [U(COT$^{(SiiPr3)2}$)(Cp^{NMe4})] with carbon dioxide

Addition of excess $^{13}CO_2$ to a solution of [U(COT$^{(SiiPr3)2}$)(Cp^{NMe4})] (**2.5**) resulted in the formation of an initial product (**4.7**) within minutes of gas addition. This species was characterised by a singlet at -60.7 ppm in the $^{13}C\{^1H\}$ NMR spectrum and a single silicon resonance at -93.1 ppm. Within several days however, these resonances had diminished and were replaced by a carbon resonance at -7.1 ppm and a silicon resonance at -79.7 ppm. These resonances corresponded to a second product, [{U(COT$^{(SiiPr3)2}$)}$_2$(μ-O){μ-η^1:η^1-O$_2$C(NC$_4$Me$_4$)}$_2$], which was formed by formal oxidation of uranium and insertion of carbon dioxide into the uranium–nitrogen bonds (**4.8, Figure 4.17**). ^{1}H NMR showed the overall conversion of **2.5** to **4.8** to be quantitative, and analytically pure samples of this complex were isolated in 62% yield.

In order to trap **4.7**, the reaction was repeated with varying stoichiometries of carbon dioxide. These studies found that one mole equivalent CO_2 per uranium centre gave rise to a mixture of **4.7** and **4.8**, but that using 0.5 equivalents exclusively yielded **4.7** and ^{13}CO. Single crystals and analytically pure samples of **4.7** however could not be obtained and this complex remains unidentified. It is therefore not possible to determine a mechanism for the transformation of **2.5** to **4.8**.

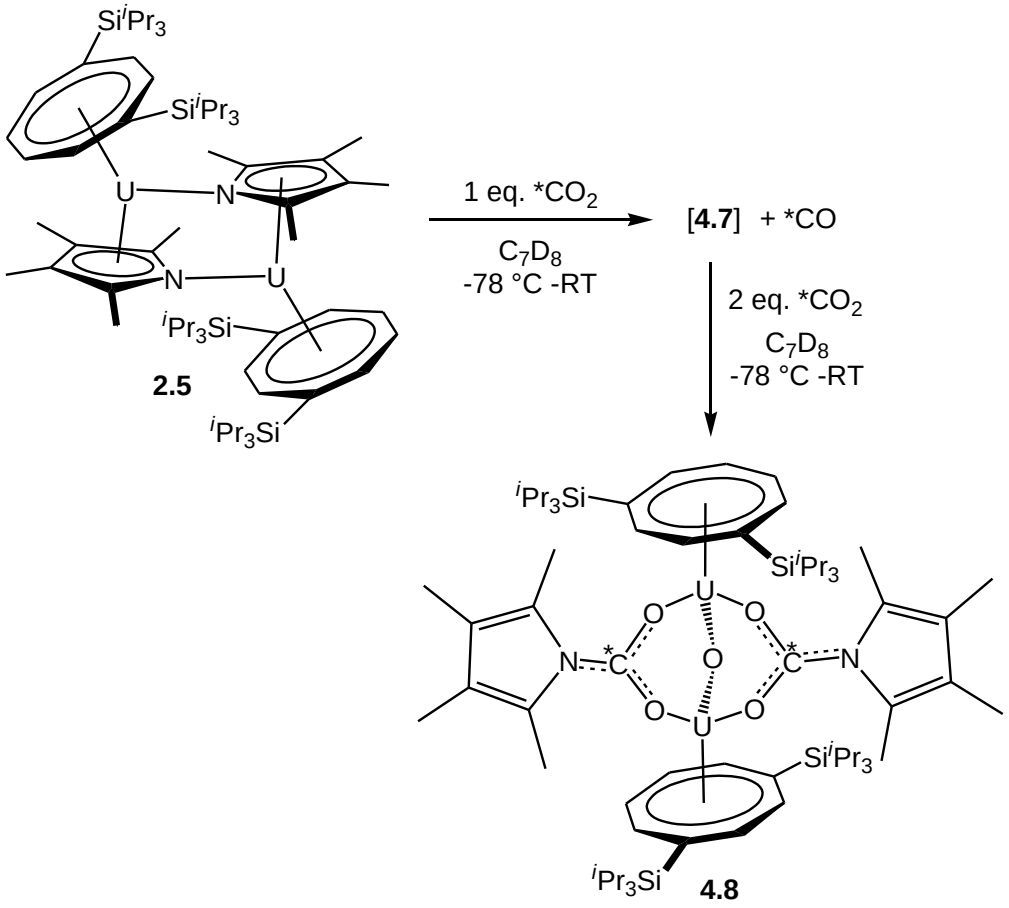

Figure 4.17 Reactivity of [U(COT$^{(SiiPr3)2}$)(Cp^{NMe4})] with carbon dioxide.

4.3.1.1 Characterisation of **4.8**

The NMR spectra of **4.8** showed the complex was dynamic in solution, however the COT-ring protons could not be observed regardless of sample concentration. Mass spectrometry supported the formulation of the complex; however microanalysis values were consistently low for carbon over repeated measurements due to the thermal instability of the complex.

XRD data for **4.8** (**Figure 4.18, Table 4.5**) illustrate that the U–Ct distances are slightly shorter in **4.8** than for the THF adduct and base-free parent mixed-sandwich complexes (**2.5THF** and **2.5**). However these distances are still within the range of U–Ct distances

for the uranium(III) mixed-sandwich complexes synthesised by Cloke *et al.* (1.8891(7) – 1.977(5) Å, see Appendix II).

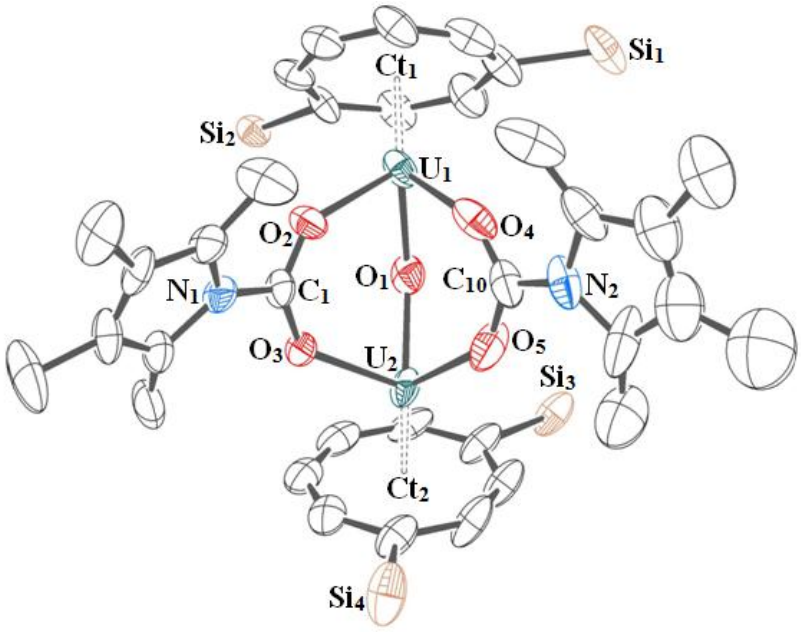

Figure 4.18 ORTEP view of **4.8** with thermal ellipsoids at 50% probability; hydrogen atoms and COT *iso*-propyl groups have been omitted for clarity.

The bridging oxo, O_1, is positioned slightly off-centre, and lies within the range of similar fragments reported in the literature (1.905(10) – 2.372(10) Å).[33,34] The U–O–U angle, however lies at the lower end of the literature range (128.8(5) – 180.0°), illustrating the constraints the carbamate ligands impose on this fragment. The carbamate moieties are asymmetrical, which is observed by the varied U–O and O–C bond lengths.

Distances (Å)					
U_1–Ct_1	1.923(7)	U_2–Ct_2	1.9121(5)	U_1–U_2	3.9087(8)
U_1–O_1	2.096(10)	U_1–O_2	2.350(8)	U_1–O_4	2.378(11)
U_2–O_1	2.067(10)	U_2–O_3	2.353(8)	U_2–O_5	2.320(11)
C_1–O_2	1.260(14)	C_1–O_3	1.261(15)	C_{10}–O_4	1.241(19)
C_{10}–O_5	1.27(2)	C_1–E_1	1.385(12)	C_{10}–E_2	1.410(15)
Angles (°)					
O_2–C_1–O_3	125.2(11)	O_4–C_{10}–O_5	117.8(11)	O_2–C_1–E_1	116.9(11)
O_4–C_{10}–E_2	123.5(15)	O_3–C_1–E_1	119.5(16)	O_5–C_{10}–E_2	117.0(14)
U_1–O_1–U_2	139.8(5)				

Table 4.5 Bond lengths, distances and angles for **4.8**. Ct_1 and Ct_2 are the centroids for the $COT^{(Si\textit{i}Pr3)2}$ ligands.

The pyrrole rings retain a degree of aromaticity despite the formation of the N–C bond, which is illustrated in **Figure 4.19** by the similar C–C bond distances in this fragment. This arises from overlap of the nitrogen lone pair with the diene unit, evidenced by the almost linear Ct–N–C angles (169.2(10) and 179.2(12)°). There is also a pronounced twist (*ca.* 30°) in the pyrrole rings in relation to the N–CO_2 plane, in order to avoid close contact of the pyrrole methyl substituents with the *iso*-propyl groups.

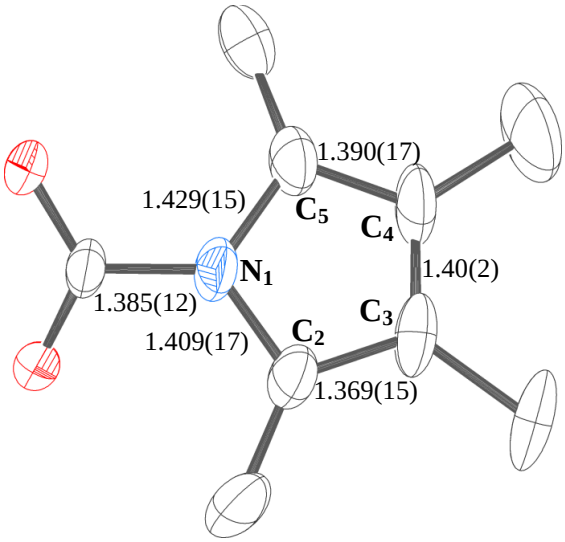

Figure 4.19 ORTEP view of the $[Me_4C_4NCO_2]^-$ fragment in **4.8** with bond lengths.

A similar core structure was reported by Arnold and co-workers for a dimeric uranium aryloxide complex with bridging oxo and carbonate fragments (**Figure 4.20**).[44] The metrics of the oxo fragment are similar to those in **4.8** ($U–O_1$ 2.095(3) Å, $U–O_1–U$ 140.4(5)°) and the carbonate fragments also exhibit the same asymmetry. Another uranium complex with bridging oxo and acetate moieties also has similar metrics within the core unit, illustrating that the constraints imposed by the three bridging moieties keep the metrics within a narrow range.[45]

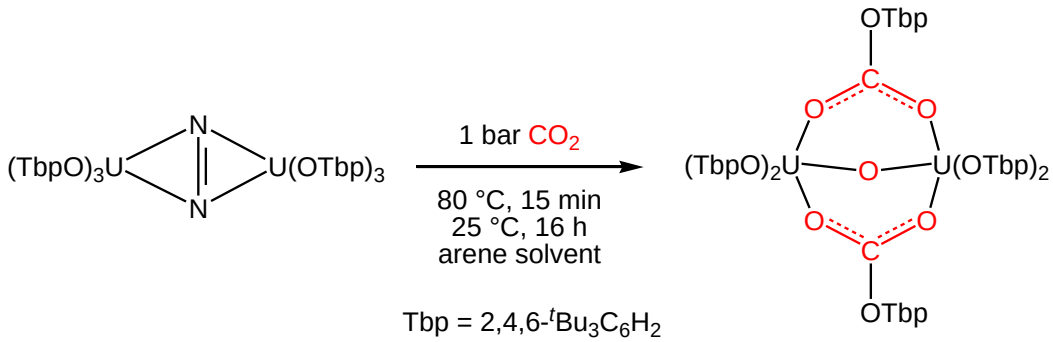

Figure 4.20 Reactivity of a uranium(trisaryloxide) complex with carbon dioxide.[44]

4.3.2 Reactivity of [U(COT$^{(SiiPr3)2}$)(Cp^{NMe4})] with nitrous oxide

The formation of the bridging oxo fragment in **4.8** and the observed formation of CO in the reaction mixture gave rise to the hypothesis that a bridging oxo complex was an intermediate in the reaction. In order to test this, [U(COT$^{(SiiPr3)2}$)(Cp^{NMe4})] (**2.5**) was reacted with nitrous oxide.

Addition of N_2O to a solution of **2.5** resulted in the instantaneous formation of one paramagnetic species (**4.9**), which was identified by XRD studies as [{(COT$^{(SiiPr3)2}$)(η^1-Cp^{NMe4})U}(μ-O)(μ-η^1:η^5-Cp^{NMe4}){U(COT$^{(SiiPr3)2}$)}] (**Figure 4.21**).

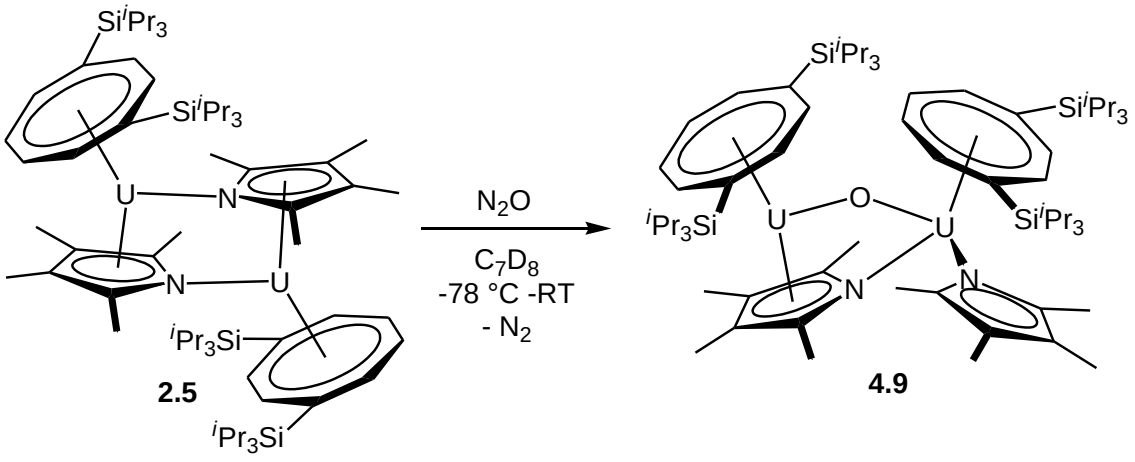

Figure 4.21 Synthesis of **4.9** by reaction of the mixed-sandwich complex with N_2O.

The asymmetric structure of **4.9** gives rise to complicated NMR spectra. Four silicon resonances and individual protons are observed, giving rise to overlapping resonances between +13 and -12 ppm in the ^{1}H NMR spectrum. A molecular ion could not be observed by mass spectrometry due to the thermal lability of this species, however microanalysis agreed with the proposed formulation.

The asymmetric nature of this complex is ascribed to the steric properties around the U–O–U centre. Due to the propensity of the pyrrolyl ring to coordinate in both η^5 and η^1-modes, one of the rings forms a second bridge between the two metal centres (**Figure 4.22**). This is observed by the near identical U–N distances, in addition to the typical U–Ct(pyrrolyl) distance. Not only does this prevent η^5-coordination of the second pyrrolyl ring, but also gives rise to inequivalent COT rings.

The U–O–U core metrics fall within the range of values published in the literature (U–O 1.905(10) – 2.372(10) Å and U–O–U 128.8(5) – 180.0°), however the 0.06 Å difference in the U–O bond distances within the complex is more unusual.[33,34] The U–O–U bond angle is more acute than uranium(IV) mixed-sandwich oxo complexes previously observed (154.5(3) and 159.6(3)°), and the U–U distance is *ca.* 0.3 Å shorter (4.1140(4) – 4.1600(8) Å), due to the additional bridge formed by the pyrrolyl ligand.[46,47]

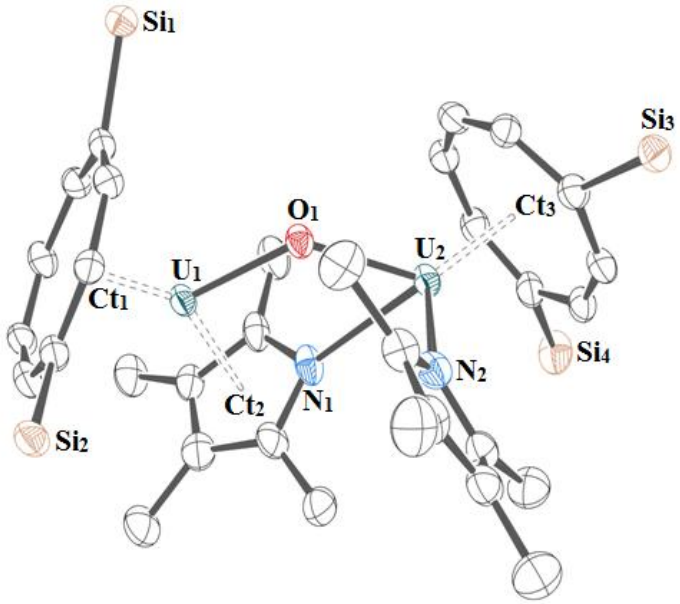

Figure 4.22 ORTEP view of **4.9** with thermal ellipsoids at 50% probability; hydrogen atoms and COT *iso*-propyl groups have been omitted for clarity.

Distances (Å)					
Ct_1–U_1	1.9430(3)	**Ct_2–U_1**	2.5498(4)	**Ct_3–U_2**	1.9798(2)
U_1–N_1	2.661(6)	**U_2–N_1**	2.653(6)	**U_2–N_2**	2.352(6)
U_1–O_1	2.059(4)	**U_2–O_1**	2.121(4)	**U_1–U_2**	3.7977(5)
Angles (°)					
Ct_1–U_1–Ct_2	135.253(10)	**Ct_3–U_2–N_2**	126.052(6)	**U_1–O_1–U_2**	130.6(2)
N_1–U_2–N_2	97.9378(10)	**O_1–U_2–N_2**	88.140(7)	**U_1–N_1–U_2**	91.238(4)
Ct_1–U_1–U_2–Ct_3	68.960(3)			**Ct_2–U_1–U_2–N_2**	104.399(4)

Table 4.6 Bond lengths, distances and angles for **4.9**. Ct_1 and Ct_3 are the centroids for the $COT^{(Si\textit{i}Pr3)2}$ ligands and Ct_2 is the centroid for the pyrrolyl ligands.

4.3.2.1 Reactivity of **4.9** with carbon dioxide

Addition of one equivalent CO_2 to a solution of **4.9** resulted in the gradual conversion of this complex to **4.8** *via* **4.7** by NMR. This confirms that **4.9** is an intermediate in the formation of the carbamate complex (**Figure 4.23**). However, as the identity of **4.7** remains unknown, it is not possible to deduce a mechanism for the transformation that occurs.

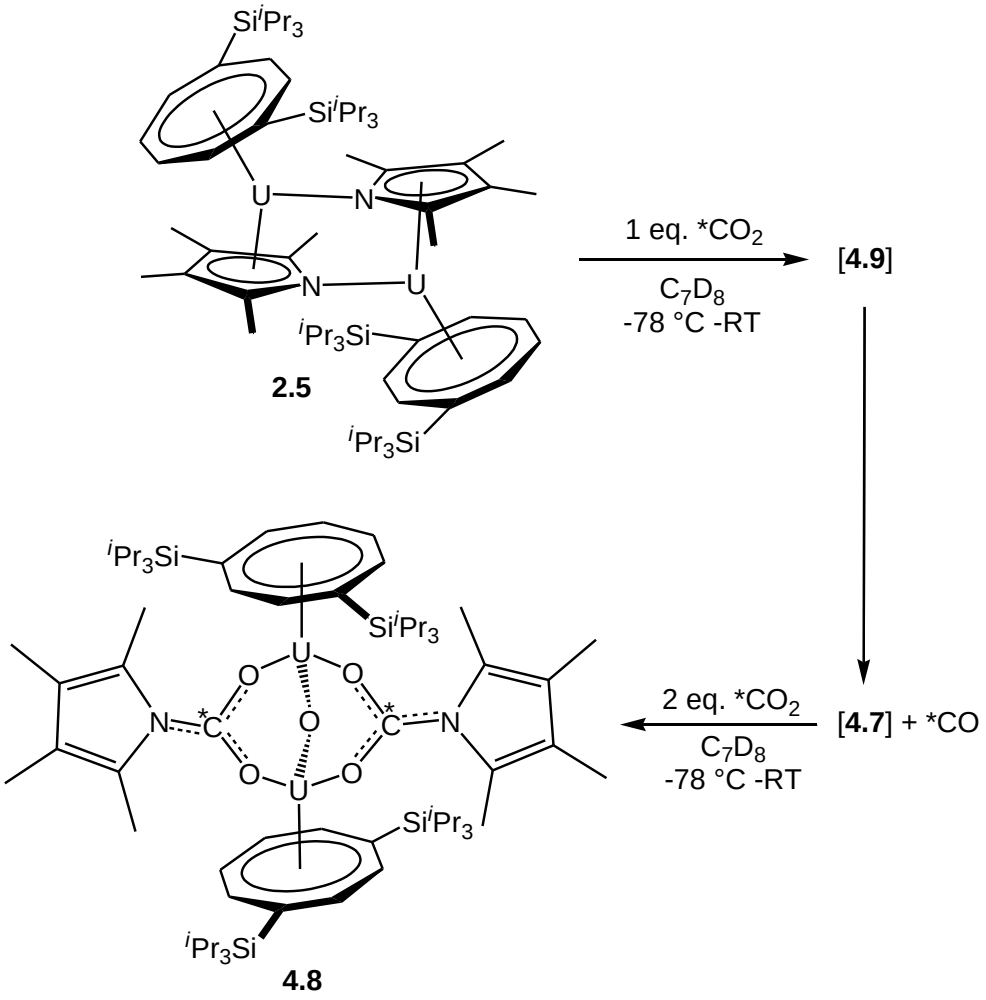

Figure 4.23 Reactivity of [U(COT$^{(SiiPr3)2}$)(Cp^{NMe4})] with CO_2.

4.3.3 Reactivity of [U(COT$^{(SiiPr3)2}$)(Cp^{PMe4})] with carbon dioxide

Addition of excess $^{13}CO_2$ to a solution of [U(COT$^{(SiiPr3)2}$)(Cp^{PMe4})] (**2.6**) gave rise to an instantaneous colour change from purple to red/brown. Analysis of the solution revealed complete consumption of the mixed-sandwich complex within minutes of gas addition and formation of an initial product (**4.10**), which was characterised by a singlet at -108.2 ppm in the $^{13}C\{^1H\}$ NMR spectrum. Within 48 hours however, this resonance had disappeared and two doublets corresponding to a second product (**4.11**) were present at -43.3 and -46.6 ppm. **4.11** was identified as [{U(COT$^{(SiiPr3)2}$)}$_2$(μ-O){μ-η^1:η^1-$O_2C(PC_4Me_4)$}$_2$], the phospholyl analogue of **4.8** (**Figure 4.24**). However, the

formation of **4.11** is observed to occur more quickly than the analogous carbamate complex, which is postulated to be due to the dimeric nature of [U(COT$^{(Si\textit{i}Pr3)2}$)(Cp^{NMe4})] in solution.

Reaction of **2.6** with 0.5 equivalents carbon dioxide resulted in the exclusive formation of **4.10**, indicating that this complex is analogous to the pyrrolyl intermediate, **4.7**. Heteronuclear NMR studies of the solution illustrated that in addition to the singlet in the $^{13}C\{^{1}H\}$ NMR spectrum, two silicon resonances (-72.8 and -93.3 ppm) and a broad phosphorus resonance were observed. However, further characterisation of **4.10** was not achieved as neither single crystals or analytically pure samples were obtained. As a consequence a mechanism for the formation of **4.11** cannot be determined.

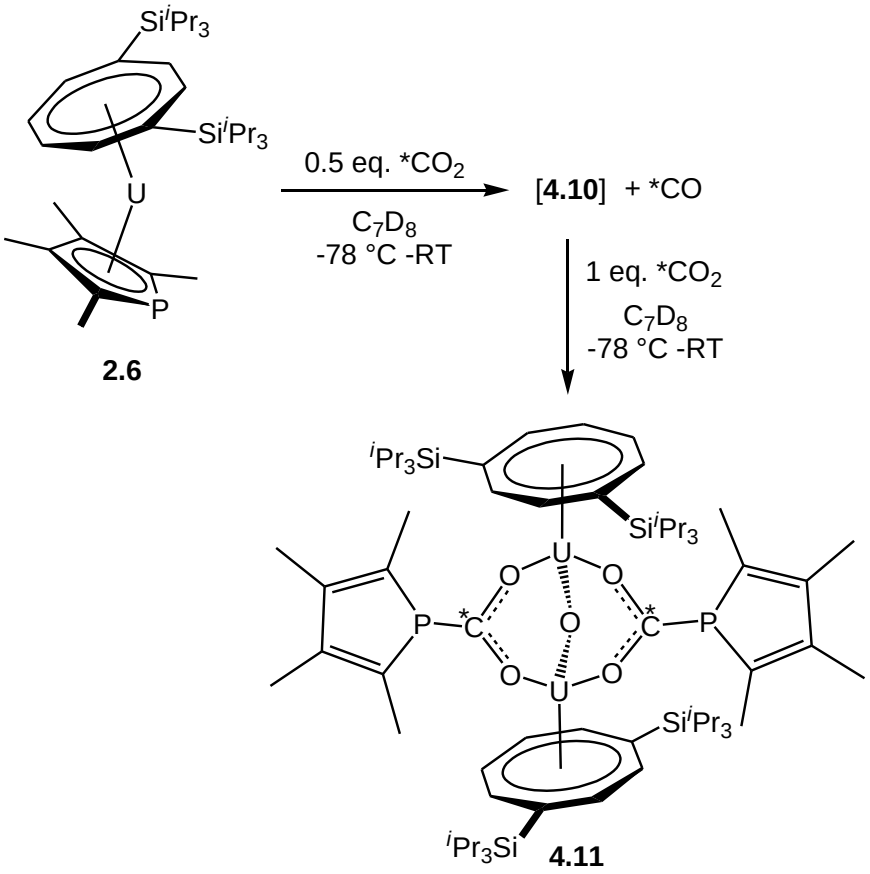

Figure 4.24 Reactivity of [U(COT$^{(Si\textit{i}Pr3)2}$)(Cp^{PMe4})] with carbon dioxide.

4.3.3.1 Characterisation of **4.11**

NMR analysis of **4.11** suggested that this complex is fluxional at ambient temperature, which gives rise to broad overlapping resonances in the $^{31}P\{^{1}H\}$ NMR spectrum and major and minor doublets at -46.6 and -43.3 ppm respectively in the $^{13}C\{^{1}H\}$ NMR spectrum. Cooling the probe to -20 °C removed the degeneracy; however definitive assignment of the resonances could not be achieved due to overlap with impurity resonances. The non-trivial formation of **4.11** was confirmed by the presence of three phosphorus resonances at -50 °C for the crude reaction mixture and the low yields of analytically pure solids (25%). However, mass spectrometry and combustion analysis confirmed the proposed formulation.

The crystallographic data obtained for **4.11** illustrate the similarity between this complex and its carbamate analogue (**4.8, Figure 4.25**). However, O_1 is positioned exactly between the two uranium centres in **4.11**, although the U–O–U angle is identical to this angle in **4.8** within error.

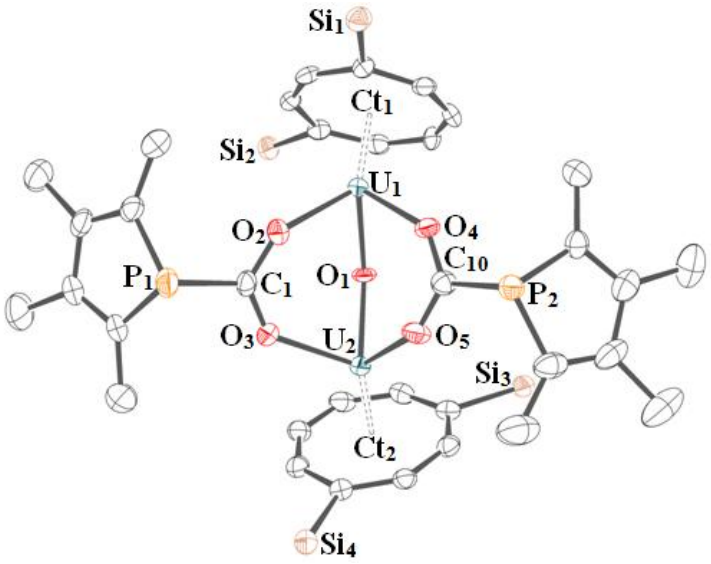

Figure 4.25 ORTEP view of **4.11** with thermal ellipsoids at 50% probability; hydrogen atoms and COT *iso*-propyl groups have been omitted for clarity.

There is also a slight contraction in the U–Ct distances in **4.11** compared to **4.8** as the longer C–P bonds preclude close contact between the phosphole methyl substituents and the *iso*-propyl groups. A further consequence of this is that the phosphole moieties do not twist with respect to the PCO_2 plane.

Unlike the carbamate fragments in **4.8**, the phosphacarbonate moieties are no longer aromatic, which is illustrated in **Figure 4.26** by discreet single and double bonds. Further evidence that the phosphorus lone pair does not participate in delocalisation of the diene unit is illustrated by the Ct–P–C angles (116.6(2) and 116.2(3)°), illustrating a trigonal pyramidal geometry around the phosphorus atoms.

Distances (Å)					
U_1–Ct_1	1.9320(3)	**U_2–Ct_2**	1.9323(3)	**U_1–U_2**	3.9313(3)
U_1–O_1	2.096(3)	**U_1–O_2**	2.346(4)	**U_1–O_4**	2.391(4)
U_2–O_1	2.096(3)	**U_2–O_3**	2.362(3)	**U_2–O_5**	2.343(4)
C_1–O_2	1.260(6)	**C_1–O_3**	1.262(6)	**C_{10}–O_4**	1.260(6)
C_{10}–O_5	1.286(6)	**C_1–E_1**	1.855(6)	**C_{10}–E_2**	1.850(6)
Angles (°)					
O_2–C_1–O_3	124.3(5)	**O_4–C_{10}–O_5**	123.7(5)	**O_2–C_1–E_1**	119.4(4)
O_4–C_{10}–E_2	118.8(4)	**O_3–C_1–E_1**	116.1(4)	**O_5–C_{10}–E_2**	117.3(4)
U_1–O_1–U_2	139.38(19)				

Table 4.7 Bond lengths, distances and angles for **4.11**. Ct_1 and Ct_2 are the centroids for the $COT^{(Si\textit{i}Pr3)2}$ ligands.

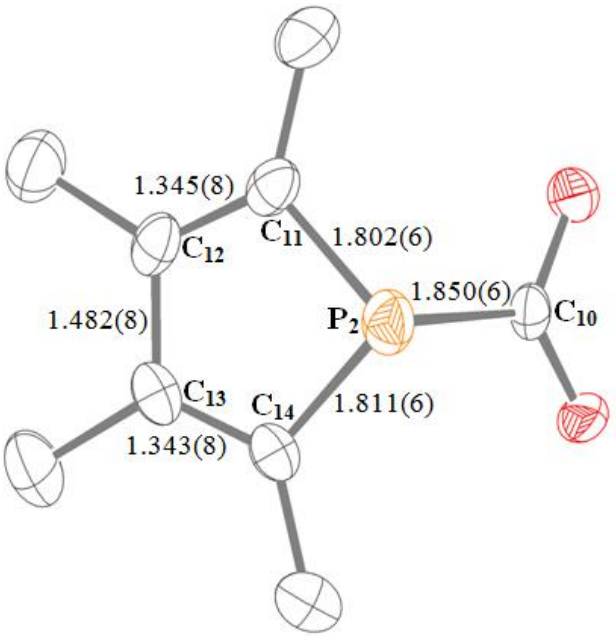

Figure 4.26 ORTEP view of a $[Me_4C_4PCO_2]^-$ fragment in **4.11** with bond lengths.

4.3.4 Reactivity of [U(COT$^{(SiiPr3)2}$)(Cp^{PMe4})] with nitrous oxide

During the formation of **4.10** using 0.5 mole equivalents carbon dioxide, another intermediate was observed (**4.12**), which had no ^{13}C-enriched resonance in the $^{13}C\{^1H\}$ NMR spectrum. It was speculated that **4.12** could be an oxo intermediate analogous to **4.9**. Nitrous oxide was therefore employed to independently synthesise **4.12**.

Addition of N_2O to a solution of [U(COT$^{(SiiPr3)2}$)(Cp^{PMe4})] (**2.6**) resulted in complete consumption of **2.6** within minutes. However the observed species disappeared over several hours to yield **4.12** as the predominant paramagnetic species in solution. This implied the presence of another observable intermediate; however repetition of this reaction with varying stoichiometries of N_2O yielded the same result. The only other paramagnetic species observed in solution were the two uranocene complexes, [U(COT$^{1,4\text{-Si}i\text{Pr3}}$)$_2$] and [U(COT$^{1,3\text{-Si}i\text{Pr3}}$)(COT$^{1,4\text{-Si}i\text{Pr3}}$)], which were present in varying ratios as minor products.

4.12 was identified as [{(COT$^{(SiiPr3)2}$)U}$_2$(μ-O)$_2$] by the XRD analysis of the DME and THF adducts of this complex (**4.12DME** and **4.12THF** respectively). This complex forms by abstraction of one oxygen atom from N_2O per uranium complex and loss of the phospholyl ring, demonstrating the lability of this ligand in comparison to the pyrrolyl ligand. The phospholyl rings couple to give [1,1'-bis(2,3,4,5-tetramethylphosphole)] (**4.13**), which was the only phosphorus incorporated species present in solution (**Figure 4.27**).

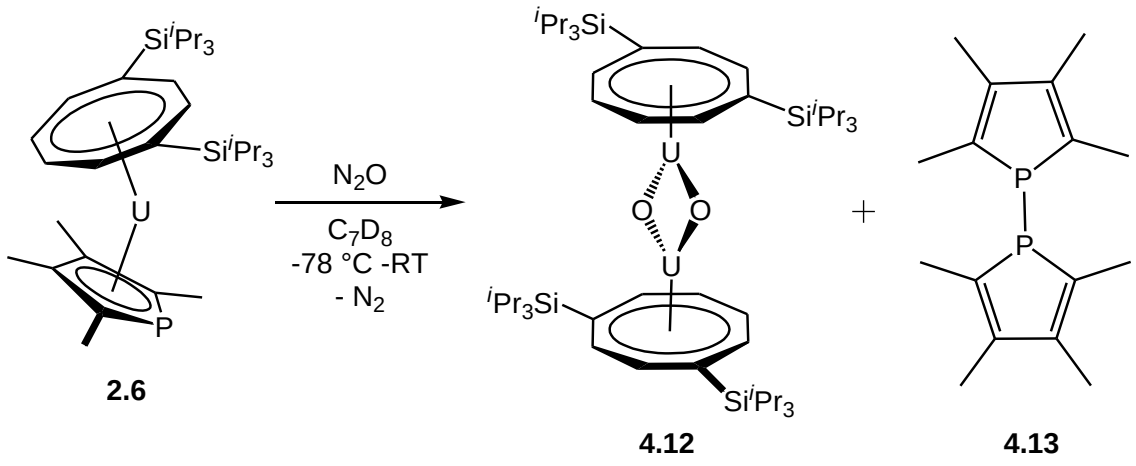

Figure 4.27 Reactivity of [U(COT$^{(SiiPr3)2}$)(Cp^{PMe4})] with N_2O.

4.3.2.1 Characterisation of [{(COT$^{(SiiPr3)2}$)U}$_2$(μ-O)$_2$] (**4.12**)

Analysis of **4.12** by NMR spectroscopy revealed the dynamic behaviour of this complex in solution is non-trivial, precluding definitive assignment of the resonances between -80 and +100 °C. At ambient temperature only one silicon resonance is observed at -85.4 ppm, however overlapping resonances in the proton spectra preclude assignment. Below -20 °C some of these resonances are observed to split, which is consistent with a fluxional structure that adopts a static conformation in solution below this temperature. Mass spectrometry exhibited a parent ion for the complex at *m/z* = 1341, and

microanalysis results from a powder sample obtained in the absence of coordinating solvent supported the proposed formulation.

Data from crystals of the DME adduct, [{U(COT$^{(Si\textit{i}Pr3)2}$)(DME)}$_2$(μ-O)$_2$] (**4.12DME, Figure 4.28**) show the molecular structure has longer U–Ct distances than the parent mixed-sandwich complex, **4.8** and **4.11** as a consequence of DME coordination.

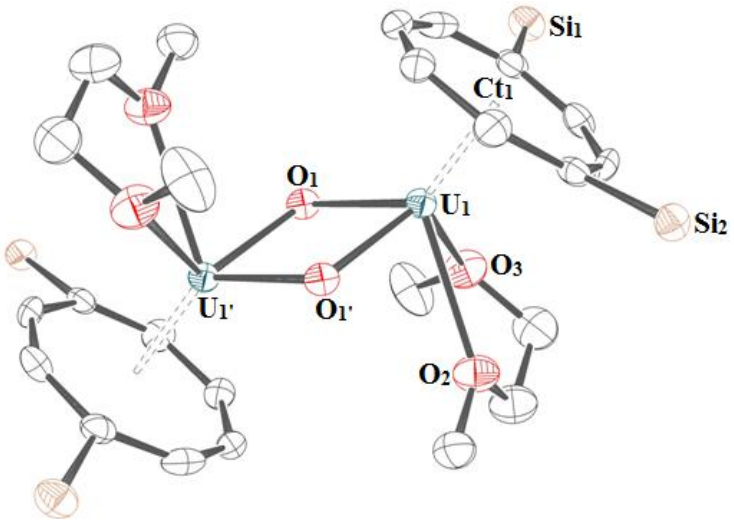

Figure 4.28 ORTEP view of **4.12DME** with thermal ellipsoids at 50% probability; hydrogen atoms and COT *iso*-propyl groups have been omitted for clarity. Selected bond distances (Å) and angles (°): U_1–Ct_1 2.059(2), 2.049(3), U_1–O_1 2.111(4), 2.107(5), U_1–$O_{1'}$ 2.131(5), 2.128(5), U_1–O_2 2.618(6), 2.627(5), U_1–O_3 2.651(6), 2.653(6), U_1–$U_{1'}$ 3.4081(5), 3.4027(6), U_1–O_1–$U_{1'}$ 106.93(18), 106.93(18).

The U–O bond lengths for the oxo fragments are within the reported range for analogous complexes (2.034(4) – 2.2012(16) Å), and the U–O–U angles allow the oxygen atoms to adopt a pseudo-tetrahedral geometry.[48–54] The U–U distance is also typical of bis-μ-oxo complexes (3.3557(5) – 3.5090(4) Å), which is *ca.* 0.5 Å shorter

than in **4.8** and **4.11** due to the absence of the bridging carbamate and phosphacarbonate fragments.

A similar complex, [{($COT^{(SiMe3)2}$)U}(μ-O)$_2${U(Cp*)$_2$}], synthesised by Cloke and Tsoureas by reaction of [U($COT^{(SiMe3)2}$)(Cp*)(THF)] with N_2O, exhibits similar U–O bond distances in the bridging oxo fragments (2.099(7) to 2.134(7) Å), but more acute U–O–U angles (104.8(2) – 105.2(2)°).[55] The U–Ct distance is also slightly shorter (1.932(4) Å), as the absence of coordinated solvent allows for closer proximity of the ring to the metal centre.

The THF adduct of **4.12**, [{U($COT^{(SiiPr3)2}$)(THF)}$_2$(μ-O)$_2$] (**4.12THF**) also yielded crystals. However the data obtained from these samples could not be fully refined and only illustrate connectivity (**Figure 4.29**). Consequently, the metrics of this complex cannot be compared to those of **4.12DME**.

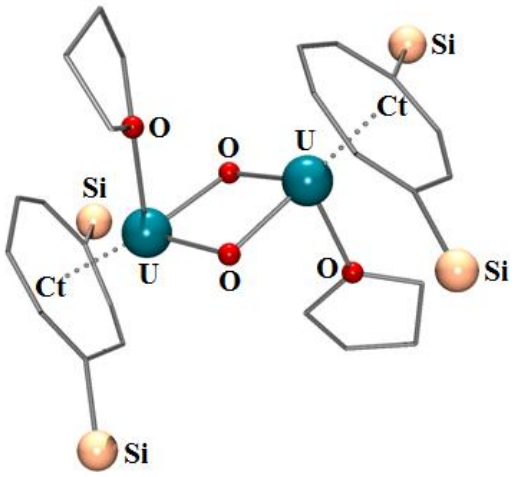

Figure 4.29 POV-Ray depiction of an unrefined molecular structure of **4.12THF**. COT *iso*-propyl groups have been omitted for clarity.

4.3.2.1 Characterisation of [1,1'-bis(2,3,4,5-tetramethylphosphole)] (**4.13**)

4.13 was obtained as an oil and the low quantities of this species precluded thorough purification and characterisation. However, mass spectrometry exhibited the molecular ion at *m/z* = 278 and this species was characterised by NMR spectroscopy (**Figure 4.30**). The proton resonance at 1.8 ppm exhibited two-bond coupling to phosphorus (4.9 Hz), and correlation experiments supported the proposed formulation of **4.13** by the absence of coupling in the ^{1}H-^{31}P HSQC.

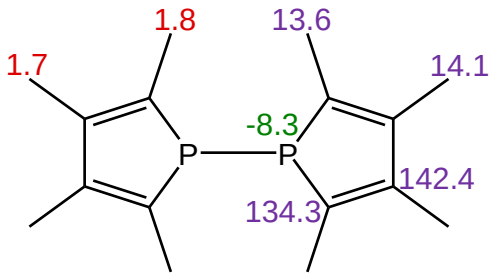

Figure 4.30 NMR assignments (δ) of **4.13**. Proton resonances are shown in red, carbon resonances are shown in blue and the phosphorus resonance is shown in green.

*4.3.4 Reactivity of **4.12** and **4.13** with carbon dioxide*

Addition of CO_2 to a mixture of **4.12** and **4.13** resulted in the formation of **4.10** then **4.11**, illustrating that **4.12** and **4.13** are intermediates in the formation of the phosphacarbonate complex (**4.11**). However it should be noted that an oxygen atom has been lost in the formation of **4.11**, demonstrating that the mechanism for the transformation is not trivial.

Reactivity of **4.12** and **4.13** with CO was attempted, however no changes were observed by NMR, illustrating that CO is not a reactive species in the transformation. Analytically pure samples of **4.13** were also found to be unreactive towards carbon

dioxide; however addition of CO_2 to **4.12** yielded a new unidentified paramagnetic species that had not been previously observed. This demonstrates that both **4.12** and **4.13** need to be present as a mixture in order for **4.11** to be formed, however further deductions about the mechanism could not be determined (**Figure 4.31**).

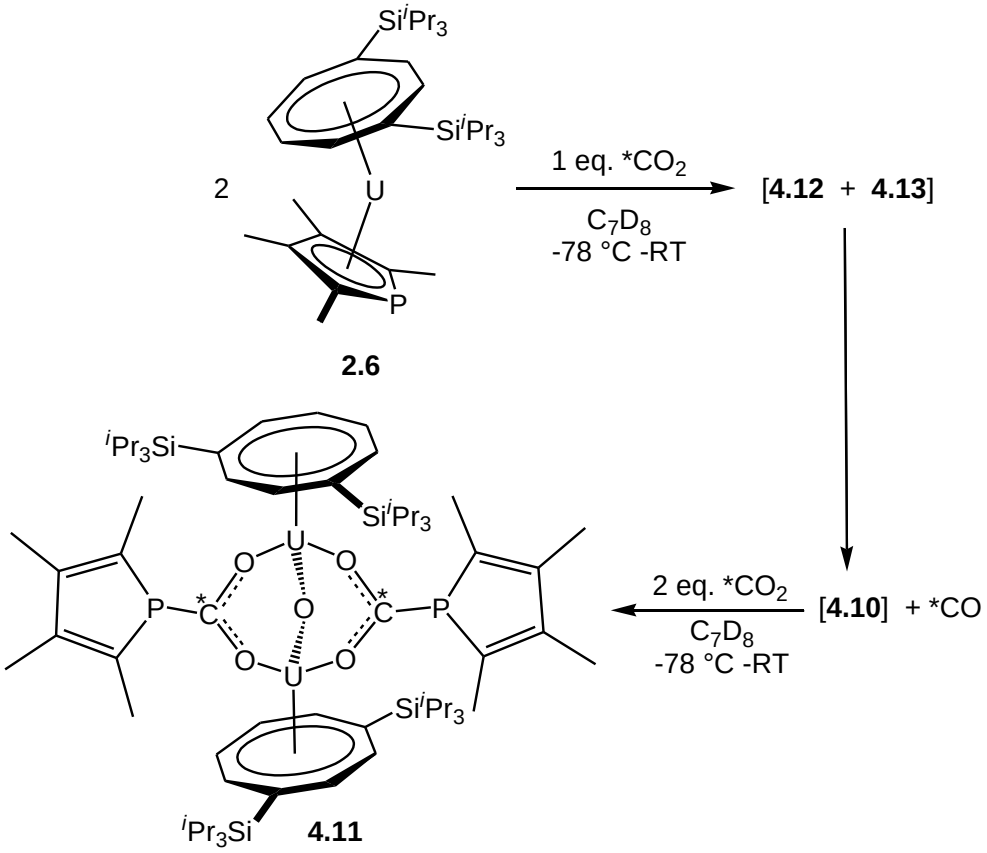

Figure 4.31 Reactivity of [U(COT$^{(SiiPr3)2}$)(Cp^{PMe4})] with CO_2.

4.3.5 Reactivity of [U(COT$^{(SiiPr3)2}$)(Cp^{AsMe4})] with carbon dioxide

The reaction of [U(COT$^{(SiiPr3)2}$)(Cp^{AsMe4})] (**2.7**) with carbon dioxide formed a fluxional species, which was observed to have one set of *iso*-propyl environments at ambient temperature and two sets of resonances at -30 °C. However the only ^{13}C-enriched carbon environment observed was assigned to ^{13}CO at 184.5 ppm. Attempts to

characterise this complex were precluded by its instability, and reactivity of **2.7** with CO_2 was therefore not pursued.

4.3.6 Removal of the phosphacarbonate moiety

In an attempt to cleave the phosphacarbonate fragment from **4.11**, reactions with TMSX (X = Cl, I or OTf) were conducted. The purpose of this was twofold: replacing the carboxyl fragment with a halide would allow subsequent ligand metathesis reactions, thereby allowing the synthesis of other complexes with the $[\{(COT^{(SiiPr3)2})U\}_2(\mu\text{-}O)]$ backbone. It was also anticipated that this method would allow elucidation of the structure of **4.10** by identification of the organic and organometallic species from these reactions. In order to achieve the latter goal, reactions of **4.10** and $[\{U(COT^{(SiiPr3)2})\}_2(\mu\text{-}O)\{\mu\text{-}\eta^1\text{:}\eta^1\text{-}O_2C(PC_4Me_4)\}_2]$ (**4.11**) with TMSX reagents were explored so that comparisons could be made. Initial studies found that these complexes were unreactive towards TMSX, however the reactions proceeded when heated to 70 °C.

Thermolysis of **4.11** with two equivalents TMSOTf yielded $[\{U(COT^{(SiiPr3)2})\}_2(\mu\text{-}O)(\mu\text{:}\eta^1\text{:}\eta^1\text{-}O_3SCF_3)_2]$ (**4.3**) by cleavage of the phosphacarbonate unit from the uranium complex, and coordination of the triflate anion. However, whilst reaction of **4.10** with TMSOTf yielded the same paramagnetic fragment, identification of the organic compounds from the two reactions was precluded by the complicated mixture of species observed by GC-MS and NMR.

The $^{31}P\{^1H\}$ NMR spectra of both reaction mixtures contained several resonances, but three major species were identified from the reaction of **4.11**. The first of these was [1,1'-bis(2,3,4,5-tetramethylphosphole)] (**4.13**), which was identified by its characteristic $^{31}P\{^1H\}$ NMR resonance at -8.3 ppm. The second species, **4.14**, had ^{13}C-enriched carbon incorporation, which coupled to a phosphorus resonance at 16.7 ppm

(19.3 Hz). This species was anticipated to be the silylated phosphcarbonate moiety, however it was not observed in all the reaction mixtures.

Full characterisation of the silylated phosphacarbonate was achieved by independent synthesis according to **Figure 4.32**. However, **4.14** was found to be unstable over several days under 1 bar inert atmosphere, and extruded CO_2 to yield the silylated phosphole (**4.15**, **Figure 4.33**). **4.15** was found to be the dominant phosphorus-incorporated species present in all solutions and its formation from **4.14** justifies the absence of this species from the crude reaction mixtures.

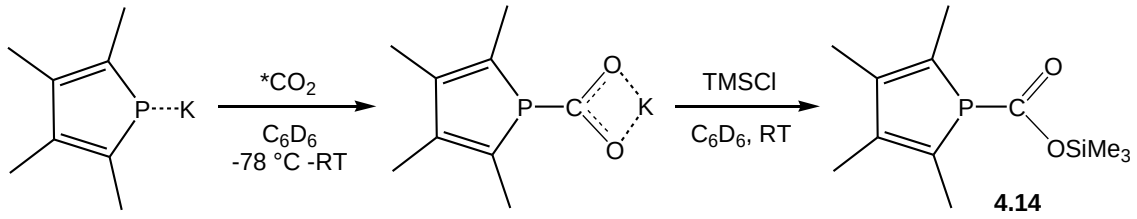

Figure 4.32 Synthesis of the silylated phosphacarbonate (**4.14**) from K[Cp^{PMe4}]

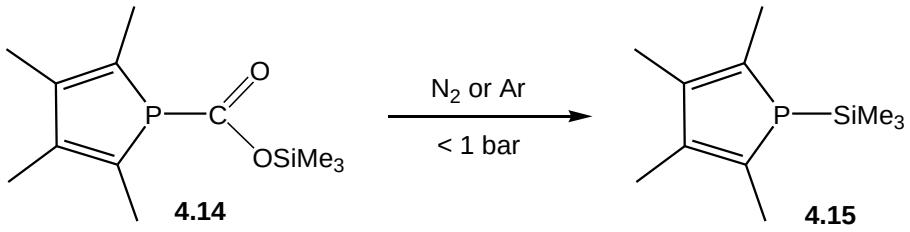

Figure 4.33 Extrusion of CO_2 from the silylated phosphacarbonate to yield the silyl phosphole (**4.15**).

Owing to the reactivity observed using TMSOTf, it was anticipated that analogous reactivity would occur with a trimethylsilyl halide. Repetition of the reaction using excess TMSCl or TMSI yielded **4.13**, **4.14** and **4.15** by $^{31}P\{^{1}H\}$ NMR, in addition to a

paramagnetic species, which was identified as $[\{(COT^{(SiiPr3)2})U(OSiMe_3)\}_2(\mu\text{-}X)_2]$ (X = Cl (**4.16**) or I (**4.17**), **Figure 4.34**).

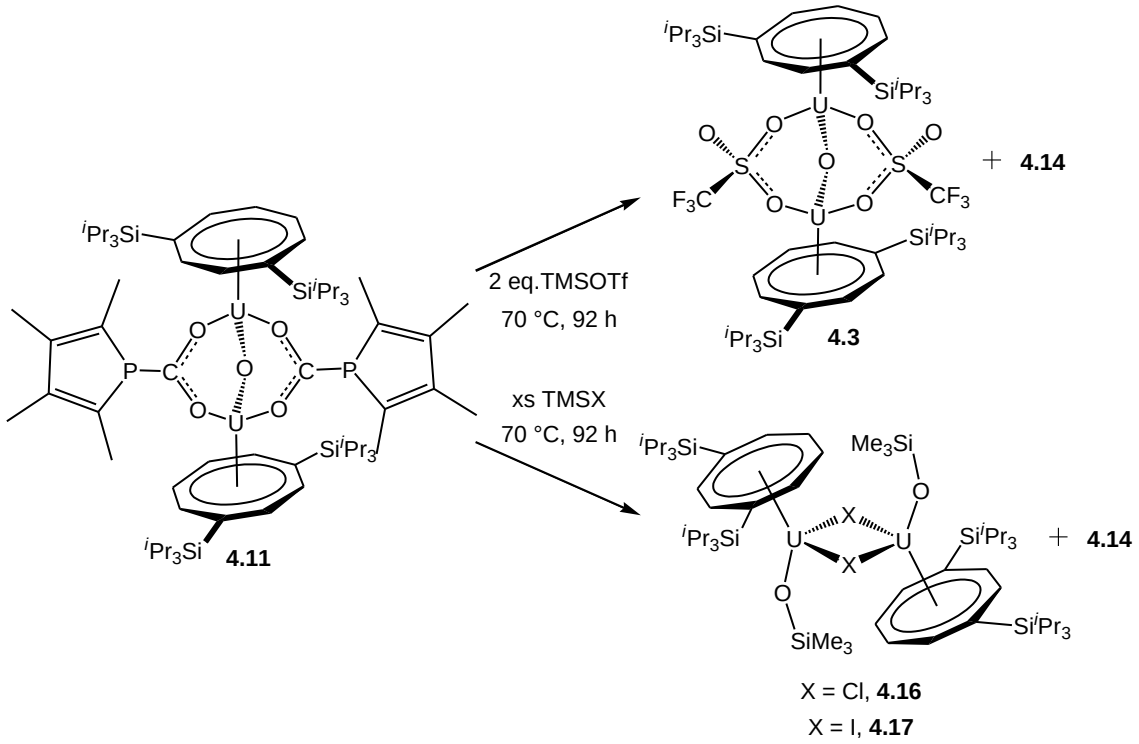

Figure 4.34 Extraction of **4.14** from **4.11** using TMSOTf or TMSX (X = Cl or I).

The silylation of the bridging oxo fragment and the addition of a second siloxy fragment to give symmetrical dimeric complexes was an unexpected result. However the formation of multiple products, observed by GC-MS and $^{31}P\{^1H\}$ NMR, illustrates that the reactions of **4.11** with TMSX are non-trivial and further studies were therefore not pursued.

4.3.6.1 Characterisation of **4.16** and **4.17**

The NMR spectra of **4.16** and **4.17** were found to exhibit two resonances for each proton and silicon environment, indicating non-trivial behaviour in solution. For the

chloride complex, one resonance was dominant, and the corresponding minor resonance was shifted upfield. The iodide complex however, showed both resonances were of equal intensity. Mass spectrometry characterised the molecular ion for both complexes, illustrating that **4.16** and **4.17** are also dimeric under these conditions, however microanalysis results could only be obtained for [{(COT$^{(SiiPr3)2}$)U(OSiMe$_3$)}$_2$(μ-Cl)$_2$] due to the low yields of the iodide complex.

Single crystal XRD analysis of both complexes showed dimeric structures, which have a centre of inversion (**Figure 4.35**). The U_2X_2 core is planar with parallel COT rings, resembling [{(COT$^{(SiiPr3)2}$)U(DME)$_2$}$_2$(μ-O)$_2$] (**4.12DME**), however the U–Ct distances are shorter in **4.16** and **4.17** due to the decreased sterics around the metal centres. Contrastingly the U–U distance is almost 1 Å longer in **4.16** than **4.12DME** due to the larger covalent radius of chlorine (0.99 Å) than oxygen (0.66 Å).[56]

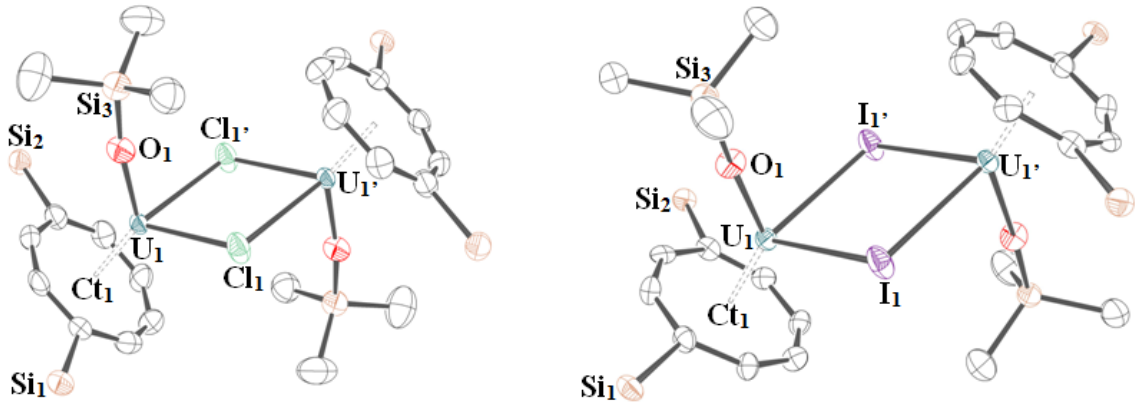

Figure 4.35 ORTEP views of **4.16** (left) and **4.17** (right) with thermal ellipsoids at 50% probability; hydrogen atoms and COT *iso*-propyl groups have been omitted for clarity.

Comparison of **4.16** and **4.17** with similar published bridging halide complexes reveal typical uranium–chloride and uranium–iodide bond lengths (**Figure 4.36**) and angles

(U–I–U 99.23(1) – 103.551(13)° and I–U–I 76.449(13) – 79.58(9)°; U–Cl–U 83.28(10) – 111.91(8)° and Cl–U–Cl 66.71(12) – 86.60(4)°) within the planar core.[49,57–61]

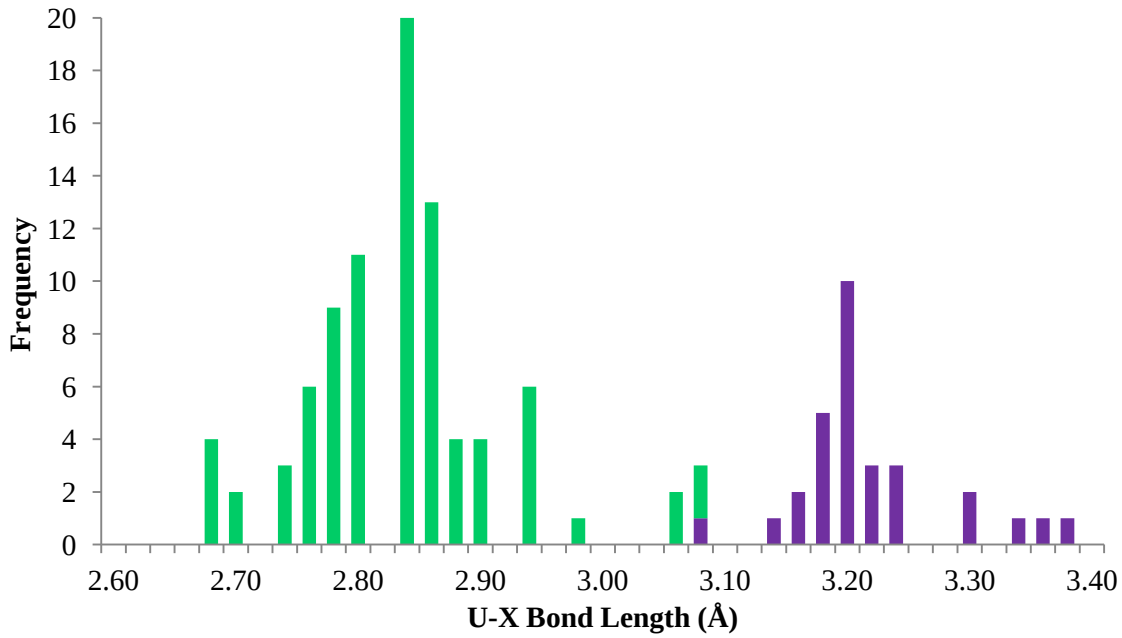

Figure 4.36 Published U–Cl bond lengths (green) and U–I bond lengths (purple) for complexes with bridging halide ligands.[33,34]

The uranium-siloxide fragment, which is perpendicular to the U_2X_2 plane, has an almost linear U–O–Si bond angle. Comparison of this fragment with published complexes featuring similar fragments reveals the angle varies extensively from 153.5(5) to 179.25(15)°.[50,62–69] This may be attributed to the steric environment around this complex which demands a more linear angle than would otherwise be expected. In the case of complex **4.16**, the 171(2)° angle enables the siloxide group to be positioned exactly between the *iso*-propyl groups on the nearest COT ring and the ring atoms on the furthest COT ring, so that there is a minimum separation distance between this fragment and the nearest carbon atoms of 3.5 Å.

Comparison of the U–O distances in these complexes also reveals shorter than expected bond lengths reminiscent of uranium(V) siloxide species.[50,62–66] These range from 1.975(7) to 2.034(9) Å, whereas uranium(IV) siloxide complexes exhibit U–O bond lengths in the range of 2.065(6) – 2.173(9) Å.[64–69]

Distances (Å)					
U_1–Ct_1	1.9(6) *1.9113(4)*	**U_1–X_1**	2.8(11) *3.1782(8)*	**U_1–X_1'**	2.8(8) *3.1788(8)*
U_1–O_1	2.1(5) *2.034(6)*	**O_1–Si_3**	1.7(4) *1.674(7)*	**U_1–U_2**	4.4(11) *4.8796(8)*
Angles (°)					
U_1–X_1–U_1'	105(10) *100.28(2)*	**X_1–U_1–X_1'**	75(10) *79.72(2)*	**U_1–O_1–Si_3**	171(2) *176.3(4)*
U_1'–U_1–O_1	87.33(26) *86.6(2)*	**Ct_1–U_1–O_1**	133(9) *133.7(2)*	**Ct_1–U_1–U_1'–Ct_1'**	180.00(34) *180.0(3)*

Table 4.8 Bond lengths, distances and angles for **4.16** and **4.17** (*italicised*). Ct_1 and $Ct_{1'}$ are the centroids for the $COT^{(SiiPr3)2}$ ligands.

4.4 Alternative heteroallenes

4.4.1 Introduction

Despite the prominent reactivity of organouranium complexes with carbon dioxide in the literature, few studies have employed analogous heteroallenes to observe how the

reactivity changes with alteration of one or more functional groups. Some research groups have carried out comparative reactivity studies with carbonyl sulfide and carbon disulfide in order to observe the effect of an isoelectronic, but softer analogue. In some cases these reagents give rise to analogous reactivity, which has been primarily observed for insertion of CO_2, COS or CS_2 into uranium–carbon bonds.[70,71] However some of these complexes exhibit different bonding modes whereby the carboxylate fragment is delocalised but the dithiocarboxylate fragment has defined uranium–sulfur single and dative bonds.[72] Alternatively, the number of insertions that occur can vary, as exemplified by a 'double tuck-in' complex, whereby double insertion of CO_2 takes place in comparison to single insertion of CS_2 (**Figure 4.37**).[73,74]

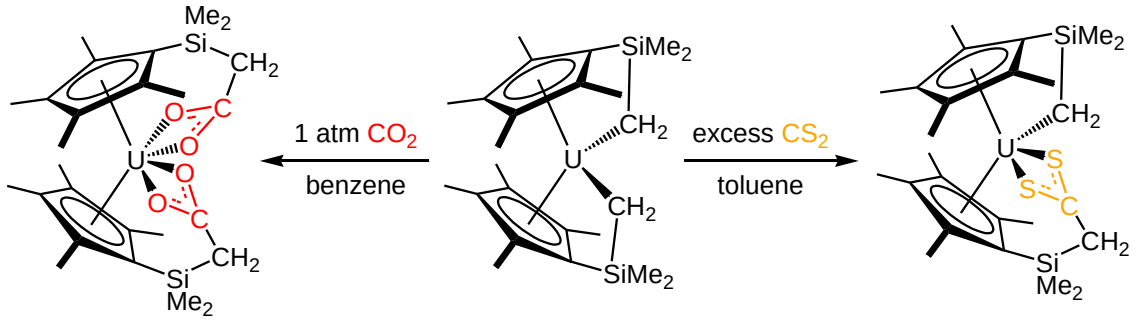

Figure 4.37 Comparative reactivity of carbon dioxide and carbon disulfide with a 'double tuck-in' complex.[73,74]

In other instances, carbonyl sulfide and carbon disulfide have given rise to products that are not analogous to their carbon dioxide derivatives. Mazzanti and co-workers found that reaction of a trivalent uranium siloxide complex with carbon dioxide yielded a bimetallic carbonate complex, whilst reaction with carbon disulfide yielded a dimeric complex with a U-CS_2-U core.[75] This type of reactivity has also been observed by Cloke *et al.* for titanium bis(pentalene) complexes and Andersen and co-workers for tris(cyclopentadienyl)uranium species.[76–78]

Carbonyl sulfide and carbon disulfide reactions have also provided insight into the mechanism by which carbon dioxide reactions occur. Studies by Maron and co-workers have found the sulfur-based complexes are often analogous to suggested intermediates in the formation of the carbon dioxide derived species.[79] Calculations of the Gibbs free energy for these species have shown that the thio analogue is more thermodynamically stable than its oxo counterpart and/or that the activation barrier to the next transition state is too large to overcome, thereby giving rise to different reaction products.

These examples demonstrate that whilst isoelectronic reagents often follow a similar reaction pathway, the reaction products observed can vary from their carbon dioxide analogues giving rise to a wealth of unexpected products, or previously unobtainable intermediates. In order to gain further insight into the transformations that give rise to **4.7** – **4.11**, reactions of [U(COT$^{(Si\textit{i}Pr3)2}$)(Cp^{PMe4})(THF)] with COS and CS_2 were conducted.

4.4.2 Reactivity of [U(COT$^{(SiiPr3)2}$)(Cp^{PMe4})(THF)] with carbonyl sulfide

Condensation of one mole equivalent COS to a degassed solution of [U(COT$^{(Si\textit{i}Pr3)2}$)(Cp^{PMe4})(THF)] (**2.6THF**) resulted in the instantaneous formation of one paramagnetic species (**4.18**, **Figure 4.38**), which was identified crystallographically as [{U(COT$^{(Si\textit{i}Pr3)2}$)(Cp^{PMe4})}$_2$(μ-S)]. Attempts to form the carbonyl sulphide analogue of **4.8** and **4.11** by addition of excess COS to **2.6THF** were unsuccessful and no further reactivity was observed.

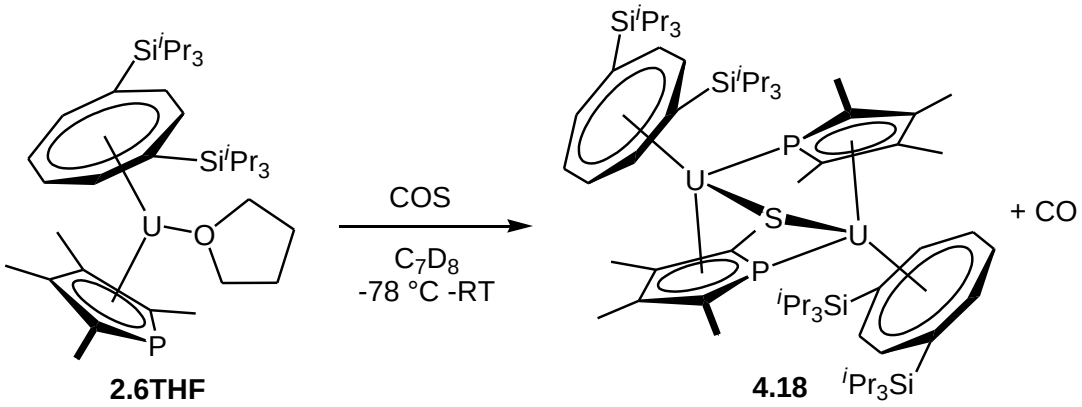

Figure 4.38 Synthesis of [{U(COT$^{(Si\textit{i}Pr3)2}$)(Cp^{PMe4})}$_2$(μ-S)] (**4.18**) using COS.

Due to the limited availability of COS, alternative synthetic routes to **4.18** were explored (**Figure 4.39**). Addition of triphenylphosphine sulfide to **2.6THF** resulted in instantaneous formation of **4.18**. However sublimation of triphenylphosphine away from the crude complex required prolonged heating of the residue to 80 °C on a turbo assisted vacuum line. Whilst this did not degrade the sulfide complex, the procedure needed repeating to ensure all traces of the phosphine were removed.

To avoid this process, triethylphosphine sulfide was used as an alternative source of sulfide dianions. Addition of this reagent to a solution of [U(COT$^{(Si\textit{i}Pr3)2}$)(Cp^{PMe4})(THF)] at room temperature resulted in the formation of **4.18** over four days. This method required less manipulation of the crude solution, as triethylphosphine could be sublimed away from the complex within two hours at ambient temperature.

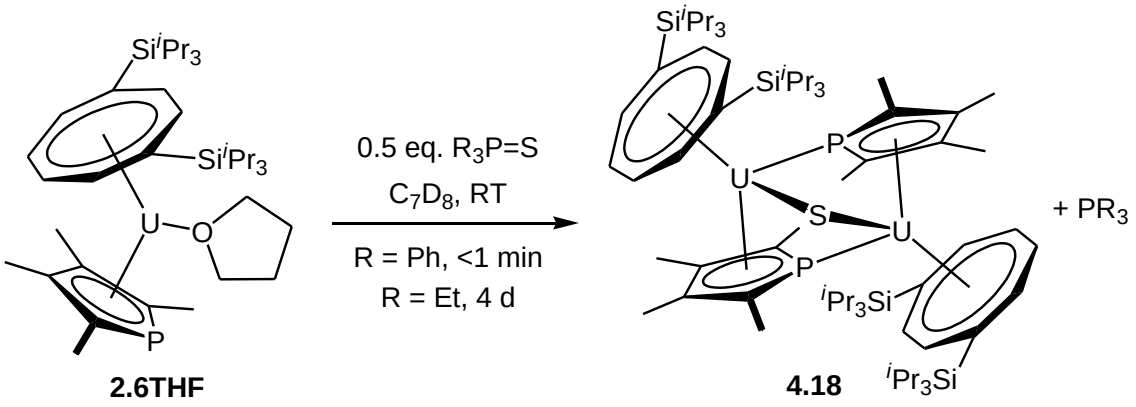

Figure 4.39 Alternative syntheses of [{U(COT$^{(Si\textit{i}Pr3)2}$)(Cp^{PMe4})}$_2$(μ-S)].

4.4.2.1 Characterisation of [{U(COT$^{(Si\textit{i}Pr3)2}$)(Cp^{PMe4})}$_2$(μ-S)]

NMR studies of **4.18** showed one set of resonances for each environment illustrating that the complex is dynamic in solution and microanalysis agreed with the proposed formulation. **4.18** could not be characterised by mass spectrometry however due to the thermal lability of the complex under electron impact and electrospray ionisation conditions.

XRD analysis of **4.18** illustrates that despite the similarity between this complex and [{(COT$^{(Si\textit{i}Pr3)2}$)(η^1-Cp^{NMe4})U}(μ-O)(μ-η^1:η^5-Cp^{NMe4}){U(COT$^{(Si\textit{i}Pr3)2}$)}] (**4.9**) there are several differences in the solid-state molecular structures. **4.18** features a more obtuse COT–U–U–COT torsion angle than **4.9** and both phospholyl units adopt bridging η^1:η^5-coordination to the two metal centres (**Figure 4.40**). These rings bond so that the phosphorus atoms lie almost exactly between the two metals, which is analogous to the bridging pyrrolyl unit in **4.9** and several dimeric phospholyl complexes in the literature.[80,81] The mixed-sandwich fragment has longer U–COT bonds than **4.9** and a more obtuse COT–U–Cp angle, which is rationalised by the increased length of U–P and U–S bonds relative to U–N and U–O bonds.

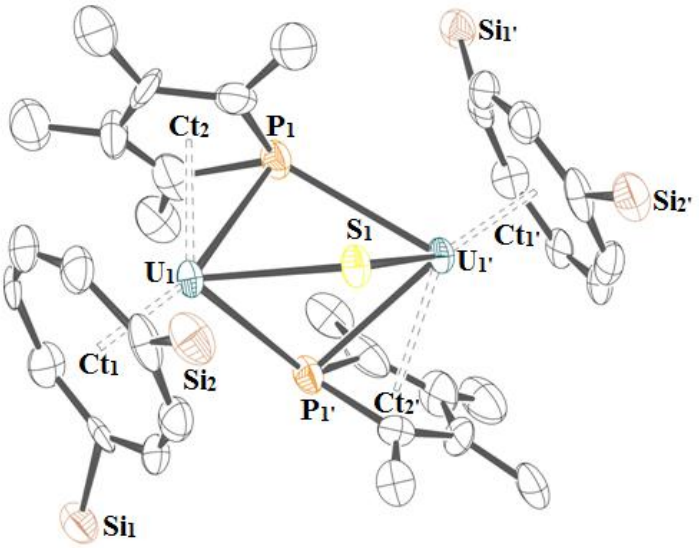

Figure 4.40 ORTEP view of **4.18** with thermal ellipsoids at 50% probability; hydrogen atoms and COT *iso*-propyl groups have been omitted for clarity.

Distances (Å)					
Ct_1–U_1	2.0001(4)	**Ct_2–U_1**	2.6199(4)	**U_1–S_1**	2.653(3)
U_1–P_1	2.904(3)	**U_1'–P_1**	3.071(4)	**U_1–U_1'**	4.16699(14)
Angles (°)					
Ct_1–U_1–Ct_2	131.92(2)	**Ct_1–U_1–P_1**	160.74(18)	**Ct_1–U_1–P_1'**	114.55(17)
U_1–P_1–U_1'	88.40(10)	**Ct_2–U_1–P_1'**	99.74(17)	**U_1–S_1–U_2**	103.50(18)
Ct_1–U_1–U_1'–Ct_1'	139.892(2)			**Ct_2–U_1–U_1'–Ct_2'**	125.056(3)

Table 4.9 Bond lengths, distances and angles for **4.18**. Ct_1 and $Ct_{1'}$ are the centroids for the $COT^{(SiiPr3)2}$ ligands and Ct_2 and $Ct_{2'}$ are the centroids for the phospholyl ligands.

Comparison of the mixed-sandwich fragment in **4.18** with the uranium(III) starting complex also shows lengthening of the U–COT and U–Cp distances by 0.026 and 0.033 Å respectively, illustrating that the molecular structure of **4.18** prohibits shortening of these bonds upon oxidation. The U–P bond however is *ca* 0.1 Å shorter in this complex than its precursor as η^1-coordination to the second uranium centre ($U_{1'}$) requires the phospholyl ring to slip so that the phosphorus atom lies closer to U_1.

The U–S–U fragment is typical of other uranium sulfide complexes in the literature, which exhibit U–S bonds in the range of 2.588(1) to 2.8124(9) Å.[51,82–84] The U–S–U angles reported in the literature however fall within two ranges: 92.17(7) – 99.63(7)° and 165.2(2) – 180.0°. This appears to be dependent on the U–S bond length and can be rationalised by partial uranium-sulfur double bond character giving rise to a near linear U–S–U angle.

4.4.3 Reactivity of [{U(COT$^{(SiiPr3)2}$)(Cp^{PMe4})}$_2$(μ-S)] with carbon dioxide

Due to the aforementioned insertion reactivity of carbon dioxide into uranium–nitrogen and uranium–phosphorus bonds, reactivity of **4.18** with CO_2 was attempted. Reaction of **4.18** with excess CO_2 yielded two major paramagnetic species. The predominant species was identified as the thiocarbonate complex [{U(COT$^{(SiiPr3)2}$)(Cp^{PMe4})}$_2$(μ-CO_2S)] (**4.19**, **Figure 4.41**), formed by insertion of one molecule of CO_2 into the uranium–sulfur bonds. The second complex (**4.20**) features a phosphacarbonate fragment in addition to the thiocarbonate unit, giving rise to an asymmetrical complex (**Figure 4.42**).

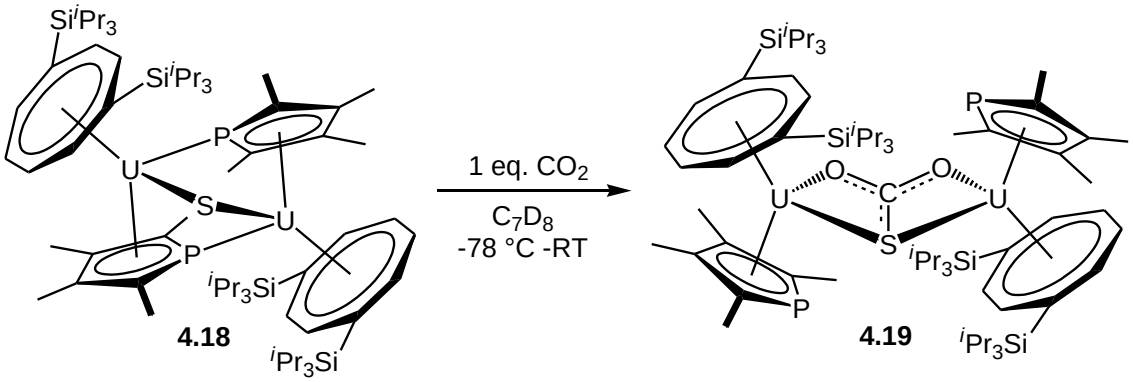

Figure 4.41 Reactivity of **4.18** with carbon dioxide to form **4.19**.

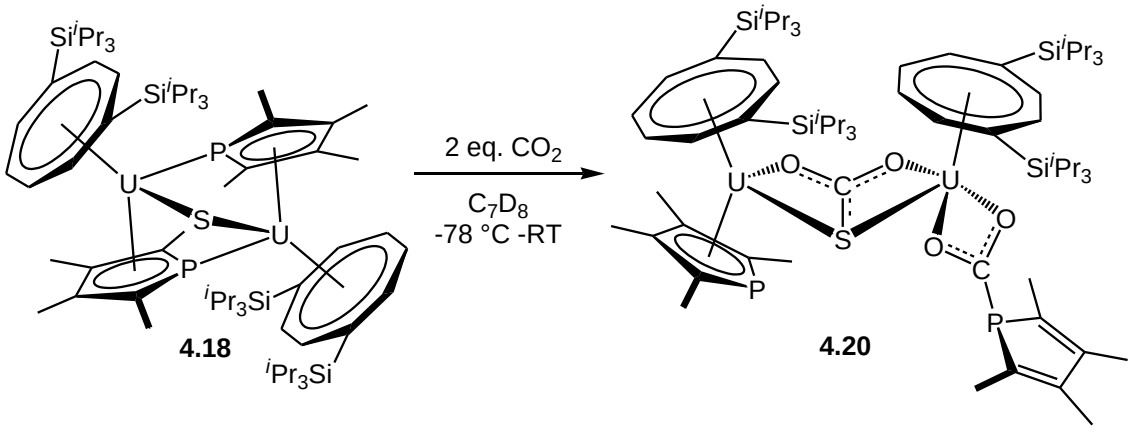

Figure 4.42 Reactivity of **4.18** with carbon dioxide to form **4.20**.

Addition of excess carbon dioxide to a mixture of **4.19** and **4.20** did not yield a triple insertion species, but lead to decomposition of both complexes. It is hypothesised that such a species may not have sufficient steric saturation to allow kinetic stabilisation, as the space-filling model of **4.20** reveals the core thiocarbonate unit to be visible (**Figure 4.43**). It is anticipated that insertion of another CO_2 molecule would open the cavities around the core further, and therefore give rise to the decomposition observed.

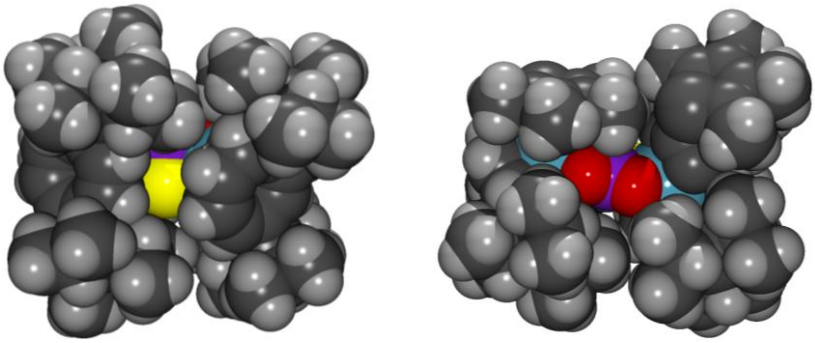

Figure 4.43 Space-filling views of **4.20** from 'above' the COT ligands (left) and 'behind' the thiocarbonate fragment (right). All non-core atoms are illustrated in grey (hydrogen atoms in pale grey) and U-CO_2S-U core atoms are shown in colour.

4.4.3.1 Characterisation of **4.19**

The NMR spectra of [{U($COT^{(SiiPr3)2}$)(Cp^{PMe4})}$_2$(μ-CO_2S)] exhibit one silicon and one phosphorus resonance (-98.8 and 602.2 ppm respectively) consistent with a structure that is dynamic in solution. Assignment of the thiocarbonate carbon resonance however was precluded by the presence of multiple resonances in the crude spectra and the low yield of analytically pure material. XRD studies illustrated the connectivity of the complex but disorder in the phospholyl and thiocarbonate units gave rise to an unrefined structure (**Figure 4.44**).

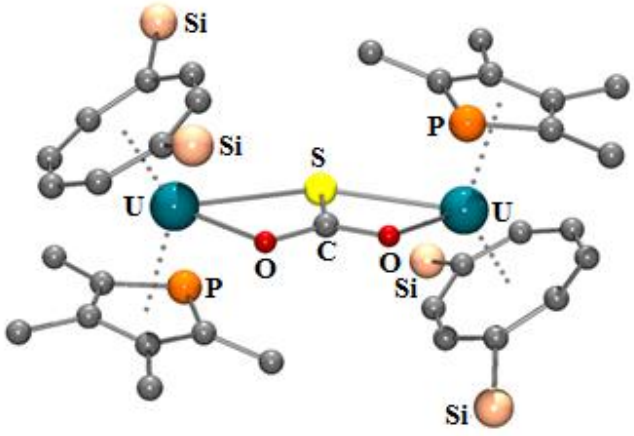

Figure 4.44 POV-Ray depiction of **4.19**, illustrating connectivity.

4.4.3.2 Characterisation of **4.20**

The NMR spectra of **4.20** illustrate two phosphorus environments corresponding to the phospholyl ring (716.6 ppm) and the phosphacarbonate fragment (54.7 ppm), and two silicon environments corresponding to each $COT^{(SiiPr3)2}$ ligand. The ^{13}C-enriched carbon resonances for this complex however could not be assigned due to low yields of analytically pure solids. This also precluded microanalysis and mass spectrometry only detected fragments of the complex due to its thermal lability. Single crystals of **4.20** were obtained from saturated pentane solutions (**Figure 4.45**) and data are presented in **Table 4.10** and with **Figure 4.46**.

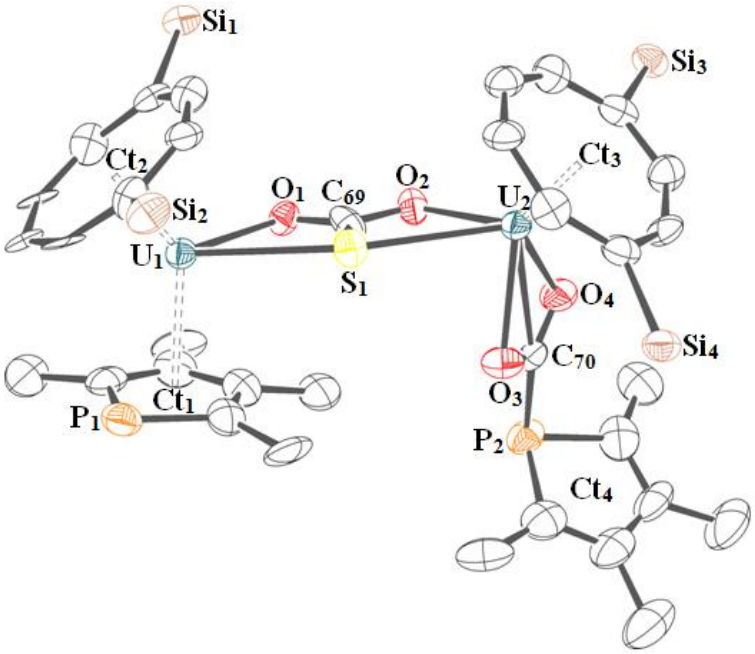

Figure 4.45 ORTEP view of **4.20** with thermal ellipsoids at 50% probability; hydrogen atoms and COT *iso*-propyl groups have been omitted for clarity.

The mixed-sandwich fragment shows contraction in the U–Ct distances in comparison to **4.18** and $[U(COT^{(SiiPr3)2})(Cp^{PMe4})(THF)]$ (**2.6THF**), indicating that expansion of the

bridge lessens the sterics around the uranium(IV) centre, allowing closer contact with the ancillary ligands. This is also proposed to be the reason for the near linear torsion angles of the ligands either side of the bridge, which contrasts to the perpendicular torsion angles observed in **4.18**. Another feature of **4.20** is the lengthening of the U_1–P_1 bond in comparison to **4.18** illustrating that the ring has slipped to increase the U–P distance. Despite this, the U–P bond is still shorter in **4.20** than in **2.6THF**.

Distances (Å)					
U_1–Ct_1	2.5299(5)	**U_1–Ct_2**	1.9519(5)	**U_2–Ct_3**	1.9031(4)
U_1–P_1	2.951(4)	**U_1–C_{69}**	3.017(14)	**U_1–C_{69}**	3.003(15)
Angles (°)					
Ct_1–U_1–Ct_2	139.06(2)	**U_1–S_1–U_2**	151.70(12)	**U_1–C_{69}–U_2**	139.3(5)
Ct_3–U_2–O_3	135.8(3)	**Ct_3–U_2–O_4**	123.5(3)	**Ct_3–U_2–C_{70}**	136.380(6)
U_2–C_{70}–P_2	170.4(7)	**Ct_4–P_2–C_{50}**	109.603(8)		
Ct_1–U_1–U_2–Ct_3	149.449(5)			**Ct_2–U_1–U_2–C_{70}**	171.9661(13)

Table 4.10 Bond lengths, distances and angles for **4.20**. Ct_2 and Ct_3 are the centroids for the $COT^{(SiiPr3)2}$ ligands and Ct_1 and Ct_4 are the centroids for the phospholyl ligands.

Only one other bimetallic uranium thiocarbonate complex has been published, and was synthesised by successive reaction of a uranium(III) tacn complex with elemental sulfur/triphenylphosphine sulfide and carbon dioxide.[51,85] This complex features μ-κ^1(O):κ^2(O,S)-coordination of the planar thiocarbonate unit, as demonstrated by varied U–S distances (2.8919(13) and 4.6512(13) Å) and slight variation in the U–O

distances (2.225(3) and 2.422(3) Å). One of the U–O–C angles is also more linear (173.9(3)°) due to κ^1-coordination of this oxygen atom to uranium. All other metrics within the thiocarbonate unit are the same as those in complex **4.20** illustrating that the varied coordination mode has no effect on the bonding within this fragment.

The phosphacarbonate fragment in **4.20** is similar to the analogous fragments in **4.11** and the carbamate fragments in **4.8**, with the exception of the O–C–O bond angle, which is 4° more acute due to η^2-coordination to one metal centre. Comparison of this unit to other U–O_2CR moieties in the literature illustrates average bond lengths and angles, and that the slight asymmetry observed is also typical of these complexes (**Figure 4.46**).[33,34]

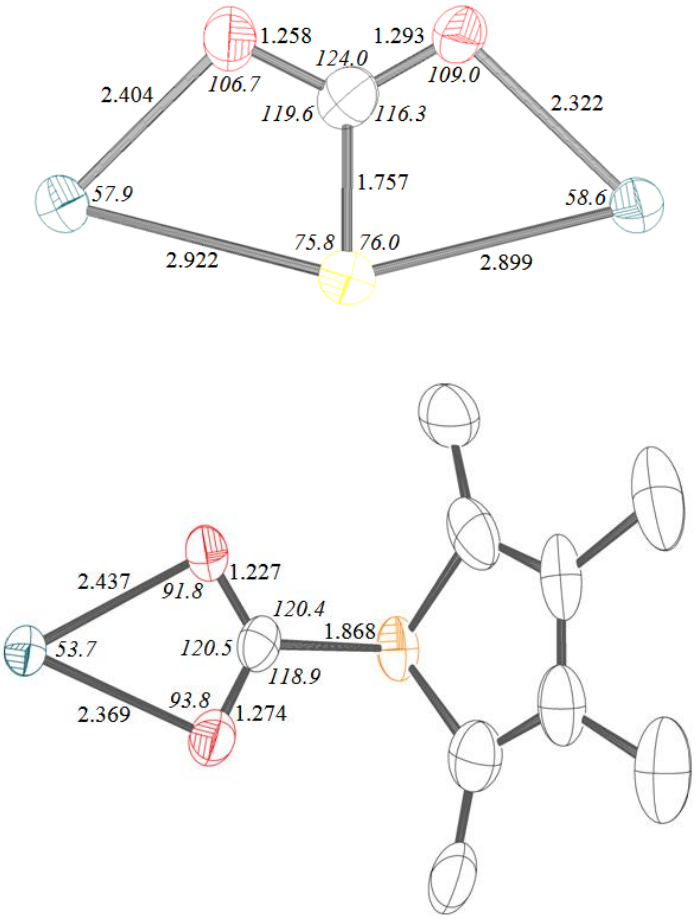

Figure 4.46 ORTEP views of the thiocarbonate fragment (above) and the phosphacarbonate fragment (below) of **4.20** with bond lengths and angles (*italicised*).

4.4.4 Carbon disulfide reactivity

4.4.4.1 Reactivity of [U($COT^{(SiiPr3)2}$)(Cp^{PMe4})] with CS_2

Addition of excess carbon disulfide to [U($COT^{(SiiPr3)2}$)(Cp^{PMe4})] (**2.6**) resulted in the formation of a brown/black viscous solution. However, no identifiable products were observed with the exception of $COT^{(SiiPr3)2}$ and [1,1'-bis(2,3,4,5-tetramethylphosphole)] (**4.13**). The formation of a dithiophosphacarbonate complex analogous to **4.11** is believed not to occur as this would require the formation of C≡S, which is thermodynamically unfavourable. Further reactions using a stoichiometric amount of carbon disulfide were therefore not attempted.

4.4.4.2 Reactivity of **4.12** and **4.13** with CS_2

Despite the decomposition observed in the reaction of **2.6** with carbon disulfide, it was postulated that reaction of [{($COT^{(SiiPr3)2}$)U}$_2$(μ-O)$_2$] (**4.12**) and [1,1'-bis(2,3,4,5-tetramethylphosphole)] (**4.13**) with CS_2 would not present the same problem if insertion was the only type of reactivity taking place. Addition of excess carbon disulfide to a degassed solution of **4.12** and **4.13** gave rise to the formation of one paramagnetic species within minutes, evidenced by one set of proton environments, one broad phosphorus resonance at 147.2 ppm ($w_{½}$ = 813 Hz), and one silicon resonance at -103.4 ppm. However, attempts to fully characterise this complex were precluded as this species was observed to decompose over several weeks at -35 °C. Similar attempts to synthesise a dithiophosphacarbonate complex from **4.18** and CS_2 were unsuccessful.

4.5 Summary

The heterocyclic mixed-sandwich complexes, [U(COT$^{(Si\textit{i}Pr3)2}$)(Cp^{EMe4})], have illustrated a wealth of new reactivity and the synthesis of some novel fragments. Carbon monoxide reactivity has illustrated that under optimum conditions the C≡O bond can be cleaved at ambient temperature, and offers a synthetic route to the synthesis of substituted bis(arsenine) species.

Carbon dioxide has illustrated a combination of reductive and insertive reactivity in the formation of phosphacarbonate and carbamate complexes *via* two isolable intermediates. The identity of the second intermediate in both instances is unclear and precludes the formulation of a mechanism. Reactivity studies of carbonyl sulfide and carbon disulfide in an attempt to probe this mechanism resulted in the formation of thiocarbonate complexes and illustrates that these reagents cannot be used interchangeably.

4.6 Experimental details for Chapter 4

*4.6.1 Synthesis of [U(COT$^{(SiiPr3)S2}$)(Cp^{PMe4})(2-O-PC$_5$Me$_4$)] (**4.1**)*

A solution of [U(COT$^{(Si\textit{i}Pr3)2}$)(Cp^{PMe4})] (127.0 mg, 1.60 x 10^{-4} mol) in equal parts THF/toluene (4 mL) was cooled to -78 °C and freeze-thaw degassed. Excess (>3 mole equivalents) carbon monoxide was added *via* Toepler line. The mixture was slowly warmed to room temperature, and a colour change from dark purple to red/orange was observed after several hours. The mixture was stirred at ambient temperature for five days then dried *in vacuo*. The residue was dissolved in pentane and filtered to yield a red solution, from which crystals were obtained at -35 °C.

Yield: 35.7 mg (3.71 x 10^{-5} mol), 46.4% based on [U(COT$^{(Si\textit{i}Pr3)2}$)(Cp^{PMe4})].

MS (EI): *m/z* = 157 (100%, Si^{i}Pr$_3$), 962 (<1%, **^{13}C-4.1** M$^+$).

IR (NaCl): **^{13}C-4.1** 2943, 2890, 2864, 2722, 2083, 1940, 1891, 1496, 1365, 1292, 1220, 1194 cm^{-1}.

IR (methylcyclohexane, -20 °C): **4.1** 2178, 2015; **^{13}C-4.1** 2093, 1948 cm^{-1}.

^{1}H NMR (d_8-toluene, 303 K): δ 102.8 (s, br, 2H, COT-C*H*), 43.4 (s, br, 3H, phosphinine-CH_3), 15.6 (s, br, 3H, phosphinine-CH_3), 15.0 (s, br, 3H, phosphinine-CH_3), 9.3 (d, $^3J_{HP}$ = 15 Hz, 3H, phosphinine C$_5$-CH_3), 7.2 (s, br, 6H, Cp-CH_3/^{i}Pr-C*H*), -9.3 (s, br, 18H, ^{i}Pr-CH_3), -12.0 (s, br, 6H, Cp-CH_3/^{i}Pr-C*H*), -12.6 (s, br, 18H, ^{i}Pr-CH_3), -15.7 (s, br, 6H, Cp-CH_3/^{i}Pr-C*H*), -35.1 (s, br, 2H, COT-C*H*), -89.9 (s, br, 2H, COT-C*H*).

^{13}C{^{1}H} NMR (d_8-toluene, 303 K): δ 423.1 (d, $^1J_{CP}$ = 33 Hz, **^{13}C**-phosphine-C$_1$).

^{28}Si{^{1}H} NMR (d_8-toluene, 303 K): δ -132.8 (*Si*^{i}Pr$_3$).

^{31}P{^{1}H} NMR (d_8-toluene, 303 K): δ 201.4 (s, Cp *P*-ring), 191.4 (d, $^1J_{CP}$ = 33 Hz, phosphinine *P*-ring).

*4.6.2 Synthesis of [1,2-bis(1,2,3,4-tetramethylphospholyl)acetylene] (**4.2**)*

To a degassed solution of [U(COT$^{(SiiPr3)2}$)(Cp^{PMe4})] (18.0 mg, 2.26 x 10^{-5} mol) in d_8-toluene at -78 °C was added 3.2 equivalents ^{13}CO (7.35 x 10^{-5} mol). Warming of the mixture resulted in a colour change from brown to red/brown. The mixture was filtered and the residue dried *in vacuo*. Crystals of **4.2** were obtained at -35 °C from a saturated pentane solution as off-white prisms. Duplicate elemental analyses and high yields indicated that pentane molecules remained in rigorously dried samples, even though pentane was not present in the unit cell.

Yield: 3.8 mg (1.2 x 10^{-5} mol), 100% based on [U(COT$^{(SiiPr3)2}$)(Cp^{PMe4})] for $C_{16}{}^{13}C_2H_{24}P_2\cdot(C_5H_{12})_{0.4}$.

Anal. calc (found) for $C_{16}{}^{13}C_2H_{24}P_2$: C 71.69 (72.49), H 7.95 (8.04)%.

Anal. calc (found) for $C_{16}{}^{13}C_2H_{24}P_2\cdot(C_5H_{12})_{0.2}$: C 72.22 (72.49), H 8.35 (8.04)%.

MS (EI): *m/z* = 304 (100%, M^+).

IR (NaCl): 2966, 2909, 2852, 2723, 2343, 2092, 1606, 1542, 1435, 1371, 1310, 1261, 1215 cm^{-1}.

^{1}H NMR (d_6-benzene, 303 K): δ 2.0 (d, $^3J_{PH}$ = 10.9 Hz, 12H, C_1-C*H*$_3$, C_4-C*H*$_3$), 1.5 (s, 12H, C_2-C*H*$_3$, C_3-C*H*$_3$).

^{13}C{^{1}H} NMR (d_6-benzene, 303 K): δ 143.8 (m, *C*$_2$, *C*$_3$), 131.2 (d, $^1J_{CP}$ = 6.9 Hz, *C*$_1$, *C*$_4$), 103.1 (dd, $^1J_{CP}$ = 16.7 Hz, $^2J_{CP}$ = 15.4 Hz, acetylenic-***^{13}C***), 13.8 (m, C_2-*C*H$_3$, C_3-*C*H$_3$), 12.8 (d, $^2J_{CP}$ = 22.6 Hz, C_1-*C*H$_3$, C_4-*C*H$_3$).

^{31}P{^{1}H} NMR (d_6-benzene, 303 K): δ -19.4 (dd, $^1J_{CP}$ = 16.7 Hz, $^2J_{CP}$ = 15.3 Hz, *P*-ring).

*4.6.3 Synthesis of [{U(COT$^{(SiiPr3)2}$)}$_2$(μ-O)(μ-η^1: η^1-O$_2$SOCF$_3$)$_2$] (**4.3**)*

Method A:

To a degassed solution of [U(COT$^{(SiiPr3)2}$)(Cp^{PMe4})] (31.4 mg, 3.95 x 10^{-5} mol) in toluene (3 mL) at -78 °C was added *ca.* four mole equivalents carbon monoxide *via* Toepler line. The mixture was stirred for one hour between -50 and -35 °C and a colour change from dark purple to orange/red was observed. The mixture was freeze-thaw degassed and three drops TMSOTf added *via* cannula. The mixture was warmed to ambient temperature and a slight colour change from orange/red to bright red was observed. All volatiles were removed *in vacuo*, the residue dissolved in pentane and filtered.

Method B:

To a degassed solution of [U(COT$^{(SiiPr3)2}$)(Cp^{PMe4})] (98.4 mg, 1.24 x 10^{-5} mol) in toluene (2 mL) at -78 °C was added *ca.* 2 mole equivalents carbon dioxide *via* Toepler line. The mixture was warmed to room temperature and a colour change from purple to red/brown was observed. The mixture was stirred for three days then the mixture was degassed to remove residual carbon dioxide. Four drops TMSOTf was added to the solution and the mixture was heated to 80 °C for three days. The mixture was cooled and all volatiles were removed *in vacuo* to give a bright red residue. This was dissolved in pentane and filtered. Addition of tetramethylsilane to a saturated solution yielded crystals at -35 °C.

Yield: 6.6 mg (4.1 x 10^{-6} mol), 6.6% based on [U(COT$^{(SiiPr3)2}$)(Cp^{PMe4})].

MS (EI): *m/z* = 157 (100%, Si^{i}Pr$_3$), 1624 (5%, M$^+$).

^{1}H NMR (d_8-toluene, 303 K): 162.2 (br, 1H), 148.4 (br, 1H), 49.1 (br, 3H), 42.6 (br, 1H), 42.1 (br, 4H), 5.2 (br), -9.4 (br, 14H), -9.8 (br, 8H), -19.4 (br, 20H), -24.3 (br, 3H), -25.1 (br, 2H), -95.8 (br, 9H), -142.6 (br, 1H), -143.7 (br, 1H).

^{19}F{^{1}H} NMR (d_8-toluene, 303 K): δ -127.6 (C*F*$_3$).

^{29}Si{^{1}H} NMR (d_8-toluene, 303 K): -143.4 (*Si*^{i}Pr$_3$), -145.9 (*Si*^{i}Pr$_3$).

*4.6.4 Synthesis of [U(COT$^{(SiiPr3)2}$)(Cp^{AsMe4})(2-O-AsC$_5$Me$_4$)] (**4.4**)*

To a degassed solution of [U(COT$^{(SiiPr3)2}$)(Cp^{AsMe4})(THF)] (20.8 mg, 2.28 x 10^{-5} mol) in d_8-toluene at -78 °C was added 0.86 bar ^{13}CO. Warming of the mixture resulted in a colour change from brown to red/brown. After four days all volatiles were removed *in vacuo*. A solution was made up in pentane and filtered to yield a red/brown solution.

Cooling the solution to -35 °C resulted in precipitation of some solids. Filtration of the solution then removal of all volatiles gave rise to crude solids of **4.4**.

Yield of crude solids: 5.1 mg (4.9 x 10^{-6} mol), 43% based on [U(COT$^{(Si\textit{i}Pr3)2}$)(Cp^{AsMe4})(THF)].

MS (EI): *m/z* = 59 (100%), 626 (20%, [UO(COT$^{(Si\textit{i}Pr3)2}$]$^{+}$ – ^{i}Pr).

IR (NaCl): **^{13}C-4.4** 2942, 2890, 2864, 2123, 1921, 1888, 1582, 1385, 1364, 1319, 1255 (br) cm^{-1}.

^{1}H NMR (d_8-toluene, 303 K): δ 104.6 (s, br, 2H, COT-C*H*), 41.6 (s, br, 3H, arsenine-CH_3), 15.5 (s, br, 3H, arsenine-CH_3), 15.0 (s, br, 3H, arsenine-CH_3), 10.3 (s, br, 3H, arsenine-CH_3), 10.1 (s, br, 6H, Cp-CH_3/^{i}Pr-C*H*), -9.2 (d, $^{3}J_{HH}$ = 5.3 Hz, 18H, ^{i}Pr-CH_3), -12.3 (d, $^{3}J_{HH}$ = 5.0 Hz, 18H, ^{i}Pr-CH_3), -14.2 (s, br, 6H, Cp-CH_3/^{i}Pr-C*H*), -15.4 (s, br, 6H, Cp-CH_3/^{i}Pr-C*H*), -32.6 (s, br, 2H, COT-C*H*), -93.1 (s, br, 2H, COT-C*H*).

^{13}C{^{1}H} NMR (d_8-toluene, 303 K): δ 428.0 (s, **^{13}C**-arsenine-C_1).

^{28}Si{^{1}H} NMR (d_8-toluene, 303 K): δ -134.5 (*Si*^{i}Pr$_3$).

*4.6.5 Synthesis of [2,2'-bis(3,4,5,6-tetramethylarsenine)] (**4.5**)*

To a degassed solution of [U(COT$^{(Si\textit{i}Pr3)2}$)(Cp^{AsMe4})] (12.4 mg, 1.36 x 10^{-5} mol) in d_8-toluene at -78 °C was added 0.86 bar ^{13}CO. Warming of the mixture resulted in a colour change from deep pink to red/brown. After several hours all volatiles were removed *in vacuo*, and the residue was filtered in pentane. Addition of THF to the solution yielded crystals of **4.5** as colourless blocks at -35 °C.

NMR Yield: 29% in d_{12}-cyclohexane referenced to C_6H_6 internal standard.

MS (EI): *m/z* = 392 (100%, M^{+}).

^{1}H NMR (d_6-benzene, 303 K): δ 2.5 (s, 6H, CH_3), 2.2 (s, 6H, CH_3), 2.0 (s, 6H, CH_3), 1.7 (s, 6H, CH_3).

^{13}C{^{1}H} NMR (d_6-benzene, 303 K): δ 185.7 (s, **^{13}C**-C_1), 177.4 (s, aromatic-*C*), 142.9 (s, aromatic-*C*), 139.5 (s, aromatic-*C*), 133.4 (d, $^{1}J_{CC}$ = 77 Hz, C_2), 25.0 (s, *C*H$_3$), 20.4 (s, *C*H$_3$), 20.3 (s, *C*H$_3$), 14.6 (s, *C*H$_3$).

*4.6.6 Synthesis of [U(COT$^{(SiiPr3S2}$)(Cp^{PMe4})(CN^{t}Bu)] (**4.6**)*

To a solution of [U(COT$^{(SiiPr3)2}$)(Cp^{PMe4})(THF)] (74.4 mg, 8.59 x 10^{-5} mol) in pentane (3 mL) was added excess CN^{t}Bu *via* syringe (13 μL, 1.15 x 10^{-4} mol). An instant colour change from purple to black/brown was observed with precipitation of dark solids. The mixture was stirred for several hours then filtered *via* cannula to give a pale green/brown solution and dark solids. The solids were dissolved in benzene and filtered to give a dark solution. Slow evaporation of the solvent at ambient temperature yielded crystals of **4.6**.

Yield: 37.4 mg (4.26 x 10^{-5} mol), 49.6% based on [U(COT$^{(SiiPr3)2}$)(Cp^{PMe4})(THF)].

MS (EI): *m/z* = 115 (100%), 875 (2%, M^{+}-H).

IR (NaCl): 2941, 2890, 2862, 2718, 2142 (*ν*CN), 1461, 1382, 1365 cm^{-1}.

^{1}H NMR (d_6-benzene, 303 K): δ -2.2 (s, br, 9H, ^{t}Bu-CH_3), -3.6 (s, br, 24H, ^{i}Pr-CH_3, ^{i}Pr-C*H*), -4.0 (s, br, 18H, ^{i}Pr-CH_3), -12.7 (s, br, 6H, Cp-CH_3), -22.5 (s, br, 2H, COT-C*H*), -30.3 (s, br, 6H, Cp-CH_3), -46.2 (s, br, 2H, COT-C*H*), -54.9 (s, br, 2H, COT-C*H*).

^{29}Si{^{1}H} NMR (d_8-toluene, 303 K): δ -117.7 (*Si*^{i}Pr$_3$).

^{31}P{^{1}H} NMR (d_8-toluene, 303 K): δ 661.2 (br, $w_{½}$ = 466 Hz, *P*-ring).

4.6.7 Reaction of [U(COT$^{(SiiPr3)2}$)(Cp^{NMe4})] with 0.5 equivalents of $^{13}CO_2$

To a degassed solution of [U(COT$^{(SiiPr3)2}$)(Cp^{NMe4})] (37.2 mg, 4.79 x 10^{-5} mol) in d_8-toluene at -78 °C was added 0.5 equivalents $^{13}CO_2$ (2.39 x 10^{-5} mol). Warming of the mixture resulted in a colour change from brown to red/brown.

^{1}H NMR (d_8-toluene, 303 K): *Resonances could not be assigned.*

^{13}C{^{1}H} NMR (d_8-toluene, 303 K): δ -60.7 (s).

^{29}Si{^{1}H} NMR (d_8-toluene, 303 K): δ -93.1 (*Si*^{i}Pr$_3$).

*4.6.8 Synthesis of [{U(COT$^{(SiiPr3)2}$)}$_2$(μ-O){μ-η^1:η^1-O$_2$C(NC$_4$Me$_4$)}$_2$] (**4.8**)*

To a degassed solution of [U(COT$^{(SiiPr3)2}$)(Cp^{NMe4})] (34.2 mg, 4.40 x 10^{-5} mol) in d_8-toluene at -78 °C was added 0.86 bar $^{13}CO_2$. Warming the mixture to room temperature resulted in a gradual colour change from brown to red/orange. The residue was dried *in vacuo* then dissolved in hexane and filtered. Slow evaporation of the solvent at -35 °C yielded crystals.

Yield: 22.7 mg (1.37 x 10^{-5} mol), 62.2% based on [U(COT$^{(SiiPr3)2}$)(Cp^{NMe4})].

Anal. calc (found) for $C_{68}{}^{13}C_2H_{120}O_5N_2Si_4U_2$: C 50.76 (49.527), H 7.29 (7.201), N 1.69 (2.100)%.

MS (EI): *m/z* = 59 (100%), 1659 (< 1%, M^+-H).

IR (NaCl): 2917, 2858, 2346, 1513, 1443, 1396, 1344 cm^{-1}.

^{1}H NMR (d_8-toluene, 303 K): δ -1.4 (s, br, 18H, ^{i}Pr-C*H*$_3$), -2.3 (s, br, 6H, ^{i}Pr-C*H*), -2.6 (s, br, 18H, ^{i}Pr-C*H*$_3$), -10.0 (s, br, 6H, Cp-C*H*$_3$), -27.7 (s, br, 6H, Cp-C*H*$_3$).

^{13}C{^{1}H} NMR (d_8-toluene, 303 K): δ -7.1 (s, carbamate-**^{13}*C***).

$^{29}Si\{^{1}H\}$ NMR (d_8-toluene, 303 K): δ -79.7 ($Si^{i}Pr_3$).

*4.6.9 Synthesis of [(COT$^{(SiiPr3)2}$)(Cp^{NMe4})U(μ-O)(μ-η^1:η^5-Cp^{NMe4})U(COT$^{(SiiPr3)2}$)] (**4.9**)*

To a degassed solution of [U(COT$^{(SiiPr3)2}$)(Cp^{NMe4})] (30 mg, 3.9 x 10^{-5} mol) in d_8-toluene at -78 °C was added 0.86 bar N_2O. A colour change from purple/brown to red/brown was observed which persisted as the solution was warmed to room temperature. All volatiles were removed *in vacuo* six hours after gas addition. The residue was taken up in pentane and filtered. Single crystals of **4.9** were obtained from a saturated diethyl ether solution at -35 °C.

Yield: 21.2 mg (1.35 x 10^{-5} mol), 69% based on [U(COT$^{(SiiPr3)2}$)(Cp^{NMe4})].

Anal. calc (found) for $C_{68}H_{120}ON_2Si_4U_2$: C 52.02 (51.504), H 7.70 (7.460), N 1.78 (1.468)%.

^{1}H NMR (d_8-toluene, 303 K): δ 171.8 (s, br, 1H, COT-C*H*), 141.7 (s, br, 1H, COT-C*H*), 127.7 (s, br, 1H, COT-C*H*), 124.8 (s, br, 1H, COT-C*H*), 35.2 (s, br, 1H, COT-C*H*), 12.4 (s, br, 3H, ^{i}Pr-C*H*/Cp-CH_3), 10.4 (s, br, 9H, ^{i}Pr-CH_3), 8.2 (s, br, 3H, ^{i}Pr-C*H*/Cp-CH_3), 7.4 (s, br, 3H, ^{i}Pr-C*H*/Cp-CH_3), 5.3 (s, br, 9H, ^{i}Pr-CH_3), 3.5 (s, br, 3H, ^{i}Pr-C*H*/Cp-CH_3), -0.3 (s, br, overlapping), -1.1 (s, br, overlapping), -1.5 (s, br, overlapping), -2.5 (s, br, 3H, ^{i}Pr-C*H*/Cp-CH_3), -3.8 (s, br, overlapping, 9H, ^{i}Pr-CH_3), -4.2 (s, br, overlapping, 9H, ^{i}Pr-CH_3), -5.4 (s, br, 9H, ^{i}Pr-CH_3), -8.0 (s, br, 9H, ^{i}Pr-CH_3), -10.2 (s, br, overlapping, 3H, ^{i}Pr-C*H*/Cp-CH_3), -10.7 (s, br, overlapping, 3H, ^{i}Pr-C*H*/Cp-CH_3), -11.0 (s, br, overlapping, 3H, ^{i}Pr-C*H*/Cp-CH_3), -24.0 (s, br, 3H, ^{i}Pr-C*H*/Cp-CH_3), -76.8 (s, br, overlapping, 1H, COT-C*H*), -77.3 (s, br, overlapping, 1H, COT-C*H*), -80.9 (s, br, 1H, COT-C*H*), -88.1 (s, br, 1H, COT-C*H*), -97.4 (s, br, overlapping, 3H, ^{i}Pr-C*H*/Cp-CH_3), -97.9 (s, br, overlapping, 1H, COT-C*H*), -100.6 (s, br, 3H, ^{i}Pr-C*H*/Cp-CH_3), -101.6 (s, br, 1H, COT-C*H*), -104.2 (s, br, 1H, COT-C*H*).

$^{29}Si\{^{1}H\}$ NMR (d_8-toluene, 303 K): δ -41.7 ($Si^{i}Pr_3$), -46.8 ($Si^{i}Pr_3$), -87.7 ($Si^{i}Pr_3$), -154.1 ($Si^{i}Pr_3$).

4.6.10 Reaction of [U(COT$^{(SiiPr3)2}$)(Cp^{PMe4})] with 0.5 equivalents of $^{13}CO_2$

To a degassed solution of [U(COT$^{(SiiPr3)2}$)(Cp^{PMe4})] (55.9 mg, 7.04 x 10^{-5} mol) in d_8-toluene at -78 °C was added 0.5 equivalents $^{13}CO_2$ (3.48 x 10^{-5} mol). Warming of the mixture resulted in a colour change from brown to red/brown.

IR (NaCl): 2961, 2920, 2863, 1448, 1261 cm^{-1}.

^{1}H NMR (d_8-toluene, 303 K): δ 13.3 (br), 10.7 (br), 6.3 – 1.8 (br, overlapping), -0.1 (br), -5.1 (br), -9.5 (br), -15.7 (br), -19.5 (br), -57.4 (br).

$^{13}C\{^{1}H\}$ NMR (d_8-toluene, 303 K): δ -108.2 (s).

$^{29}Si\{^{1}H\}$ NMR (d_8-toluene, 303 K): δ -72.8 ($Si^{i}Pr_3$), -93.3 ($Si^{i}Pr_3$).

$^{31}P\{^{1}H\}$ NMR (d_8-toluene, 303 K): δ -20.9 (br).

*4.5.11 Synthesis of [{U(COT$^{(SiiPr3)2}$)}$_2$(μ-O){μ-η^1:η^1-O$_2$C(PC$_4$Me$_4$)}$_2$] (**4.11**)*

To a frozen, degassed solution of [U(COT$^{(SiiPr3)2}$)(Cp^{PMe4})] (191.5 mg, 2.21 x 10^{-4} mol) in pentane at -196 °C was added 3.2 equivalents CO_2 (7.06 x 10^{-4} mol). Thawing of the mixture and warming resulted in a colour change from brown to red/brown. The mixture was stirred for two days then filtered *via* cannula and crystals of **4.11** were obtained at -35 °C.

Yield: 47.5 mg (2.81 x 10^{-5} mol), 25.4% based on [U(COT$^{(SiiPr3)2}$)(Cp^{PMe4})].

Anal. calc (found) for $C_{70}H_{120}O_5P_2Si_4U_2$: C 49.69 (49.937), H 7.15 (7.332)%.

MS (EI): *m/z* = 1070 (100%, $[U(COT^{(SiiPr3)2})_2]^+$), 1692 (< 1%, M^+).

IR (NaCl): 2945, 1509, 1360, 1309 cm^{-1}.

^1H NMR (d_8-toluene, 303 K): δ 6.0 – -4.0 (br, overlapping), -9.7 (br), -19.0 (br).

^1H NMR (d_8-toluene, 363 K): δ 1.8 (s, br, 6H, Cp-CH_3/^{i}Pr-C*H*), 0.9 (s, br, 18H, ^{i}Pr-CH_3), 0.2 (s, br, 18H, ^{i}Pr-CH_3), -7.3 (s, br, 6H, Cp-CH_3/^{i}Pr-C*H*), -15.0 (s, br, 6H, Cp-CH_3/^{i}Pr-C*H*).

$^{13}C\{^1H\}$ NMR (d_8-toluene, 303 K): δ -43.3 (d, $^1J_{CP}$ = 18.0 Hz, phosphacarbonate-***^{13}C***), -46.6 (d, $^1J_{CP}$ = 20.3 Hz, phosphacarbonate-***^{13}C***).

$^{29}Si\{^1H\}$ NMR (d_8-toluene, 303 K): δ -75.7 (Si^iPr_3).

$^{31}P\{^1H\}$ NMR (d_8-toluene, 303 K): δ 15.0 – 9.0 (br, overlapping), -14.5 (br).

*4.6.12 Synthesis of [{(COT$^{(SiiPr3)2}$)U}$_2$(μ-O)$_2$] (**4.12**) and [Me$_4$C$_4$P]$_2$ (**4.12**)*

To a degassed solution of $[U(COT^{(SiiPr3)2})(Cp^{PMe4})]$ (124.5 mg, 1.57 x 10^{-4} mol) in toluene at -78 °C was added 0.86 bar N_2O. Warming of the mixture resulted in a colour change from brown to red/brown. Solvent was removed *in vacuo* and the residue was dissolved in a mixture of hexane/DME to give crystals of **4.12DME**.

Characterisation of $[\{(COT^{(SiiPr3)2})U\}_2(\mu\text{-}O)_2]$ (**4.12**):

Yield: 59.8 mg (4.46 x 10^{-5} mol), 56.8% based on $[U(COT^{(SiiPr3)2})(Cp^{PMe4})]$.

Anal. calc (found) for $C_{52}H_{96}O_2Si_4U_2$: C 46.55 (45.690), H 7.21 (6.966)%.

MS (EI): *m/z* = 59 (100%), 1341 (4%, M^+).

IR (NaCl): 3050-2700 (br, overlapping), 1455, 1365, 1294, 1252, 1218 cm^{-1}.

^{1}H NMR (d_8-toluene, 303 K): δ 30.1 (br, 1H), 6 – 1.5 (br, overlapping), -10.0 (br, 1H), -39.3 (br, 1H), -63.7 (br, 1H), -93.1 (br, 1H).

^{29}Si{^{1}H} NMR (d_8-toluene, 303 K): δ -85.1 ($Si^{i}Pr_3$).

Characterisation of [1,1'-bis(2,3,4,5-tetramethylphosphole)] (**4.13**):

MS (EI): *m/z* = 140 (100%, $[Me_4C_4PH]^+$), 278 (55%, M^+).

^{1}H NMR (d_8-toluene, 303 K): δ 1.8 (t, $^{3}J_{HP}$ = 4.9 Hz, 6H, C_3- CH_3, C_4-CH_3), 1.7 (s, 6H, C_2- CH_3, C_5-CH_3).

^{13}C{^{1}H} NMR (d_8-toluene, 303 K): δ 142.4 (m, 3,4-*C*CH_3), 134.3 (m, 2,5-*C*CH_3), 14.1 (s, 3,4-*C*H_3), 13.6 (m, 2,5-*C*H_3).

^{31}P{^{1}H} NMR (d_8-toluene, 303 K): δ -8.3 (*P*-ring).

*4.6.13 Synthesis of [$C_4Me_4P^{13}CO_2SiMe_3$] (**4.14**)*

A suspension of K[Cp^{PMe4}] (11.5 mg, 6.45 x 10^{-5} mol) in d_6-benzene in a Young's tube was frozen at -78 °C and degassed prior to addition of 0.86 bar $^{13}CO_2$. During the three hours after gas addition the suspension became white. The mixture was freeze-thaw degassed then TMSCl was added dropwise *via* syringe until all solids had reacted. White solids (presumably KCl) were observed to precipitate leaving a yellow solution.

MS (EI): *m/z* = 73 (100%, $[SiMe_3]^+$), 258 (15%, M^++H).

^{1}H NMR (d_6-benzene, 303 K): δ 2.2 (d, $^{3}J_{PH}$ = 10.5 Hz, 6H, C_1-CH_3, C_4-CH_3), 1.6 (s, 6H, C_2-CH_3, C_3-CH_3), 0.2 (s, 9H, Si(CH_3)$_3$).

^{13}C{^{1}H} NMR (d_6-benzene, 303 K): δ 176.1 (d, $^{1}J_{CP}$ = 19.2 Hz, P-^{13}***C***O_2), 158.1 (s), 151.1 (s), 35.6 (s, 2,5-*C*H_3), 23.3 (s, 3,4-*C*H_3).

$^{29}Si\{^{1}H\}$ NMR (d_6-benzene, 303 K): δ 30.0 ($Si^{i}Pr_3$).

$^{31}P\{^{1}H\}$ NMR (d_6-benzene, 303 K): δ 16.7 (d, $^{1}J_{CP}$ = 19.3 Hz, *P*-ring).

*4.6.14 Characterisation of [$C_4Me_4PSiMe_3$] (**4.15**)*

MS (EI): *m/z* = 73 (100%, $[SiMe_3]^+$), 212 (20%, M^+).

^{1}H NMR (d_6-benzene, 303 K): δ 2.0 (d, $^{3}J_{PH}$ = 10.2 Hz, 6H, C_1-C*H*$_3$, C_4-C*H*$_3$), 1.9 (s, 6H, C_2-C*H*$_3$, C_3-C*H*$_3$), 0.0 (d, $^{3}J_{PH}$ = 4.1 Hz, 9H, Si(C*H*$_3$)$_3$).

$^{13}C\{^{1}H\}$ NMR (d_6-benzene, 303 K): δ 142.9 (d, $^{2}J_{CP}$ = 5.7 Hz, *C*$_2$, *C*$_3$), 131.9 (d, $^{1}J_{CP}$ = 8.4 Hz, *C*$_1$, *C*$_4$), 14.6 (d, $^{2}J_{CP}$ = 22.8 Hz, C_1-*C*H$_3$, C_4-*C*H$_3$), 14.0 (d, $^{3}J_{CP}$ = 2.2 Hz, C_2-*C*H$_3$, C_3-*C*H$_3$), -1.7 (d, $^{2}J_{CP}$ = 10.1 Hz, Si(*C*H$_3$)$_3$).

$^{29}Si\{^{1}H\}$ NMR (d_6-benzene, 303 K): δ 3.1 ($Si^{i}Pr_3$).

$^{31}P\{^{1}H\}$ NMR (d_6-benzene, 303 K): δ -33.4 (s, *P*-ring).

*4.6.15 Synthesis of [{U(COT$^{(SiiPr3)2}$)(OTMS)}$_2$(μ-Cl)$_2$] (**4.16**)*

To a degassed solution of [U(COT$^{(SiiPr3)2}$)(Cp^{PMe4})] (150.0 mg, 1.89 x 10^{-4} mol) in toluene (5 mL) at -78 °C was added three equivalents CO_2. The mixture was warmed to ambient temperature, stirred for 24 hours, then freeze-thaw degassed. Excess TMSCl (5 drops) was added and the mixture was heated to 90 °C for 72 hours. The residue was dried *in vacuo*, dissolved in pentane and filtered. Slow evaporation of the solvent at -35 °C yielded red crystals.

Yield: 60.8 mg (3.90 x 10^{-5} mol), 41.3% based on [U(COT$^{(SiiPr3)2}$)(Cp^{PMe4})].

Anal. calc (found) for $C_{58}H_{114}Cl_2O_2Si_6U_2$: C 44.68 (44.718), H 7.37 (7.390)%.

MS (EI): *m/z* = 59 (100%), 1557 (1%, M^+).

^{1}H NMR (d_8-toluene, 303 K): δ 158.9 (s, br, 2H, COT-C*H*), 148.5 (s, br, 2H, COT-C*H*), 47.3 (s, br, 9H, TMS-CH_3), 46.0 (s, br, 9H, TMS-CH_3), -12.3 (s, br, 18H, ^{i}Pr-CH_3), -12.4 (s, br, 18H, ^{i}Pr-CH_3), -17.0 (s, br, 2H, COT-C*H*), -17.6 (s, br, 2H, COT-C*H*), -20.6 (s, br, 18H, ^{i}Pr-CH_3), -21.6 (s, br, 18H, ^{i}Pr-CH_3), -23.8 (s, br, 18H, ^{i}Pr-C*H*), -25.1 (s, br, 18H, ^{i}Pr-C*H*), -137.2 (s, br, 2H, COT-C*H*), -139.6 (s, br, 2H, COT-C*H*).

^{29}Si{^{1}H} NMR (d_8-toluene, 303 K): δ -139.8 (*Si*R$_3$), -143.3 (*Si*R$_3$).

*4.6.16 Synthesis of [{U(COT$^{(SiiPr3)2}$)(OTMS)}$_2$(μ-I)$_2$] (**4.17**)*

To a degassed solution of [U(COT$^{(SiiPr3)2}$)(Cp^{PMe4})(THF)] (98.3 mg, 1.13 x 10^{-4} mol) in toluene (5 mL) at -78 °C was added three mole equivalents carbon dioxide. Warming the mixture to room temperature resulted in a gradual colour change from brown to red/orange. The mixture was stirred for 24 hours then stripped to dryness. The residue was taken up in d_6-benzene and excess TMSI (four drops) was added. The mixture was heated to 75 °C for 24 hours then stripped to dryness. The residue was extracted in pentane and filtered to yield a bright red solution which yielded crystals at -35 °C.

Yield: 30.7 mg (1.76 x 10^{-5} mol), 15.6% based on [U(COT$^{(SiiPr3)2}$)(Cp^{PMe4})(THF)].

MS (EI): *m/z* = 827 (100%, [U(COT$^{(SiiPr3)2}$)(OTMS)I]$^+$ - $SiCH_3$), 1741 (1%, M^+).

^{1}H NMR (d_6-benzene, 303 K): δ 176.5 (s, br, 2H, COT-C*H*), 159.1 (s, br, 2H, COT-C*H*), 52.0 (s, br, 9H, TMS-CH_3), 48.7 (s, br, 9H, TMS-CH_3), -11.4 (s, br, 18H, ^{i}Pr-CH_3), -11.8 (s, br, 18H, ^{i}Pr-CH_3), -12.8 (s, br, 2H, COT-C*H*), -13.8 (s, br, 2H, COT-C*H*), -19.8 (s, br, 18H, ^{i}Pr-CH_3), -20.3 (s, br, 18H, ^{i}Pr-CH_3), -26.6 (s, br, 6H, ^{i}Pr-C*H*), -27.2 (s, br, 6H, ^{i}Pr-C*H*), -148.8 (s, br, 2H, COT-C*H*), -152.5 (s, br, 2H, COT-C*H*).

^{29}Si{^{1}H} NMR (d_6-benzene, 303 K): δ -149.3 (*Si*R$_3$), -154.5 (*Si*R$_3$).

4.6.17 Synthesis of [{U(COT$^{(SiiPr3)2}$)(Cp^{PMe4})}$_2$(μ-S)] ***(4.18)***

Method A:

A solution of [U(COT$^{(SiiPr3)2}$)(Cp^{PMe4})(THF)] (90.5 mg, 1.04 x 10^{-4} mol) in toluene (2 mL) was cooled to -78 °C and degassed. To this solution was added two mole equivalents COS *via* Toepler line. The mixture was slowly warmed to room temperature and a colour change from purple to brown was observed. The mixture was stirred for 24 hours then all volatiles were removed *in vacuo*. The residue was filtered in pentane and crystals of **4.18** were obtained at -35 °C.

Yield: 46.3 mg (2.86 x 10^{-5} mol), 55.0% based on [U(COT$^{(SiiPr3)2}$)(Cp^{PMe4})(THF)].

Method B:

A mixture of [U(COT$^{(SiiPr3)2}$)(Cp^{PMe4})(THF)] (197.5 mg, 2.28 x 10^{-4} mol) and triphenylphosphine sulfide (72.0 mg, 2.45 x 10^{-5} mol) were cooled to -78 °C and toluene (5 mL) was added. The mixture was warmed to ambient temperature and a colour change from purple to brown was observed within minutes. The mixture was stirred for 24 hours then all volatiles were removed *in vacuo*. The residue was extracted in pentane and filtered then solvent and triphenylphosphine were sublimed away from the product at 80 °C at 10^{-7} mbar. The complex was extracted in pentane and filtered to give a saturated solution from which crystals were obtained at -35 °C.

Yield: 126.3 mg (7.79 x 10^{-5} mol), 68.4% based on [U(COT$^{(SiiPr3)2}$)(Cp^{PMe4})(THF)].

Anal. calc (found) for $C_{68}H_{120}P_2SSi_4U_2$: C 50.41 (50.495), H 7.47 (7.333)%.

IR (NaCl): 2942, 2889, 2864, 1463, 1380, 1260, 1224, 1146,1071, 1022 cm^{-1}.

^{1}H NMR (d_6-benzene, 303 K): δ 77.2 (s, br, 2H, COT-C*H*), 43.8 (s, br, 2H, COT-C*H*), 12.2 (s, br, 6H, Cp-CH_3), 1.9 (s, br, 2H, COT-C*H*), 0.3 (s, br, 18H, ^{i}Pr-CH_3), 0.1 (s, br,

36H, ^{i}Pr-CH_3), -0.6 (s, br, 6H, ^{i}Pr-C*H*), -0.7 (s, br, 6H, ^{i}Pr-C*H*), -2.0 (s, br, 18H, ^{i}Pr-CH_3), -6.4 (s, br, 6H, Cp-CH_3), -22.8 (s, br, 6H, Cp-CH_3), -33.6 (s, br, 2H, COT-C*H*), -47.2 (s, br, 6H, Cp-CH_3), -48.4 (s, br, 2H, COT-C*H*), -81.4 (s, br, 2H, COT-C*H*).

^{29}Si{^{1}H} NMR (d_6-benzene, 303 K): δ -94.3 (*Si*^{i}Pr$_3$), -123.2 (*Si*^{i}Pr$_3$).

^{31}P{^{1}H} NMR (d_6-benzene, 303 K): δ 1669.4 (br, $w_{½}$ = 432 Hz, *P*-ring).

4.6.18 Reactivity of [{U(COT$^{(SiiPr3)2}$)(Cp^{PMe4})}$_2$(μ-S)] with CO_2.

Method A:

A solution of **4.18** was prepared from reaction of [U(COT$^{(SiiPr3)2}$)(Cp^{PMe4})(THF)] (176.4 mg, 2.04 x 10^{-4} mol) and triethylphosphine sulfide (31.3 mg, 2.08 x 10^{-4} mol) over seven days. All volatiles were removed *in vacuo* and triethylphosphine was sublimed away from the product at 60 °C at 10^{-2} mbar. The complex was extracted in pentane and filtered to give a crude solution which was degassed at -78 °C. To this was added excess carbon dioxide (2.36 x 10^{-4} mol), and the mixture was warmed resulting in a yellow/brown solution. NMR spectroscopy illustrated the formation of [{U(COT$^{(SiiPr3)2}$)(Cp^{PMe4})}$_2$(μ-CO_2S)] **4.19**. All volatiles were removed *in vacuo*, and the residue was extracted in pentane and filtered. Crystals of **4.19** were obtained at -35 °C.

Yield 17.9 mg (1.08 x 10^{-5} mol), 10.5% based on [U(COT$^{(SiiPr3)2}$)(Cp^{PMe4})(THF)].

MS (EI): *m/z* = 115 (100%), 1479 (15%, M^+ - [$O_2{}^{13}CPC_4Me_4$]).

^{1}H NMR (d_6-benzene, 303 K): δ 26.3 (2H), 5.0 (br, overlapping), 3.8 (br, overlapping), -1.5 (br, overlapping), -2.9 (br, overlapping), -4.7 (br, overlapping), -5.5 – -8.0 (br, overlapping), -10.7 (br, overlapping), -12.8 (br, overlapping), -21.1 (1H), -33.7 (1H), -60.4 (2H).

$^{13}C\{^{1}H\}$ NMR (d_6-benzene, 303 K): *Resonances could not be assigned.*

$^{29}Si\{^{1}H\}$ NMR (d_6-benzene, 303 K): δ -98.8 ($Si^{i}Pr_3$).

$^{31}P\{^{1}H\}$ NMR (d_6-benzene, 303 K): δ 602.2 (br, $w_{½}$ = 123.7 Hz, *P*-ring).

Method B:

A solution of **4.18** was prepared from [U($COT^{(SiiPr3)2}$)(Cp^{PMe4})(THF)] (17.3 mg, 2.00 x 10^{-5} mol) and COS. Once the reaction had reached completion, the mixture was degassed, cooled to -78 °C and two mole equivalents CO_2 was added *via* Toepler line. The mixture was warmed to room temperature and a subtle colour change from red/brown to yellow/brown was observed. NMR spectroscopy illustrated the formation of [{U($COT^{(SiiPr3)2}$)(Cp^{PMe4})}$_2$(μ-CO_2S)] (**4.19**) and [{U($COT^{(SiiPr3)2}$)(Cp^{PMe4})}(μ-CO_2S){U($COT^{(SiiPr3)2}$)(η^1:η^1-$O_2CPC_4Me_4$)}] (**4.20**) . All volatiles were removed *in vacuo*, and the residue was extracted in pentane and filtered. Crystals of **4.20** were obtained at -35 °C.

Yield: 4.5 mg (2.63 x 10^{-6} mol), 26.3% based on [U($COT^{(SiiPr3)2}$)(Cp^{PMe4})(THF)].

MS (EI): *m/z* = 115 (100%), 961 (45%, [U($COT^{(SiiPr3)2}$)(Cp^{PMe4})]$^+$ + [$O_2{}^{13}CPC_4Me_4$])

^{1}H NMR (d_8-toluene, 303 K): δ 6.0 (br), 5.1 (br), 3.1 (br, overlapping), 2.9 (br, overlapping), 1.2 (br), -5.2 (br, overlapping), -5.3 (br, overlapping), -5.4 (br, overlapping), -6.8 (br), -7.3 (br).

$^{13}C\{^{1}H\}$ NMR (d_8-toluene, 303 K): *Resonances could not be assigned.*

$^{29}Si\{^{1}H\}$ NMR (d_8-toluene, 303 K): δ -79.9 ($Si^{i}Pr_3$), -90.3 ($Si^{i}Pr_3$).

$^{31}P\{^{1}H\}$ NMR (d_8-toluene, 303 K): δ 716.6 (br, $w_{½}$ = 88.5 Hz, *P*-ring), 54.7 (d, $^{1}J_{CP}$ = 26.9 Hz, phosphacarbonate-*P*).

4.7 References

1 O. T. Summerscales, F. G. N. Cloke, P. B. Hitchcock, J. C. Green and N. Hazari, *J. Am. Chem. Soc.*, 2006, **128**, 9602–9603.

2 O. T. Summerscales, F. G. N. Cloke, P. B. Hitchcock, J. C. Green and N. Hazari, *Science*, 2006, **311**, 829–831.

3 O. T. Summerscales, A. S. P. Frey, F. G. N. Cloke and P. B. Hitchcock, *Chem. Commun.*, 2009, 198–200.

4 A. S. P. Frey, F. G. N. Cloke, M. P. Coles, L. Maron and T. Davin, *Angew. Chem. Int. Ed.*, 2011, **50**, 6881–6883.

5 C. E. Kefalidis, A. S. P. Frey, S. M. Roe, F. G. N. Cloke and L. Maron, *Dalton Trans.*, 2014, **43**, 11202–11208.

6 J. A. Higgins, F. G. N. Cloke and S. M. Roe, *Organometallics*, 2013, **32**, 5244–5252.

7 C. Villiers, R. Adam and M. Ephritikhine, *J. Chem. Soc., Chem. Commun.*, 1992, 1555–1556.

8 M. Weydert, J. G. Brennan, R. A. Andersen and R. G. Bergman, *Organometallics*, 1995, **14**, 3942–3951.

9 J. A. Higgins, DPhil Thesis, University of Sussex, 2014.

10 R. E. Cramer, K. T. Higa and J. W. Gilje, *Organometallics*, 1985, **4**, 1140–1141.

11 Y. Mao and F. Mathey, *Chem. Eur. J.*, 2011, **17**, 10745–10751.

12 K. H. Dötz, A. Tiriliomis and K. Harms, *Tetrahedron*, 1993, **49**, 5577–5597.

13 K. H. Dötz, A. Tiriliomis, K. Harms, M. Regitz and U. Annen, *Angew. Chem. Int. Ed.*, 1988, **27**, 713–714.

14 Paolucci, Gino, Rossetto, Gilberto, Zanella, Pierino, Yünlü, Kenan and Fischer, R Dieter, *J. Organomet. Chem.*, 1984, **272**, 363–383.

15 P. J. Fagan, J. M. Manriquez, S. H. Vollmer, C. S. Day, V. W. Day and T. J. Marks, *J. Am. Chem. Soc.*, 1981, **103**, 2206–2220.

16 M. del Mar Conejo, J. S. Parry, E. Carmona, M. Schultz, J. G. Brennan, S. M. Beshouri, R. A. Andersen, R. D. Rogers, S. Coles and M. B. Hursthouse, *Chem. Eur. J.*, 1999, **5**, 3000–3009.

17 R. K. Sheline and J. L. Slater, *Angew. Chem. Int. Ed.*, 1975, **14**, 309–313.

18 W. J. Evans, S. A. Kozimor, G. W. Nyce and J. W. Ziller, *J. Am. Chem. Soc.*, 2003, **125**, 13831–13835.

19 J. S. Parry, E. Carmona, S. Coles and M. B. Hursthouse, *J. Am. Chem. Soc.*, 1995, **117**, 2649–2650.

20 A. S. P. Frey, F. G. N. Cloke, P. B. Hitchcock, I. J. Day, J. C. Green and G. Aitken, *J. Am. Chem. Soc.*, 2008, **130**, 13816–13817.

21 G. Aitken, N. Hazari, A. S. P. Frey, F. G. N. Cloke, O. T. Summerscales and J. C. Green, *Dalton Trans.*, 2011, 11080–11088.

22 J. G. Brennan, R. A. Andersen and J. L. Robbins, *J. Am. Chem. Soc.*, 1986, **108**, 335–336.

23 L. Maron, O. Eisenstein and R. A. Andersen, *Organometallics*, 2009, **28**, 3629–3635.

24 I. Castro-Rodriguez and K. Meyer, *J. Am. Chem. Soc.*, 2005, **127**, 11242–11243.

25 John A. Timney, *Encyclopedia of Inorganic and Bioinorganic Chemistry*, 2006.

26 E. Pretsch, P. Bühlmann and M. Badertscher, *Structure Determination of Organic Compounds*, Springer, Berlin Heidelberg, 4th edn., 2009.

27 J. C. J. Bart, *Acta Cryst. Sect. B*, 1969, **B25**, 489–497.

28 J. Svara, E. Fluck, J. J. Stezowski and A. Maier, *Z. Anorg. Allg. Chem*, 1987, **545**, 47–55.

29 F. Laporte, F. Mercier, L. Ricard and F. Mathey, *J. Am. Chem. Soc.*, 1994, **116**, 3306–3311.

30 F. H. Allen, O. Kennard, D. G. Watson, L. Brammer, A. G. Orpen and R. Taylor, *J. Chem. Soc. Perkin Trans. 2*, 1987, S1–S19.

31 L. Natrajan, M. Mazzanti, J.-P. Bezombes and J. Pécaut, *Inorg. Chem.*, 2005, **44**, 6115–6121.

32 W. J. Evans, J. R. Walensky, F. Furche, J. W. Ziller, A. G. DiPasquale and A. L. Rheingold, *Inorg. Chem.*, 2008, **47**, 10169–10176.

33 F. H. Allen, *Acta Cryst. Sect. B*, 2002, **B58**, 380–388.

34 I. J. Bruno, J. C. Cole, P. R. Edgington, M. Kessler, C. F. Macrae, P. McCabe, J. Pearson and R. Taylor, *Acta Cryst. Sect. B*, 2002, **B58**, 389–397.

35 F. Sanz and J. J. Daly, *J. Chem. Soc. Dalton Trans.*, 1973, 511–514.

36 G. Maerkl, S. Dietl and K. Polborn, *Private Communication*, 2002.

37 C. Boisson, J.-C. Berthet, M. Lance, M. Nierlich and M. Ephritikhine, *J. Organomet. Chem.*, 1997, **548**, 9–16.

38 W. J. Evans, T. J. Mueller and J. W. Ziller, *Chem. Eur. J.*, 2010, **16**, 964–975.

39 J.-C. Berthet, M. Lance, M. Nierlich and M. Ephritikhine, *Chem. Commun.*, 1998, 1373–1374.

40 S. M. Beshouri and A. Zalkin, *Acta Cryst. Sect. C*, 1989, **C45**, 1221–1222.

41 A. Zalkin and S. M. Beshouri, *Acta Cryst. Sect. C*, 1989, **C45**, 1080–1082.

42 J. H. Farnaby, F. G. N. Cloke, M. P. Coles, J. C. Green and G. Aitken, *Comptes Rendus Chimie*, 2010, **13**, 812–820.

43 J. H. Farnaby, DPhil Thesis, University of Sussex, 2011.

44 S. M. Mansell, N. Kaltsoyannis and P. L. Arnold, *J. Am. Chem. Soc.*, 2011, **133**, 9036–9051.

45 J. Rebizant, M.-R. Spirlet, C. Apostolidis and B. Kanellakopulos, *Acta Cryst. Sect. C*, 1992, **48**, 452.

46 N. Tsoureas, L. Castro, A. F. R. Kilpatrick, F. G. N. Cloke and L. Maron, *Chem. Sci.*, 2014, **5**, 3777–3788.

47 A. S. P. Frey, F. G. N. Cloke, M. P. Coles and P. B. Hitchcock, *Chem. Eur. J.*, 2010, **16**, 9446–9448.

48 A. Zalkin and S. M. Beshouri, *Acta Cryst. Sect. C*, 1988, **C44**, 1826–1827.

49 W. W. Lukens, P. G. Allen, J. J. Bucher, N. M. Edelstein, E. A. Hudson, D. K. Shuh, T. Reich and R. A. Andersen, *Organometallics*, 1999, **18**, 1253–1258.

50 P. L. Arnold, G. M. Jones, S. O. Odoh, G. Schreckenbach, N. Magnani and J. B. Love, *Nature Chemistry*, 2012, **4**, 221–227.

51 O. P. Lam, F. W. Heinemann and K. Meyer, *Chem. Sci.*, 2011, **2**, 1538–1547.

52 T. Le Borgne, P. Thuéry and M. Ephritikhine, *Acta Cryst. Sect. C*, 2002, **C58**, m8–m9.

53 A.-C. Schmidt, F. W. Heinemann, W. W. Lukens and K. Meyer, *J. Am. Chem. Soc.*, 2014, **136**, 11980–11993.

54 J. G. Reynolds, A. Zalkin, D. H. Templeton and N. M. Edelstein, *Inorg. Chem.*, 1977, **16**, 1090–1096.

55 F. G. N. Cloke and N. Tsoureas, *Unpublished Results*.

56 R. D. Shannon, *Acta Cryst.*, 1976, **A32**, 751–767.

57 A. Zalkin, A. L. Stuart and R. A. Andersen, *Acta Cryst. Sect. C*, 1988, **C44**, 2106–2108.

58 P. C. Blake, M. F. Lappert, R. G. Taylor, J. L. Atwood, W. E. Hunter and H. Zhang, *J. Chem. Soc., Chem. Commun.*, 1986, 1394–1395.

59 L. Maria, Â. Domingos and I. Santos, *Inorg. Chem.*, 2003, **42**, 3323–3330.

60 D. P. Mills, F. Moro, J. McMaster, J. V. Slageren, W. Lewis, A. J. Blake and S. T. Liddle, *Nature Chemistry*, 2011, **3**, 454–460.

61 B. M. Gardner, W. Lewis, A. J. Blake and S. T. Liddle, *Inorg. Chem.*, 2011, **50**, 9631–9641.

62 P. L. Arnold, A.-F. Pécharman and J. B. Love, *Angew. Chem. Int. Ed.*, 2011, **50**, 9456–9458.

63 J. L. Brown, G. Wu and T. W. Hayton, *J. Am. Chem. Soc.*, 2010, **132**, 7248–7249.

64 J. L. Brown, C. C. Mokhtarzadeh, J. M. Lever, G. Wu and T. W. Hayton, *Inorg. Chem.*, 2011, **50**, 5105–5112.

65 D. D. Schnaars, G. Wu and T. W. Hayton, *Inorg. Chem.*, 2011, **50**, 4695–4697.

66 D. D. Schnaars, G. Wu and T. W. Hayton, *Inorg. Chem.*, 2011, **50**, 9642–9649.

67 S. Fortier, N. Kaltsoyannis, G. Wu and T. W. Hayton, *J. Am. Chem. Soc.*, 2011, **133**, 14224–14227.

68 M. Porchia, N. Brianese, U. Casellato, F. Ossola, G. Rossetto, P. Zanella and R. Graziani, *J. Chem. Soc. Dalton Trans.*, 1989, 677–681.

69 G. Zi, L. Jia, E. L. Werkema, M. D. Walter, J. P. Gottfriedsen and R. A. Andersen, *Organometallics*, 2005, **24**, 4251–4264.

70 C. Lescop, T. Arliguie, M. Lance, M. Nierlich and M. Ephritikhine, *J. Organomet. Chem.*, 1999, **580**, 137–144.

71 A. L. Arduini, J. D. Jamerson and J. Takats, *Inorg. Chem.*, 1981, **20**, 2474–2479.

72 E. M. Matson, W. P. Forrest, P. E. Fanwick and S. C. Bart, *J. Am. Chem. Soc.*, 2011, **133**, 4948–4954.

73 N. A. Siladke, J. LeDuc, J. W. Ziller and W. J. Evans, *Chem. Eur. J.*, 2012, **18**, 14820–14827.

74 W. J. Evans, N. A. Siladke and J. W. Ziller, *Comptes Rendus Chimie*, 2010, **13**, 775–780.

75 V. Mougel, C. Camp, J. Pécaut, C. Copéret, L. Maron, C. E. Kefalidis and M. Mazzanti, *Angew. Chem. Int. Ed.*, 2012, **51**, 12280–12284.

76 A. F. R. Kilpatrick, DPhil Thesis, University of Sussex, 2014.

77 J. G. Brennan, R. A. Andersen and A. Zalkin, *Inorg. Chem.*, 1986, **25**, 1756–1760.

78 J. G. Brennan, R. A. Andersen and A. Zalkin, *Inorg. Chem.*, 1986, **25**, 1761–1765.

79 L. Castro and L. Maron, *Chem. Eur. J.*, 2012, **18**, 6610–6615.

80 D. Baudry, M. Ephritikhine, F. Nief, L. Ricard and F. Mathey, *Angew. Chem. Int. Ed.*, 1990, **29**, 1485–1486.

81 P. Gradoz, M. Ephritikhine, M. Lance, J. Vigner and M. Nierlich, *J. Organomet. Chem.*, 1994, **481**, 69–73.

82 J. L. Brown, G. Wu and T. W. Hayton, *Organometallics*, 2013, **32**, 1193–1198.

83 L. R. Avens, D. M. Barnhart, C. J. Burns, S. D. Mckee and W. H. Smith, *Inorg. Chem.*, 1994, **33**, 4245–4254.

84 T. Arliguie, P. Thuéry, P. Le Floch, N. Mézailles and M. Ephritikhine, *Polyhedron*, 2009, **28**, 1578–1582.

85 O. P. Lam, S. M. Franke, F. W. Heinemann and K. Meyer, *J. Am. Chem. Soc.*, 2012, **134**, 16877–16881.

CHAPTER 5: STERIC EFFECTS OF THE FIVE-MEMBERED RING

5.1 Introduction

The terms ‘steric effects’ or ‘steric properties’ have seen a great deal of attention in the literature for several decades as chemists have tried to gain a better understanding of the consequences of changing functional groups on a molecule of choice. In organometallic chemistry, the effects of size are often used as a justification for the observed chemistry, whether anticipated or unexpected. In some instances the rationale is evident, and no further evidence is required to persuade peers. However, in some cases the alteration of a functional group can lead to indecision about the type or degree of change that has taken place. As a consequence, chemists have spent the last four decades developing methods for evaluating the steric properties of their complexes in a quantitative way so that they can better understand and predict their reactivity.[1,2]

Earliest studies were carried out by Tolman, who required a numerical definition for the size of phosphine ligands when coordinated to a nickel centre.[3] Using a physical representation constructed from space-filling atomic models and an angle measuring device, the steric parameters were determined. Using the model as a cone with the metal centre at the apex, the boundaries of the cone were just wide enough to enclose the van der Waals radii of the outermost atoms (**Figure 5.1**). This approach was found to have reasonable accuracy (± 2° error) for phosphine ligands where the R groups have limited flexibility. However, in cases where the substituents possess internal degrees of freedom, the model assumed the ligand ‘packed’ into the smallest cone possible, leading to substantial errors of up to 10°. In addition, further studies into the effect of cone angle against strain energy found that a better relationship between cone angle and ligand dissociation was obtained when the strain energy was close to zero.[4] A second problem with this method is that it didn’t cater for unsymmetrical phosphine ligands.

The model was therefore adjusted to generate the ‘effective cone angle’, which is the averaged sum of each half cone angle, as defined by **Equation 5.1**. This method was also used in the calculation of chelating ligands, whereby $\theta_i/2$ is the angle between one metal–phosphorus bond and the bisector of the phosphorus–metal–phosphorus angle.

$$\Theta = \frac{2}{3}\sum_{i=1}^{3}\frac{\theta_i}{2}$$

Equation 5.1 The effective cone angle, calculated from the half angle of each substituent.

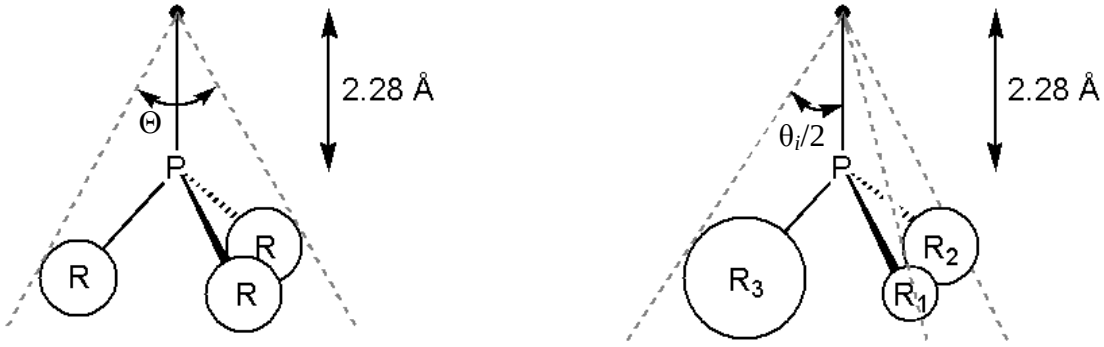

Figure 5.1 A pictorial representative of the cone angle (left) and the effective cone angle (right) for a phosphine ligand bonded to a nickel atom, whereby the phosphorus-nickel distance is set to 2.28 Å.[3,4]

Despite the improved model and the adjustments made for the effects of strain within the ligand, Tolman reported that this method contained many flaws.[2] Firstly, there is variation in the metal-phosphorus bond length, which whilst accounting for a difference of ± 4° in the cone angle, is not a significant error when compared to the variation in cone angle due to uncertainties in the measurements. Secondly, it was observed that the

angles around the phosphorus atom are generally distorted from a perfect tetrahedron, and this distortion can sometimes be enhanced by changes in the crowding around the ligand. A third aspect is that the model assumes a cylindrical ligand, which allows no overlap with another ligand. However, in order to achieve higher coordination numbers substituents have been known to 'mesh', allowing for more ligands to fit around a metal centre than is predicted by the model.

Since then, several models based on experimental and computational methods have been established with varying degrees of success. Brown developed a molecular mechanics model which calculates the ligand repulsive energy, E_R, based on van der Waals interactions of phosphine and phosphite ligands with a $Cr(CO)_5$ binding site.[5] Hirota and co-workers used molecular mechanics to define a steric constant for organic substituents, Ω_s,[6,7] and Coville and co-workers developed an algorithm for calculating the solid angle, Ω, as a function of distance from the metal centre.[8–10] These and other methods[11–14] all have their own advantages and disadvantages and several reviews cover the models and their applications.[1,15,16]

In 2006 an algorithm was released that calculates the steric parameters of ligands with more accuracy.[17] Unlike previous methods which often employed unspecified van der Waals radii and were only used to compare the size of one ligand *vs* another without consideration of other coordinating ligands, the 'Solid-G' software utilises atomic radii, which are smaller than the van der Waals radii published by Bondi,[18] but are larger than covalent radii. This allows more accurate values to be obtained when looking at ligand-ligand interactions. It also removes the variation found in van der Waals radii that arises from the environment in which the atom resides.

By building on Coville's definition of the solid angle, which is described as the 'measure of shadow' cast on the surface of a sphere by the ligand if the metal at the centre were a source of light, Solid-G calculates the solid angle, Ω (**Equation 5.3**), using the surface area of a sphere (**Equation 5.2**).[8,17] As the maximum solid angle is 4π,

the solid angle can be converted into the percentage shielding of the sphere, or the 'G-parameter' using **Equation 5.4**. The values obtained for the area of shadow can be calculated either by the coordinates obtained from XRD analysis of single crystals, or from the coordinates calculated by molecular mechanics.

$$A = 4\pi r^2 \qquad \textbf{Equation 5.2}$$

$$\Omega = \frac{A}{r^2} \qquad \textbf{Equation 5.3}$$

$$G = 100\,\frac{\Omega}{4\pi} \qquad \textbf{Equation 5.4}$$

Equation 5.2 (top) the surface area of a sphere; **Equation 5.3** (middle) calculating the solid angle, Ω; and **Equation 5.4** (bottom) converting the solid angle into the G-parameter (percentage shielding).[8,17]

There are several advantages of the Solid-G software over other algorithms/models available. Firstly, expressing the G-parameter as a percentage enables straightforward comparison with other ligands around the metal centre, as well as informing the analyst of the number of such ligands that can fit around the metal. This feature also allows the sterics of several ligands to be evaluated simultaneously so that both individual ligands and the complex as a whole can be viewed in terms of the shielding. Secondly, the G-parameter is independent of ligand size, shape and hapticity, allowing facile comparison of chelating ligands with monodentate ligands. Additional features of the software include the calculation of unfavourable contacts, and calculation of the overlap parameter, Gγ, which describes the amount of 'meshing' that occurs between

substituents/ligands and is especially useful when a complex contains functional groups with several degrees of freedom.

Due to the nature of the algorithm there is scope for variation in the values obtained, particularly with regard to conformational changes that the ligand can adopt. This is especially true when calculating G-parameters from crystallographic data where the effects of lattice packing, solvent and temperature can influence the atomic coordinates. Similarly with molecular mechanics calculations, the number of conformations calculated will affect the range and standard deviation of the steric values obtained.

Since the release of Solid-G, many research groups have employed its use for evaluating the steric properties and effects on reactivity in a quantitative manner. One application of the algorithm is its use in determining the steric effects on catalysis. Holland and co-workers used both this method and the $\%V_{bur}$ parameter (percent buried volume parameter calculated using Samb*V*ca)[19] to evaluate the effects of altering carbene substituents on palladium complexes used in Sonogashira coupling reactions.[20] The $\%V_{bur}$ parameter calculated was found to be unreliable for these complexes because the calculation only measures the sterics within 3.5 Å of the metal centre, and the substituents that were being studied were positioned over 6 Å away from palladium. The G-parameter however, effectively showed the changes in overall shielding of the metal centre, and the values obtained correlated well with reactivity studies, showing that increasing the sterics on the carbene ligand increases the catalytic activity. Similar results were also obtained for palladium catalysts with phosphine ligands, which had previously found the cone angle model inaccurate for evaluating the steric parameters,[21] and in tris(carbene)borate complexes of nickel nitrosyl, which found that bulkier ligands stabilised low-coordination numbers without blocking the metal centre.[22]

Other studies by Holland and co-workers on iron(III) imido complexes supported by di- and tri-substituted β-diketiminate ligands found that there was only a slight increase in the G-parameter from 62.2 to 63.8% on exchange of di-*iso*-propyl substituents on the

phenyl ring for triphenyl substituents (**Figure 5.2**).[23] However, the observed reactivity with hydrocarbons is significantly increased because the shape of the binding pocket is altered due to increased bending in the imido Fe–N–C angle. The good correlation between ligand size/shape and catalytic reactivity has given rise to studies which aim to design ligands with particular steric and electronic properties in mind.[24] Molecular mechanics calculations are also being used to track changing steric properties in intermediates in order to gain a better understanding of how changing the sterics changes reactivity.[25]

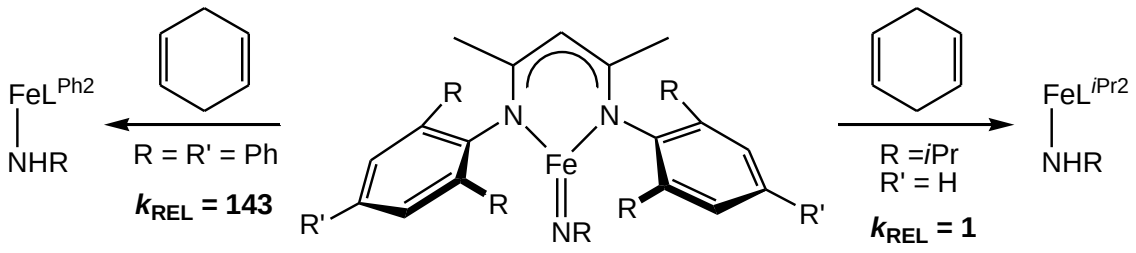

Figure 5.2 The iron(III) complexes supported by β-diketiminate ligands and their relative rate constants for comparable hydrogen atom transfer reactions.[23]

Solid-G has also been employed to explain crystallographic features. For a pyridine-2-tellurenyl chloride complex the small degree of shielding (28.1 and 28.3% for each telluride centre) results in dimerisation of the complex and a shortening of Te···Cl intermolecular contacts (**Figure 5.3**). The combination of these effects increases the shielding of each metal centre to approximately 73%.[26] Contrastingly, calculations of the shielding in bimetallic molybdenum complexes with a silicon-containing linker showed that a trimetallic complex could not be synthesised as the silicon atom was already shielded by over 95%.[27]

Other studies of the scandium complex [Sc(q^{Me})$_4$H] (q^{Me} = 2-methyl-8-quinolinolate) found that only two of the four q^{Me} ligands could chelate to the scandium centre whilst the other two were monodentate (**Figure 5.3**).[28] Overall, the shielding in this complex is almost 90% with approximately 28% arising from each bidentate q^{Me} ligand and 18% arising from each monodentate q^{Me} ligand. It was also observed that one of the ligands has a proton coordinated to the nitrogen atom in order to maintain neutrality.

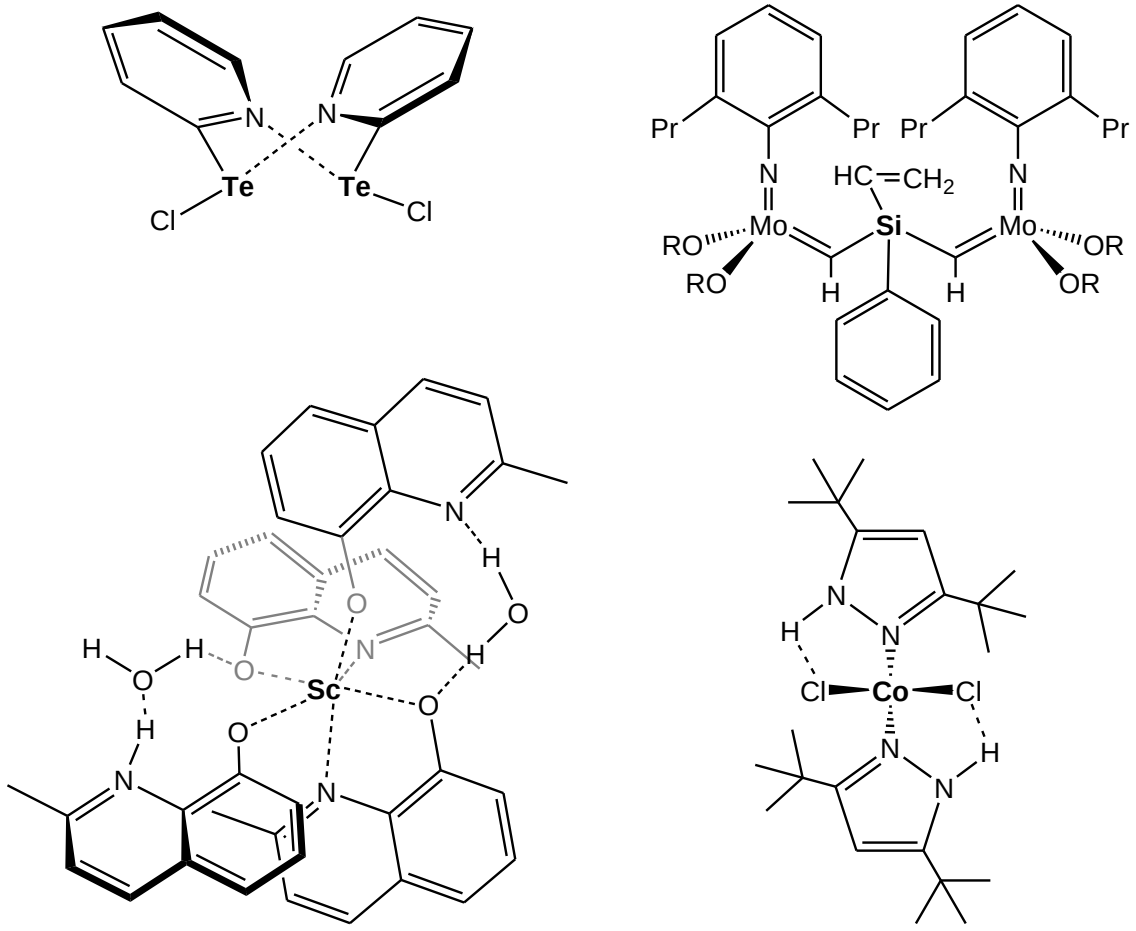

Figure 5.3 The pyridine-2-tellurenyl chloride complex (top left), bimetallic molybdenum complex (top right), scandium quinolinolate complex (bottom left) and the cobalt pyrazole complex (bottom right). The atoms for which G-parameters were calculated are shown in bold.[26–29]

Further research by Guzei has found that subtle changes in the steric shielding can lead to unusual interactions. Crystallographic studies of dichlorobis(3,5-di-*tert*-butyl-1*H*-pyrazole-κN2)cobalt(II) have shown that there are two N–H···Cl intramolecular hydrogen bonds within the complex, interactions which are not seen with related complexes (**Figure 5.3**).[30,31] This is due to the *tert*-butyl groups increasing the shielding parameter of the ligand by approximately 3%, preventing the formation of intermolecular bonds.[29]

The steric parameters of lanthanide complexes have also been investigated to determine how altering the lanthanide metal causes changes in ligand conformation. Studies by Fukin and co-workers found that reaction of $LnCl_3$ with two equivalents of the lithium guanidinate ligand resulted in the formation of a bimetallic complex with bridging chloride ligands for the larger lanthanides, but the formation of a lanthanide ate-complex for the smaller lanthanides (**Figure 5.4**).[32]

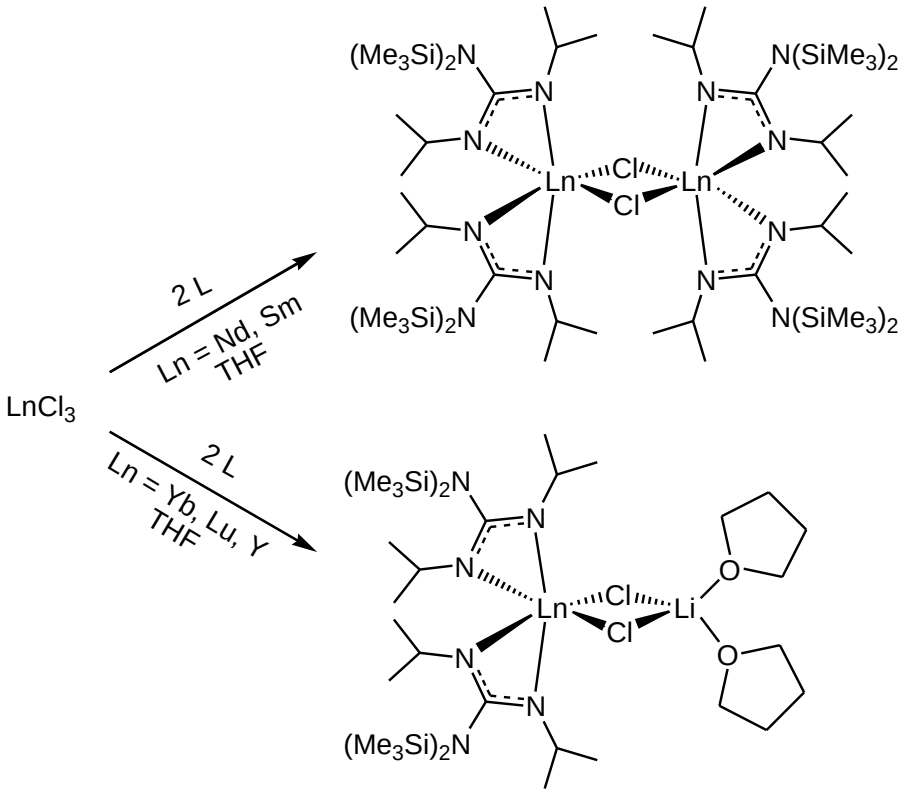

Figure 5.4 Synthesis of lanthanide guanidinate complexes from $LnCl_3$.[32]

Studies of analogous bimetallic lanthanide hydride complexes showed the guanidinate ligands have an eclipsed arrangement for the larger lanthanides (neodymium, samarium and gadolinium) but a staggered conformation for the smaller lanthanides (yttrium, ytterbium and lutetium).[32] This is justified by a decrease in the lanthanide radii shortening the Ln–Ln and Ln–ligand distances. The ligands therefore impart more shielding on the metal centre and the changing orientation allows the release of steric stress. Another feature noted with these complexes is that the overlap parameter, Gγ, increases as the lanthanide becomes smaller in order to reduce the overall shielding. Furthermore, monomeric lanthanide guanidinate complexes bearing bis(trimethylsilyl)amide ligands feature agostic C–H···Ln interactions, which are illustrated in the molecular structures by short Ln–C contacts (**Figure 5.5**).[33] This has the effect of increasing the G-parameter of these ligands by up to 10%, providing a significant increase in the total shielding.

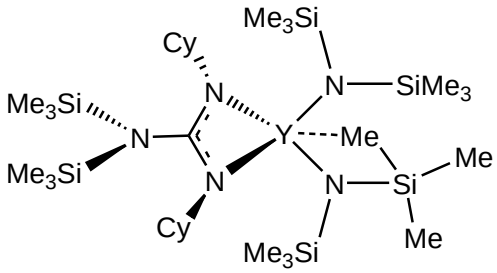

Figure 5.5 A monomeric yttrium guanidinate complex illustrating the agostic C–H···Y interaction (dashed lines) between the metal and the ligand.[33]

Comparison of the values obtained for all the complexes studied show that the overall shielding in mono- and bis(guanidinate) lanthanide complexes lies in the range of 85 – 88%, and that tris(guanidinate) complexes lie in the range of 84 – 92%, This illustrates

that achieving an optimum level of steric saturation is a key feature of lanthanide complexes.[32–35]

Other studies on lanthanide complexes have been used to determine the extent of ligand-ligand interaction. For $NdI_3(^iPrNH_2)_4$ it was found that the Nd–I bond lengths (3.1130(2) – 3.1711(2) Å) are longer than the corresponding Nd–I distances in $NdI_3(THF)_4$ (3.0714(4) – 3.1468(4) Å) in order to achieve a similar degree of shielding. It was therefore concluded that there are less non-bonding ligand-ligand interactions in the amine complex when compared to the THF complex due to the elongation of the Nd–I bonds.[36]

5.2 Calculating the steric parameters

As demonstrated by the above examples, there is considerable scope for study using the Solid-G algorithm, in terms of explaining the properties of a complex and its reactivity. It was therefore deemed an appropriate method for evaluating the steric properties of the mixed-sandwich complexes discussed in Chapter 2. In order to achieve the best overview of the steric properties, all mixed sandwich complexes incorporating the $COT^{(Si\mathit{i}Pr3)2}$ ligand and a five-membered aromatic ring were evaluated. In some cases however, comparison of $[U(COT^{(Si\mathit{i}Pr3)2})(Cp^{NMe4})]$ (**2.5**) with other complexes was inappropriate because dimerisation in the solid state was expected to give biased results.

Analyses of the base-free complexes and THF adducts have been kept separate due to the variation in values as a consequence of THF coordination, and where appropriate, values for **2.5** have been compared with both the THF adducts and base-free complexes. This is illustrated in **Figures 5.10** and **5.11** (*vide infra*). Values for **2.5THF** must be considered approximate due to the limitations of XRD data but have been included for comparative purposes. All G-parameters calculated for the complexes and individual ligands are included in Appendix II.

5.3 Steric effects on molecular structures

At first glance of the crystallographic data in Appendix II, there appeared to be a correlation between the size of the five-membered ring and the Cp–U–COT angle (measured for the centroids of each ligand). When these data were plotted however, there was a fair correlation for the THF adducts but no correlation for the base-free complexes (**Figure 5.6**). Comparison of the G-parameters obtained for the complexes with the Cp–U–COT angles also gave rise to similar results. The only observed correlation pertaining to the Cp–U–COT angle related to the G-parameter for THF, which showed that as the G-parameter decreases (and U–THF bond length increases), the angle increases.

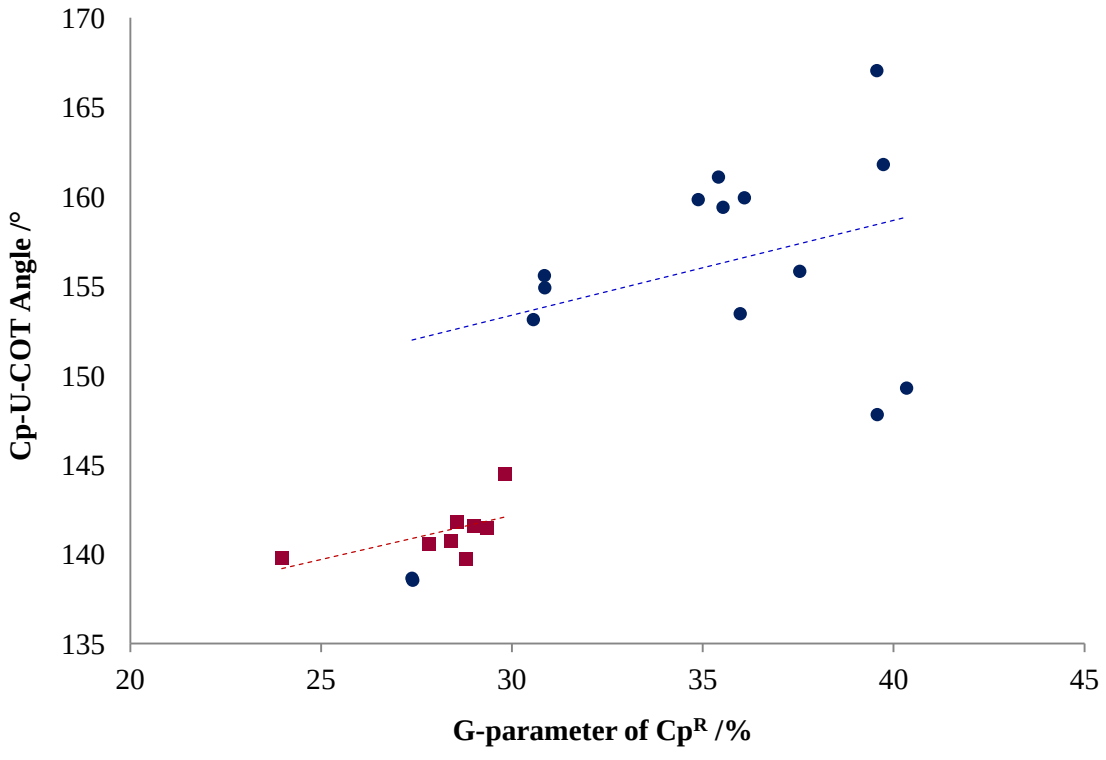

Figure 5.6 Comparison of the calculated G-parameters for substituted cyclopentadienyl rings (Cp^R) with the Cp–U–COT angle for base-free complexes excluding **2.5** (blue dots, y = 0.5299x + 137.5, R^2 = 0.09) and THF-adducts (red squares, y = 0.4923x + 127.4, R^2 = 0.35).

It was also observed that despite keeping the $COT^{(Si\mathit{i}Pr3)2}$ ring constant, the G-parameter for this ligand varied from 48.4 to 54.1% and normalisation of the U–COT distance to 2.28 Å only increased the variation (40.6 – 48.8%). The cause of variation was hypothesised to arise from the slight bending of the silyl groups away from the uranium centre caused by partial sp^3 character of the aromatic ring. Changes to the degree of sp^3 character would therefore give rise to significant variation in the perceived size of the ligand. In addition, the *iso*-propyl groups possess several degrees of freedom, a feature which highlights the limitations of using XRD data, as other conformations of these substituents present in solution and at varying temperatures are not accounted for in the calculations.

To observe the effect of partial sp^3 character for the COT ring carbons, the Ct–C–Si angles were compared to the $COT^{(Si\mathit{i}Pr3)2}$ G-parameters (**Figure 5.7**). These data show a strong correlation, and fair correlation is also observed when the aforementioned substituent angle is compared to the U–COT distance (**Figure 5.8**), illustrating that shorter uranium carbon bonds result in less sp^3 character in the aromatic ring carbons.

The same features were also expected of the five-membered rings. However, the differing substituents on these ligands make comparison with U–C(cyclopentadienyl) distances inappropriate as the contribution due to the number and size of the substituents and the degree of sp^3 character in the aromatic ring would be impossible to distinguish.

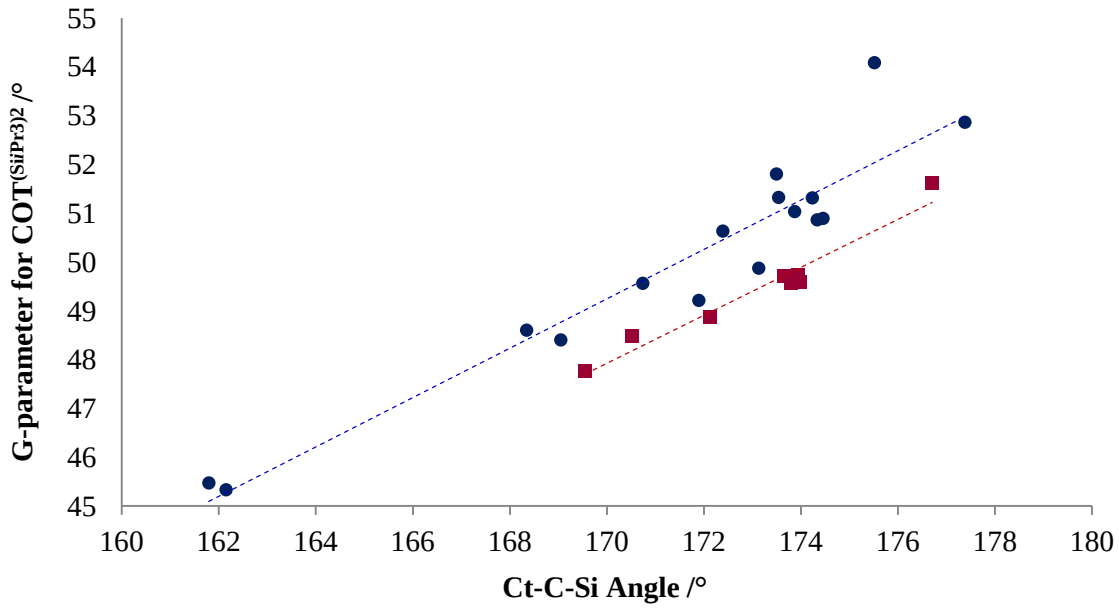

Figure 5.7 Comparison of the silyl bending angle with calculated G-parameters for $COT^{(SiiPr3)2}$ for the base-free complexes (blue dots, y = 0.5058x – 36.74, R^2 = 0.90) and THF adducts (red squares, y = 0.4914x – 35.61 R^2 = 0.95).

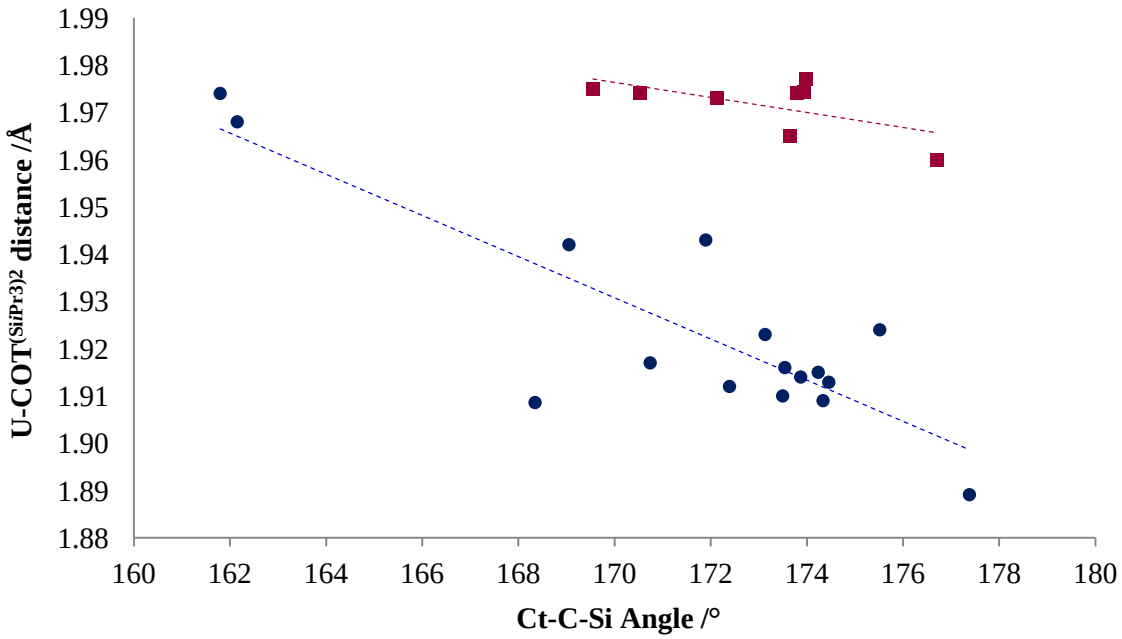

Figure 5.8 Comparison of the silyl bending angle with U–COT distances for the base-free complexes (blue dots, y = -0.0044x + 2.671, R^2 = 0.73) and THF adducts (red squares, y = -0.0016x + 2.247, R^2 = 0.37).

Further analysis of the COT G-parameters showed that with decreasing U–COT distances the shielding increases. A less expected result however, is that the COT G-parameters show some dependence on the Cp^R G-parameters (**Figure 5.9**). It is therefore postulated that there is an ideal steric saturation in these complexes as was observed by Fukin and co-workers for lanthanide complexes (*vide supra*).[32–35] For the mixed sandwich complexes, this is remediated by the coordination of THF in the smaller complexes, bending of the substituents away from linearity and varying the uranium–ligand distance.

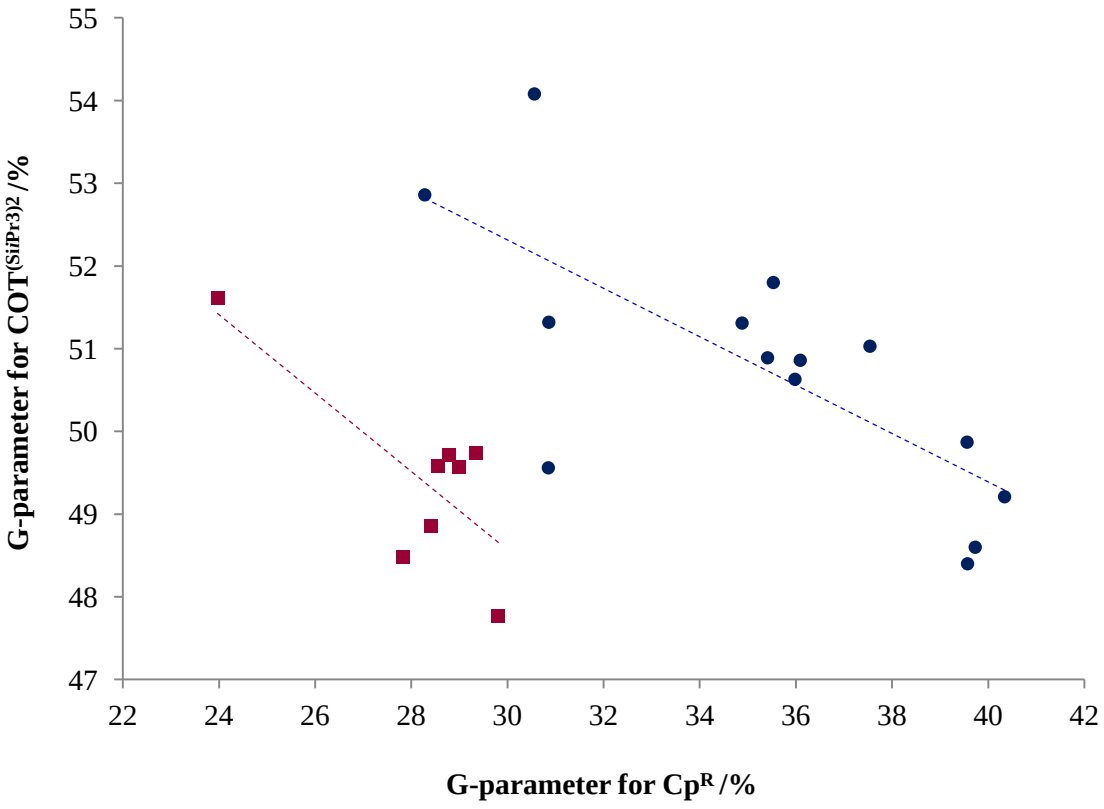

Figure 5.9 Comparison of the Cp^R G-parameter with the $COT^{(SiiPr3)2}$ G-parameter for the base-free complexes excluding **2.5** (blue dots, y = -0.2927x + 61.10, R^2 = 0.53) and THF adducts (red squares, y = -0.4742x + 62.79, R^2 = 0.58).

5.4 Steric effects on reactivity

The primary purpose of calculating the G-parameters was to provide a quantitative measure of how altering the steric saturation around the metal centre affects the observed reactivity with small molecules. As observed from the previous work by Cloke *et al.* and the reactivity studies of the mixed-sandwich complexes discussed in Chapter 3, varying the size of the cyclopentadienyl ring alters the reactivity with small molecules.[37–40] Arranging the ligands in ascending order of the G-parameter (**Figure 5.10**) allows both quantitative comparison of the ligands and the formulation of a trend for the observed small molecule reactivity. This could be useful for the synthesis of other complexes, which could be tailored with particular sterics (and reactivity) in mind.

Comparison of the ligand G-parameters in **Figure 5.10** shows the shielding varies from 24 to 40% as the number and the size of the substituents increases. However there is some variation in the values obtained for the THF adducts and base-free complexes $[U(COT^{(Si\mathit{i}Pr3)2})(Cp^*)(THF)_n]$ and $[U(COT^{(Si\mathit{i}Pr3)2})(Cp^{\mathit{t}Bu})(THF)_n]$ due to the coordination of the solvent molecule.

Another point to note is the subtle change in sterics upon changing E in Cp^{EMe4} from C to a heteroatom. In the series $Cp^{Me4} < Cp^{NMe4} < Cp^{PMe4} < Cp^{AsMe4} < Cp^{Me5}$ (Cp*), the G-parameter increases by 0.21 to 0.46% as E increases in size. This increase may affect the reactivity observed with small molecules. However the observed non-innocence of the Cp^{EMe4} ligands prevents conclusive deductions about the effects of sterics on reactivity for these complexes (see Chapter 4).

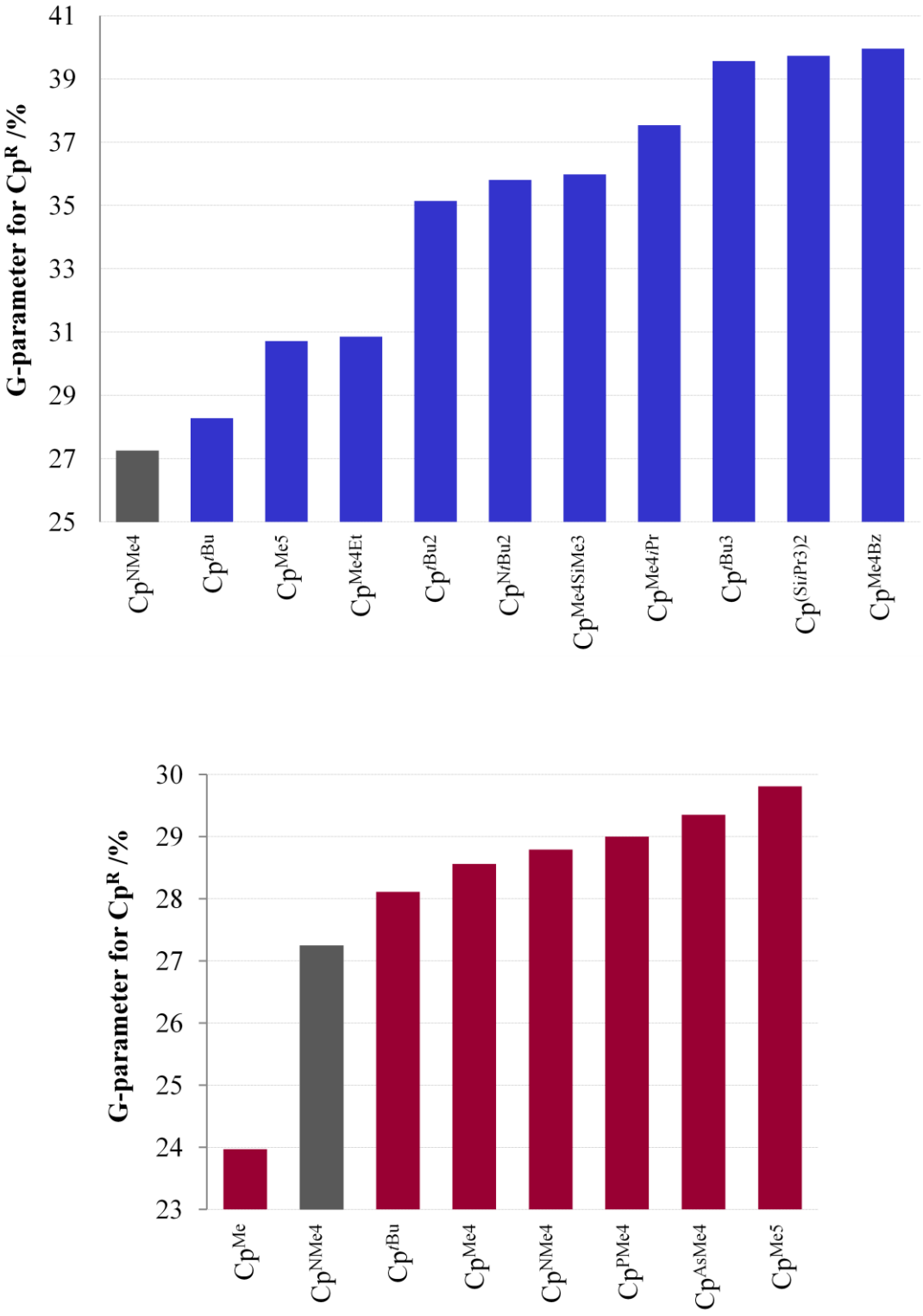

Figure 5.10 The G-parameter for Cp^R in ascending order for the base-free complexes (blue) and the THF adducts (red). The pyrrolyl ligand in [U($COT^{(SiiPr3)2}$)(Cp^{NMe4})] (**2.5**) is shown in grey.

For some complexes, it is also observed that there is a significant degree of 'meshing', evidenced by larger values of Gγ, which gives rise to less steric saturation than would otherwise be expected. This is exemplified by [U(COT$^{(Si\textit{i}Pr3)2}$)(Cp^{NMe4})(THF)] (**2.5**), which has an overlap parameter of 0.61%, giving rise to its displacement in the series and the impression of an anomalous result (**Figure 5.11**). Contrastingly, [U(COT$^{(Si\textit{i}Pr3)2}$)(Cp^{Me4Et})] exhibits no ligand meshing and has a $G_{complex}$ value which is almost 3% lower than [U(COT$^{(Si\textit{i}Pr3)2}$)(Cp*)]. It is postulated that this is due to the increased sp^3 character of the COT ring carbon atoms, as the Ct–C–Si angles for [U(COT$^{(Si\textit{i}Pr3)2}$)(Cp^{Me4Et})] (170°) bear resemblance to the larger complexes, [U(COT$^{(Si\textit{i}Pr3)2}$)(Cp^{Me4Bz})] and [U(COT$^{(Si\textit{i}Pr3)2}$)(Cp$^{(Si\textit{i}Pr3)2}$)]. These results further demonstrate that caution must be applied to the interpretation of results obtained from crystallographic data, as degrees of freedom exhibited in solution and at varying temperatures cannot be modelled.

Analysis of the steric parameters of [U(COT$^{(Si\textit{i}Pr3)2}$)(Cp^{NMe4})] (**2.5**) supports the idea of an ideal degree of steric saturation. Due to dimerisation it would be anticipated that each metal centre would be shielded to a greater extent than the other complexes. Whilst this is the case when looking at the dimeric unit, calculations illustrate that the pyrrolyl ring is the smallest of all the five-membered rings with the exception of the Cp^{Me} ligand due to lengthening of the U–Cp distance (2.548(3) – 2.567(3) Å). This coupled with the longest U–COT distances (1.967(3) – 1.975(3) Å) and most acute Cp–U–COT angles (138.55(10) and 138.57(11)°) partially counteracts the increase in the $G_{complex}$ value, so that the metal exhibits *ca.* 91% shielding. Whilst these values are almost 10% higher than the G-parameter for [U(COT$^{(Si\textit{i}Pr3)2}$)(Cp*)], they are only 2 – 3% higher than those obtained for the three largest mixed-sandwich complexes and [U(COT$^{(Si\textit{i}Pr3)2}$)(Cp*)(THF)].

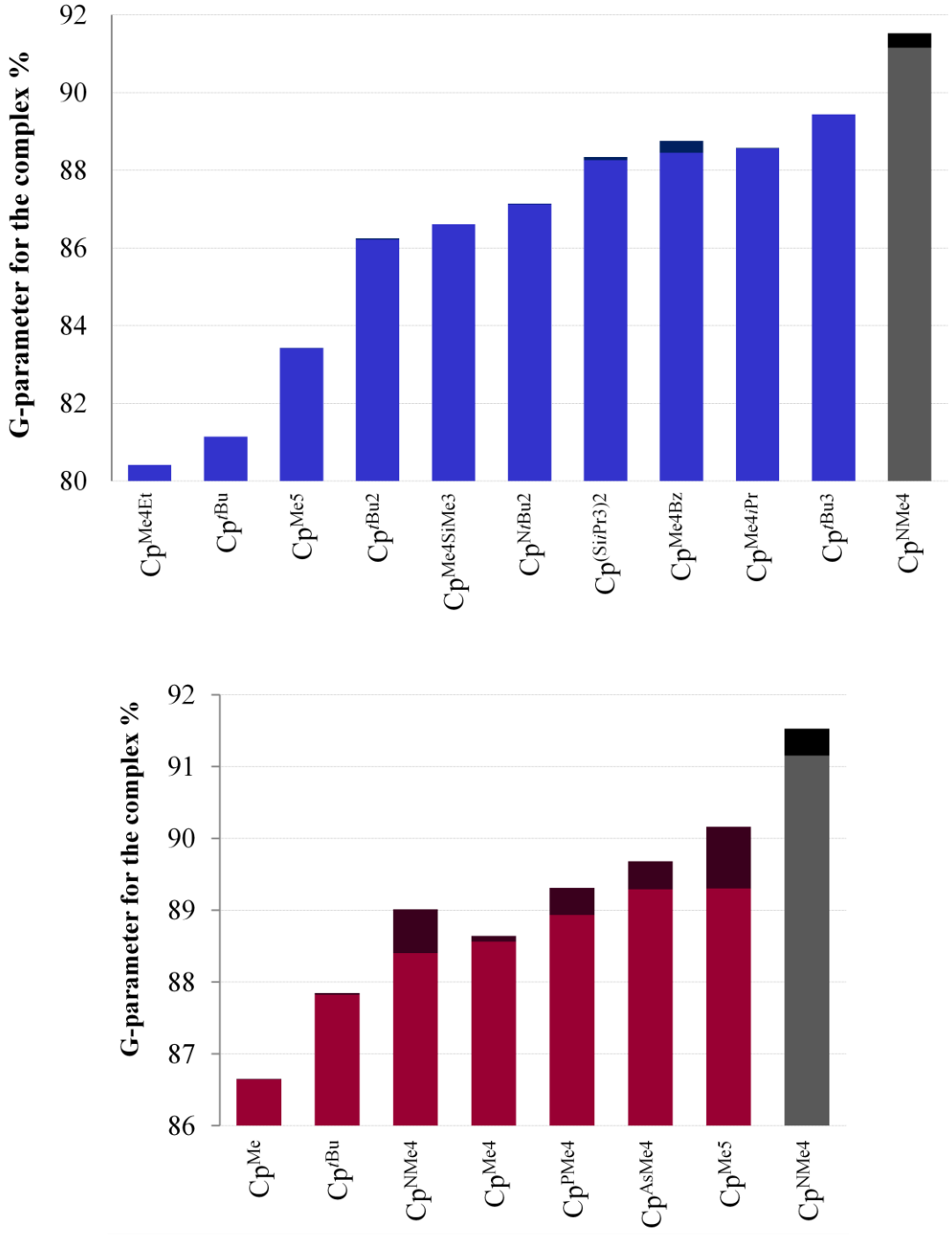

Figure 5.11 The G-parameter ($G_{complex}$) for the mixed-sandwich complexes in ascending order for the base-free complexes (blue) and the THF adducts (red). The pyrrolyl ligand in [U(COT$^{(SiiPr3)2}$)(Cp^{NMe4})] (**2.5**) is shown in grey. The paler colour represents the total shielding (G) and the darker colour represents the overlap parameter (Gγ).

Overlaying the results obtained from carbon monoxide reactivity studies with the calculated Cp^R G-parameters shows that within the [U(COT$^{(SiiPr3)2}$)(Cp^R)] series, any Cp^R ligand that provides more than 35% shielding of the uranium centre precludes reductive activation, and that optimum results are obtained for ligands within the 28 – 31% range (**Figure 5.12**, **Table 5.1**). Given that [U(COT$^{(SiiPr3)2}$)(Cp^{Me4Et})] gives rise to the ynediolate complex contaminated by the deltate complex, it is anticipated that a ligand which provides shielding in the range of 31 – 35% would give rise exclusively to the ynediolate complex.[39]

Comparison of carbon monoxide reactivity with values of $G_{complex}$ however is more difficult because of the anomalous result obtained for [U(COT$^{(SiiPr3)2}$)(Cp^{Me4Et})], and the differing values obtained for THF adducts and base-free complexes. However, it can be ascertained that for the base-free complexes, no reaction occurs when the G-parameter is greater than 86%. Conversely, if the uranium centre is less than 82% shielded there is insufficient steric saturation to stabilise an oxocarbon product and the complex decomposes.

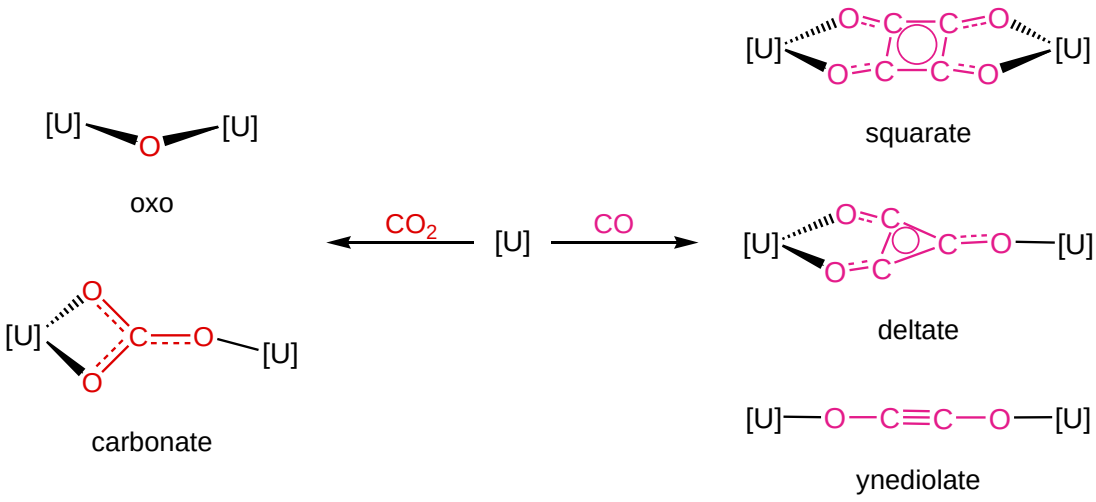

Figure 5.12 Summary of the observed reactivity with CO and CO_2 for the uranium(III) mixed-sandwich complexes studied, with the exception of [U(COT$^{(SiiPr3)2}$)(Cp^{EMe4})] (E = N, P or As), where [U] represents [U(COT$^{(SiiPr3)2}$)(Cp^R)$(THF)_n$].

R	$G_{complex}$	G_{CpR}	Outcome with CO	Outcome with CO_2
Me	*86.64*	*23.97*	unknown	unknown
^{t}Bu	81.14	28.28	decomposition	carbonate
Me_4	*88.56*	*28.56*	squarate	carbonate
Me_5	83.42	30.71	deltate	carbonate
Me_4Et	80.41	30.85	ynediolate and deltate	unidentified mixture
$^t Bu_2$	86.22	35.14	no reaction	oxo
N^tBu_2	8712	35.81	no reaction	oxo
Me_4SiMe_3	86.61	35.98	no reaction	oxo
$Me_4{}^iPr$	88.56	37.54	no reaction	oxo
$^t Bu_3$	89.44	39.56	no reaction	oxo
$(Si^iPr_3)_2$	88.26	39.73	no reaction	oxo
Me_4Bz	88.44	39.96	no reaction	oxo

Table 5.1 Comparison of the shielding parameter G with the observed reactivity for [U(COT$^{(SiiPr3)2}$)(Cp^R)] complexes, where R ≠ EMe_4 (E = N, P or As). All values of G are given for the base-free complexes except when R = Me_4 and R = Me, where values obtained from the THF adduct are shown in italics.

An exception to the trend arises with [U(COT$^{(SiiPr3)2}$)(Cp^{NMe4})], which despite having the highest degree of steric saturation is reactive towards carbon monoxide. However, it was observed during the course of the reactivity studies that the mixture required

heating to initiate, and that the reaction proceeded at a slower rate than the corresponding phospholyl and arsolyl analogues even when heated to 100 °C. It can therefore be concluded that steric saturation still plays a pivotal role in the reactions with the heterocyclic mixed-sandwich complexes.

Reactivity with carbon dioxide can also be compared to the steric saturation of the complexes. In this case, all ligands that impart less than 31% shielding give rise to the bridging carbonate complex, and all ligands with greater than 35% shielding give rise to the bridging oxo complex (**Figure 5.12**, **Table 5.1**). An exception is [U(COT$^{(Si\textit{i}Pr3)2}$)(Cp^{Me4Et})] which gave rise to an unidentified mixture of species.[40] However, in order to obtain a clearer understanding of the steric saturation required for the switch from carbonate to oxo to occur, a ligand that is more sterically saturated than Cp^{Me4Et} (30.85%) but less than Cp$^{\textit{t}Bu2}$ (35.14%) would be required. This would bridge the large gap observed in the $G_{complex}$ values (**Figures 5.10** and **5.11**) and would also provide further insight into carbon monoxide reactivity.

Studies of [U(COT$^{(SiMe3)2}$)(Cp^{R})] complexes by Cloke and Tsoureas have shown the same dependence on sterics regarding the activation of carbon monoxide and carbon dioxide.[39,40] However, whilst calculation of the G-parameters was carried out for these complexes by the author, disorder of some of the structures precluded meaningful comparison with the results discussed here.

5.5 Summary

The G-parameters calculated for the mixed-sandwich complexes synthesised by Cloke *et al.* reveal trends pertaining to the molecular structures and the observed reactivity with carbon monoxide and carbon dioxide. Despite this, anomalies in the data illustrate the shortcomings of using XRD data for the calculations. The data also reveal a sudden increase in the sterics of the mixed-sandwich complexes around the upper limit of

carbon monoxide reactivity and illustrate that more studies are needed to find the precise shielding value that would preclude reactivity.

5.6 Computational details for Chapter 5

The G-parameter was calculated using the Solid-G algorithm, based on the surface area of a sphere.[17] G-parameters were calculated for all individual ligands ($COT^{(Si\mathit{i}Pr3)2}$, Cp^{R} and THF) and $G_{complex}$. Values for the overlap parameter, Gγ, were obtained by summation of the individual G values less $G_{complex}$. All calculated values, their comparison with XRD data and error analyses are given in Appendix II. For the purpose of consistency hydrogen atoms were included in all the calculations. Where there is disorder in the XRD data or multiple complexes in the unit cell, the G-parameters have been calculated for all variants and the average value or range quoted.

G-parameters were calculated for the given XRD data and for normalised data, where the central atom (in all cases uranium) is set to 2.28 Å from a geometrical centre (COT or Cp centroids, THF oxygen atoms or η^1-pyrrolyl nitrogen atoms). Normalised values have not been discussed as the overall trends from both sets of data are the same but the results from these calculations are included in Appendix II.

Analyses of the base-free complexes and THF adducts were kept separate due to the variation in values as a consequence of THF coordination, and where appropriate, values for $[U(COT^{(Si\mathit{i}Pr3)2})(Cp^{NMe4})]$ were compared with both desolvated and solvated complexes.

5.7 References

1 N. Fey, A. G. Orpen and J. N. Harvey, *Coord. Chem. Rev.*, 2009, **253**, 704–722.

2 C. A. Tolman, *Chem. Rev.*, 1977, **77**, 313–348.

3 C. A. Tolman, *J. Am. Chem. Soc.*, 1970, **92**, 2956–2965.

4 C. A. Tolman, W. C. Seidel and L. W. Gosser, *J. Am. Chem. Soc.*, 1974, **96**, 53–60.

5 T. L. Brown, *Inorg. Chem.*, 1992, **31**, 1286–1294.

6 T. Komatsuzaki, K. Sakakibara and M. Hirota, *Tetrahedron Lett.*, 1989, **30**, 3309–3312.

7 M. Hirota, K. Sarakibara, T. Komatsuzaki and I. Akai, *Computers Chem.*, 1991, **15**, 241–248.

8 D. White, B. C. Tavener, P. G. L. Leach and N. J. Coville, *J. Organomet. Chem.*, 1994, **478**, 205–211.

9 B. C. Taverner, *J. Comp. Chem.*, 1996, **17**, 1612–1623.

10 D. P. White, J. C. Anthony and A. O. Oyefeso, *J. Org. Chem*, 1999, **64**, 7707–7716.

11 R. D. Fischer and L. Xing-Fu, *J. Less Common Metals*, 1985, **112**, 303–325.

12 J. M. Smith, S. C. Pelly and N. J. Coville, *J. Organomet. Chem.*, 1996, **525**, 159–166.

13 S. Tryka, *Applied Radiation and Isotopes*, 2012, **70**, 2466–2470.

14 J. A. Bilbrey, A. H. Kazez, J. Locklin and W. D. Allen, *J. Chem. Theory Comput.*, 2013, **9**, 5734–5744.

15 N. Fey, *Dalton Trans.*, 2010, **39**, 296–310.

16 T. L. Brown and K. J. Lee, *Coord. Chem. Rev.*, 1993, **128**, 89–116.

17 I. A. Guzei and M. Wendt, *Dalton Trans.*, 2006, 3991–3999.

18 A. Bondi, *J. Phys. Chem*, 1964, **68**, 441–451.

19 A. Poater, B. Cosenza, A. Correa, S. Gludice, F. Ragone, V. Scarano and L. Cavallo, *Eur. J. Inorg. Chem.*, 2009, 1759–1766.

20 B. R. Dible, R. E. Cowley and P. L. Holland, *Organometallics*, 2011, **30**, 5123–5132.

21 M. R. an der Heiden, H. Plenio, S. Immel, E. Burello, G. Rothenberg and H. C. J. Hoefsloot, *Chem. Eur. J.*, 2008, **14**, 2857–2866.

22 S. B. Muñoz III, W. K. Foster, H.-J. Lin, C. G. Margarit, D. A. Dickie and J. M. Smith, *Inorg. Chem.*, 2012, **51**, 12660–12668.

23 R. E. Cowley and P. L. Holland, *Inorg. Chem.*, 2012, **51**, 8352–8361.

24 J. R. McAtee, G. P. A. Yap and D. A. Watson, *J. Am. Chem. Soc.*, 2014, **136**, 10166–10172.

25 F. T. I. Marx, J. H. L. Jordaan, G. Lachmann and H. C. M. Vosloo, *J. Comp. Chem.*, 2014, **35**, 1457–1463.

26 A. V. Borisov, Z. V. Matsulevich, G. K. Fukin and E. V. Baranov, *Russ. Chem. Bull.*, 2010, **59**, 581–583.

27 Y. P. Barinova, Y. E. Begantsova, N. E. Stolyarova, I. K. Grigorieva, A. V. Cherkasov, G. K. Fukin, Y. A. Kurskii, L. N. Bochkarev and G. A. Abakumov, *Inorg. Chim. Acta*, 2010, **363**, 2313–2317.

28 M. A. Katkova, V. A. Ilichev, G. K. Fukin and M. N. Bochkarev, *Inorg. Chim. Acta*, 2009, **362**, 1393–1395.

29 I. A. Guzei, L. C. Spencer, M. K. Ainooson and J. Darkwa, *Acta Cryst. Sect. C*, 2010, **C66**, m336–m338.

30 F. H. Allen, *Acta Cryst. Sect. B*, 2002, **B58**, 380–388.

31 I. J. Bruno, J. C. Cole, P. R. Edgington, M. Kessler, C. F. Macrae, P. McCabe, J. Pearson and R. Taylor, *Acta Cryst. Sect. B*, 2002, **B58**, 389–397.

32 G. K. Fukin, I. A. Guzei and E. V. Baranov, *J. Coord. Chem.*, 2007, **60**, 937–944.

33 G. K. Fukin, I. A. Guzei and E. V. Baranov, *J. Coord. Chem.*, 2008, **61**, 1678–1688.

34 G. G. Skvortsov, D. M. Lyubov, M. V. Yakovenko, G. K. Fukin, A. V. Cherkasov and A. A. Trifonov, *Russ. Chem. Bull. Int. Ed*, 2009, **58**, 1126–1131.

35 G. G. Skvortsov, M. V. Yakovenko, G. K. Fukin, A. V. Cherkasov and A. A. Trifonov, *Russ. Chem. Bull. Int. Ed*, 2007, **56**, 1742–1748.

36 M. E. Burin, G. K. Fukin and M. N. Bochkarev, *Russ. Chem. Bull.*, 2007, **56**, 1736–1741.

37 O. T. Summerscales, F. G. N. Cloke, P. B. Hitchcock, J. C. Green and N. Hazari, *J. Am. Chem. Soc.*, 2006, **128**, 9602–9603.

38 O. T. Summerscales, F. G. N. Cloke, P. B. Hitchcock, J. C. Green and N. Hazari, *Science*, 2006, **311**, 829–831.

39 N. Tsoureas, O. T. Summerscales, F. G. N. Cloke and S. M. Roe, *Organometallics*, 2013, **32**, 1353–1362.

40 N. Tsoureas, L. Castro, A. F. R. Kilpatrick, F. G. N. Cloke and L. Maron, *Chem. Sci.*, 2014, **5**, 3777–3788.

CHAPTER 6: STUDIES TOWARDS A URANIUM(II) METALLOCENE

The key to life is to have high hopes and no expectations.

6.1 Introduction

Uranium in the +2 oxidation state was, until recently, unisolable. The reductive chemistry exhibited by uranium(III) complexes led to the belief that a uranium(II) complex would not only be a more powerful reducing agent, but would donate two electrons per uranium centre and therefore facilitate an even broader range of reductive transformations.

Despite the recent synthesis of two anionic uranium(II) complexes (**Figure 6.1**), a neutral, formal uranium(II) complex has yet to be reported.[1,2] Evans *et al.* also reported that [K(crypt)][U(Cp^{SiMe3})$_3$] cleaves dihydrogen to yield the uranium(III) anionic complex [K(crypt)][UH(Cp^{SiMe3})$_3$], however further reactivity studies have yet to be published.[1] It is therefore still desirable to synthesise a neutral uranium(II) complex by using sterically demanding cyclopentadienyl ligands.

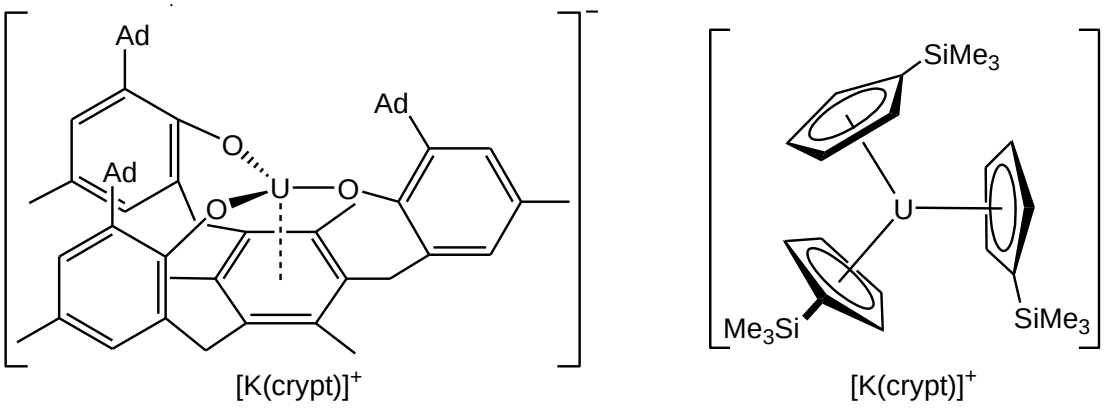

Figure 6.1 The two ionic uranium(II) complexes.[1,2]

6.2 Synthesis of bis(cyclopentadienyl)uranium(III) iodides

*6.2.1 Synthesis and characterisation of [{U(Cp^{tBu2})$_2$}$_2$(μ-I)$_2$] (**6.1**)*

As detailed in Chapter 2, **6.1** was observed as a side product in the synthesis of [U(COT$^{(Si\mathit{i}Pr3)2}$)(Cp$^{\mathit{t}Bu2}$)] (**2.2**). However, direct synthesis could be achieved by reaction of UI_3 with two equivalents of K[Cp$^{\mathit{t}Bu2}$] (**Figure 6.2**). The ^{1}H NMR spectrum of **6.1** exhibits three broad resonances corresponding to two ring-proton environments at 85.8 and -68.5 ppm and a *tert*-butyl resonance at -4.2 ppm. Mass spectrometry and microanalysis were consistent with the proposed formulation.

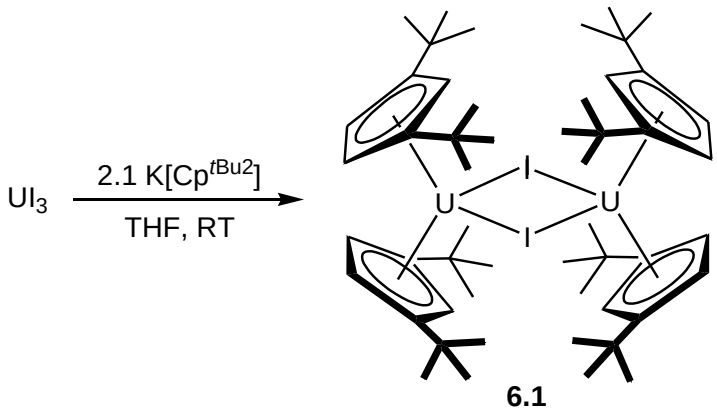

Figure 6.2 Synthetic route to [{U(Cp$^{\mathit{t}Bu2}$)$_2$}$_2$(μ-I)$_2$] (**6.1**).

XRD analysis of **6.1** (**Figure 6.3**) revealed eclipsed cyclopentadienyl rings and a planar U_2I_2 core, which has U–I bond lengths and U–I–U angles that are similar to [{(COT$^{(Si\mathit{i}Pr3)2}$)U(OSiMe$_3$)}$_2$(μ-I)$_2$] (**4.17**) and fall within the range of values reported in the literature (U–I 3.0764(12) – 3.3768(7) Å, U–I–U 99.23(1) – 103.551(13)° and I–U–I 76.449(13) – 79.58(9)°).[3–5] A similar complex synthesised by Cloke *et al.*, [{U(Pn$^{(Si\mathit{i}Pr3)2}$)(Cp*)}$_2$(μ-I)$_2$], exhibits slightly longer uranium-iodide distances

(3.1997(8) to 3.3584(9) Å) and more acute I–U–I angles (70.98(2) and 71.46(2)°).[6] These differences may be attributed to the larger size of the pentalene ligand relative to the cyclopentadienyl ligand, which encourages longer U–I distances in order to minimise steric crowding.

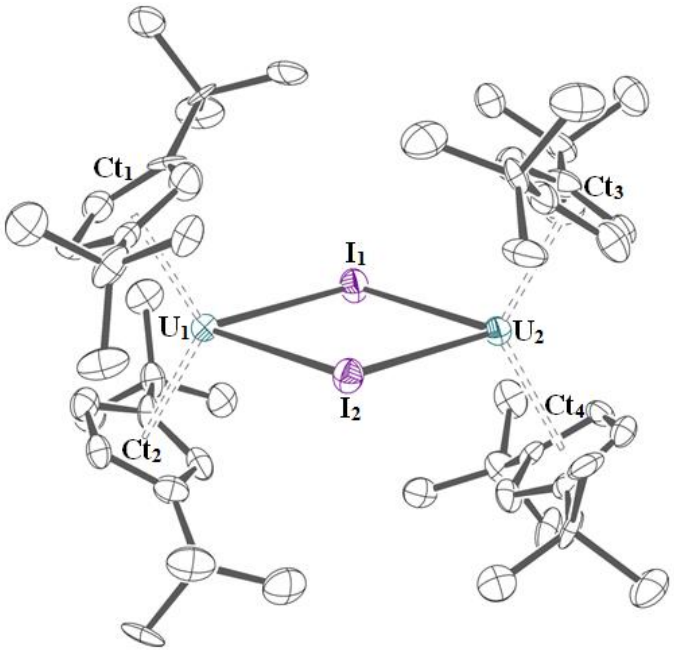

Figure 6.3 ORTEP view of **6.1** with thermal ellipsoids at 50% probability; hydrogen atoms have been omitted for clarity.

Several structures of the type $[\{(Cp^{R})_2U\}_2(\mu\text{-}X)_2]$ have previously been reported. $[\{(Cp^{tBu2})_2U\}_2(\mu\text{-}Cl)_2]$, synthesised by Andersen and co-workers, has very similar U–Ct distances to **6.1** (2.517(8) and 2.515(7) Å) with variation in the U–X bond distances and angles arising from the smaller halide.[7] This is also true for $[\{(Cp^{(SiMe3)2})_2U\}_2(\mu\text{-}X)_2]$ complexes (X = Br, Cl or F) and further demonstrates that the U–U distance shortens as the halide becomes smaller (4.335(7) Å for Br, 4.357(1) Å for Cl and 3.8505(9) Å for F).[8,9]

Distances (Å)					
Ct_1–U_1	2.5154(6)	**Ct_2–U_1**	2.5210(6)	**Ct_3–U_2**	2.5110(6)
Ct_4–U_2	2.5145(6)	**U_1–I_1**	3.1894(11)	**U_2–I_1**	3.1929(11)
U_1–I_2	3.1990(11)	**U_2–I_2**	3.2113(11)	**U_1–U_2**	4.93430(18)
Angles (°)					
Ct_1–U_1–Ct_2	123.71(3)	**Ct_3–U_2–Ct_4**	123.97(3)	**U_1–I_1–U_2**	101.27(3)
U_1–I_2–U_2	100.66(3)	**I_1–U_1–I_2**	79.15(3)	**I_1–U_2–I_2**	78.92(3)

Table 6.1 Bond lengths, distances and angles for **6.1**. $Ct_1 – Ct_4$ are the centroids for the Cp^{tBu2} ligands.

*6.2.2 Synthesis and characterisation of [{U(Cp$^{(SiiPr3)2}$)$_2$}$_2$(μ-I)$_2$] (**6.2**)*

Following the successful synthesis of **6.1**, the larger analogue, [{U(Cp$^{(SiiPr3)2}$)$_2$}$_2$(μ-I)$_2$] (**6.2**) was prepared. However, despite the steric crowding imposed by the substituents, three different samples were isolated, including the base-free complex (**6.2**), the THF adduct, [UI(Cp$^{(SiiPr3)2}$)$_2$(THF)] (**6.2THF**), and the DME solvated ate-complex, [U(Cp$^{(SiiPr3)2}$)$_2$I$_2$K(DME)$_2$] (**6.2DME**, **Figure 6.4**).

6.2THF was obtained as a bright green complex from a solution of UI_3 and K[Cp$^{(SiiPr3)2}$] in THF. However, removal of the coordinated solvent molecule proved difficult and was achieved either by heating the residue *in vacuo* (10^{-6} mbar) at 100 °C, or by removal of toluene *in vacuo* from a crude solution at the same temperature. However both methods of desolvation were ineffective for large quantities of the complex and rarely removed all traces of THF. Repetition of the reaction in other ethereal solvents resulted in the formation of the ate-complex [U(Cp$^{(SiiPr3)2}$)$_2$I$_2$K(DME)$_2$] (**6.2DME**) from

DME, and the desired base-free complex [{U($Cp^{(SiiPr3)2}$)$_2$}$_2$(μ-I)$_2$] (**6.2**) from diethyl ether. NMR spectroscopy revealed **6.2**, **6.2THF** and **6.3DME** are dynamic in solution, illustrating that the bulky substituents do not impede rotation of the $Cp^{(SiiPr3)2}$ ligands at ambient temperature.

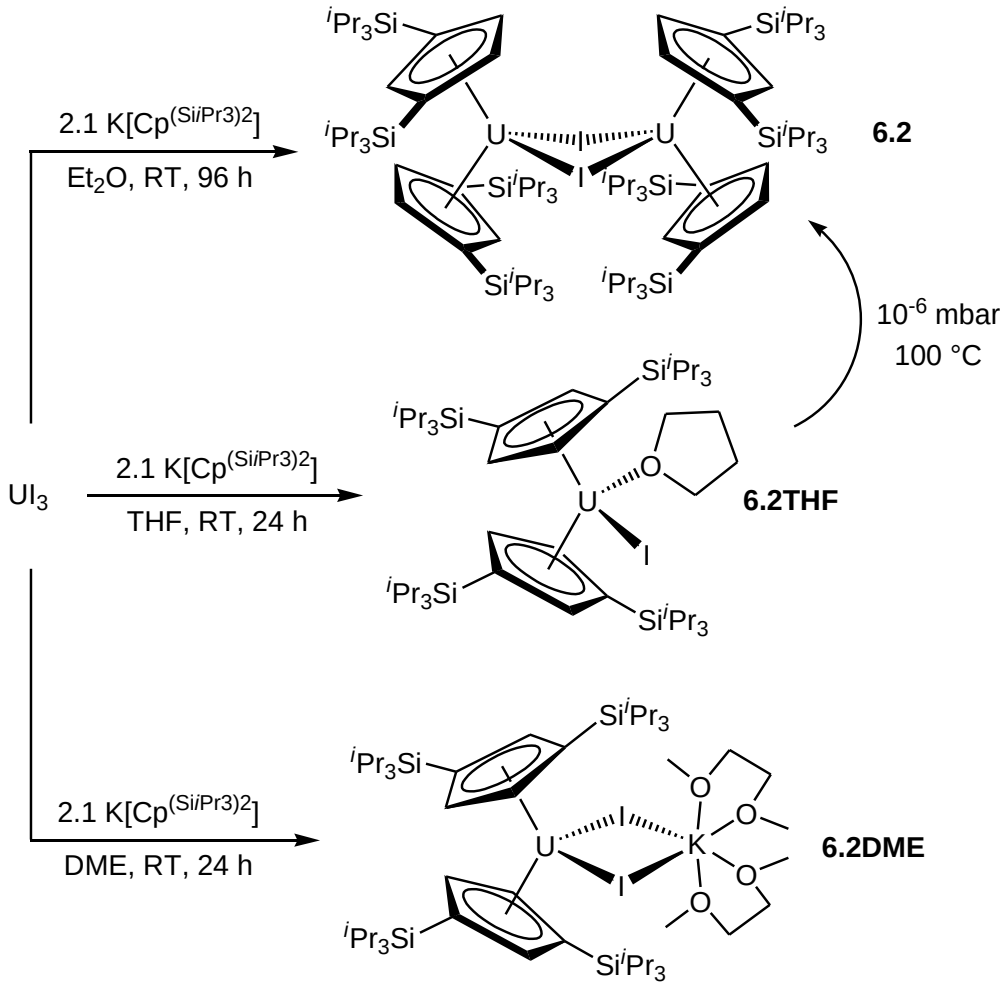

Figure 6.4 Synthetic routes to [{U($Cp^{(SiiPr3)2}$)$_2$}$_2$(μ-I)$_2$] (**6.2**).

6.2.2.1 Molecular structure of [{U($Cp^{(SiiPr3)2}$)$_2$}$_2$(μ-I)$_2$] (**6.2**).

There are two notable features about the solid-state structure of **6.2** in comparison to **6.1** and other [{(Cp^R)$_2$U}$_2$(μ-X)$_2$] complexes (**Figure 6.5**). Firstly, the cyclopentadienyl rings are not eclipsed due to steric repulsion of the silyl groups. This allows the U–Ct distances to remain at *ca.* 2.5 Å, although has given rise to obtuse Ct–U–Ct angles. The

second feature of this complex is that the iodides lie 0.4341(5) Å below the plane, thereby maintaining the normal bond lengths and angles within the unit despite the increased sterics of this complex.

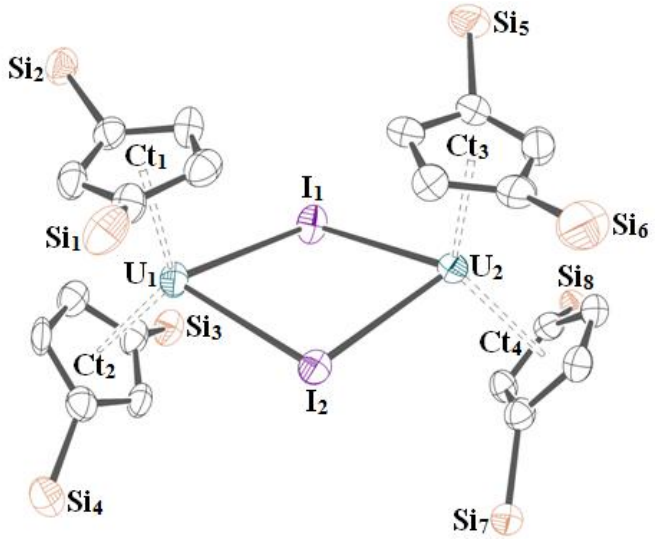

Figure 6.5 ORTEP view of **6.2** with thermal ellipsoids at 50% probability; hydrogen atoms and Cp *iso*-propyl groups have been omitted for clarity.

Distances (Å)					
Ct_1–U_1	2.5038(5)	**Ct_2–U_1**	2.5154(5)	**Ct_3–U_2**	2.5184(5)
Ct_4–U_2	2.5094(5)	**U_1–I_1**	3.1961(7)	**U_2–I_1**	3.1938(7)
U_1–I_2	3.2364(7)	**U_2–I_2**	3.1846(7)	**U_1–U_2**	4.9099(6)
Angles (°)					
Ct_1–U_1–Ct_2	128.225(17)	**Ct_3–U_2–Ct_4**	130.047(17)	**U_1–I_1–U_2**	100.420(19)
U_1–I_2–U_2	99.751(18)	**I_1–U_1–I_2**	77.382(17)	**I_1–U_2–I_2**	78.166(17)

Table 6.2 Bond lengths, distances and angles for **6.2**. Ct_1 – Ct_4 are the centroids for the $Cp^{(SiiPr3)2}$ ligands.

6.2.2.2 Molecular structures of [UI($Cp^{(SiiPr3)2}$)$_2$(THF)] and [U($Cp^{(SiiPr3)2}$)$_2$I$_2$K(DME)$_2$]

Single crystals of **6.2THF** and **6.2DME** were obtained by cooling saturated pentane solutions to -35 °C. **6.2THF** was solved with two molecules in the unit cell (**Figure 6.6**), and **6.2DME** exhibited a mirror plane (**Figure 6.7**).

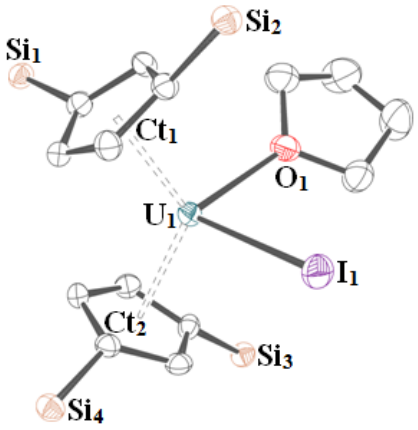

Figure 6.6 ORTEP view of **6.2THF** with thermal ellipsoids at 50% probability; hydrogen atoms and Cp *iso*-propyl groups have been omitted for clarity. Selected bond distances (Å) and angles (°): U_1–Ct_1 2.5274(3), 2.5132(3); U_1–Ct_2 2.5170(3), 2.5201(3); U_1–I_1 3.0673(5), 3.0554(5); U_1–O_1 2.534(4), 2.557(5); Ct_1–U_1–Ct_2 123.612(12), 122.795(12).

Comparison of **6.2THF** and **6.2DME** with the base-free complex shows a marginal increase in the U–Ct distances and a large decrease in the Ct–U–Ct angles, so that these complexes bear more resemblance to **6.1**. The U–I distance in **6.2THF** is slightly shorter than the other complexes as the iodide is terminal instead of bridging. The angles within the UI_2K core are also more distorted than in the cores of **6.1** and **6.2** due to the longer potassium–iodide contacts. Other uranium halide ate-complexes have also been structurally characteried.[10] XRD analysis of [($Cp^{(SiMe3)2}$)$_2$$UCl_2$Li(THF)$_2$] and [($Cp^{(SiMe3)2}$)$_2$$UCl_2$Li(pmdta)$_2$] show both complexes have a planar UCl_2Li unit and staggered Cp conformations.

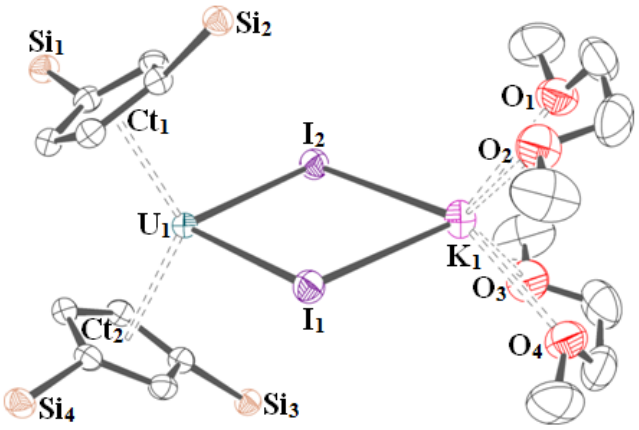

Figure 6.7 ORTEP view of **6.2DME** with thermal ellipsoids at 50% probability; hydrogen atoms and Cp *iso*-propyl groups have been omitted for clarity. Selected distances (Å) and angles (°): U_1–Ct_1 2.52954(14); U_1–I_1 3.1350(2); K_1–I_1 3.3993(8); U_1–K_1 4.73608(6); Ct_1–U_1–Ct_2 123.909(12); U_1–I_1–K_1 92.816(13); I_1–U_1–I_2 91.596(8); I_1–U_1–I_2 82.77(2).

*6.2.3 Cyclic voltammetry of [{U(Cp^{tBu2})$_2$}$_2$(μ-I)$_2$] (**6.1**) and [UI(Cp$^{(SiiPr3)2}$)$_2$(THF)]$_2$ (**6.2THF**)*

As the U^{IV}/U^{III} redox couple for mixed-sandwich complexes is already very negative (*ca.* -2.1 V *vs* $[FeCp_2]^{+/0}$), it was anticipated that the U^{III}/U^{II} redox couple would occur at a potential more negative than -2.5 V, and might occur outside the electrochemical window of the $[^nBu_4N][PF_6]$/THF medium. Studies of **6.1** and **6.2THF** were conducted under comparable conditions and sections of the cyclic voltammograms are shown in **Figure 6.8**.

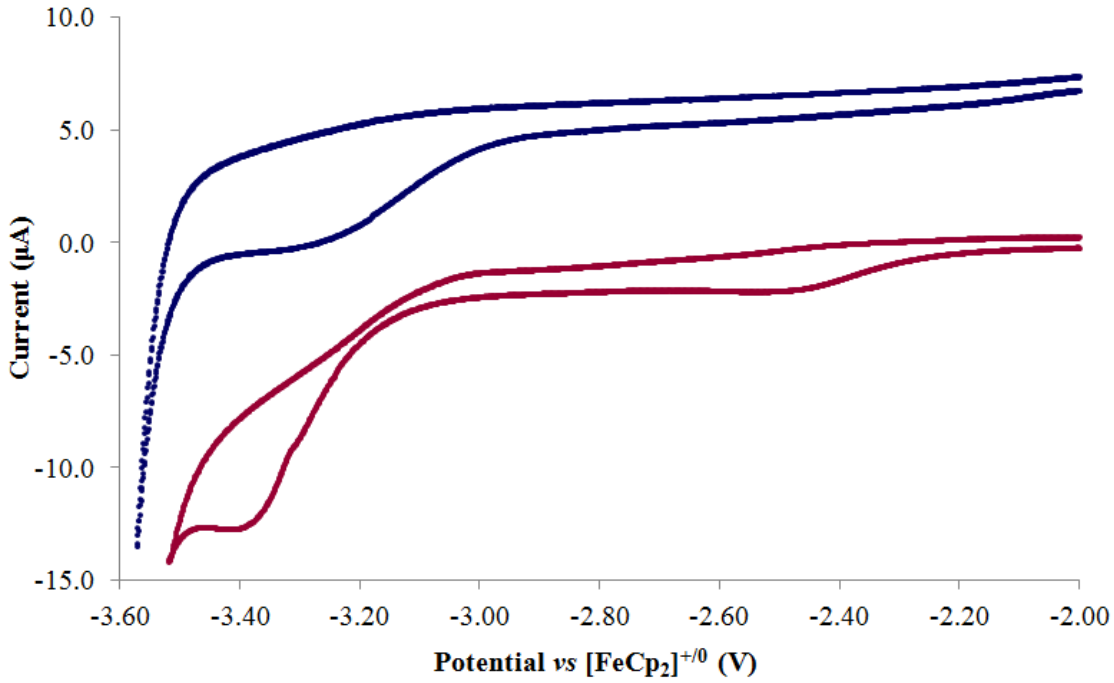

Figure 6.8 Cyclic voltammograms of 5.0 mM solutions of **6.1** (bottom) and **6.2b** (top) in 0.05 M [^{n}Bu$_4$N][PF$_6$]/THF at 100 mVs^{-1}, showing the first cycle only.

Both complexes exhibit an irreversible half-wave close to the solvent breakdown. Repeated scans between -2.8 and -3.5 V gave rise to loss of the half-wave and fouling of the working electrode, illustrating the instability of the observed species. As a consequence the potentials at which these processes occur can only be considered approximate, although Ep_c values were found to be *ca.* -3.4 V *vs* $[FeCp_2]^{+/0}$ for $[\{U(Cp^{tBu2})_2\}_2(\mu\text{-}I)_2]$ and in the region of -3.1 to -3.4 V for $[UI(Cp^{(SiiPr3)2})_2(THF)]$. If these processes correspond to the U^{III}/U^{II} redox couple, their highly negative potentials illustrate that the uranium(II) oxidation state will highly reactive (for example towards solvents) and as a consequence may not be isolable.

6.2.4 Calculating the G-parameter for bis(cyclopentadienyl)uranium(III) iodides

One of the main considerations when choosing an appropriate cyclopentadienyl ligand for a uranium(II) metallocene is the steric properties imposed by the substituents. As previous calculations illustrated the larger size of the $Cp^{(Si\mathit{i}Pr3)2}$ ligand in comparison to $Cp^{\mathit{t}Bu2}$ (Chapter 5), it was considered that **6.2** might provide the additional steric stabilisation required. However, XRD studies have shown that despite the size of this ligand, coordination of solvent molecules, and dimerisation of the base-free complex still occurs, illustrating that this complex is not coordinatively saturated. Calculations of the G-parameter, for the four complexes and their ligands discussed thus far are presented in **Table 6.3**.

	6.1	**6.2**	**6.2THF**	**6.2DME**
$\mathbf{G_{complex}}$	91.06 - 91.14	95.21 - 95.36	92.83 - 93.65	95.35
Gγ	0.48 - 0.54	3.86 - 4.97	1.17 - 1.41	0.00
$\mathbf{G_{CpR}}$	31.74 - 32.01	33.44 - 35.88	34.79 - 36.07	36.30
$\mathbf{G_{iodide}}$	10.15 - 10.32	9.98 - 10.37	11.27 - 11.38	10.73 - 10.76
$\mathbf{G_{THF}}$	-	-	12.09 - 12.49	-

Table 6.3 The steric parameters, G, calculated for **6.1** and **6.2**, including values for the individual ligands and the overlap parameter, Gγ. All values are expressed as a percentage, and a range of values is given where more than one value was obtained.

The values for the G-parameter show that the shielding in all the complexes is high, with $[\{U(Cp^{(Si\mathit{i}Pr3)2})_2\}_2(\mu\text{-}I)_2]$ (**6.2**) and **6.2DME** exhibiting the most sterically protected

metal centres. This further rationalises the differences in the molecular structures for [{U(Cp^{tBu2})$_2$}$_2$(μ-I)$_2$] (**6.1**) and [{U($Cp^{(SiiPr3)2}$)$_2$}$_2$(μ-I)$_2$] **6.2** in regards to a non-planar core and staggered cyclopentadienyl rings. It is also observed for **6.2** that the silyl substituents are able to mesh effectively, thereby lowering the values of $G_{complex}$ by up to 5%.

Analysis of the only monomeric complex, [UI($Cp^{(SiiPr3)2}$)$_2$(THF)] (**6.2THF**), illustrates that the U–I and U–Cp bonds are shorter and the overlap parameter is reduced in comparison to **6.2** in order to compensate for the size difference of THF *vs* a second [U($Cp^{(SiiPr3)2}$)$_2$)$_2$I] unit. The degree to which the ligands shield the metal is illustrated by the space-filling model in **Figure 6.9**, which shows small scattered areas in which the metal complex exhibits no shielding (no colour). These results demonstrate the conformational changes complexes undergo in order to maintain an ideal steric environment. It is therefore difficult to conclude whether the steric parameters of **6.1** and **6.2** are sufficient to stabilise a uranium(II) metallocene, as it is anticipated that conformational changes would arise in order to fill the coordination sphere to compensate for the loss of the iodide and solvent ligands.

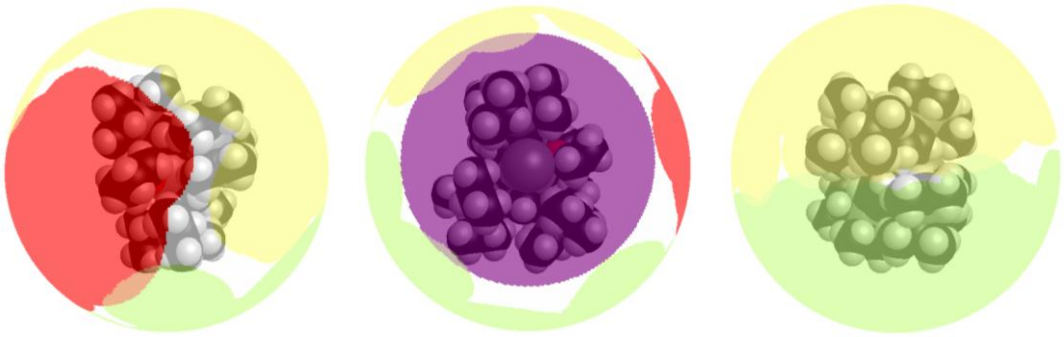

Figure 6.9 Three space-filling views of **6.2THF**. The $Cp^{(SiiPr3)2}$ ligands are represented by yellow and green shadows, THF is shown by the red shadow and the iodide ligand is illustrated by the purple shadow. White areas between the ligands represent parts of the metal centre that are not shielded.

6.3 Reactivity of [{U(Cp^{R})$_2$}$_2$(μ-I)$_2$] with reducing agents

Although there is insufficient evidence to suggest that the sterics of the Cp$^{(SiiPr3)2}$ and Cp^{tBu2} ligands are large enough to sterically protect a uranium(II) centre, reactivity of these complexes with reducing agents was explored. The electrochemical data suggest that the U^{III}/U^{II} redox couple is in the order of magnitude of the M^{+}/M redox couples for the alkali metals, and potassium based reducing agents were therefore employed for these reactions.[11]

*6.3.1 Attempted reduction of [{U(Cp$^{(SiiPr3)2}$)$_2$}$_2$(μ-I)$_2$] (**6.2**)*

Attempts to reduce **6.2** with potassium graphite or sodium-potassium alloy were unsuccessful and the results varied according to the stoichiometry of reducing agent employed. With one mole equivalent, little change was observed and the resulting solution predominantly contained the uranium(III) complex with traces free Cp$^{(SiiPr3)2}$ ligand. However as the stoichiometry of reducing agent was increased the degree of decomposition increased until the Cp$^{(SiiPr3)2}$ ligand was the only characterised species remaining in solution. Repetition of these reactions with [UI(Cp$^{(SiiPr3)2}$)$_2$(THF)] and [U(Cp$^{(SiiPr3)2}$)$_2$I$_2$K(DME)$_2$] yielded similar results with the formation of dark solutions from which crystals of the sodium/potassium salt of the cyclopentadienyl ligand were obtained.

*6.3.2 Reactivity of [{U(Cp^{tBu2})$_2$}$_2$(μ-I)$_2$] (**6.1**) with potassium graphite*

Addition of potassium graphite to a solution of **6.1** resulted in a gradual colour change from green to olive. Monitoring the reaction by NMR spectroscopy illustrated the quantitative conversion of [{U(Cp^{tBu2})$_2$}$_2$(μ-I)$_2$] to a new complex (**6.3**) over several

days (**Figure 6.10**). This complex was identified crystallographically as [U(Cp^{tBu2})$_3$], possibly formed by the reduction of [{U(Cp^{tBu2})$_2$}$_2$(μ-I)$_2$] and disproportionation of [U(Cp^{tBu2})$_2$]. This species can alternatively be synthesised by salt metathesis of UI_3 and K[Cp^{tBu2}], however the isolated yields from this reaction are poor (<10%) and synthesis of **6.3** by reaction of **6.1** with potassium graphite was the more efficient route (29% yield with respect to UI_3).

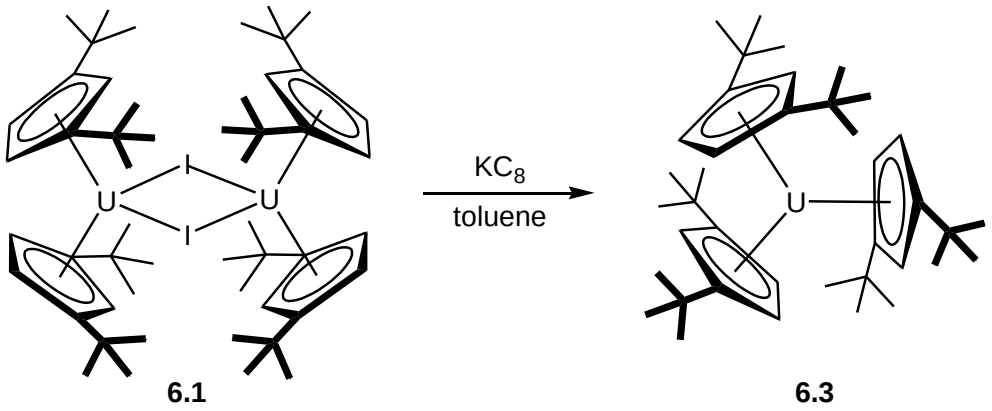

6.1 **6.3**

Figure 6.10 The synthesis of [U(Cp^{tBu2})$_3$].

6.3.1.1 Characterisation of [U(Cp^{tBu2})$_3$] (**6.3**)

The ^{1}H NMR spectrum of **6.3** displays three resonances corresponding to two ring proton environments at 26.3 and -16.0 ppm and a *tert*-butyl resonance at -11.2 ppm. Mass spectrometry also confirmed the formulation of **6.3**; however characterisation by microanalysis repeatedly yielded low values of carbon and hydrogen as the complex was found to slowly decompose in the absence of solvent. Single crystals of **6.3** were obtained by slow cooling a saturated pentane solution to -35 °C and selected data are presented with **Figure 6.11**.

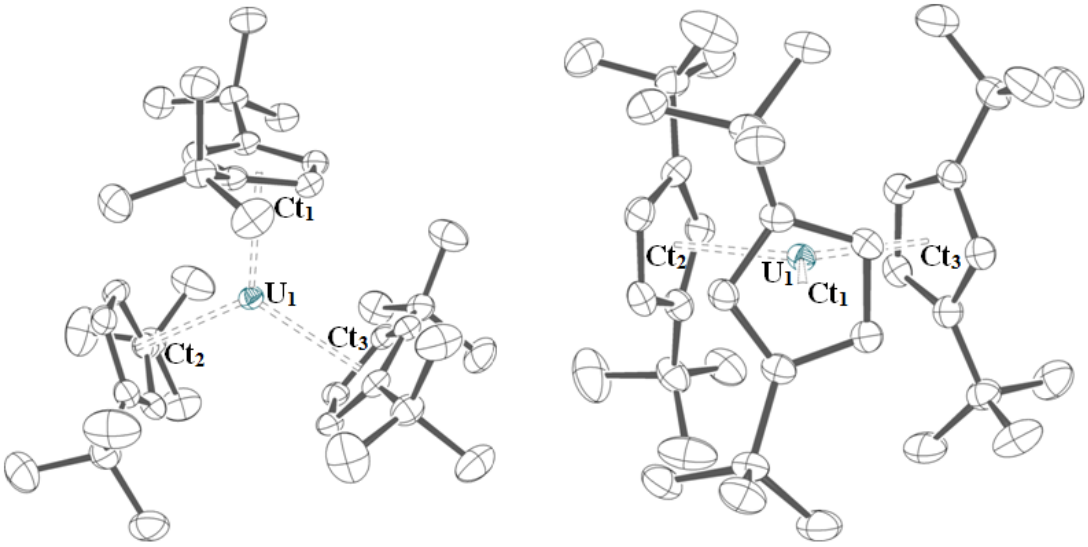

Figure 6.11 ORTEP views of **6.3** from the side (left) and top (right) with thermal ellipsoids at 50% probability; hydrogen atoms have been omitted for clarity. Selected bond distances (Å) and angles (°): U_1–Ct_1 2.5657(3), U_1–Ct_2 2.5807(3), U_1–Ct_3 2.5635(3), U_1–C_n 2.729(3) – 2.939(3), Ct_1–U_1–Ct_2 119.883(13), Ct_1–U_1–Ct_3 119.691(13), Ct_2–U_1–Ct_3 120.426(13).

Seven other $[U(Cp^R)_3]$ complexes have been published, all of which exhibit *ca*. 120° Ct–U–Ct angles in order to maintain maximum separation of the rings and their substituents.[12–17] It is observed that as the number and size of the substituents increase the U–Ct and U–C(Cp) distances increase, however the degree of ring slippage appears to be dependent only on the number of substituents so that a symmetrical ring such as Cp* exhibits slightly less slippage (U_1–C_n 2.813(2) – 2.920(5) Å) than $Cp^{(SiMe3)2}$ (U_1–C_n 2.741(11) – 2.86(1) Å). An analogous cerium complex, $[Ce(Cp^{tBu2})_3]$, also exhibits a similar structure with a *ca*. 120° Ct–Ce–Ct angle but less ring slippage than **6.3** (Ce_1–C_n 2.766(8) – 2.929(7) Å).[18]

6.3.3 Reactivity of [{U(Cp^R)$_2$}$_2$(μ-I)$_2$] with potassium graphite in the presence of a Lewis acid

It was speculated that the formation of [U(Cp^{tBu2})$_3$] from [{U(Cp^{tBu2})$_2$}$_2$(μ-I)$_2$] proceeds *via* a uranium(II) species, which then disproportionates to yield **6.3** and uranium metal. If this were the case it was postulated that the uranium(II) complex could be trapped by the addition of a Lewis acid. This could result in the formation of an adduct, whereby the uranium centre donates electron density to the acid in order to stabilise the +2 oxidation state. Alternatively the transient uranium(II) species could reductively activate the Lewis acid to yield a uranium(III) or uranium(IV) complex. Attempts to trap an intermediate using excess CO were unsuccessful and either resulted in the formation of contaminated [U(Cp^{tBu2})$_3$] or led to decomposition. Therefore alternative Lewis acids were considered.

The propensity for group 13 molecules to accept electron density from Lewis bases is well documented and a small borane was therefore considered a good choice of electron-acceptor to trap a uranium(II) species. Reactivity of [{U(Cp^{tBu2})$_2$}$_2$(μ-I)$_2$] with potassium graphite and BH$_3$·THF gave rise to the formation of multiple species which included a significant yield of [U(Cp^{tBu2})$_3$]. Separation of these species by filtration and crystallisation resulted in the formation of a borane/borohydride containing complex, [{U(Cp^{tBu2})$_2$}$_2$(μ-BH$_x$)$_2$] (**6.4, Figure 6.12**) which was dimeric in the solid state.

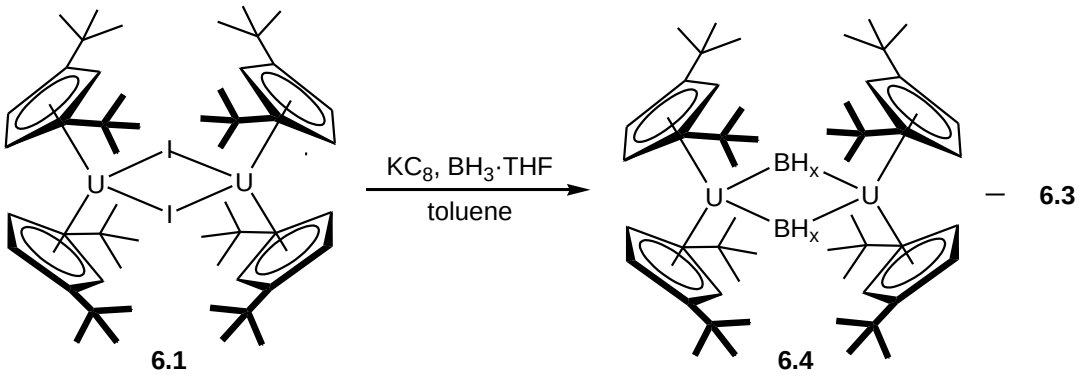

Figure 6.12 Reactivity of [{U(Cp^{tBu2})$_2$}$_2$(μ-I)$_2$] with BH$_3$·THF and potassium graphite.

Applying the same reaction conditions to [{U($Cp^{(Si\mathit{i}Pr3)2}$)$_2$}$_2$(μ-I)$_2$] gave rise to the formation of one or more new species, evidenced by two boron resonances at 211 and 181 ppm, and two silicon resonances at 109 and 124 ppm. Mass spectrometry however showed a peak at *m/z* = 1007, indicating the formation of an analogous borane/borohydride species [{U($Cp^{(Si\mathit{i}Pr3)2}$)$_2$}$_2$(μ-BH_x)$_2$] (**6.5**). Further characterisation of this species was precluded by the complex mixture of products in solution.

Boranes have seen limited use in organoactinide chemistry. However, reactions of BH_3·THF with [UCp_3X] complexes, where X is an amide, alkoxide or alkyl ligand, illustrate the formation the borohydride complex, [$Cp_3U(BH_4)$] by migratory insertion of borane into the U–E bond (E = N, O, or C), followed by σ-bond methathesis.[19–21] Few uranium(III) borohydride complexes have been reported, and the closest analogues to **6.4** are the dimeric tetramethylphospholyl complexes, [(Cp^{PMe4})$_2$U(BH_4)] and [(Cp^{PMe4})(Cp*)U(BH_4)].[22–24] However, the samarium complex, [{(Cp^*)$_2$Sm}$_2$(μ-$AlMe_4$)$_2$], bears the most structural resemblance to **6.4**, and was synthesised by reaction of the samarium(II) metallocene with $AlMe_3$.[25] The synthesis of **6.4** therefore represents a method for the synthesis of novel organouranium complexes derived from group 13 Lewis acids.

6.3.3.1 Characterisation of [{U($Cp^{t\mathrm{Bu}2}$)$_2$}$_2$(μ-BH_x)$_2$] (**6.4**)

NMR characterisation of **6.4** revealed four proton environments corresponding to the cyclopentadienyl resonances and the BH_x unit. However the linewidths and overlap of these resonances precludes assignment of all but the *tert*-butyl environment and inhibits definitive assignment of x in the BH_x unit. Mass spectrometry confirmed the formulation of **6.4** with a parent ion at *m/z* = 607. However, whilst this value indicates a borohydride unit, the exact value of x cannot be inferred using this method.

XRD analysis of **6.4** was complicated by twinning, which was present in samples obtained from several solutions. The data must therefore be treated with a degree of caution; however the molecular structure is shown to be dimeric, with BH_x units perpendicular to the [U(Cp^{tBu2})$_2$] fragment (**Figure 6.13**). The BH_x moieties appear to be in-plane with the uranium atoms, and the cyclopentadienyl ligands are eclipsed giving rise to a structure that is very similar to the iodide precursor. Approximate U–B distances in this complex lie in the range of 2.9 – 3.2 Å, which are comparable to both terminal uranium borohydride complexes (2.489(17) – 2.921(11) Å) and bridging uranium borohydride complexes (2.85(3) – 2.88(3) Å).[26,27] However, the nature of the BH_x unit cannot be inferred from these data.

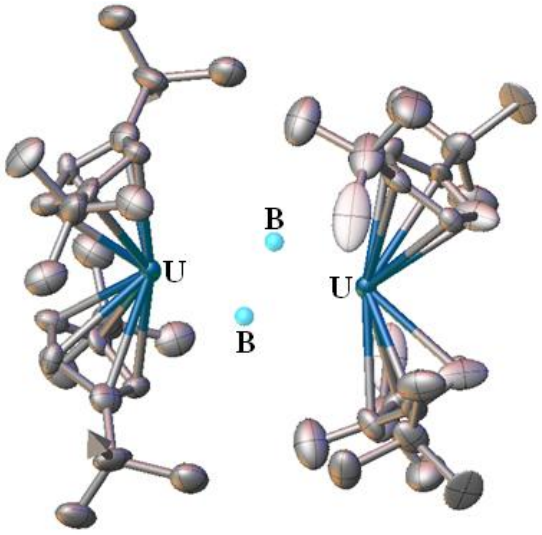

Figure 6.13 Olex2 view of **6.4** with thermal ellipsoids at 50% probability for carbon and uranium atoms and isotropic boron atoms; hydrogen atoms have been omitted for clarity.

6.4 Synthesis of a uranium tetraphenylborate complex

An alternative strategy for synthesising a uranium(II) species involved synthesis of a uranium(III) cation, which may or may not coordinate the tetraphenylborate counterion. The steric properties of such cationic species could also be evaluated and compared to the uranium(III) iodide precursors, thereby providing further evidence of the suitability (or otherwise) of these ligands for the synthesis of a uranium(II) metallocene.

Uranium(III) tetraphenylborate complexes are known in the literature, and studies by Evans *et al.* on the synthesis of the $[(Cp^*)_2U]^+$ moiety illustrate that in the presence of a coordinating solvent, discreet ions are formed (**Figure 6.14**).[28] However in the absence of the solvent, uranium interacts in an η^1-fashion to two of the phenyl rings in order to saturate its coordination sphere. The Cp^{Me4} analogue was also synthesised but only coordinates through one phenyl ring *via* an η^3-interaction.[29]

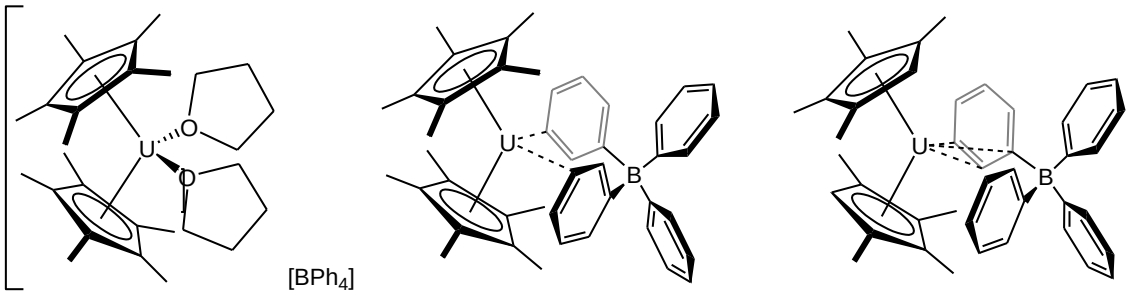

Figure 6.14 Three bis(cyclopentadienyl)uranium tetraphenylborate complexes.[28,29]

6.4.1 Reactivity of $[\{U(Cp^R)_2\}_2(\mu\text{-}I)_2]$ with potassium benzyl and $[NEt_3H][BPh_4]$

The three complexes discussed above were synthesised by protonolysis of the uranium(III) alkyl complexes, $[(Cp^R)_2UMe_2K]$.[28,29] An adaptation of this methodology was therefore employed in the attempted synthesis of a bis(cyclopentadienyl)uranium cation. The strategy outlined in **Figure 6.15**, was to replace the iodide ligand with a

benzyl moiety, which could then be protonated to yield toluene and the desired cationic complex.

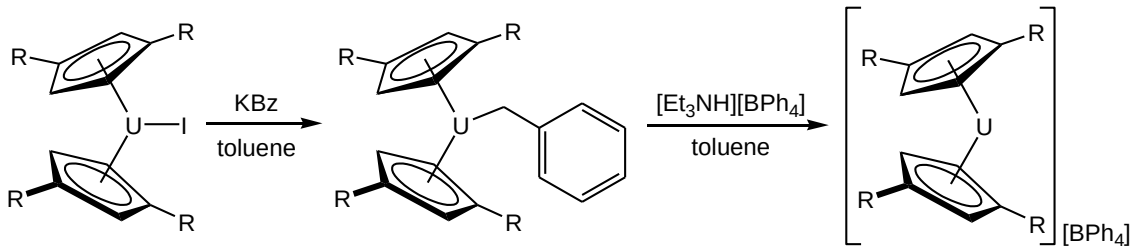

Figure 6.15 Synthetic route to $[U(Cp^{R})_2][BPh_4]$ complexes, where R = ^{t}Bu or Si^{i}Pr$_3$.

Characterisation of the benzyl complexes was not achieved due to difficulties in obtaining analytically pure samples. Nevertheless, the second step of the reaction was undertaken using the crude material from the reaction. Addition of $[NEt_3H][BPh_4]$ to the solutions in d_8-toluene gave rise to changes in the NMR spectra over several days. Identification and characterisation of the Cp$^{t\mathrm{Bu2}}$-based complex was not achieved, however, XRD analysis of crystals of the Cp$^{\mathrm{Si}i\mathrm{Pr3}}$-based product revealed the loss of one of the cyclopentadienyl rings to yield a mono(cyclopentadienyl)uranium tetraphenylborate complex, $[(Cp^{(\mathrm{Si}i\mathrm{Pr3})2})U(\mu\text{-}Ph)_2BPh_2]$ (**6.6**) in 60% yield **(Figure 6.16**).

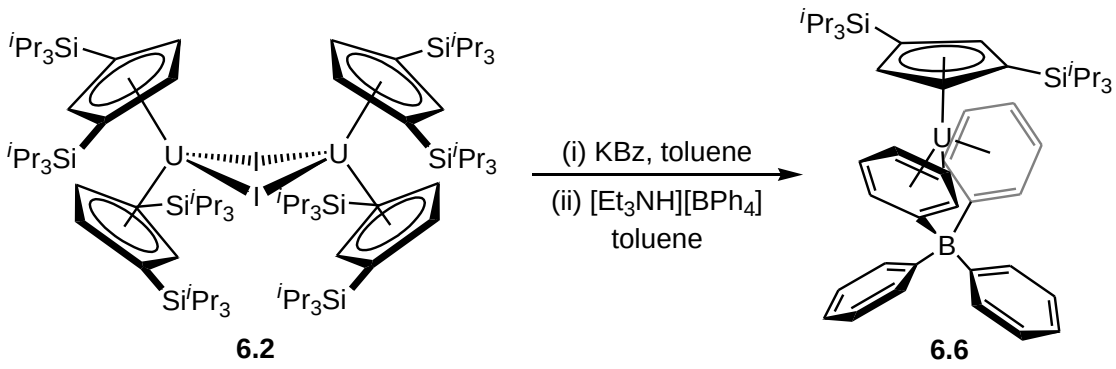

Figure 6.16 Synthesis of $[(Cp^{(\mathrm{Si}i\mathrm{Pr3})2})U(\mu\text{-}Ph)_2BPh_2)]$.

6.4.1.1 Characterisation of $[(Cp^{(SiiPr3)2})U(\mu\text{-}Ph)_2BPh_2]$

The ^1H NMR spectrum of a solution of **6.6** was complicated due to the number of overlapping resonances. However a single silicon resonance at -104.5 ppm illustrated that the complex is dynamic in solution. Microanalysis of the complex supported the formulation, and the mass spectrum showed two peaks at *m/z* = 770 and 1100 for $M^+ - BPh_2$ and $M^+ + BPh_2$ respectively. Attempts to determine the presence of a hydride bound to the uranium centre were inconclusive by these methods and infrared spectroscopy, due to the number of absorption bands between 1350 and 1500 cm^{-1}.

The molecular structure of **6.6** could only be partially refined due to twinning, but illustrates η^6-interactions of the two coordinated phenyl moieties which are positioned between the silyl substituents in order to fill the coordination sphere (**Figure 6.17**). The complex also has a trigonal planar geometry of aromatic ligands around the metal centre, and the uranium atom lies on this plane.

Comparison of this structure with the two base-free complexes synthesised by Evans illustrates that the η^3-interaction in $[(Cp^{Me4})_2U(\mu\text{-}Ph)BPh_3]$ has longer $U–C_{Ph}$ bond lengths than **6.6** (2.868(4) – 2.957(5) Å) and the non-coordinating atoms in the bridging phenyl ring have $U–C_{Ph}$ distances in excess of 2.99 Å.[29] Similar distances are observed in $[(Cp^*)_2U(\mu\text{-}Ph)_2BPh_2]$, whereby the two η^1-bound phenyl rings have $U–C_{Ph}$ bond lengths of 2.857(8) and 2.879(9) Å, whereas the adjacent carbon atoms have $U–C_{Ph}$ distances of 3.137(8) – 3.166(8) Å.[28] These interactions give rise to variation in the arene C–C bond lengths which range from 1.377(12) to 1.411(11) Å.

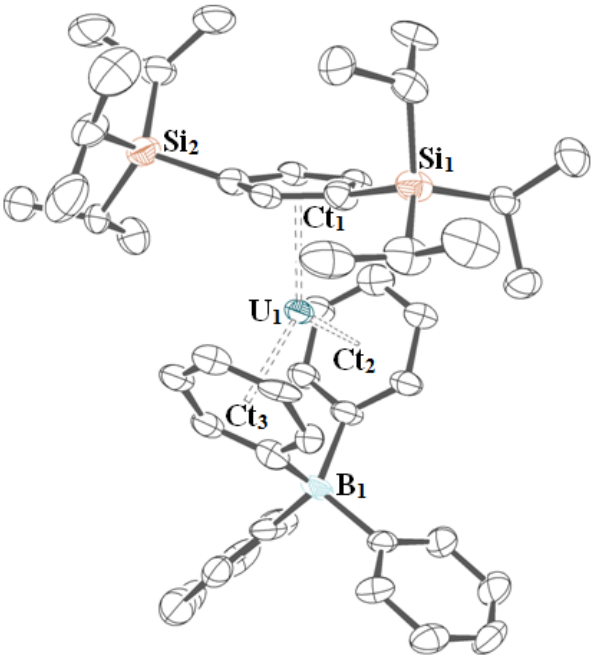

Figure 6.17 ORTEP view of **6.6** with thermal ellipsoids at 50% probability; hydrogen atoms have been omitted for clarity. Selected bond distances (Å) and angles (°): U–Ct_1 2.4623(9); U–Ct_2 2.4184(10); U–Ct_3 2.4272(9); U_1–B_1 3.567(16); U_1–C_{Ph} 2.749(16) – 2.8323(10); C_{Ph}–C_{Ph} 1.3900(2) – 1.390(15);Ct_1–U–Ct_2 119.30(3); Ct_1–U–Ct_3 125.43(4); Ct_2–U–Ct_3 115.21(3).

Non-activated uranium monoarene complexes in the literature have similar U–C_{Ph} bond distances to **6.6** (2.729(3) – 2.964(3) Å).[2,30–33] Inverse-sandwich complexes however, illustrate the activated arene rings exhibit shorter U–C_{Ph} bond lengths (*ca.* 2.532(2) – 2.749(10) Å) due to a strong δ-interaction.[4,34–41] However the arene C–C distances show little variation from the free arenes, and the maximum elongation was reported to be *ca.* 0.07 Å, illustrating that the assignment of the oxidation state of uranium in these complexes cannot be based on the uranium-phenyl interactions or the arene C–C bond distances alone.[42]

DFT analysis was performed by Professor Maron using the hybrid functional B2PW91. These calculations indicate that the ground state of **6.6** has 65% U^{2+} character,

comprised of three f orbitals and one f+d orbital. There is also a significant contribution (35%) of U^{3+} character, from three f orbitals and one π*(tetraphenylborate) orbital (**Figure 6.18**).

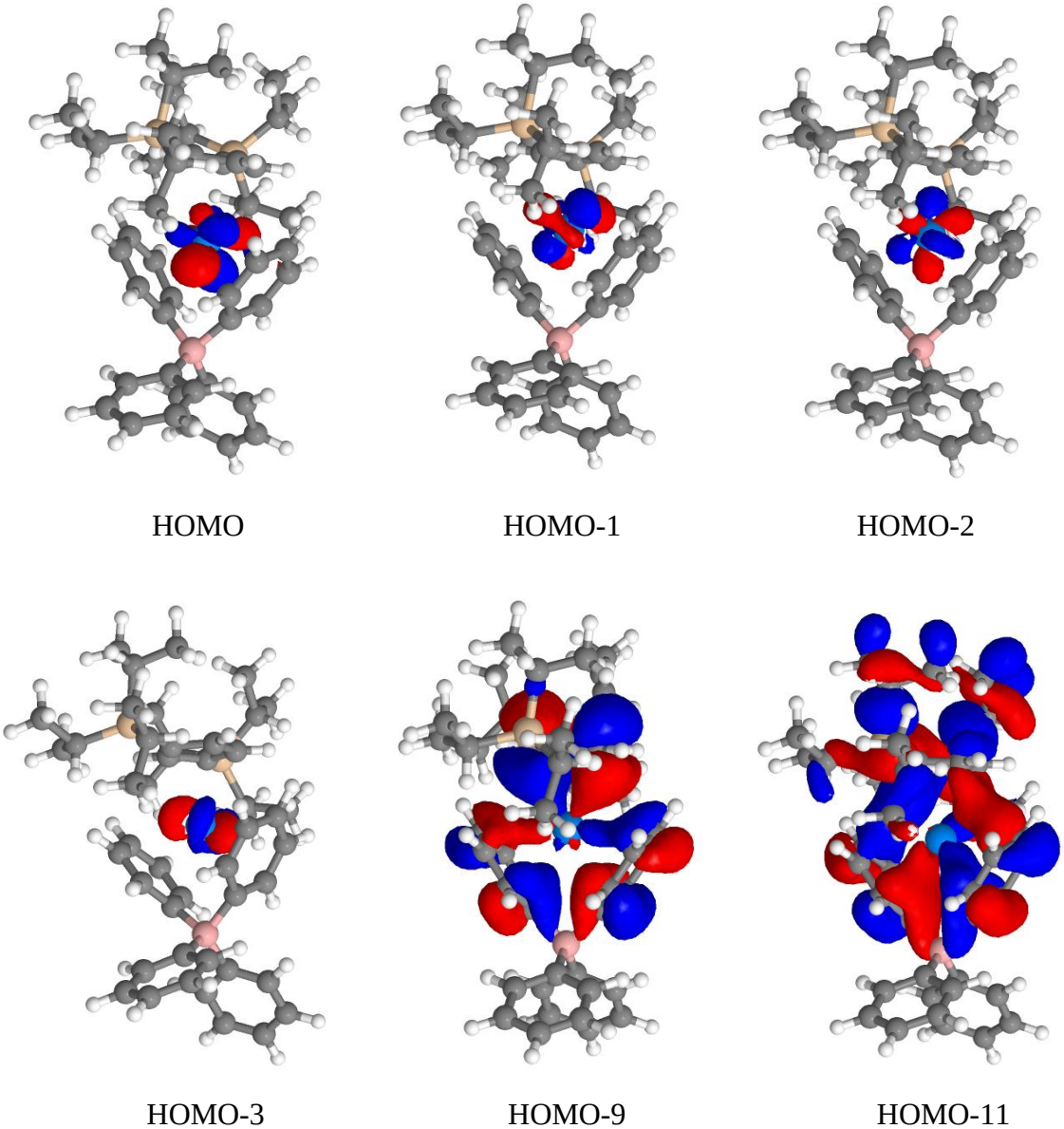

Figure 6.18 The calculated MOs for **6.6**

These studies illustrate that assignment of an oxidation state is not trivial, and that in order to complete characterisation of **6.6**, further studies are required. Investigation of the magnetic properties of this complex as a function of temperature would give further information on the ground state of this complex.

6.5 Summary

The results discussed herein demonstrate that although a uranium(II) metallocene was not synthesised, uranium(III) complexes exhibit interesting reactivity in the presence of reducing agents. Attempts to trap intermediates in these reactions gave rise to the formation of bridging borane/borohydride complexes and illustrate the potential for novel uranium-based fragments to be synthesised under optimum conditions. Attempts to synthesis a bis(cyclopentadienyl)uranium(III) cation also failed to yield the expected complex and the formation of $[(Cp^{(Si\textit{i}Pr3)2})U(\mu\text{-}Ph)_2BPh_2]$ was instead observed. This complex warrants further characterisation, but could be used to yield organouranium complexes based on the $[(Cp^{(Si\textit{i}Pr3)2})U]$ unit.

6.6 Experimental details for Chapter 6

*6.6.1 Synthesis of $[\{U(Cp^{tBu2})_2\}_2(\mu\text{-}I)_2]$ (**6.1**)*

To a mixture of UI_3 (0.600 g, 0.970 mmol) and $K[Cp^{tBu2}]$ (0.4216 g, 1.95 mmol) was added THF (100 mL) at ambient temperature. A bright green suspension was formed instantaneously and the mixture was stirred for six hours. The residue was dried *in vacuo* then extracted in toluene, filtered and crystallised from toluene at -50 °C.

Yield: 0.458 g (0.318 mmol), 65.7% based on UI_3.

Anal. calc (found) for $C_{52}H_{84}I_2U_2$: C 43.40 (43.777), H 5.88 (6.078)%.

MS (EI): *m/z* = 719 (100%, [UI(Cp^{tBu2})$_2$]).

^{1}H NMR (d_6-benzene, 303 K): δ 86.2 (s, br, 2H, Cp-C*H*), -4.2 (s, br, 36H, ^{t}Bu-CH_3), -68.8 (s, br, 4H, Cp-C*H*).

*6.6.2 Synthesis of [{U($Cp^{(SiiPr3)2}$)$_2$}$_2$(μ-I)$_2$] (**6.2**)*

To a mixture of UI_3 (1.221 g, 1.973 mmol) and K[$Cp^{(SiiPr3)2}$] (1.670 g, 4.007 mmol) was added diethyl ether (150 mL). The mixture was stirred for 72 hours over which time a slow change from a suspension of dark and pale solids to a bright green solution was observed. The residue was stripped to dryness then extracted in pentane, twice filtered and crystallised from pentane at -35 °C.

Yield: 1.344 g (0.600 mmol), 60.7% based on UI_3.

MS (EI): *m/z* = 335 (100%), 1118 (< 1%, M^+).

^{1}H NMR (d_8-toluene, 303 K): δ 67.3 (s, br, 1H, Cp-C*H*), -2.0 (s, br, 6H, ^{i}Pr-C*H*), -4.7 (s, br, 18H, ^{i}Pr-CH_3), -5.9 (s, br, 18H, ^{i}Pr-CH_3), -38.7 (s, br, 2H, Cp-C*H*).

^{29}Si{^{1}H} NMR (d_8-toluene, 303 K): δ -100.5 (*Si*^{i}Pr$_3$).

*6.6.3 Synthesis of [UI($Cp^{(SiiPr3)2}$)$_2$(THF)] (**6.2THF**)*

To a solution of UI_3 (0.643 g, 1.04 mmol) in THF (30 mL), was added K[$Cp^{(SiiPr3)2}$] (0.871 g, 2.09 mmol) to yield [UI($Cp^{(SiiPr3)2}$)$_2$(THF)] and KI precipitate after 24 hours. The residue was dried *in vacuo* then extracted in pentane, filtered *via* cannula and crystallised at -35 °C.

Yield: 0.828 g (0.694 mmol), 66.8% based on UI_3.

Anal. calc (found) for $C_{50}H_{98}OISi_4U$: C 50.36 (50.178), H 8.28 (8.195)%.

MS (EI): *m/z* = 335 (100%), 1119 (< 1%, M^+ -THF).

^{1}H NMR (d_8-toluene, 303 K): δ 57.9 (s, br, 1H, Cp-C*H*), -0.8 (s, br, 6H, ^{i}Pr-C*H*), -1.7 (s, br, 18H, ^{i}Pr-C*H*$_3$), -3.2 (br, 22H, ^{i}Pr-C*H*$_3$, THF), -9.1 (s, br, 4H, THF), -39.7 (s, br, 2H, Cp-C*H*).

^{29}Si{^{1}H} NMR (d_8-toluene, 303 K): δ -106.2 (*Si*^{i}Pr$_3$).

*6.6.4 Synthesis of [U(Cp$^{(SiiPr3)2}$)$_2$I$_2$K(DME)$_2$] (**6.2DME**)*

To a mixture of UI_3 (302 mg, 0.488 mmol) and K[Cp$^{(SiiPr3)2}$] (416 mg, 0.998 mmol) was added DME (20 mL) at room temperature. An instantaneous colour change to bright green was observed. The mixture was stirred for 24 hours then dried *in vacuo*. The residue was extracted in pentane, filtered *via* cannula and recrystallised from pentane/DME at -35 °C.

Yield: 342.9 mg (0.234 mmol) 47.9% based on UI_3.

MS (EI): *m/z* = 1119 (100%, M^+ - KI(DME)$_2$).

^{1}H NMR (d_8-toluene, 303 K): δ 57.8 (s, br, 1H, Cp-C*H*), 4.0 – -1.0 (br, overlapping, ^{i}Pr-C*H*, ^{i}Pr-C*H*$_3$, DME), -43.5 (s, br, 2H, Cp-C*H*).

^{29}Si{^{1}H} NMR (d_8-toluene, 303 K): δ -115.9 (*Si*^{i}Pr$_3$).

*6.6.5 Synthesis of [U(Cp^{tBu2})$_3$] (**6.3**)*

A solution of [{U(Cp^{tBu2})$_2$}$_2$(μ-I)$_2$] (60 mg, 4.2 x 10^{-5} mol) in toluene (15 mL) was added to sodium/potassium alloy (14 mg, 0.10 mmol) in toluene (2 mL) at -78 °C. The solution was warmed to ambient temperature and stirred for five days during which time

dark solids precipitated. Filtration of the olive solution and analysis by NMR illustrated quantitative conversion to **6.3**. Rigorous drying of the residue and cooling of a saturated pentane solution yielded crystals at -35 °C.

Yield: 14.1 mg (1.83 x 10^{-5} mol), 44% based on [{U(Cp^{tBu2})$_2$}$_2$(μ-I)]$_2$.

Anal. calc (found) for $C_{39}H_{63}U$: 60.84 (60.059), H 8.25 (8.106)%.

MS (EI): *m/z* = 147 (100%), 769 (15%, M^+).

^{1}H NMR (d_8-toluene, 303 K): δ 26.3 (s, br, 3H, Cp-C*H*), -11.2 (s, br, 54H, ^{t}Bu-CH_3), -16.0 (s, br, 6H, Cp-C*H*).

*6.6.6 Synthesis of [{U(Cp^{tBu2})$_2$}$_2$(BH_x)]$_2$ (**6.4**)*

A solution of BH_3·THF (0.7 mL, 1.0 M in THF) was diluted in toluene (20 mL), then added to a mixture of [{U(Cp^{tBu2})$_2$}$_2$(μ-I)$_2$] (234.6 mg, 1.63 x 10^{-4} mol) and KC_8 (51.2 mg, 3.79 x 10^{-4} mol) at -50 °C. Additional toluene was added (20 mL) and the mixture was allowed to warm to ambient temperature. The mixture was stirred for seven days then all volatiles were removed *in vacuo*. The residue was extracted in pentane and filtered to yield a crude solution of **6.3** and **6.4**. Crystals of **6.4** were obtained from saturated pentane solutions at -35 °C.

Yield: 57.5 mg (4.74 x 10^{-5} mol), 29.0% based on [{U(Cp^{tBu2})$_2$}$_2$(μ-I)$_2$].

MS (EI): *m/z* = 57 (100%, ^{t}Bu), 607 (12%, [U(Cp^{tBu2})$_2$$BH_4$]).

^{1}H NMR (d_6-benzene, 303 K): δ 73.7 (br), 61.7 (br), -4.1 (s, br, 36H, ^{t}Bu-CH_3), -11.7 (br).

^{11}B{^{1}H} NMR (d_6-benzene, 303 K): δ 462.5 (br, $w_{½}$ = 834 Hz, *B*H_x).

*6.6.7 Synthesis of [{U(Cp$^{(SiiPr3)2}$)$_2$}$_2$(BH$_x$)] (**6.5**)*

To a mixture of [{U(Cp$^{(SiiPr3)2}$)$_2$}$_2$(μ-I)$_2$] (52.0 mg, 2.32 x 10^{-5} mol) and KC_8 (8.2 mg, 6.06 x 10^{-5} mol) in toluene (5 mL) was added two drops BH_3·THF (0.7 ml, 1.0 M in THF) at -78 °C. The mixture was warmed to ambient temperature and stirred for 24 hours. Removal of all volatiles and dissolution in d_6-benzene allowed partial characterisation of **6.5**.

MS (EI): *m/z* = 761 (100%), 1007 (49%, [U(Cp$^{(SiiPr3)2}$)$_2$BH$_4$]).

^{1}H NMR (d_6-benzene, 303 K): *Resonances could not be definitively identified.*

^{11}B{^{1}H} NMR (d_6-benzene, 303 K): δ 211.7 (br, $w_{½}$ = 374.1 Hz, *B*H$_x$), 181.1 (br, $w_{½}$ = 251.5 Hz, *B*H$_x$).

^{29}Si{^{1}H} NMR (d_6-benzene, 303 K): δ -109.1 (*Si*^{i}Pr$_3$), -123.8 (*Si*^{i}Pr$_3$).

*6.6.8 Synthesis of [(Cp$^{(SiiPr3)2}$)U(BPh$_4$)] (**6.6**)*

To a mixture of [{U(Cp$^{(SiiPr3)2}$)$_2$}$_2$(μ-I)$_2$] (150.3 mg, 6.71 x 10^{-5} mol) and KBz (18.3 mg, 1.40 x 10^{-4} mol) was added pentane (15 mL) to give a teal/black solution with orange solids. The mixture was stirred for three days to give an olive/green solution, which was filtered *via* cannula then stripped to dryness to give an olive residue with a crude yield of 133 mg. To this was added [Et$_3$NH][BPh$_4$] (56.9 mg, 1.35 x 10^{-4} mol) and toluene (7 mL) to form a suspension. The mixture was stirred for three days then stripped to dryness. The brown residue was taken up in pentane, filtered then cooled to -35 °C. Dull brown microcrystalline solids of **6.6** were obtained from a red/brown supernatant.

Yield: 76.0 mg (8.13 x 10^{-5} mol), 60.7% based on [{U(Cp$^{(SiiPr3)2}$)$_2$}$_2$(μ-I)$_2$].

Anal. calc (found) for $C_{47}H_{65}BSi_2U$: C 60.37 (60.611), H 7.01 (7.412)%.

MS (EI): *m/z* = 59 (100%), 770 (11%, M$^+$ - BPh$_2$), 1100 (2%, M$^+$ + BPh$_2$).

IR (NaCl): 2943, 2890, 2865, 1700 – 1500 (br), 461, 1433, 1383, 1363, 1316, 1241, 1185, 1071, 1040, 1015 cm^{-1}.

^{1}H NMR (d_6-benzene, 303 K): δ 11.9 (br, 1H), 5.8 (br, 2H), 4.0 (br, overlapping), 3.4 (br, overlapping), 3.0 (br, overlapping), 0.7 (br, 1H), -0.2 (br, 2H), -1.2 (br, 2H), -1.8 (br, 2H), -2.1 (br, 2H), -2.4 (br, 2H), -2.9 (br, 1H), -4.2 (br, overlapping), -4.6 (br, overlapping), -5.4 (br, 2H), -6.0 (br), -6.6 (br, 6H), -8.1 (br, 1H), -8.4 (br, 1H).

$^{11}B\{^{1}H\}$ NMR (d_6-benzene, 303 K): δ 1.3 (br, overlapping, BPh_4), 0.8 (br, overlapping, BPh_4).

$^{29}Si\{^{1}H\}$ NMR (d_6-benzene, 303 K): δ -104.5 ($Si^{i}Pr_3$).

6.7 References

1 M. R. MacDonald, M. E. Fieser, J. E. Bates, J. W. Ziller, F. Furche and W. J. Evans, *J Am Chem Soc*, 2013, **135**, 13310–13313.

2 H. S. La Pierre, A. Scheurer, F. W. Heinemann, W. Hieringer and K. Meyer, *Angew Chem Int Ed*, 2014, **53**, 7158–7162.

3 B. M. Gardner, W. Lewis, A. J. Blake and S. T. Liddle, *Inorg Chem*, 2011, **50**, 9631–9641.

4 D. P. Mills, F. Moro, J. McMaster, J. V. Slageren, W. Lewis, A. J. Blake and S. T. Liddle, *Nat. Chem.*, 2011, **3**, 454–460.

5 L. Maria, Â. Domingos and I. Santos, *Inorg Chem*, 2003, **42**, 3323–3330.

6 O. T. Summerscales, DPhil Thesis, University of Sussex, 2007.

7 A. Zalkin, A. L. Stuart and R. A. Andersen, *Acta Cryst Sect C*, 1988, **C44**, 2106–2108.

8 W. W. Lukens, P. G. Allen, J. J. Bucher, N. M. Edelstein, E. A. Hudson, D. K. Shuh, T. Reich and R. A. Andersen, *Organometallics*, 1999, **18**, 1253–1258.

9 P. C. Blake, M. F. Lappert, R. G. Taylor, J. L. Atwood, W. E. Hunter and H. Zhang, *J Chem Soc Chem Commun*, 1986, 1394–1395.

10 P. C. Blake, M. F. Lappert, R. G. Taylor, J. L. Atwood and H. Zhang, *Inorg Chim Acta*, 1987, **139**, 13–20.

11 N. G. Connelly and W. E. Geiger, *Chem Rev*, 1996, **96**, 877–910.

12 A. Zalkin, J. G. Brennan and R. A. Andersen, *Acta Cryst Sect C*, 1988, **C44**, 2104–2106.

13 J. Meunier-Piret, J. P. Declercq, G. Germain and M. van Meerssche, *Bull Soc Chim Belg*, 1980, **89**, 121.

14 W. J. Evans, K. J. Forrestal and J. W. Ziller, *Angew Chem Int Ed*, 1997, **36**, 774–776.

15 N. A. Siladke, J. W. Ziller and W. J. Evans, *Z Anorg Allg Chem*, 2010, **636**, 2347–2351.

16 J.-C. Berthet, J.-F. Le Maréchal, M. Lance, M. Nierlich, J. Vigner and M. Ephritikhine, *J Chem Soc Dalton Trans*, 1992, 1573–1577.

17 M. del Mar Conejo, J. S. Parry, E. Carmona, M. Schultz, J. G. Brennan, S. M. Beshouri, R. A. Andersen, R. D. Rogers, S. Coles and M. B. Hursthouse, *Chem Eur J*, 1999, **5**, 3000–3009.

18 C. D. Sofield and R. A. Andersen, *J Organomet Chem*, 1995, **501**, 271–276.

19 G. Rossetto, M. Porchia, F. Ossola, P. Zanella and R. D. Fischer, *J Chem Soc Chem Commun*, 1985, 1460–1461.

20 M. Porchia, G. Rossetto, N. Brianese, F. Ossola, P. Zanella and R. D. Fischer, *J Common Met.*, 1986, 603.

21 M. Porchia, N. Brianese, F. Ossola, G. Rossetto and P. Zanella, *J Chem Soc Dalton Trans*, 1987, 691–694.

22 D. Baudry, M. Ephritikhine, F. Nief, L. Ricard and F. Mathey, *Angew Chem Int Ed*, 1990, **29**, 1485–1486.

23 P. Gradoz, D. Baudry, M. Ephritikhine, F. Nief and F. Mathey, *J Chem Soc Dalton Trans*, 1992, 3047–3051.

24 P. Gradoz, M. Ephritikhine, M. Lance, J. Vigner and M. Nierlich, *J Organomet Chem*, 1994, **481**, 69–73.

25 W. J. Evans, L. R. Chamberlain, T. A. Ulibarri and J. W. Ziller, *J Am Chem Soc*, 1988, **110**, 6423–6432.

26 F. H. Allen, *Acta Cryst Sect B*, 2002, **B58**, 380–388.

27 I. J. Bruno, J. C. Cole, P. R. Edgington, M. Kessler, C. F. Macrae, P. McCabe, J. Pearson and R. Taylor, *Acta Cryst Sect B*, 2002, **B58**, 389–397.

28 W. J. Evans, G. W. Nyce, K. J. Forrestal and J. W. Ziller, *Organometallics*, 2002, **21**, 1050–1055.

29 W. J. Evans, S. A. Kozimor, W. R. Hillman and J. W. Ziller, *Organometallics*, 2005, **24**, 4676–4683.

30 S. M. Franke, B. L. Tran, F. W. Heinemann, W. Hieringer, D. J. Mindiola and K. Meyer, *Inorg Chem*, 2013, **52**, 10552–10558.

31 F. A. Cotton and W. Schwotzer, *Organometallics*, 1985, **4**, 942–943.

32 M. Cesari, U. Pedretti, A. Zazzetta, G. Lugli and W. Marconi, *Inorg Chim Acta*, 1971, **5**, 439–444.

33 F. A. Cotton and W. Schwotzer, *Organometallics*, 1987, **6**, 1275–1280.

34 D. Patel, F. Moro, J. McMaster, W. Lewis, A. J. Blake and S. T. Liddle, *Angew Chem Int Ed*, 2011, **50**, 10388–10392.

35 D. Baudry, E. Bulot, P. Charpin, M. Ephritikhine, M. Lance, M. Nierlich and J. Vigner, *J Organomet Chem*, 1989, **371**, 155–162.

36 P. L. Diaconescu and C. C. Cummins, *J Am Chem Soc*, 2002, **124**, 7660–7661.

37 W. J. Evans, C. A. Traina and J. W. Ziller, *J Am Chem Soc*, 2009, **131**, 17473–17481.

38 M. J. Monreal, S. I. Khan, J. L. Kiplinger and P. L. Diaconescu, *Chem Commun*, 2011, **47**, 9119–9121.

39 P. L. Diaconescu and C. C. Cummins, *Inorg Chem*, 2012, **51**, 2902–2916.

40 V. Mougel, C. Camp, J. Pécaut, C. Copéret, L. Maron, C. E. Kefalidis and M. Mazzanti, *Angew Chem Int Ed*, 2012, **51**, 12280–12284.

41 C. Camp, V. Mougel, J. Pécaut, L. Maron and M. Mazzanti, *Chem Eur J*, 2013, **19**, 17528–17540.

42 W. J. Evans, S. A. Kozimor, J. W. Ziller and N. Kaltsoyannis, *J Am Chem Soc*, 2004, **126**, 14533–14547.

APPENDIX I: GENERAL EXPERIMENTAL DETAILS

AI.1 General Procedures

The manipulation of air- and moisture-sensitive compounds and their spectroscopic measurements were conducted using standard Schlenk techniques[1] under an atmosphere of nitrogen or argon, or in a MBraun glovebox under nitrogen or argon atmospheres (O_2 and H_2O levels <1 ppm). Nitrogen and argon gases were supplied by BOC Gases UK, and argon was catalytically dried and deoxygenated by passing through a column containing BASF R3-11(G) catalyst and activated 4 Å molecular sieves prior to use. All glassware was dried at 160 °C and cooled under dynamic vacuum prior to use. Filtrations were conducted using filter cannulae or pipettes equipped with Whatman 25 mm glass microfiber filters, which were pre-dried at 160 °C prior to use. Celite 545 filter aid was pre-dried at 200 °C then flame dried under dynamic vacuum prior to use

AI.2 Purification of Solvents

Solvents were pre-dried over sodium wire for a minimum of 72 hours before refluxing over drying agents under an atmosphere of nitrogen: sodium/potassium alloy (pentane, hexane, diethyl ether, petroleum ether 40:60 and tetramethylsilane) potassium (THF, methylcyclohexane, DME, pyridine and *tert*-butyl methyl ether), sodium (toluene and hexamethyldisiloxane) or calcium hydride (DCM and acetonitrile). Dried solvents were collected, degassed and stored under argon in potassium mirrored ampoules (pentane, hexane, toluene, methylcyclohexane and hexamethyldisiloxane) or activated 4 Å molecular sieves (DCM, DME, THF, pyridine, diethyl ether and *tert*-butyl methyl ether). Tetramethylsilane was stored over activated 4 Å molecular sieves at -35 °C.

Deuterated solvents (d_6-benzene, d_8-toluene, d_{12}-cyclohexane, d_8-THF and d_5-pyridine) were obtained from Aldrich and were freeze-thaw degassed thrice prior to drying by reflux over potassium for 72 hours. Solvents were vacuum distilled and degassed prior to storage under nitrogen in a MBraun glovebox.

AI.3 Instrumentation

NMR analysis was undertaken by the author using Varian VNMR5 400 MHz and 500 MHz spectrometers or by Dr I. J. Day using a Varian VNMR 600 MHz spectrometer. Chemical shifts are reported in parts per million or δ, and half-height linewidths ($w_{½}$) and coupling constrants (J) are reported in Hz. ^{1}H and ^{13}C spectra were referenced internally to the residual protic solvent signals. ^{11}B, ^{19}F, ^{29}Si and ^{31}P spectra were referenced externally to $BF_3{\cdot}OEt_2$, $CFCl_3$ (10%), $SiMe_4$ and H_3PO_4 (85%) respectively. Heteronuclei NMR spectra were ^{1}H-decoupled unless otherwise stated.

Infrared spectra were recorded on a Perkin-Elmer 1600 Fourier Transform spectrometer. Samples were prepared by evaporation of a solution sandwiched between two NaCl discs under inert atmosphere. Solution phase IR spectra were recorded on a Mettler-Toledo ReactIR^{TM} 45 m FTIR system with iC IR 4.1 software. The spectra were recorded for samples in a gas-tight IR cell under a dinitrogen or reactive gas atmosphere using methylcyclohexane as the solvent. Background spectra were recorded of the starting complex at ambient temperature prior to the reaction.

MS-EI spectra were obtained with a VG autospec Fisons instrument at 70 eV, and GC-MS spectra were performed on a Quattro micro^{TM} GC by Dr A. Abdul-Sada. MS-EI samples were prepared in capillary tubes under inert atmosphere and sealed. Solution based-samples were prepared in crimp top vials with aluminium caps with PTFE/red rubber septa under inert atmosphere.

Elemental analyses were carried out at Mikroanalytisches Labor Pascher in Remagen, Germany or by Mr Davis at the Microanalytical Laboratoy, University of Bristol.

Cyclic voltammetry studies were conducted under argon by the author using a BASi Epsilon-EC potentiostat under computer control. *iR* drop was compensated for by using the feedback method. All experiments were conducted using a gold disc (2.0 mm^2) or glassy carbon disc (7.0 mm^2) working electrode, platinum wire counter electrode and silver wire pseudo-reference electrode. Ferrocene or decamethylferrocene (*ca.* 1 mg) was added to all solutions after initial voltammograms had been obtained to obtain the $[FeCp_2]^{+/0}$ reference couple. Samples were prepared by dissolving the analyte (5 – 10 mM) in a solution of supporting electrolyte (5 mM $[^nBu_4N][PF_6]$ or $[^nBu_4N][B(C_6F_5)]$ in 1 ml THF).

Single crystal XRD data were collected by Dr S. M. Roe or the author using a Enraf-Nonius CAD4 diffractometer with graphite-monochromated Mo K α radiation (λ = 0.71073) source or an Agilent Technologies Xcalibur Gemini ultra diffractormer with a Mo K α radiation (λ = 0.71073) source or a Cu K α radiation (λ = 1.54184) source and a Eos CCD area detector. The data were collected at 173 K using an Oxford Cryosystems Cobra low temperature device and were processed using KappaCCD software or CrysAlisPro.[2] An empirical absorption correction was carried out using the MULTI-SCAN program.[3,4] Single crystal XRD data for **2.8**, **4.3**, **4.8**, **4.9**, **4.12THF**, **6.2** and **6.6** were collected by the UK National Crystallography Service at the University of Southampton,[5] and an empirical absorption correction was carried out using the MULTI-SCAN program. Full details of structures are provided in Appendix IV.

Single crystal XRD data were solved by the author and Dr S. M. Roe using SHELXL-2013,[6] SHELXL-97,[6] SHELXT[6] and SUPERFLIP.[7] Data were refined using SHELX-2013 with Olex2 or WinGX software.[8,9] All non-hydrogen atoms were refined with anisotropic displacement parameters except **2.8**, **4.12THF** and **4.19**. All hydrogen atoms

were refined using a riding model. Disordered solvent molecules were modelled using the SQUEEZE[10] function in PLATON[11] (**4.8**) or 'solvent mask' in Olex2.[8]

AI.4 Commercially Supplied Reagents

The following reagents were purchased from Aldrich and used as received: [^{n}Bu$_4$N][PF$_6$] (electrochemical grade), ^{i}Pr$_3$SiOTf, 1,5-cyclooctadiene, KH, AlCl$_3$ (reagent grade, 98%), 2-butyne, 2-bromo-2-methyl propane, dibenzo-18-crown-6, tributylphosphine, P,P-dichlorophenylphosphine, lithium granules (99% under Ar) and 1,4-dichlorobutane.

The following reagents were purchased from Aldrich and purified/dried prior to use,[12] and stored under inert atmosphere: CS_2, Ph_3PS, Et_3PS, dicyclopentadiene, NaH, Me_3SiI, Me_3SiCl and Me_3SiOTf. Potassium metal was purchased from Fischer Scientific. The oxide layer was removed and the remaining metal washed in hexane prior to use. COT was purchased from Alfa Aesar and stored over 4 Å molecular sieves prior to use. HCp^{NMe4} was purchased from Alfa Aesar and degassed before use. Solutions of ^{n}BuLi (*ca.* 2.5 M in hexanes) were supplied by Acros Organics and titrated to determine the exact molarity prior to use.

CO (99.999%), H_2 (>99.999%) and CO_2 (99.99%) were supplied by Union Carbide and used with a high-purity regulator. N_2O (>99.998%) was supplied by Fluka. Isotopically enriched gases ^{13}CO (99.7%) and $^{13}CO_2$ (99%) were supplied by Euriso-top and Cambridge Isotopes respectively.

Isonitriles (CNMe and CN^{t}Bu), were kindly donated by colleagues and were stored over molecular sieves and degassed before use. NaCp, $FeCp_2$, [Fe(Cp*)$_2$], [Et_3NH][BPh_4], KBz, and K[N(SiMe$_3$)$_2$] were also donated by colleagues. KC_8 and [^{n}Bu$_4$N][B(C$_6$F$_5$)] were kindly donated by Professor Cloke. COS (97% Aldrich) was kindly donated by Professor Meyer and KCp^{AsMe4} was kindly donated by Professor Nief.

AI.5 Literature Preparations

The following compounds were prepared according to published procedures: HCp^{tBu},[13] HCp^{tBu2},[13] HCp^{tBu3},[13] $K[Cp^{(SiiPr3)2}]$,[14] $K[Cp^{PMe4}]$,[15,16] $K[NH_2]$, $K_2[COT^{(SiiPr3)2}]$,[17] and UI_3.[18] KCp^{tBu}, KCp^{tBu2}, KCp^{tBu3} and KCp^{NMe4} were prepared by deprotonation of the neutral ligands with KH in THF/toluene.

AI.6 DFT calculations

DFT calculations were carried out by Professor Laurent Maron at Université de Toulouse for compound **6.6**. The uranium atom was treated with either small core Stuttgart-Dresden ECPs[19,20] or the 5*f*-in-core ECP with their associated basis set augmented by either sets of *g* or *f* polarization functions respectively.[21] Carbon, boron and hydrogen atoms have been described with a 6-31G(d,p) double-ζ basis set.[22] Calculations were carried out at the DFT level of theory using the hybrid functional B3PW91.[23] Geometry optimizations were performed without any symmetry restrictions and the nature of the minima was verified with analytical frequency calculations. Gibbs free energies were obtained at T = 298.15 K within the harmonic approximation. DFT calculations were carried out with the Gaussian09 suite of programs.[24] CASSCF calculations were also carried out using the Gaussian03 one.[25]

AI.6 References

1 D. F. Shriver, *The Manipulation of Air-Sensitive Compounds*, Wiley-Interscience, 2nd edn., 1986.

2 Agilent Technologies, *CrysalisPro 1.171.36.32*, 2011.

3 R. H. Blessing and D. A. Langs, *J. Appl. Crystallogr.*, 1987, **20**, 427–428.

4 R. H. Blessing, *Acta Crystallogr., A, Found. Crystallogr.*, 1995, **51**, 33–38.

5 S. J. Coles and P. A. Gale, *Chem. Sci.*, 2012, **3**, 683–689.

6 G. M. Sheldrick, *Acta Crystallogr., A, Found. Crystallogr.*, 2008, **64**, 112–122.

7 L. Palatinus and G. Chapuis, *J. Appl. Crystallogr.*, 2007, **40**, 786–790.

8 O. V. Dolomanov, L. J. Bourhis, R. J. Gildea, J. A. K. Howard and H. Puschmann, *J. Appl. Crystallogr.*, 2009, **42**, 339–341.

9 L. J. Farrugia, *J. Appl. Crystallogr.*, 1999, **32**, 837–838.

10 P. Van Der Sluis and A. L. Spek, *Acta Crystallogr., A, Found. Crystallogr.*, 1990, **46**, 194–201.

11 A. L. Spek, *J. Appl. Crystallogr.*, 2003, **36**, 7–13.

12 D. Perrin and W. Armarego, *Purification of Laboratory Chemicals*, Pergamon Press, 1988.

13 E. V. Dehmlow and C. Bollmann, *Z. Naturforsch B*, 1993, **48b**, 457–460.

14 F. G. N. Cloke and D. R. Johnston, .

15 F. Nief, F. Mathey and L. Ricard, *Organometallics*, 1988, **7**, 921–926.

16 P. Gradoz, D. Baudry, M. Ephritikhine, F. Nief and F. Mathey, *J. Chem. Soc. Dalton Trans.*, 1992, 3047–3051.

17 N. C. Burton, F. G. N. Cloke, P. B. Hitchcock, H. C. de Lemos and A. A. Sameh, *J. Chem. Soc., Chem. Commun.*, 1989, 1462–1464.

18 F. G. N. Cloke and P. B. Hitchcock, *J. Am. Chem. Soc.*, 2002, **124**, 9352–9353.

19 Küchle, W.; Dolg, M.; Stoll, H.; Preuss, H. *J. Chem. Phys.* **1994**, *100*, 7535.

20 Cao, X.; Dolg, M.; Stoll, H. *J. Chem. Phys.* **2003**, *118*, 487.

21 Moritz, A.; Dolg, M. *Theor. Chem. Acc.* **2008**, *121*, 297.

22 Hehre, W. J.; Ditchfie, R.; Pople, J. A. *J. Chem. Phys.* **1972**, *56*, 2257.

23 (a) J. J. P. Perdew and Y. Wang, *Phys. Rev. B*, 1992, **45**, 13244. (b) A. D. Becke, *J. Chem. Phys.*, 1993, **98**, 5648. (c) K. Burke, J. P. Perdew and W. Yang, *Electronic Density Functional Theory: Recent Progress and New Directions*, J. F. Dobson, G. Vignale, and M. P. Das, Eds., Plenum, New York, NY. **1998.**

24 Gaussian 09, Revision A.1, Frisch, M. J.; Trucks, G. W.; Schlegel, H. B.; Scuseria, G. E.; Robb, M. A.; Cheeseman, J. R.; Scalmani, G.; Barone, V.; Mennucci, B.; Petersson, G. A.; Nakatsuji, H.; Caricato, M.; Li, X.; Hratchian, H. P.; Izmaylov, A.

F.; Bloino, J.; Zheng, G.; Sonnenberg, J. L.; Hada, M.; Ehara, M.; Toyota, K.; Fukuda, R.; Hasegawa, J.; Ishida, M.; Nakajima, T.; Honda, Y.; Kitao, O.; Nakai, H.; Vreven, T.; Montgomery, Jr., J. A.; Peralta, J. E.; Ogliaro, F.; Bearpark, M.; Heyd, J. J.; Brothers, E.; Kudin, K. N.; Staroverov, V. N.; Kobayashi, R.; Normand, J.; Raghavachari, K.; Rendell, A.; Burant, J. C.; Iyengar, S. S.; Tomasi, J.; Cossi, M.; Rega, N.; Millam, J. M.; Klene, M.; Knox, J. E.; Cross, J. B.; Bakken, V.; Adamo, C.; Jaramillo, J.; Gomperts, R.; Stratmann, R. E.; Yazyev, O.; Austin, A. J.; Cammi, R.; Pomelli, C.; Ochterski, J. W.; Martin, R. L.; Morokuma, K.; Zakrzewski, V. G.; Voth, G. A.; Salvador, P.; Dannenberg, J. J.; Dapprich, S.; Daniels, A. D.; Farkas, Ö.; Foresman, J. B.; Ortiz, J. V.; Cioslowski, J.; Fox, D. J. Gaussian, Inc., Wallingford CT, 2009.

25 Frisch, M. J.; Trucks, G. W.; Schlegel, H. B.; Scuseria, G. E.; Robb, M. A.; Cheeseman, J. R.; Montgomery, J., J. A.; ; Vreven, T.; Kudin, K. N.; Burant, J. C.; Millam, J. M.; Iyengar, S. S.; Tomasi, J.; Barone, V.; Mennucci, B.; Cossi, M.; Scalmani, G.; Rega, N.; Petersson, G. A.; Nakatsuji, H.; Hada, M.; Ehara, M.; Toyota, K.; Fukuda, R.; Hasegawa, J.; Ishida, M.; Nakajima, T.; Honda, Y.; Kitao, O.; Nakai, H.; Klene, M.; Li, X.; Knox, J. E.; Hratchian, H. P.; Cross, J. B.; Bakken, V.; Adamo, C.; Jaramillo, J.; Gomperts, R.; Stratmann, R. E.; Yazyev, O.; Austin, A. J.; Cammi, R.; Pomelli, C.; Ochterski, J. W.; Ayala, P. Y.; Morokuma, K.; Voth, G. A.; Salvador, P.; Dannenberg, J. J.; Zakrzewski, V. G.; Dapprich, S.; Daniels, A. D.; Strain, M. C.; Farkas, O.; Malick, D. K.; Rabuck, A. D.; Raghavachari, K.; Foresman, J. B.; Ortiz, J. V.; Cui, Q.; Baboul, A. G.; Clifford, S.; Cioslowski, J.; Stefanov, B. B.; Liu, G.; Liashenko, A.; Piskorz, P.; Komaromi, I.; Martin, R. L.; Fox, D. J.; Keith, T.; Al-Laham, M. A.; Peng, C. Y.; Nanayakkara, A.; Challacombe, M.; Gill, P. M. W.; Johnson, B.; Chen, W.; Wong, M. W.; Gonzalez, C.; Pople, J. A.; Gaussian, Inc.: Pittsburgh, 2003.

APPENDIX II: DATA AND ERROR ANALYSIS OF THE G-PARAMETERS GENERATED BY SOLID-G

AII.1 XRD data and calculated G-parameters

Ct–C–Si	Cp–U–COT	Gγ	$G_{complex}$	$G_{THF/pyrrole}$	O/N–U	G_{COT}	U–COT	G_{CpR}	U–Cp	R
177.38	174.660	0.00	81.14			52.86	1.8891	28.28	2.4950	^{t}Bu
174.46	161.090	0.00	86.29			50.89	1.9129	35.41	2.4706	$^{t}Bu_2$
174.24	159.830	0.06	86.14			51.31	1.9150	34.88	2.4772	
173.13	167.040	0.00	89.44			49.87	1.9230	39.56	2.4810	$^{t}Bu_3$
168.35	161.790	0.08	88.26			48.60	1.9086	39.73	2.4830	$(Si^{i}Pr_3)_2$
171.90	149.290	0.03	89.21			49.21	1.9430	40.34	2.4830	Me_4Bz
169.05	147.810	0.28	87.68			48.40	1.9420	39.57	2.4770	
173.54	154.900	0.00	82.19			51.32	1.9160	30.86	2.4610	Me_5
175.52	153.120	0.00	84.64			54.08	1.9240	30.56	2.4710	
170.74	155.580	0.00	80.41			49.56	1.9170	30.85	2.4630	Me_4Et
173.87	155.820	0.02	88.56			51.03	1.9140	37.54	2.4500	$Me_4{}^{i}Pr$
172.39	153.450	0.00	86.61			50.63	1.9120	35.98	2.4580	Me_4SiMe_3
174.34	159.930	0.00	86.95			50.86	1.9090	36.09	2.4590	$N^{t}Bu_2$
173.50	159.400	0.03	87.30			51.8	1.9100	35.53	2.466	
162.15	138.660	0.27	88.09	16.19	2.616	45.35	1.9680	26.82	2.5480	NMe_4
161.80	138.550	0.45	88.29	15.90	2.599	45.44	1.9740	27.4	2.5680	
170.53	140.574	0.00	87.33	11.03	2.671	48.48	1.9740	27.82	2.5061	^{t}Bu
172.13	140.768	0.05	88.31	11.09	2.673	48.86	1.9730	28.40	2.5046	
173.79	141.602	0.38	88.93	10.74	2.717	49.57	1.9740	29.00	2.5873	PMe_4
169.55	144.500	0.86	89.30	12.58	2.695	47.77	1.9750	29.81	2.4990	Me_5
173.98	141.800	0.08	88.56	10.5	2.737	49.58	1.9770	28.56	2.5060	Me_4
176.71	139.800	0.01	86.64	11.07	2.697	51.61	1.9600	23.97	2.5000	Me
173.94	141.482	0.39	89.29	10.58	2.726	49.74	1.9744	29.35	2.5962	$AsMe_4$
173.65	139.735	0.61	88.80	10.9	2.651	49.71	1.9649	28.79	2.4867	NMe_4

AII.2 Normalised G-parameters from normalised data

Normalised data fixes all U–COT, U–Cp, U–O(THF) and U–N(η^1-pyrrolyl) distances to 2.28 Å. The G-parameters calculated from this data are compared with the original XRD data in the table below.

$G_{complex}$	Cp–U–COT	$G_{THF/pyrrole}$	O/N–U	G_{COT}	U–COT	G_{CpR}	U–Cp	R
78.63	174.660			46.87	1.8891	31.76	2.4950	^{t}Bu
83.56	161.090			45.21	1.9129	38.35	2.4706	^{t}Bu$_2$
83.45	159.830			45.57	1.9150	37.88	2.4772	
86.83	167.040			44.34	1.9230	42.49	2.4810	^{t}Bu$_3$
85.31	161.790			42.74	1.9086	42.57	2.4830	(Si^{i}Pr$_3$)$_2$
86.90	149.290			44.07	1.9430	42.83	2.4830	Me$_4$Bz
85.01	147.810			43.07	1.9420	41.94	2.4770	
78.75	154.900			45.56	1.9160	33.19	2.4610	Me$_5$
81.80	153.120			48.76	1.9240	33.04	2.4710	
77.21	155.580			43.97	1.9170	33.24	2.4630	Me$_4$Et
85.16	155.820			45.30	1.9140	39.86	2.4500	Me$_4$^{i}Pr
83.08	153.450			44.80	1.9120	38.28	2.4580	Me$_4$SiMe$_3$
83.99	159.930			45.15	1.9090	38.84	2.4590	N^{t}Bu$_2$
84.42	159.400			46.02	1.9100	38.4	2.466	
71.64	138.660			40.65	1.9680	30.99	2.5480	NMe$_4$
71.83	138.550			40.69	1.9740	31.14	2.5680	
89.46	140.574	14.14	2.671	43.80	1.9740	31.52	2.5061	^{t}Bu
90.53	140.768	14.25	2.673	44.18	1.9730	32.10	2.5046	
92.65	141.602	14.14	2.717	44.92	1.9740	33.59	2.5873	PMe$_4$
91.72	144.500	15.9	2.695	43.24	1.9750	32.58	2.4990	Me$_5$
90.67	141.800	14.02	2.737	45.00	1.9770	31.65	2.5060	Me$_4$
88.63	139.800	14.38	2.697	46.73	1.9600	27.52	2.5000	Me
93.40	141.482	14.03	2.726	45.09	1.9744	34.28	2.5962	AsMe$_4$
90.19	139.735	13.93	2.651	44.86	1.9649	31.40	2.4867	NMe$_4$

AII.3 Scatter graphs generated from the XRD data and calculated G-parameters

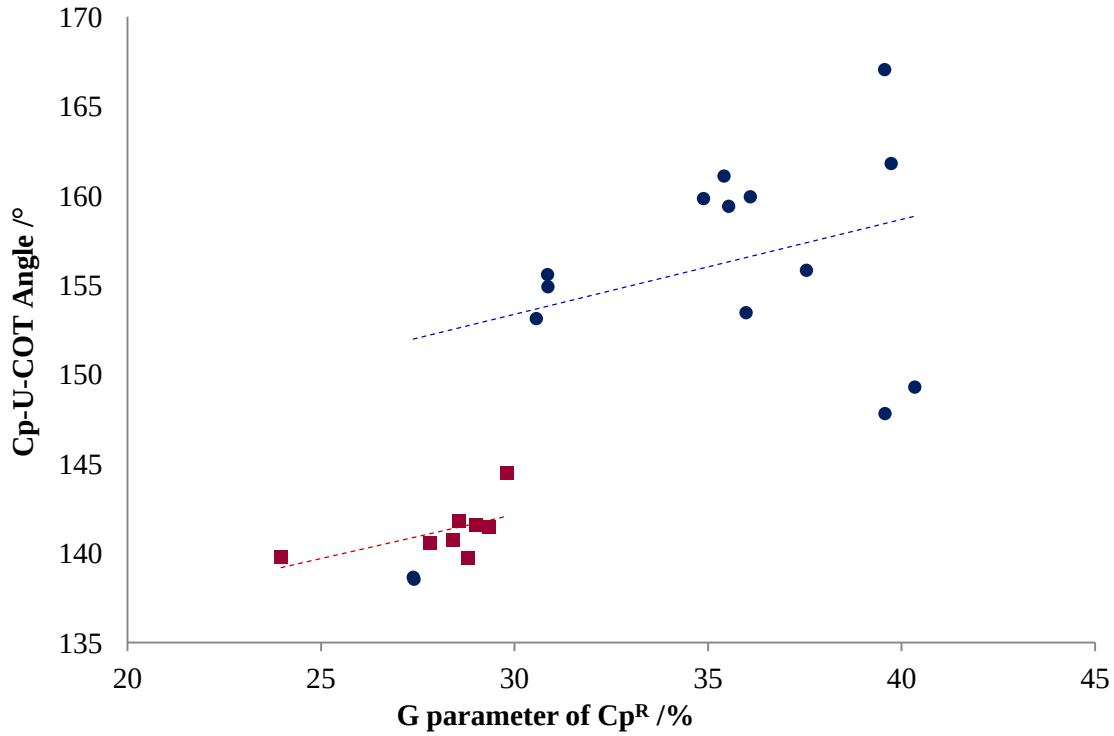

[U(COT$^{(Si\mathit{i}Pr3)2}$)(Cp^{R})] - blue

y = 0.5463x + 136.9, R^2 = 0.073 (all data)

[U(COT$^{(Si\mathit{i}Pr3)2}$)(Cp^{R})(THF)] - red

y = 0.4923x + 127.4, R^2 = 0.347 (all data)

No trend is observed between the Cp^{R} G-parameter and the Cp–U–COT angle for the base-free complexes.

A slight trend is observed between the Cp^{R} G-parameter and the Cp–U–COT angle for the THF adducts, illustrating that the Cp–U–COT angle increases as the G-parameter for Cp^{R} increases.

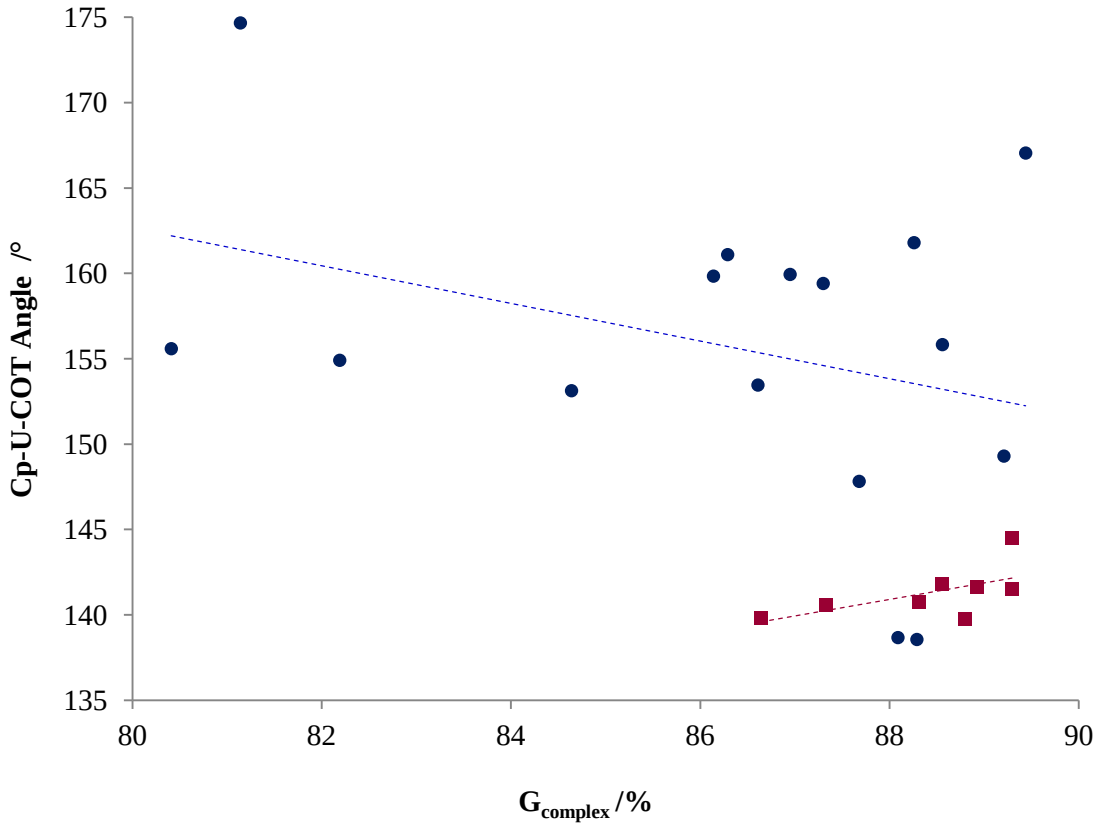

[U(COT$^{(Si\textit{i}Pr3)2}$)(Cp^{R})] - blue
y = -1.101x + 250.7, R^2 = 0.111 (all data)

[U(COT$^{(Si\textit{i}Pr3)2}$)(Cp^{R})(THF)] - red
y = 0.9685x + 55.67, R^2 = 0.368 (all data)

No trend is observed between the values of $G_{complex}$ and the Cp–U–COT angle for the base-free complexes.

A slight trend is observed between the values of $G_{complex}$ and the Cp–U–COT angle for the THF adducts, illustrating that the Cp–U–COT angle increases as $G_{complex}$ increases.

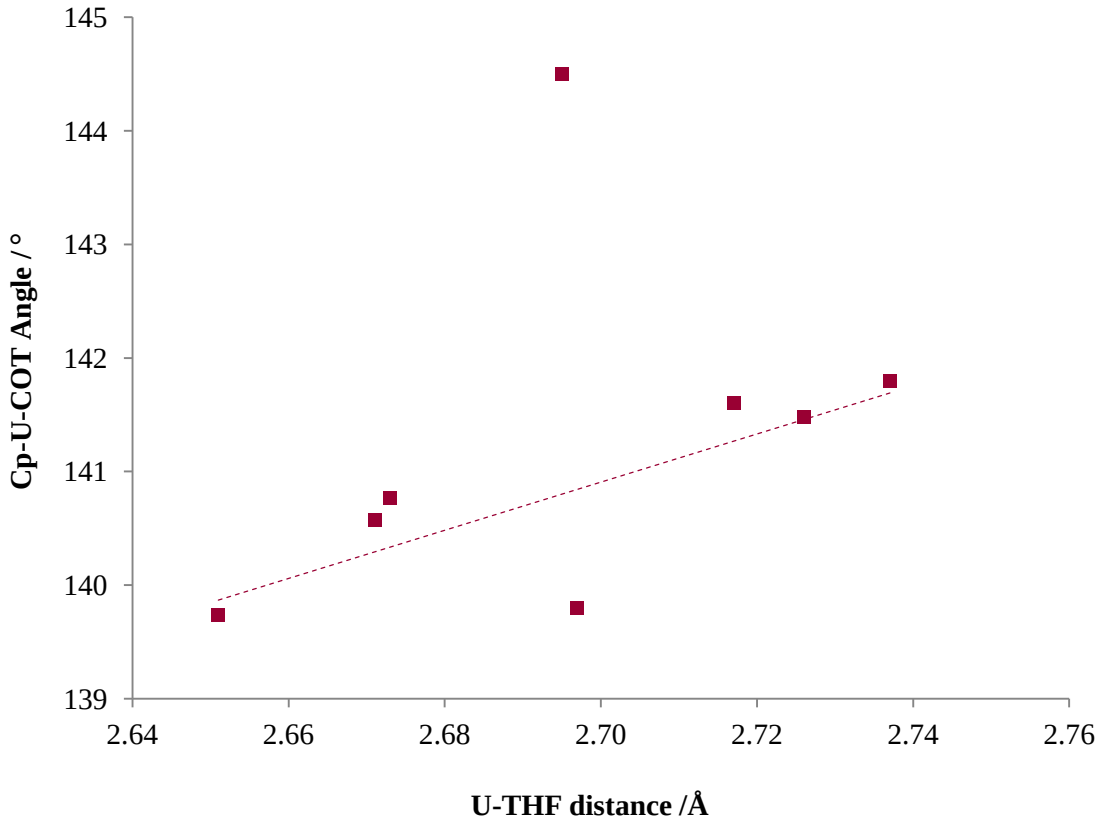

[U(COT$^{(Si\textit{i}Pr3)2}$)(Cp^{R})(THF)]
y = 20.70x + 85.48, R^2 = 0.165 (all data, not shown)
y = 21.22x + 83.61, R^2 = 0.651 (excluding the outlier {R = Me_5})

A reasonable trend is observed between the U-O(THF) distance and the Cp–U–COT angle for the THF adducts, with the exception of [U(COT$^{(Si\textit{i}Pr3)2}$)(Cp*)(THF)]. This illustrates that the Cp–U–COT angle decreases as the U–THF distance increases. Cp* is presumed to cause the outlier due to the symmetrical nature of the ligand precluding a shorter U–O(THF) bond.

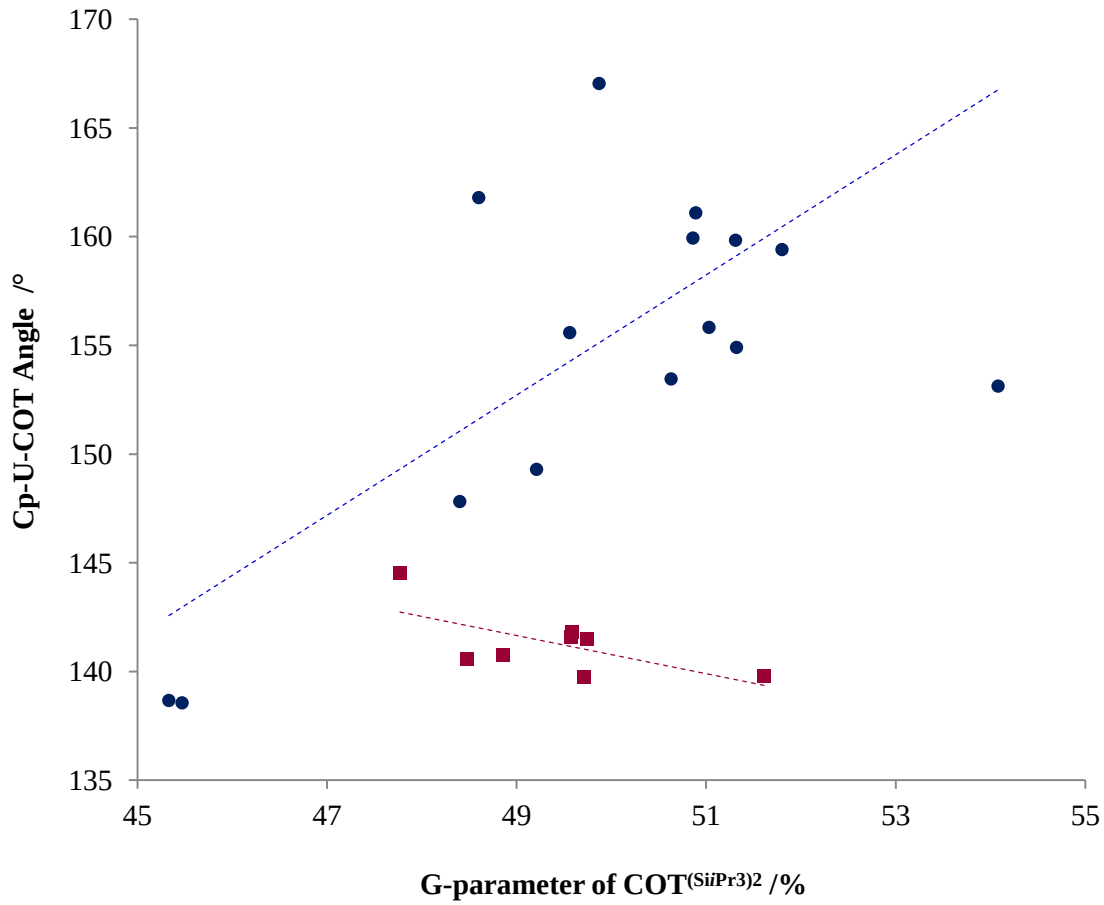

[U(COT$^{(SiiPr3)2}$)(Cp^{R})] - blue
y = 2.762x + 17.35, R^2 = 0.481 (all data)

[U(COT$^{(SiiPr3)2}$)(Cp^{R})(THF)] - red
y = -0.8777x + 184.6, R^2 = 0.428 (all data)

A reasonable trend is observed for the COT G-parameter and the Cp–U–COT angle for both types of complex, illustrating that as the COT G-parameter increases the Cp–U–COT angle also increases.

A slight trend is observed between the values of $G_{complex}$ and the Cp–U–COT angle for the THF adducts, illustrating that as the COT G-parameter increases the Cp–U–COT angle decreases.

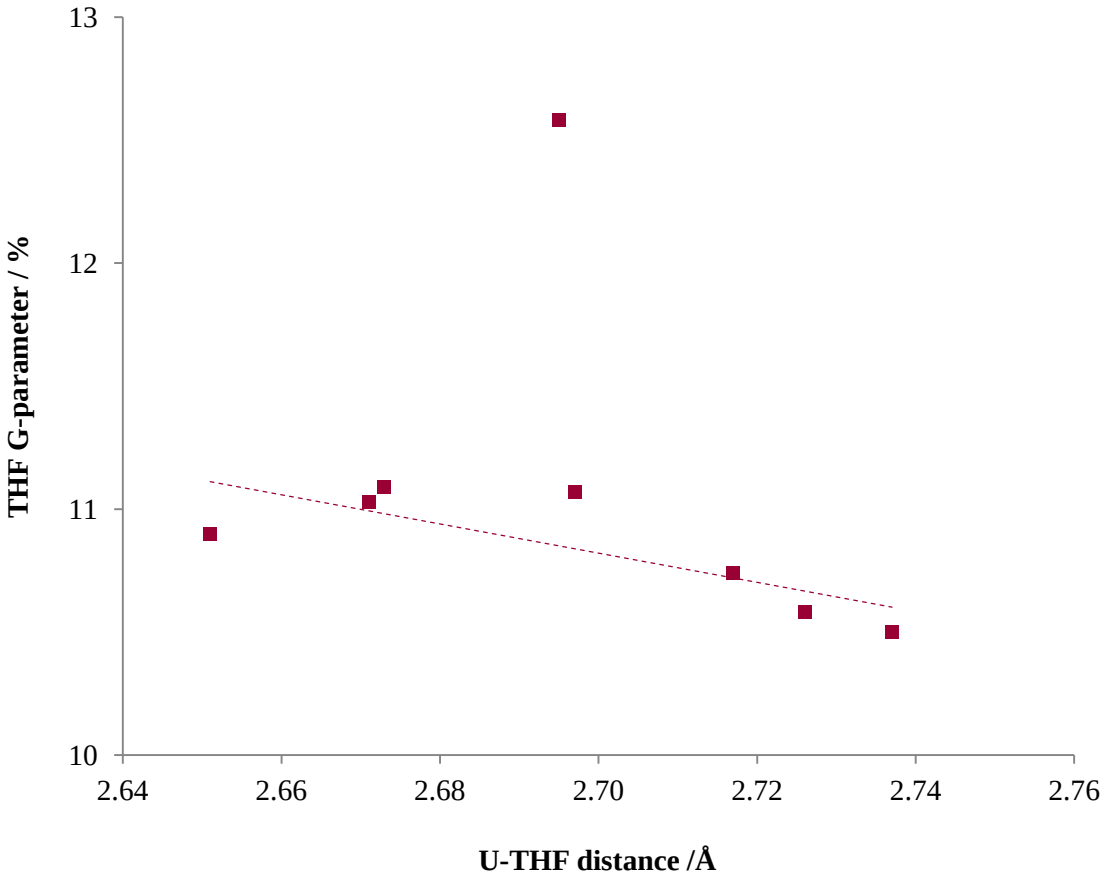

[U(COT$^{(Si\mathit{i}Pr3)2}$)(Cp^{R})(THF)]

y = -6.179x + 27.7, R^2 = 0.0794 (all data. not shown)

y = -5.935x + 26.85, R^2 = 0.627 (excluding the outlier {R = Me_5})

A reasonable trend is observed for the U– (THF) distance and the THF G-parameter with the exception of [U(COT$^{(Si\mathit{i}Pr3)2}$)(Cp*)(THF)], confirming that the shielding decreases and the U–O bond length increases.

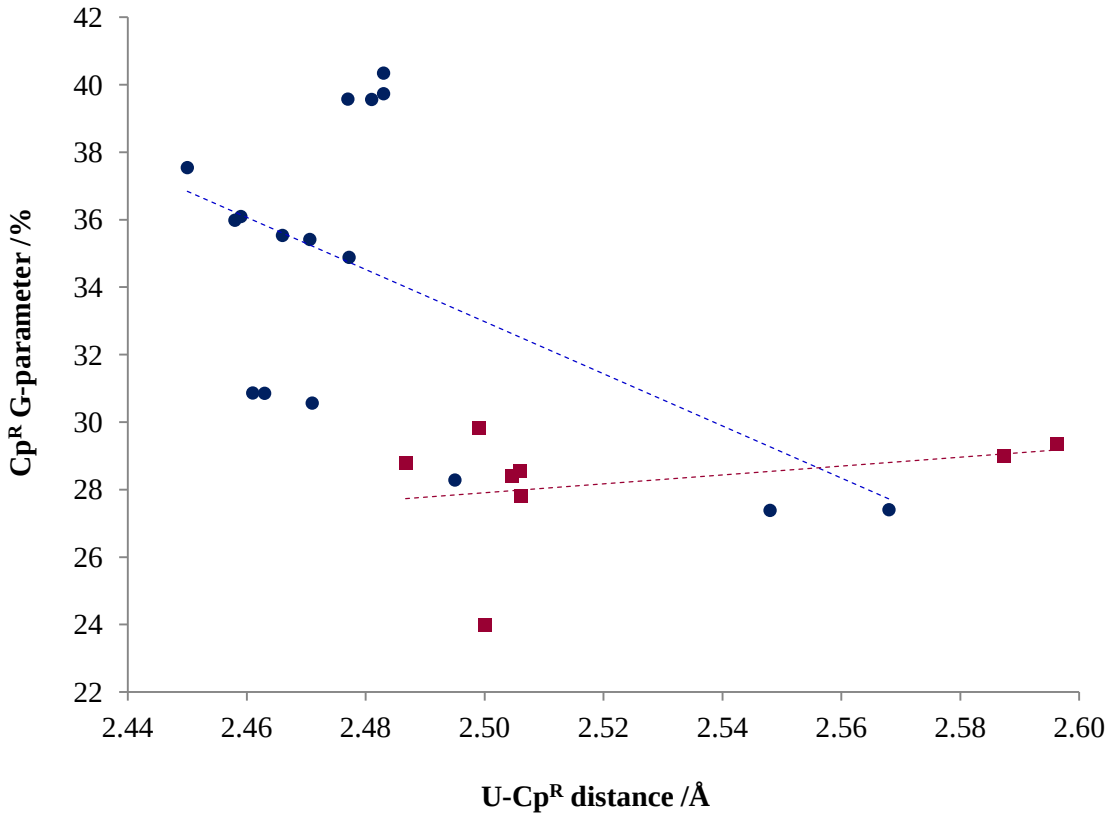

[U(COT$^{(SiiPr3)2}$)(Cp^{R})] - blue
y = -77.21x + 226, R^2 = 0.296 (all data)

[U(COT$^{(SiiPr3)2}$)(Cp^{R})(THF)] - red
y = 13.21x - 5.118, R^2 = 0.0969 (all data)

A slight trend is observed for the U–Cp^{R} distance and the U–Cp^{R} G-parameter indicating that the shielding is only partially dependent on the U–Cp distance.

No trend is observed for the THF adducts.

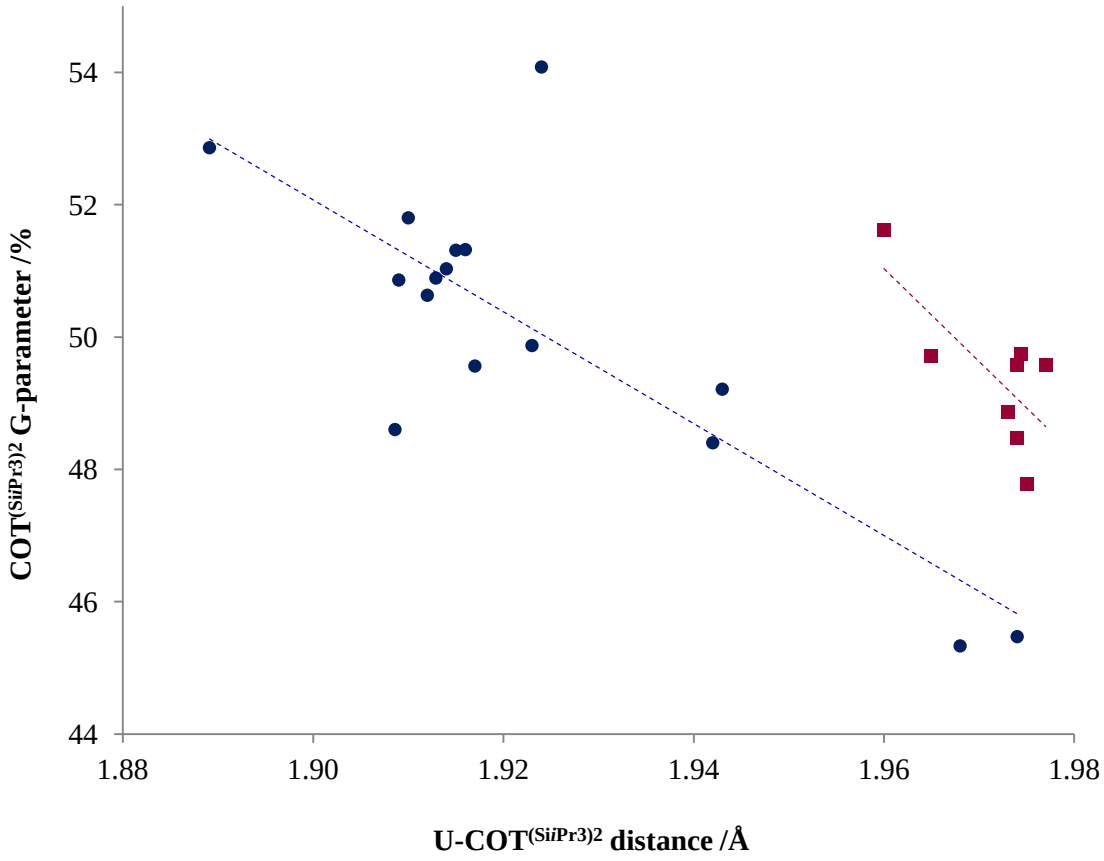

[U(COT$^{(Si\mathit{i}Pr3)2}$)(Cp^{R})] - blue
y = -84.58x + 212.77, R^2 = 0.658 (all data)

[U(COT$^{(Si\mathit{i}Pr3)2}$)(Cp^{R})(THF)] - red
y = -140.3x + 326.0, R^2 = 0.531 (all data)

A reasonable trend is observed for the COT G-parameter and the U–COT distance, illustrating that the decreasing sterics from the COT ring is only partially due to increasing the U–COT distance.

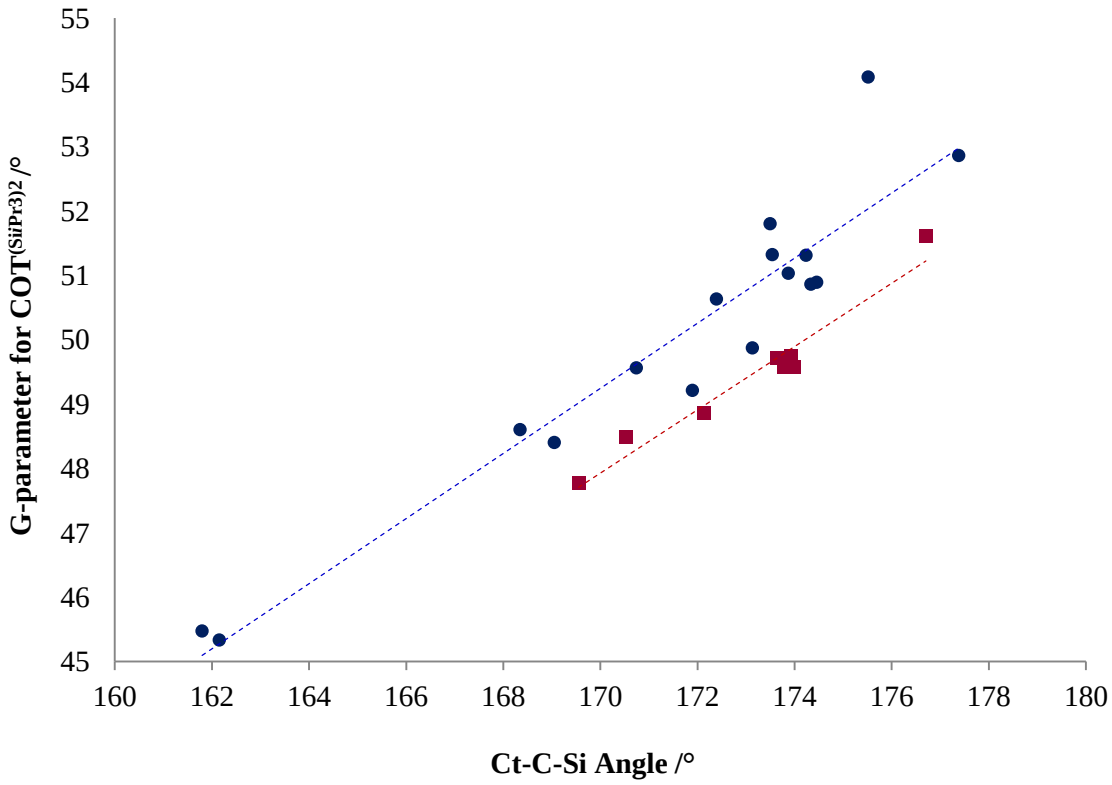

[U(COT$^{(Si\mathit{i}Pr3)2}$)(Cp^{R})] - blue
y = 0.5058x - 36.74, R^2 = 0.904 (all data)

[U(COT$^{(Si\mathit{i}Pr3)2}$)(Cp^{R})(THF)] - red
y = 0.9545x - 35.61, R^2 = 0.954 (all data)

A good trend is observed for the COT G-parameter and the Ct–C–Si substituent angle for both types of complex, illustrating that as the degree of sp^3 character of the COT ring increases, the ligand imparts less shielding on the uranium centre.

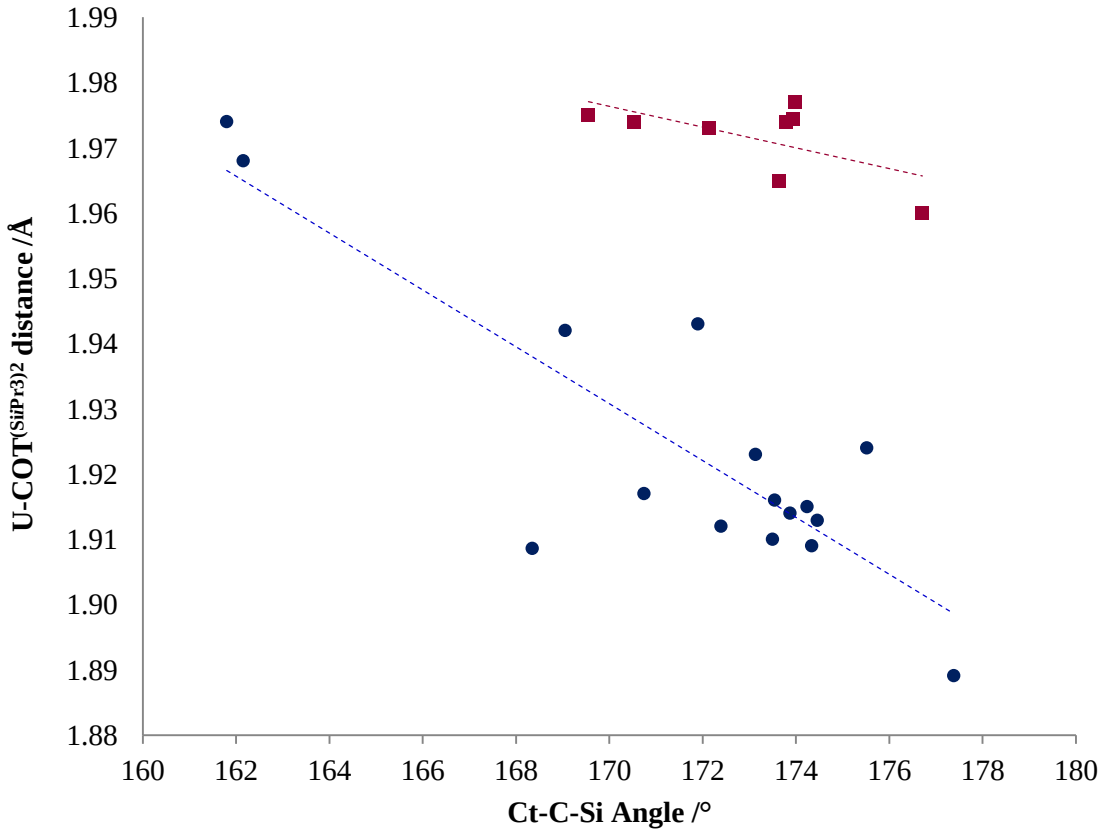

[U(COT$^{(SiiPr3)2}$)(Cp^{R})] - blue
y = -0.0044x + 2.671, R^2 = 0.729 (all data)

[U(COT$^{(SiiPr3)2}$)(Cp^{R})(THF)] - red
y = -0.0016x + 2.247, R^2 = 0.372 (all data)

A good trend is observed for the Ct–C–Si substituent angle and the U–COT distance for the desolvated complexes illustrating that as the sp^3 character of the COT ring carbons increases the U–COT distance increases.

A slight trend is observed for the Ct–C–Si substituent angle and the U–COT distance for the THF adducts illustrating that as the sp^3 character of the COT ring carbons increases the U–COT distance increases.

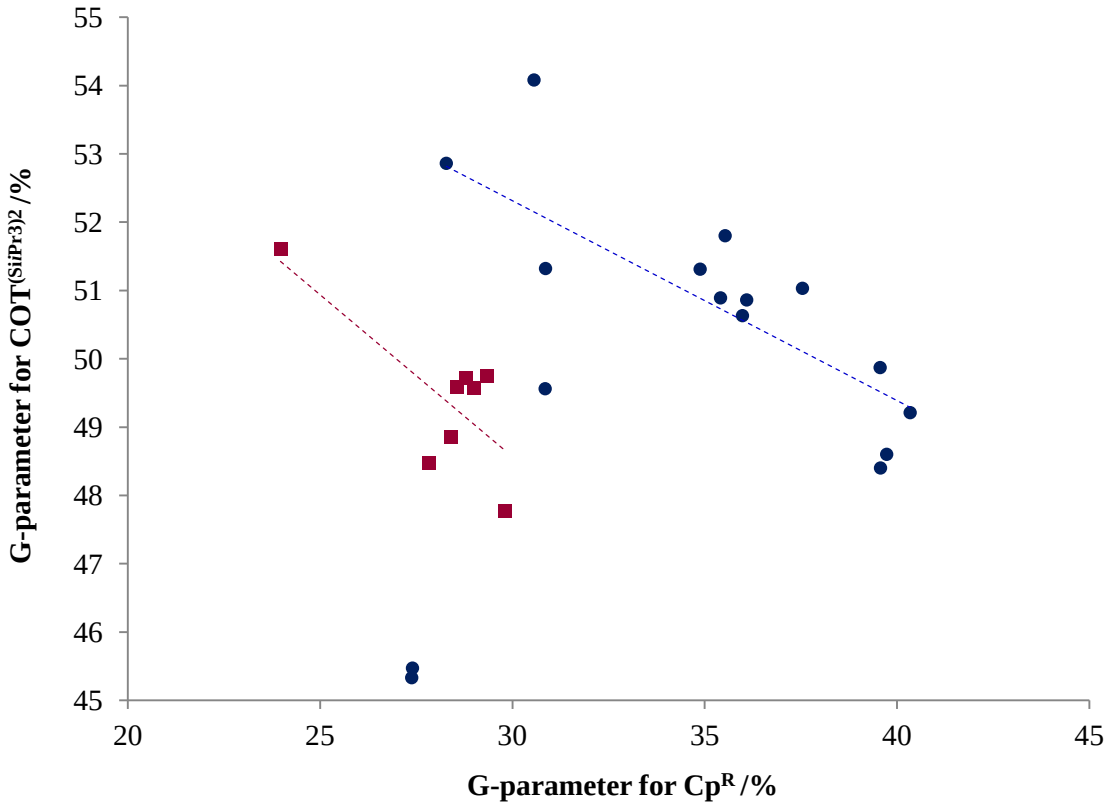

[U(COT$^{(SiiPr3)2}$)(Cp^{R})] - blue
y = 0.0600x + 48.02, R^2 = 0.0139 (all data, not shown)
y = -0.2927x + 61.10, R^2 = 0.531 (excluding the two outliers {R = NMe_4})

[U(COT$^{(SiiPr3)2}$)(Cp^{R})(THF)] - red
y = -0.4742x + 62.79, R^2 = 0.581 (all data)

A reasonable trend is observed for the COT G-parameter and the Cp^{R} G-parameter for both types of complex, excluding the desolvated pyrrolyl complex, [U(COT$^{(SiiPr3)2}$)(Cp^{NMe4})]. This illustrates that as the Cp^{R} ligand becomes larger the COT ligand compensates for the increased sterics by increasing the U-COT distance and/or increasing the amount of sp^3 character.

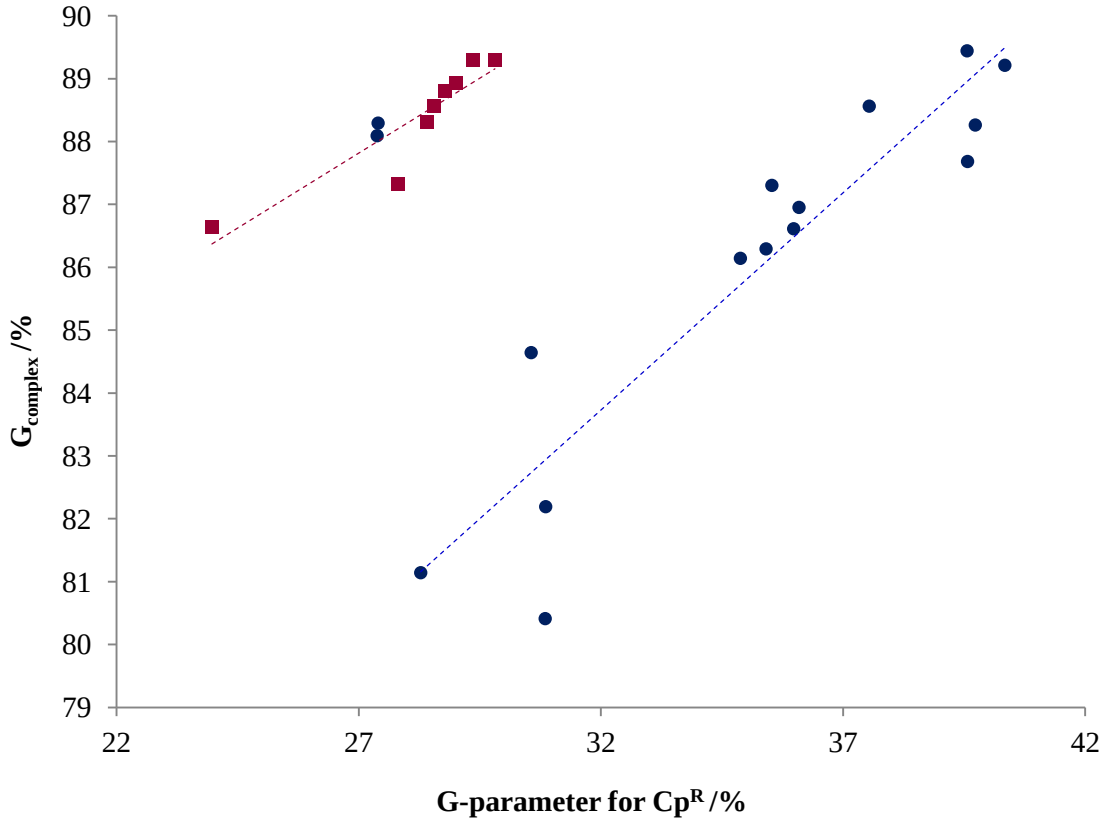

[U(COT$^{(SiiPr3)2}$)(Cp^{R})] - blue
y = 0.3471x + 74.40, R^2 = 0.315 (all data, not shown)
y = 0.6911x + 61.62, R^2 = 0.857 (excluding the two outliers {R = NMe_4})

[U(COT$^{(SiiPr3)2}$)(Cp^{R})(THF)] - red
y = 0.4471.5x + 74.96, R^2 = 0.832 (all data)

A good trend is observed for the Cp^{R} G-parameter and $G_{complex}$ for both types of complex, illustrating that the total shielding increases as the Cp^{R} ligand becomes larger.

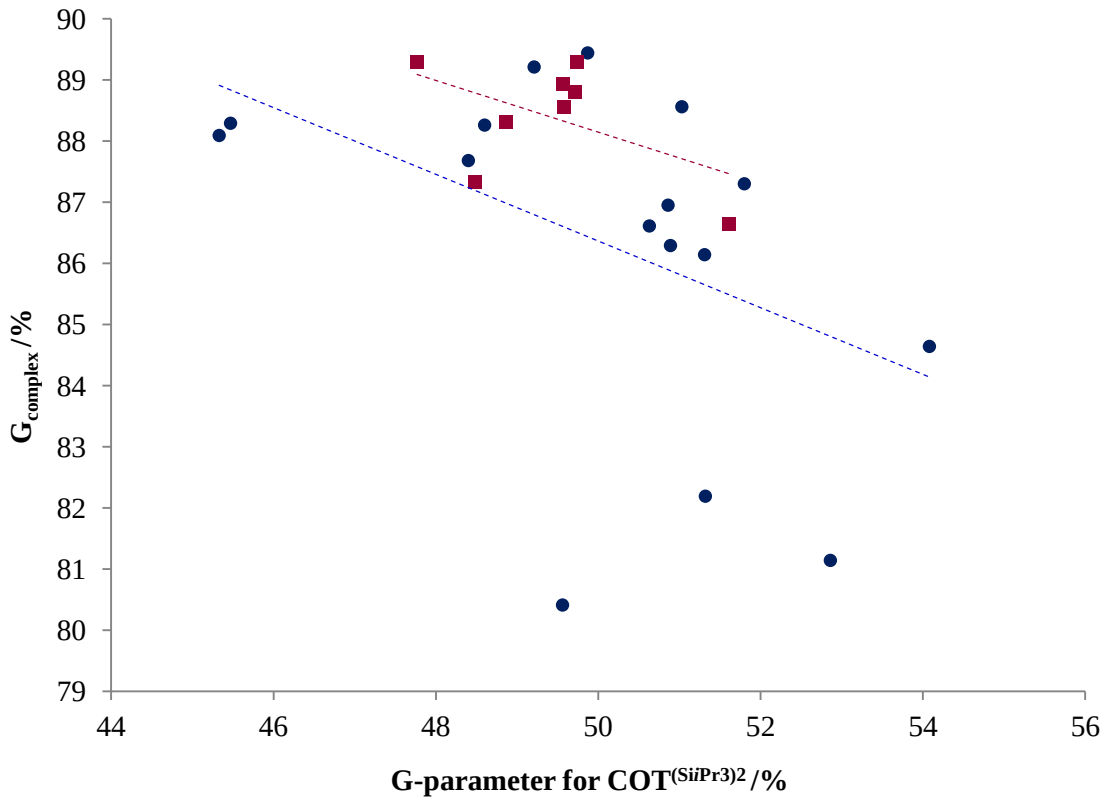

[U(COT$^{(SiiPr3)2}$)(Cp^{R})] - blue
y = -0.5549x + 113.6, R^2 = 0.205 (all data)

[U(COT$^{(SiiPr3)2}$)(Cp^{R})(THF)] - red
y = -0.4221x + 109.25, R^2 = 0.252 (all data)

A meaningful trend cannot be determined from these data

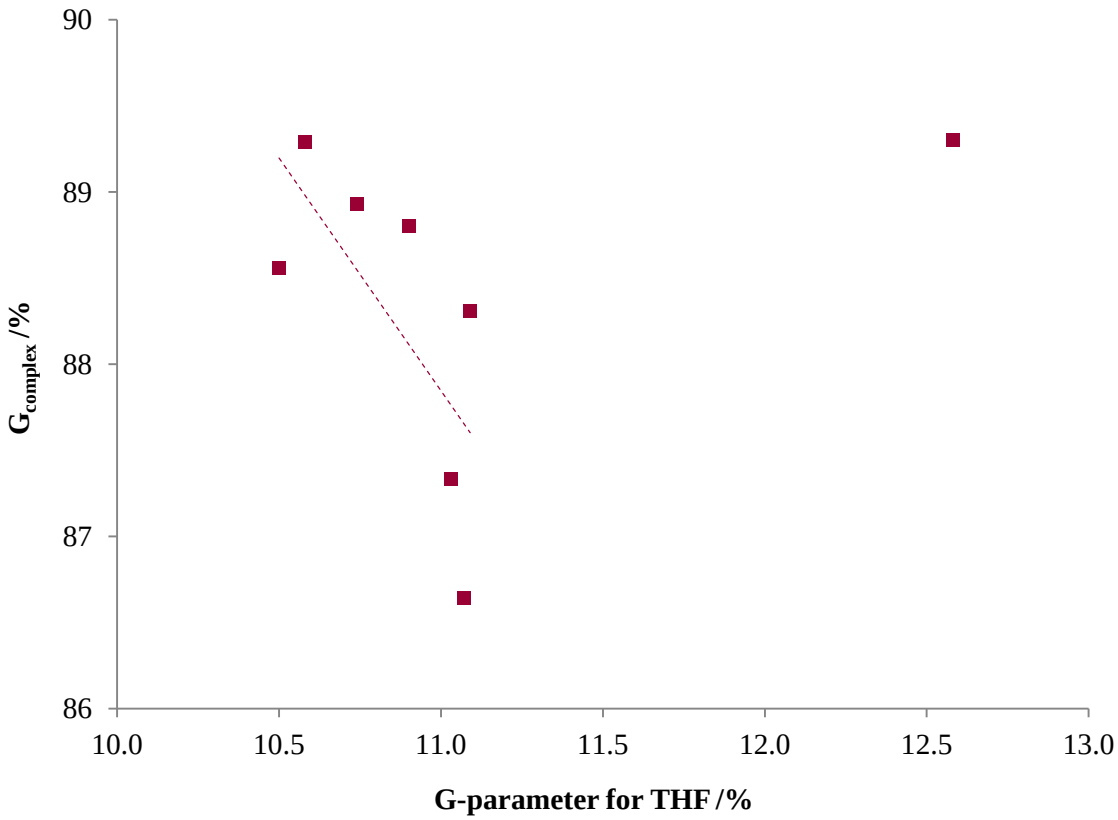

[U(COT$^{(Si\mathit{i}Pr3)2}$)(Cp^{R})(THF)]
y = 0.211x + 86.06, R^2 = 0.021 (all data, not shown)
y = -2.704x + 117.6, R^2 = 0.473 (excluding the outlier {R = Me_5})

A slight trend is observed for the THF G-parameter and $G_{complex}$ with the exception of [U(COT$^{(Si\mathit{i}Pr3)2}$)(Cp*)(THF)], illustrating that as the total shielding increases the G-parameter for THF becomes smaller, implying that the U–O(THF) distance increases to compensate for the increased sterics around the uranium centre.

APPENDIX III: DATA AND ERROR ANALYSIS FOR THE CALCULATION OF THE EQUILIBRIUM CONSTANT FOR [U(COT$^{(SIIPR3)2}$)(CP^{NME4})].

AIII.1 Experimental details and data for the calculation of the equilibrium constant K_b and ΔG

The equilibrium constant and ΔG were calculated according to:

$$K_b = \frac{(b_{2.5THF})^2}{(b_{2.5})(b_{THF})^2}$$

$$\Delta G = -RTLnK_b$$

with units of kg·mol^{-1} and kJ·mol^{-1} respectively.

The sample was made up using 14.5 mg **2.5** ([U(COT$^{(SiiPr3)2}$)(Cp^{NMe4})]) and 339 mg d_6-benzene. Each data point was obtained by adding a known mass of d_8-THF to the sample and recording the ^{1}H NMR spectrum at 30 °C. Data are included below.

mass(THF)	n(THF)	Ratio 2.5THF : 2.5	n(2.5)	n(2.5THF)	K(THF)	K(2.5)	K_b	ΔG
0	0	0	1	9.33×10^{-06}	0	0	2.75×10^{-02}	
0.9×10^{-06}	1×10^{-05}	0.05	0.95	8.86×10^{-06}	9.33×10^{-07}	0.0331	2.61×10^{-02}	0.264	3.35
3.6×10^{-06}	4.5×10^{-05}	0.1	0.9	8.4×10^{-06}	1.87×10^{-06}	0.132	2.48×10^{-02}	0.0697	6.71
8.8×10^{-06}	1.1×10^{-04}	0.18	0.82	7.65×10^{-06}	3.36×10^{-06}	0.324	2.26×10^{-02}	0.0415	8.02
1.20×10^{-05}	1.50×10^{-04}	0.23	0.77	7.18×10^{-06}	4.29×10^{-06}	0.442	2.12×10^{-02}	0.0388	8.19
1.71×10^{-05}	2.13×10^{-04}	0.32	0.68	6.34×10^{-06}	5.97×10^{-06}	0.629	1.87×10^{-02}	0.0419	7.99
2.48×10^{-05}	3.09×10^{-04}	0.39	0.61	5.69×10^{-06}	7.28×10^{-06}	0.913	1.68×10^{-02}	0.0330	8.60
3.23×10^{-05}	4.03×10^{-04}	0.46	0.54	5.04×10^{-06}	8.58×10^{-06}	1.19	1.49×10^{-02}	0.0305	8.79
3.88×10^{-05}	4.84×10^{-04}	0.53	0.47	4.39×10^{-06}	9.89×10^{-06}	1.43	1.29×10^{-02}	0.0323	8.65
4.54×10^{-05}	5.66×10^{-04}	0.57	0.43	4.01×10^{-06}	1.06×10^{-05}	1.67	1.18×10^{-02}	0.0298	8.85
5.53×10^{-05}	6.90×10^{-04}	0.64	0.36	3.36×10^{-06}	1.19×10^{-05}	2.04	9.91×10^{-03}	0.0302	8.81
6.28×10^{-05}	7.83×10^{-04}	0.67	0.33	3.08×10^{-06}	1.25×10^{-05}	2.31	9.08×10^{-03}	0.0280	9.00
7.10×10^{-05}	8.86×10^{-04}	0.71	0.29	2.71×10^{-06}	1.32×10^{-05}	2.61	7.98×10^{-03}	0.0280	9.00
7.91×10^{-05}	9.87×10^{-04}	0.73	0.27	2.52×10^{-06}	1.36×10^{-05}	2.91	7.43×10^{-03}	0.0256	9.22
8.81×10^{-05}	1.10×10^{-03}	0.76	0.24	2.24×10^{-06}	1.42×10^{-05}	3.24	6.60×10^{-03}	0.0252	9.27
9.69×10^{-05}	1.21×10^{-03}	0.79	0.21	1.96×10^{-06}	1.47×10^{-05}	3.57	5.78×10^{-03}	0.0257	9.22
1.09×10^{-04}	1.36×10^{-03}	0.81	0.19	1.77×10^{-06}	1.51×10^{-05}	4.01	5.23×10^{-03}	0.0237	9.43
1.50×10^{-05}	1.87×10^{-03}	0.89	0.11	1.03×10^{-06}	1.66×10^{-05}	5.52	3.03×10^{-03}	0.0260	9.19
1.81×10^{-05}	2.26×10^{-03}	0.91	0.09	8.40×10^{-07}	1.70×10^{-05}	6.66	2.48×10^{-03}	0.0229	9.52

Mass valus are given in kg, n is the number of moles (mol); K is the molality ($mol \cdot kg^{-1}$), K_b is given in $kg \cdot mol^{-1}$ and ΔG is given in $kJ \cdot mol^{-1}$.

AIII.2 Error analysis for the values of relative intensity.

The errors in the data arise from the mass measurements (error in the x-axis) and the integration of the ^{1}H NMR resonances (y-axis).

The error of the balance used is ±0.05 mg. Therefore the error when calculating the solvent composition in percentage THF is:

$$error\ in\ solvent\ composition = \frac{\frac{(mass_{THF} \pm 0.05)}{80.16}}{\left[\frac{mass_{THF} \pm 0.05}{80.16}\right] + \left[\frac{mass_{benzene} \pm 0.05}{84.15}\right]}\ \%THF$$

The percentage error in each value for x can therefore be calculated as

$$100 \times \frac{error\ in\ x}{x}$$

Value of x	Error in x	Percentage Error
0.000	0.0155	
0.278	0.0154	0.0554
1.10	0.0151	0.0137
2.65	0.0147	0.00553
3.58	0.0144	0.00402
5.03	0.0140	0.00278
7.13	0.0134	0.00187
9.09	0.0128	0.00141
10.7	0.0123	0.00115
12.3	0.0119	0.000965
14.6	0.0113	0.000772
16.3	0.0108	0.000666
18.0	0.0104	0.000577
19.7	0.00999	0.000508
21.4	0.00956	0.000446
23.1	0.00916	0.000397
25.2	0.00866	0.000343
31.7	0.00722	0.000228
35.9	0.00636	0.000177

The percentage error values obtained illustrate that the error in the values of x is low, and therefore would not be seen with error bars.

The error associated with the relative intensity of each resonance is 0.005. However, significant line broadening gave rise to overlap of several resonances and the errors associated with the integral values could not be quantified further. Detailed error analysis was therefore not conducted.